



**ENGINEERING SERVICE CENTER**  
**Port Hueneme, California 93043-4370**

## **CONTRACT REPORT**

### **CR-10-012-ENV**

## **FINAL REPORT - PREDICTING THE MOBILITY AND BURIAL OF UNDERWATER UNEXPLODED ORDNANCE (UXO) USING THE UXO MOBILITY MODEL**

**(ESTCP) 200417**

By

Jeffrey V. Wilson, Sound & Sea Technology, Inc.

Alexandra DeVisser, Naval Facilities Engineering Command Engineering Service Center

Barbara Sugiyama, Naval Facilities Engineering Command Engineering Service Center

November 2009





# **FINAL REPORT**

---

**Predicting the Mobility and Burial  
of Underwater Unexploded Ordnance (UXO) using the  
*UXO Mobility Model***

**ESTCP Project 200417**

**Nov 2009**

**Prepared by  
J.V. Wilson, A. De Visser, and B. Sugiyama**





<b>REPORT DOCUMENTATION PAGE</b>				Form Approved OMB No. 0704-0811	
The public reporting burden for this collection of information is estimated to average 1 hour per response, including the time for reviewing instructions, searching existing data sources, gathering and maintaining the data needed, and completing and reviewing the collection of information. Send comments regarding this burden estimate or any other aspect of this collection of information, including suggestions for reducing the burden to Department of Defense, Washington Headquarters Services, Directorate for Information Operations and Reports (0704-0188), 1215 Jefferson Davis Highway, Suite 1204, Arlington, VA 22202-4302. Respondents should be aware that notwithstanding any other provision of law, no person shall be subject to any penalty for failing to comply with a collection of information, if it does not display a currently valid OMB control number.					
<b>PLEASE DO NOT RETURN YOUR FORM TO THE ABOVE ADDRESS.</b>					
1. REPORT DATE (DD-MM-YYYY) 01-11-2009		2. REPORT TYPE Contract Report		3. DATES COVERED (From – To)	
4. TITLE AND SUBTITLE FINAL REPORT - Prediction the Mobility and Burial of Underwater Unexploded Ordnance (UXO) Using the UXO Mobility Model				5a. CONTRACT NUMBER N47408-02-D-8319 and N62473-06-3005	
				5b. GRANT NUMBER	
				5c. PROGRAM ELEMENT NUMBER	
6. AUTHOR(S) Jeffrey V. Wilson Sound & Sea Technology, Inc. Alexandra DeVisser and Barbara Sugiyama, Naval Facilities Engineering Command Engineering Service Center				5d. PROJECT NUMBER	
				5e. TASK NUMBER Task Orders 0056, 0076, 0041, 0060, and 0061	
				5f. WORK UNIT NUMBER	
7. PERFORMING ORGANIZATION NAME(S) AND ADDRESSES Sound and Sea Technology – 3507 Shelby Rd Lynnwood, WA 98087 Naval Facilities Engineering Command Engineering Service Center 1100 23 <sup>rd</sup> Ave Port Hueneme, CA 93030				8. PERFORMING ORGANIZATION REPORT NUMBER	
9. SPONSORING/MONITORING AGENCY NAME(S) AND ADDRESS(ES) Environmental Security Technology Certification Program (ESTCP) 901 North Stuart Street, Suite 303 Arlington, VA 22203				10. SPONSOR/MONITORS ACRONYM(S)	
				11. SPONSOR/MONITOR'S REPORT NUMBER(S)	
12. DISTRIBUTION/AVAILABILITY STATEMENT					
13. SUPPLEMENTARY NOTES					
14. ABSTRACT The ESTCP Unexploded Ordnance (UXO) Mobility Model (MM) validation program expanded the capabilities of the vortex lattice based model previously developed by the Navy for mine modeling applications and then validated the MM with surrogate ordnance in two instrumented field demonstration, one in each of the most common coastal environmental types (Trailing Edge and Biogenic Reef): U.S. Army Field Research Facility (FRF), Duck, NC, and Pacific Missile Range Facility (PMRF), Kauai, HI. The MM correctly predicted all the basic behaviors of the surrogates; the skill factor for modeling migration and burial exceeded 0.8 in both cases, a favorable result with respect to modeling coastal processes and mine burial prediction. The MM is calibrated for the most common coastal environmental and can use wither default environmental conditions or site-specific data inputs to more accurately predict overall probability of movement. It is noted that the primary cost drivers for varying levels of analysis is predicated on the amount of site data available.					
15. SUBJECT TERMS					
16. SECURITY CLASSIFICATION OF:			17. LIMITATION OF ABSTRACT		18. NUMBER OF PAGES
a. REPORT	b. ABSTRACT	c. THIS PAGE			19a. NAME OF RESPONSIBLE PERSON
U	U	U			19b. TELEPHONE NUMBER (include area code)



## Table of Contents

Table of Contents .....	i
List of Abbreviations and Acronyms .....	iii
List of Figures .....	v
List of Tables .....	ix
Acknowledgements .....	x
Executive Summary .....	xi
1.0 Introduction .....	1
1.1 Background .....	1
1.2 Objectives of the Demonstration .....	6
1.3 Regulatory Drivers .....	6
1.4 Stakeholder/End-User Issues .....	6
2.0 Technology .....	8
2.1 Technology description .....	8
2.2 Technology development .....	8
2.2.1 Processes Represented and Applicable Coastal Regions .....	10
2.2.2 User Requirements .....	15
2.2.3 Previous Mobility Model Efforts .....	16
2.3 Advantages and Limitations of the Technology .....	16
3.0 Performance Objectives .....	17
3.1 Qualitative Assessment of Multi-User Capability .....	19
3.2 Qualitative Mobility Model Performance .....	19
3.3 Field Demonstrations Collect Sufficient Data .....	19
3.4 Mobility Model Validation Successful .....	20
4.0 SITE DESCRIPTION .....	20
4.1 Site Selection .....	22
4.2 Demonstration Site/Facility History .....	25
4.3 Site Geology .....	25
4.4 Munitions Contamination .....	25
5.0 TEST DESIGN .....	26
5.1 Conceptual Experimental Design .....	26
5.1.1 Demonstration Setup and Startup .....	26
5.1.2 Period of Operation .....	27
5.2 Site Preparations .....	28
5.2.1 FRF Duck Pre-Demonstration Analysis .....	28
5.2.2 PMRF Kauai Pre-demonstration Analysis .....	29
5.3 System Specifications .....	29
5.4 Calibration Activities .....	30

6.0 DATA ANALYSIS AND PRODUCTS .....	30
6.1 Mobility Model Description .....	31
6.1.1 Required Input .....	31
6.1.2 Key Outputs .....	33
6.1.3 Field Demonstration Data Quality .....	34
6.2 Analysis of PMRF (Hawaii) Field Test Data.....	34
6.2.1 PMRF Model Initialization .....	42
6.2.2 UXO Shape Lattice .....	51
6.2.3 Burial and Migration on Planar Carbonate Sediment Beds .....	52
6.2.4 Eddies and Secondary Flows from Awa Channel Sidewalls .....	54
6.2.5 UXO Migration/Burial Model Performance at PMRF Experiment.....	57
6.3 Analysis of FRF Duck Field Test Data.....	69
6.3.1 Model Initialization.....	73
6.3.2 Burial and Migration from Mode 1 Analysis.....	84
6.3.3 UXO Migration/Burial Model Performance at FRF Experiment .....	86
7.0 Performance Assessment .....	107
7.1 Performance Criteria.....	107
7.2 Performance Confirmation Methods.....	107
7.3 Performance In Extreme Conditions.....	110
7.3.1 Background.....	111
7.3.2 Modeling Incoming Waves.....	112
7.3.3 Effect of Extreme Events on Overall Risk Analysis.....	112
7.3.4 Summary of Present Validation for Extreme Events .....	113
8.0 COST ASSESSMENT.....	113
8.1 Cost MODEL.....	113
8.1.1 Development and Validation Costs .....	114
8.2 COST DRIVERS .....	115
8.3 Cost BENEFITS.....	118
8.3.1 Cost Comparison.....	118
8.3.2 Basis of Costs.....	122
8.3.3 Cost Drivers .....	123
8.3.4 Life Cycle Costs.....	124
9.0 Implementation Issues .....	124
9.1 Environmental Checklist.....	124
9.2 Other Regulatory Issues.....	124
9.3 End-User Issues .....	124
10.0 References.....	126
Appendix A Points Of Contact .....	131
Appendix B. UXO Mobility Model Fortran Code.....	1

## List of Abbreviations and Acronyms

Acronym	Definition
ADCP	Acoustic Doppler Current Profiler
AGD	Applications Guidance Document
ARAMS	Army Risk Assessment Modeling System
ASTM	American Society for Testing and Materials
CATEX	Categorical Exclusion
CFR	U.S. Code of Federal Regulations
CRAB	Coastal Research Amphibious Buggy
DEM/VAL	Demonstration/Validation
Det.	Detachment
DoD	U.S. Department of Defense
DMA	Defense Mapping Agency
EPA	U.S. Environmental Protection Agency
ESTCP	Environmental Security Technology Certification Program
FRF	Field Research Facility
FRTR	Federal Remediation Technologies Roundtable
GIS	Geographic Information System
GPS	Global Positioning System
HASP	Health and Safety Plan
IM	Interaction Model
LARC	Lighter Amphibious Resupply Cargo
LIDAR	Light Detection and Ranging
MB	megabyte
MBBS	Multibeam Backscatter
MCBH	Marine Corps Base Hawaii
MDT	Mugu Drifter Test
MMFT	Measurement Method Field Test
NAD	Navy Ammunition Depot
NAS	Naval Air Station
NAVFAC ESC	Naval Facilities Engineering Command Engineering Service Center

NESDI	Navy Environmental Sustainability Development to Integration
NOS	National Ocean Service
NS	Naval Station
NWS	Naval Weapons Station
ONR	Office of Naval Research
PACDIV	NAVFAC Pacific Division
PMRF	Pacific Missile Range Facility
QA	Quality Assurance
QAPP	Quality Assurance Plan
QAS	Quality Assurance Specialist
RAC	Risk Assessment Code
REF/DIF	Refraction/Diffraction
ROI	Return on Investment
SAJ	Dr. Scott A. Jenkins Consulting
SCM	Site Conceptual Model
SEI	Sea Engineering, Inc.
SPAWAR	Space and Naval Warfare Systems Command
SST	Sound and Sea Technology
USACE	U.S. Army Corps of Engineers
USAESCH	U.S. Army Engineering and Support Center
USGS	U.S. Geological Survey
UXO	unexploded ordnance
VSW	Very Shallow Water
VORTEX	Vortex Lattice Model

## List of Figures

Figure 1. Site Conceptual Model for UXO showing the UXO Mobility Model Analysis as part of site quantification. ....	2
Figure 2. UXO Mobility Model of flow and scour over a 5"/38 projectile surrogate. ....	3
Figure 3. Possible UXO movement scenarios. ....	4
Figure 4. Overall process for estimating risk of human interaction with underwater UXO using the UXO Mobility Model and Interaction Model. ....	4
Figure 5. UXO Mobility Model flow diagram.....	10
Figure 6. Farfield and nearfield processes for the UXO MM.....	11
Figure 7. UXO entombment versus nearshore location and critical mass of sediment. ....	11
Figure 8. Details of UXO movement in response to nearfield forces.....	12
Figure 9. Geomorphic coastal classifications used in UXO Mobility Model (Mode 1).....	13
Figure 10. Duck, NC, is approximately 60 miles south of Norfolk, VA. ....	21
Figure 11. FRF Duck Field Demonstration configuration.....	21
Figure 12. PMRF Field Demonstration configuration.....	22
Figure 13. Field demonstration concept (PMRF Hawaii example). ....	26
Figure 14. ESTCP UXO Mobility Model program schedule. ....	28
Figure 15. Surrogate 5"/38 projectiles used in UXO Mobility Model field demonstrations.....	30
Figure 16. Dimensions of 5"/38 surrogate used in field demonstrations.....	35
Figure 17. Vortex Lattice Scour Burial Model. ....	36
Figure 18. Schematic diagram of control cells along a fringing reef coast .....	37
Figure 19. Farfield burial mechanics. ....	38
Figure 20. Vortex lattice method: (a) lattice and horseshoe vortex system, (b) horseshoe vortices inducing sediment transport in nature (photo courtesy Kimball Millikan).....	40
Figure 21. Illustration of the image vortex method. ....	41
Figure 22. Composite bathymetry from NOS data base and equilibrium profiles for wave conditions February - May 2007.....	43
Figure 23. Sample density of LIDAR high resolution bathymetry data. ....	44
Figure 24. PMRF offshore and inshore field demonstration sites .....	46
Figure 25. Refraction/Diffraction pattern at PMRF test site for highest waves occurring during the experiment (February-May 2007).....	47

Figure 26. Wave height (upper) and current magnitude (lower) at the offshore site.....	48
Figure 27. Current speed (upper) and current direction (lower) during the demonstration.....	49
Figure 28. Grain size distribution of sediment – PMRF Field Test site, Kauai, May 2007; data provided by Sea Engineering, Inc. ....	51
Figure 29. Simulation of vortex and scour field in the nearfield grid of the 5”/38 UXO surrogate. ....	53
Figure 30. Awa channel sidewall at intersection with carbonate sedimentary floor at PMRF; photo courtesy of Sea Engineering, Inc. ....	55
Figure 31. Simulation of vertical divergence and secondary flows induced by curvature of awa axis in the vicinity of the offshore site at PMRF, Kauai.....	56
Figure 32. Simulation of large scale eddies over UXO induced by encroaching shoulders of awa sidewalls in the vicinity of the offshore site at PMRF, Kauai. ....	57
Figure 33. Details of lay-down pattern of UXO surrogate fields at PMRF.....	58
Figure 34. Schematic of acoustic transponder ranging technique for locating position of UXO surrogates during the PMRF experiment. ....	59
Figure 35. VORTEX model simulation of migration and burial rates of 5”/38 UXO surrogates at the inshore site at 8.3m depth as a function of measured wave heights. ....	60
Figure 36. VORTEX Model simulation of migration and burial rates of 5”/38 UXO surrogates at the offshore site at 16.6m depth as a function of measured wave heights.....	61
Figure 37. Comparison of modeled probability density function for UXO migration (a) versus the measured probability density function (b) for all surrogates at the PMRF test sites, 13 February – 27 June 2007.....	64
Figure 38. Comparing probability density functions for UXO burial of all surrogates during the PMRF demonstration: modeled (a) versus measured (b). ....	66
Figure 39. Hatteras and Ocracoke littoral cells along the outer banks of North Carolina.....	71
Figure 40. Critical mass cross-section (a), volume (b) and thickness vs. distance (c). ....	72
Figure 41. Regional bathymetry for littoral cell and refraction/diffraction analysis. ....	74
Figure 42. Charts of FRF coastal area with locations of wave measurement and other instrumentation. ....	75
Figure 43. Refraction/diffraction pattern for storm of 25 October 2005. ....	77
Figure 44. Refraction/diffraction pattern for storm of 16 September 2005.....	78
Figure 45. Wave data during Rounds 1-4 UXO mobility demonstration at FRF Duck, NC.....	79
Figure 46. Beach profile variation during UXO demonstration, FRF Duck, NC, 28 June – 2 September 2005. ....	81



Figure 47. Beach profile variation during UXO demonstration FRF, Duck, NC, 28 June 2005 – 22 February 2006. ....	82
Figure 48. Grain size distribution of sediment for FRF Duck, #B6-S1, 1 September 2005. ....	83
Figure 49. Simulation of vortex and scour field from a Mode 1 simulation of the 5"/38 UXO surrogate. ....	85
Figure 50. Details of lay-down pattern of UXO fields at the FRF site. ....	87
Figure 51. Three dimensional rendering of UXO deployment at FRF Duck, NC, June 2005. ...	88
Figure 52. Schematic of acoustic directional ranging technique for locating position of UXO surrogates during the FRF experiment. ....	89
Figure 53. MM simulation of migration and burial sequence of 5"/38 surrogate #3, Inshore Group, Round 1, FRF Duck, 22-27 June 2005. ....	90
Figure 54. MM simulation of migration and burial sequence of 5"/38 surrogate #11, Offshore Group, Round 1, FRF Duck, 22-27 June 2005. ....	91
Figure 55. MM simulation of migration and burial sequence of 5"/38 surrogate #3, Inshore Group, Round 2, FRF Duck, 27 June – 12 August 2005. ....	91
Figure 56. MM simulation of migration and burial sequence of 5"/38 surrogate #11, Offshore Group, Round 2, FRF Duck, 27 June – 12 August 2005. ....	92
Figure 57. MM simulation of migration and burial sequence of 5"/38 surrogate #3, Inshore Group, Round 3, FRF Duck, 12 August – 20 October 2005. ....	92
Figure 58. MM simulation of migration and burial sequence of 5"/38 surrogate #11, Offshore Group, Round 3, FRF Duck, 12 August – 20 October 2005. ....	93
Figure 59. MM simulation of migration and burial sequence of 5"/38 surrogate #3, Inshore Group, Round 4, FRF Duck, 20 October 2005 – 16 February 2006. ....	93
Figure 60. MM simulation of migration and burial sequence of 5"/38 surrogate #11, Offshore Group, Round 4, FRF Duck, 20 October 2005 – 16 February 2006. ....	94
Figure 61. Predicted vs. measured UXO migration in Inshore Field, FRF Duck, NC, Rounds 1-4, 22 June 2005 – 16 February 2006. ....	98
Figure 62. Predicted vs. measured UXO migration in Offshore Field, FRF Duck, NC, Rounds 1-4, 22 June 2005 – 16 February 2006. ....	98
Figure 63. Predictive skill for all surrogate movement, Rounds 1-4, FRF Duck, NC. ....	100
Figure 64. MM simulation of migration and burial sequence of 5"/38 UXO surrogate #18 in Inshore Group, during Rounds 5-6 at FRF Duck, NC, 16 February – 3 August 2006. ....	101
Figure 65. MM simulation of migration and burial sequence of 5"/38 UXO surrogate #23 in Offshore Group, during Rounds 5-6 at FRF Duck, NC, 16 February – 3 August 2006. ....	101
Figure 66. Predictive skill for surrogate burial, Rounds 1-4, FRF Duck, NC; (a) Measured probability density function versus (b) predicted probability density function. ....	102

Figure 67. Extreme case simulation of migration trajectory for 5” naval projectile during storm series, 17 Nov - 4 Dec 2003, Pacific Beach, WA: Hmax = 20.3 ft, net migration 664 ft.....	111
Figure 68. Mare Island Naval Shipyard UXO remediation area comparison.....	120
Figure 69. Vieques range UXO remediation area comparison. ....	121
Figure 70. Kaho’olawe Island UXO remediation area comparison.....	121
Figure 71. Computer configuration.....	123

## **List of Tables**

Table 1. UXO Site Coastal Classifications.....	14
Table 2. UXO Mobility Model Validation Program Objectives.....	18
Table 3. Potential UXO Sites.....	23
Table 4. UXO Mobility Model Input Parameters. ....	32
Table 5. UXO Mobility Model Validation Performance Criteria.....	107
Table 6. Performance confirmation methods.....	108
Table 7. UXO Mobility Model program cost summary. ....	114
Table 8. Nominal cost of Mode 1 screening analysis of a single UXO site. ....	116
Table 9. Estimated cost of Mode 2 Detailed Analysis.....	117
Table 10. Mode 3 Enhanced Analysis cost estimate.....	118

## **Acknowledgements**

The UXO Mobility Model Demonstration/Validation program was funded by the Environmental Security Technology Certification Program (ESTCP). It was conducted by the Naval Facilities Engineering Command Engineering Service Center (NAVFAC ESC), with support from Sound & Sea Technology, Inc. (SST). Ms. Barbara Sugiyama and Ms. Alexandra DeVisser, with NAVFAC ESC, were the Co-Principal Investigators for this effort. The SST program was lead by Mr. Jeffrey Wilson. The UXO Mobility Model was developed by Dr. Scott Jenkins and Mr. Joe Wasyl of Scott A. Jenkins Consulting. The Model was tested and evaluated by Mr. Dennis Garrood, Mrs. Chanda Daly, and Mr. Eugene Keam of SST. The field work was directed by Mr. William Daly and Mr. Ian McKissick of SST. On-site field demonstration support was provided by Mr. Carl Miller and the staff of the U.S. Army Corps of Engineers (USACE) Field Research Facility (FRF) at Duck, NC. The supporting human Interaction Model (IM) that evaluates probability of human encounters with UXO was developed by Mr. Jeffrey Wilson of SST.

The original UXO Mobility Model was developed under the Chief of Naval Operation's (CNO) Navy Environmental Sustainability Development to Integration (NESDI) program. The NESDI program is managed for CNO-N45 by the Naval Facilities Engineering Command (NAVFAC). The model upgrades and the field demonstration and validation efforts were funded by the Environmental Security Technology Certification Program (ESTCP). This report was prepared by the combined NAVFAC ESC/SST staff.

## Executive Summary

The objective of the ESTCP UXO Mobility Model (MM) validation program was to expand and validate the MM for the most common coastal conditions in which UXO are found. The program first expanded the capabilities of the basic vortex-lattice based model (VORTEX) previously developed by the Navy for mine modeling applications and then validated the MM by two instrumented field tests, one in each of the most common coastal environment types (Trailing Edge and Biogenic Reef). The ESTCP field demonstration at the U.S. Army Corps of Engineers (USACE) Field Research Facility (FRF) Duck, NC, extended over a period of two years. The field demonstration at the Pacific Missile Range Facility (PMRF), Kauai, HI, was in place four months (i.e., one winter season). As with the previous short-term Navy tests, the MM correctly predicted all the basic behaviors of the demonstration surrogates. Only small adjustments of parameters (a few percent) were required to calibrate the MM to match the observed movements. The skill factor for migration at FRF was calculated at  $R_z = 0.87$  and  $R_h = 0.93$  for burial. The skill factor for migration,  $R_z$ , at PMRF was calculated at  $R_z = 0.88$  and  $R_h = 0.90$  for burial. For modeling of coastal processes and mine burial prediction in particular, any skill factor in excess of 0.8 is considered to be a good result.

The unusually mild weather at FRF Duck (hurricane activity was absent over the two year period), and the limited number of acceptable sites for the field demonstration in Hawaii (ideally, meandering awa sand channels), prevented the inert surrogates from encountering any “extreme” weather. There was no large-scale movement of the surrogates onto the nearby beaches or out of the demonstration area. However, the several meters of movement observed at FRF Duck was caused by occasional episodes of unburial by seasonal events, which was correctly predicted by the MM. The fact that the surrogates were actually protected by the awa channel in Hawaii, rather than being exposed to accelerated flow, was also behavior that was correctly modeled once detailed Light Detection and Ranging (LIDAR) bathymetry data were available to support the detailed Mode 3 analysis.

The MM is calibrated for the most common coastal environments; it can be used with either default environmental conditions, or with site-specific data inputs for a more accurate prediction of overall probability of movement. The MM software was run successfully on standard office computers by several contractor and government personnel. A User’s Manual was also prepared to describe the data flows, module run sequence, and module file dependencies.

SST also adapted the existing Navy interaction model that predicts interaction of fishing gear with seafloor cables to produce a human Interaction Model (IM). That IM predicts the probability of human encounters with UXO in a variety of activities (e.g., fishing, dredging, beachcombing, etc.). An Application Guidance Document is being developed to guide users through the overall process of evaluating risk of human interaction with UXO at waterfront sites, using both the IM and the MM. An Example Applications Analysis using field data from the

Lake Erie Impact Range (Camp Perry, OH) is being conducted to further refine the procedures for utilizing the combined IM/MM tools.

The operational costs of using the MM vary from \$100,000 for a Mode 1 “desktop” analysis to approximately \$1,000,000 for a detailed analysis of a large site, which would include bathymetric surveys, UXO distribution baseline surveys, etc. The primary cost driver at any level of analysis is the acquisition of site environmental data (i.e., waves, currents, seafloor sediments, and initial UXO distributions), and the conversion of those data into input tables that are consistent with the MM Fortran code.

## **1.0 INTRODUCTION**

This report is the final in a series documenting the Environmental Security Technology Certification Program (ESTCP) Unexploded Ordnance (UXO) Mobility Model (MM) demonstration. The immediate objective of the ESTCP UXO Mobility Model demonstration project was to demonstrate and validate the Navy-developed MM for two of the most important coastal classifications – Trailing Edge (east coast of the continental United States) and Biogenic Reef (typical of tropical island coastlines). The Trailing Edge environment typically exhibits a very wide, shallow continental shelf area with heavy cover of silicon-based sands and sediments. Biogenic reefs are typically characterized by more irregular seafloor shapes that are crossed by channels with limited cover of carbonate sands.

The ESTCP MM field demonstration program was comprised of two major field demonstrations that are outlined in the Demonstration Plan [1] and documented in detail in final field demonstration reports [2] and [3]. The fundamental demonstration method was to place a series of inert surrogate 5”/38 rounds at known locations off the coast and track their movement using acoustic pingers or metal detectors and diver tracking systems, while also recording the local current and wave conditions. The observed movement was then compared to the MM predictions for movement under those particular meteorological/oceanographic conditions. Using the data from the field demonstrations, the MM was first calibrated and then validated.

The first field demonstration – for a Trailing Edge coast – was conducted at the U.S. Army Corps Of Engineers (USACE) Engineering, Research & Development Center (ERDC), Field Research Facility (FRF), Duck, North Carolina. The demonstration was installed on 22 June 2005. Data on surrogate locations were collected at various times over a 22 to 34 month period. Half of the surrogate UXO demonstration items deployed were then recovered in April 2007. Weather, FRF operating schedule, and equipment difficulties precluded recovering the few remaining shallow water items until late FY08. The demonstration was documented in a final field test report [2].

The second ESTCP UXO field demonstration – for a Biogenic Reef site – was conducted off the coast of the Pacific Missile Range Facility (PMRF) on the southwestern coast of Kauai, Hawaii. The demonstration was installed 22 February 2007 and then completed with the test items recovered on 27 June 2007. The PMRF demonstration is documented in a final field test report as well [3].

Both tests were fully successful in that all the required data were obtained and the behavior of the test items matched the predictions from the MM closely enough to allow minor calibration and validation of the MM for those coastal environments.

### **1.2 1.1 Background**

Sustainable range management and readiness are vital national security interests, yet are subject to increasingly restrictive regulatory oversight and public concern for safety. In an effort to

address these concerns, the Navy through its Navy Environmental Sustainability Development to Integration (NESDI) Program funded a program to assess the environmental effects of underwater unexploded ordnance (UXO). A site conceptual model (SCM) was developed under this program and is included as Figure 1. This UXO Mobility Model program effort appears on the lower left side of the block diagram. After evaluating the SCM against existing scientific data and models, various data gaps were identified. One of these data gaps was the inability to predict the mobility and burial of UXO underwater. To meet this need, the Naval Facilities Engineering Command Engineering Service Center (NAVFAC ESC) initiated a project to modify the existing Vortex Lattice model (VORTEX), which is used to predict mine mobility and burial; the new software is called the UXO Mobility Model (MM). Because of the differences in size, shape, and weight from mines, UXO exhibit both variable responses to ambient coastal dynamics and diverse modes of mobility. The mine-movement model was modified to predict UXO mobility and burial in the underwater environment.

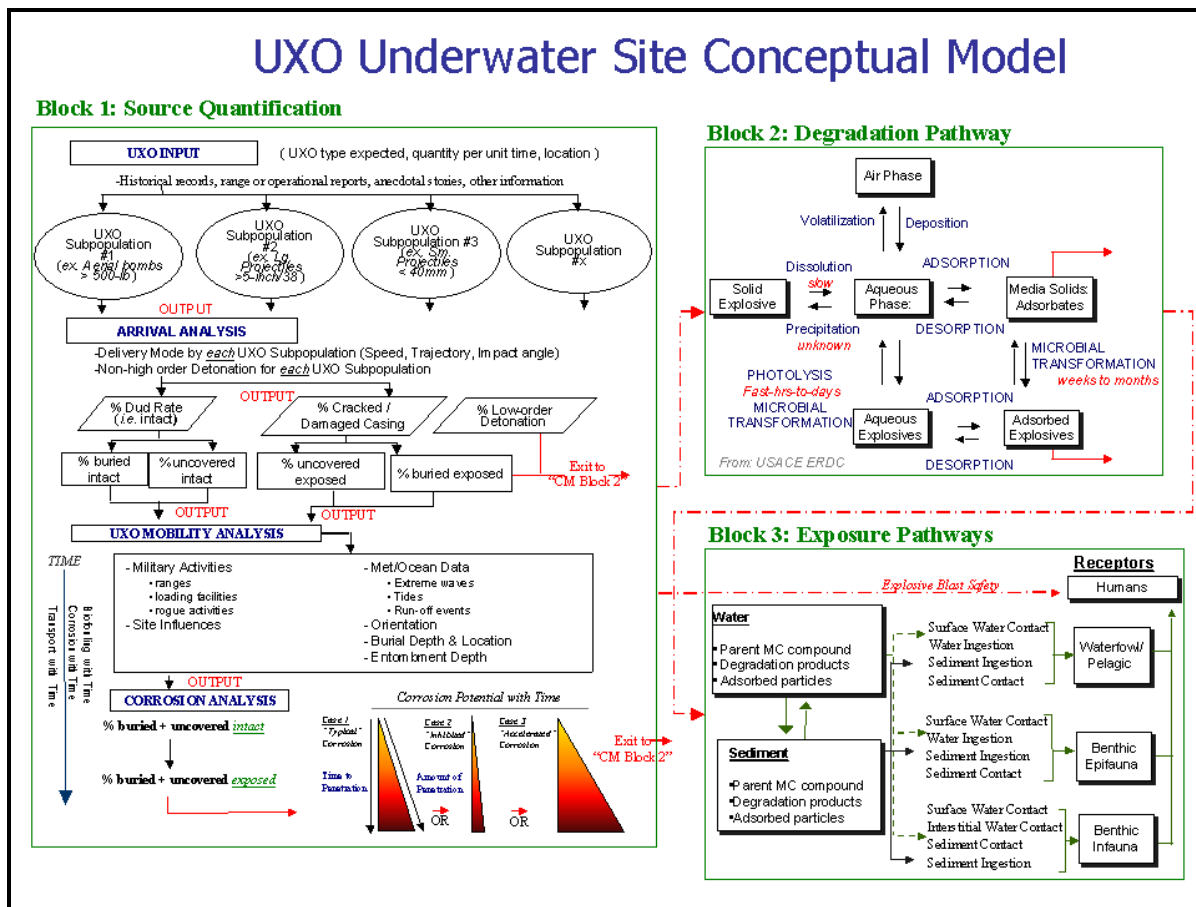


**Figure 1. Site Conceptual Model for UXO showing the UXO Mobility Model Analysis as part of site quantification.**



Figure 2 illustrates the model of the near-field flow over a partially buried UXO (5"/38 round) and the scour associated with the flow, while Figure 3 shows the various scenarios for UXO burial, unburial, movement and re-burial.

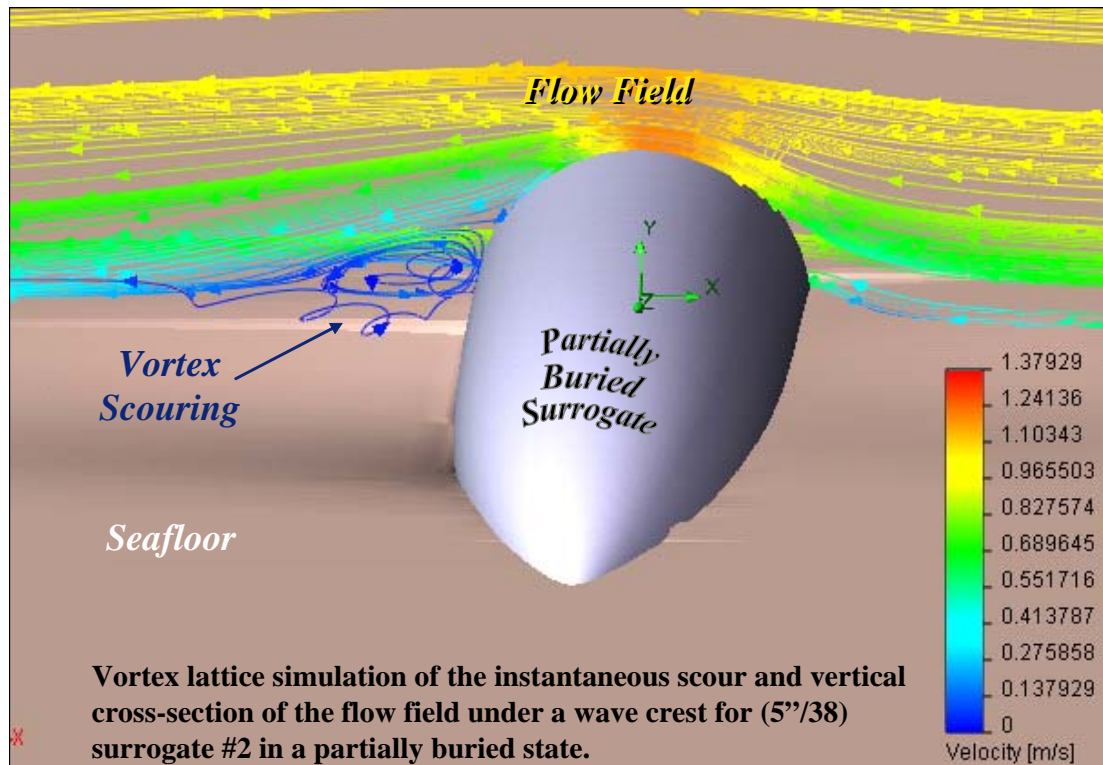


**Figure 2. UXO Mobility Model of flow and scour over a 5"/38 projectile surrogate.**

By using the MM, it is possible to predict the fate of UXO over the broad range of coastal diversity where UXO are known to exist. That information can be used as part of a comprehensive munitions response program. As a supplement to the MM development and validation program, SST and NAVFAC ESC staff adapted existing Navy models of the interaction of bottom fishing gear with seafloor cables to provide estimates of the probability of human interaction with seafloor UXO. Figure 4 outlines the general process for using the IM and MM.

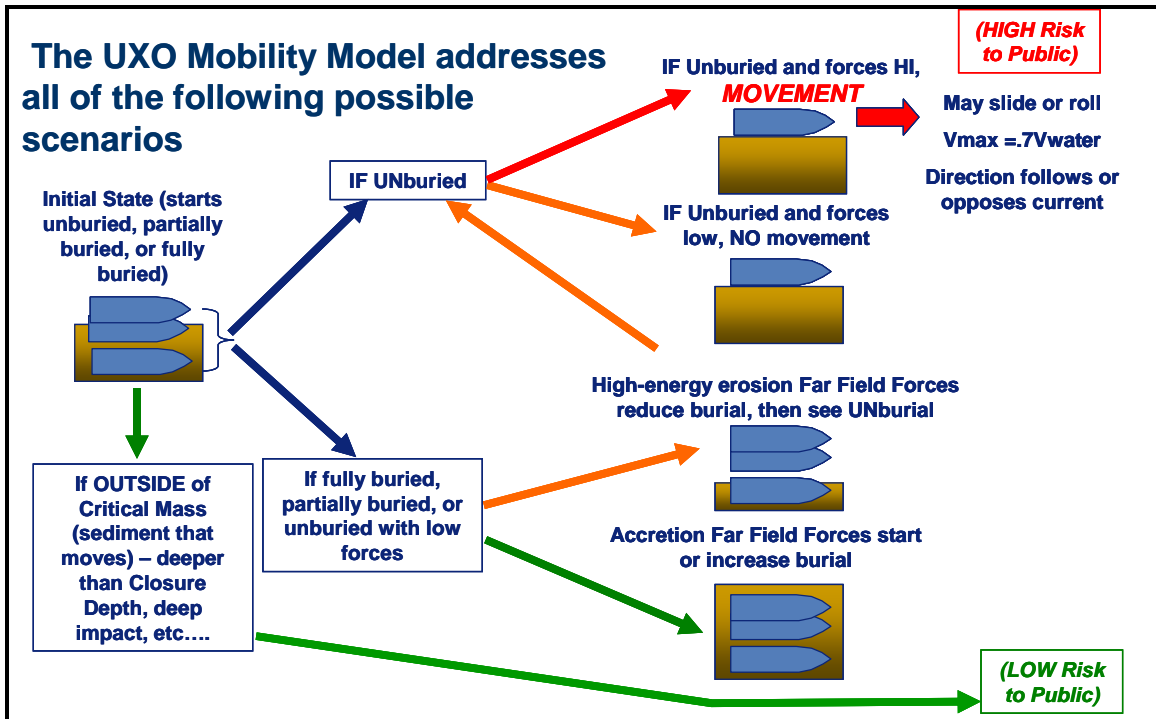


Figure 3. Possible UXO movement scenarios.

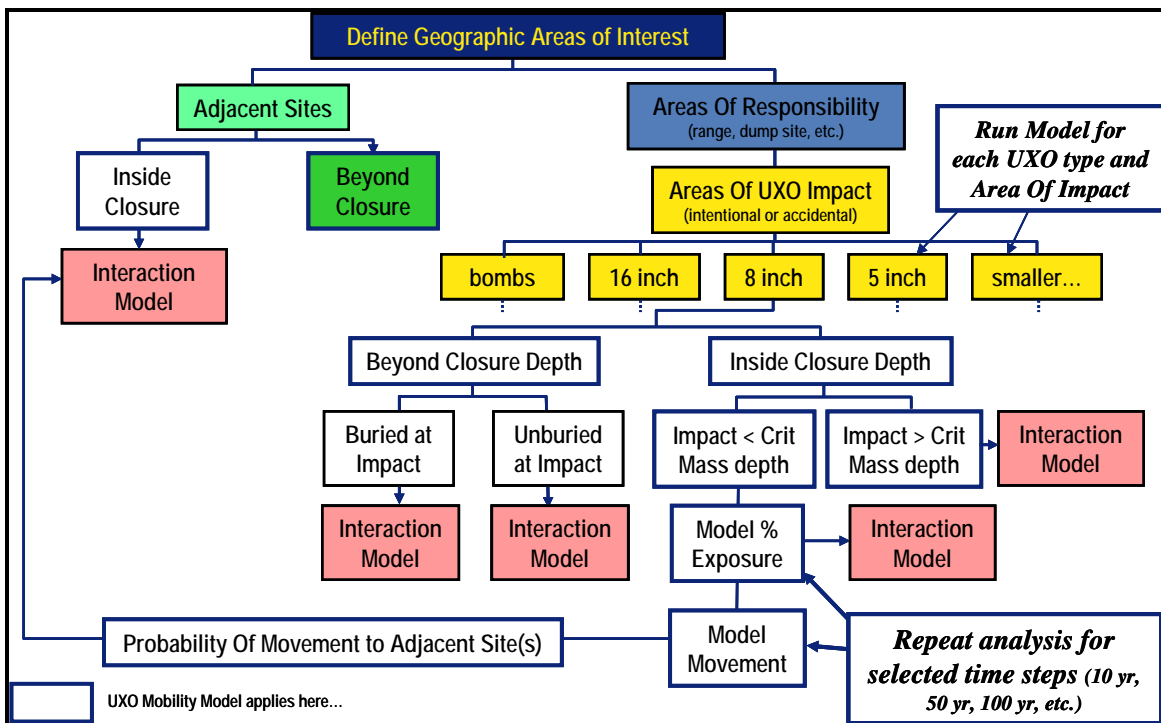


Figure 4. Overall process for estimating risk of human interaction with underwater UXO using the UXO Mobility Model and Interaction Model.

Graphical Information System (GIS) software is used to display the analysis of (a) areas of risk of human interaction with existing UXO (based on frequency of exposure), and (b) probability of UXO migration to adjacent areas that did not initially have UXO. Identifying the areas and entombment depths likely to contain UXO, also reduces costs associated with fieldwork focused on physically locating or clearing UXO items. The ultimate goal is to include the UXO mobility and burial model output data in a risk evaluation model similar specifically configured to support munitions response programs.

A preliminary search of significant Navy coastal UXO sites identified 23 locations in the United States in which underwater UXO are highly likely to exist. Using the generic coastal classification system incorporated in the MM, the sites were categorized with respect to the influence of tectonic plate movement on coastal evolution [4]. The sites can be assigned to generic classes of open ocean coastlines characterized by shelf depths, slopes, bottom materials, and dynamic wave environments. Four coastal categories are augmented with sub-category designations: collision (U.S. West Coast), trailing edge (East Coast), biogenic reef (Hawaii), and marginal seas (i.e., exposed coastlines and embayments). The MM is used to predict UXO exposure, mobility, and burial with respect to ordnance type and location (i.e., sediment characteristics or coastal classification and local waves/currents) for various marine environments.

The NESDI program supported the MM software development and a limited validation test at a single collision coastal site adjacent to Mugu Beach [5], as well as a series of Measurement Method Field Tests (MMFT 1 and 2) on the coast of Ocean Shores, Washington, in September 2004 and May 2005 [6].

The Mugu Drifter Test (MDT) was run with only small-diameter UXO (i.e., inert 20mm rounds and surrogates). This location was representative of UXO sites belonging to the collision coastline sub-category, one of the eight coastal sub-categories given in the Geomorphic Coastal Classification system [4]. Data from this test were used to validate the expected movement of small UXO in the large Santa Barbara littoral cell, a large open coastal movement area which tends to move small UXO offshore in the same manner that sand moves away from shore.

The MMFT at Ocean Shores used only larger UXO (i.e., 5"/38 inert and surrogate rounds) since it was a short-term test intended primarily to validate the effectiveness of two measurement methods for tracking UXO movement (i.e., physical tethers and acoustic pingers). The test also provided a calibration for the part of the MM that addresses movement in the high-energy breaking surf zone on a collision coastal beach.

The Navy program supported the MM development and allowed for short term, surf-zone validation for just the collision coastal type to be completed. To be useful to DoD planners, the MM needed to be validated for the remaining major coastal types. The data acquired from such validations now enables users to operate the MM either with very limited site data (Mode 1, coastal classification only) or with various levels of site-specific data inputs (Mode 2 or Mode 3).

Choosing one of the three modes also depends on the user's desire to make site-specific adaptations to the MM's configuration.

### 1.3 1.2 Objectives of the Demonstration

The primary objectives of the demonstration are listed below:

- Calibrate and validate the MM for the two most common geomorphic coastal environments in which DoD UXO are known to exist (i.e., Trailing Edge/east coast of continental United States and Biogenic Reef/tropical islands). Limited MM validation was already accomplished for the Collision Coastal environment (west coast of continental United States).
- Perform the calibration and validation steps by matching observed migration patterns of instrumented, inert surrogate UXO allowed to move freely under the influence of the local seafloor conditions in the candidate environments against the movement patterns predicted by the MM.
- Provide potential users a validated process to assist in the overall evaluation of risks associated with UXO at DoD sites. By providing credible statistical predictions of UXO movement (or non-movement), reduce costs and improve the quality of remediation.

### 1.4 1.3 Regulatory Drivers

The effort reported herein addresses the following DoD requirements:

**Navy requirements:** 1.I.2.b *Improved Marine Sediment/Dredge Spoil Remediation and Decontamination*, 1.I.1.g *Improved Methods for Removal of Unexploded Ordnance (UXO)*, and 1.III.2.n *Improved Characterization and Monitoring Techniques for Sediments*;

**Army requirements:** A(1.6.a) *Unexploded Ordnance (UXO) Screening, Detection and Discrimination*, and A(1.6.b) *Soil/Sediment Unexploded Ordnance (UXO) Neutralization/Removal/Remediation*.

These requirements imply a need for a basic ability to know where UXO is located throughout its life cycle. Even the most optimistic predictions of technology for directly measuring UXO locations through on-site surveys lead to extremely high costs, both because of the amount of area and volume to be surveyed and the considerable evidence that the surveys would have to be repeated frequently to be of value. Therefore, a model to predict movement (the MM) is essential to any monitoring of UXO and assessment of environmental or explosive safety.

### 1.5 1.4 Stakeholder/End-User Issues

The demonstration program already addressed various stakeholder or end-user decision-making factors concerning the technology.

As a supplement to the formal documentation of the ESTCP program, the team prepared an Applications Guidance Document (AGD) [7]. The AGD is the type of document the ESTCP guide refers to as a “decision support tool,” a top-level guide to using the MM in the context of comprehensive munitions response efforts. The AGD illustrates how the MM and IM can impact major decisions concerning UXO, such as determining which part of the population can safely be considered immobile, which can be considered fully entombed, and which are at risk of movement into areas of public interaction. The MM also aids planning for remediation by providing data on, for example, how long after a survey will UXO remain where they are found and what areas will stay free of UXO after remediation.

Before the MM validation was even complete, NAVFAC ESC and SST already received several inquiries concerning possible application of the MM to near-term problems:

- a. Representatives of the Army Secretariat for the Environment. The Army Secretariat is interested in using the MM to assess the stability of a large UXO dumping ground located in 30 to 150 feet of water off Waianae Sewer Outfall (Oahu, HI).
- b. Representatives of the City Of Hampton Roads, VA (Fort Monroe). The Army is transferring Fort Monroe to the city and the support contractor is investigating the risks from the UXO that have been fired offshore into Chesapeake Bay from the time of the Civil War until after WWII.
- c. USACOE, Buffalo District. The Army Corps is interested in using the MM to predict UXO movements in Lake Erie offshore off Camp Perry and the Toussaint River. There is a long and active history of thousands of UXO rounds moving onto the beach and into dredge areas. The Army postulates that the final causal mechanism responsible for movement ashore is ice rafting, but is unable to determine how the UXO migrate from their original location to the very shallow water affected by the shore ice of Lake Erie.
- d. USACOE New Orleans. The Army Corps seeks to conduct a borrow operation in sediment near a former firing range in Lake Borgne; consequently, it is necessary to determine the probability of UXO migrating to that borrow site.
- e. NAVFAC Engineering Field Division Atlantic. In charge of Munitions Response for the offshore areas of Vieques, NAVFAC would like to use the MM to assist their planning efforts.

The Lake Erie application is being addressed by NFESC and SST as an “Example Application Analysis” [8]. The Lake Erie site was selected as the Example Applications Analysis because of the excellent site data already there and the variety of conditions to be analyzed. That example application, plus the interactions with the other inquiring agencies, has identified several specific applications not previously considered – but which are all supportable by the MM and risk

evaluation process. To date, none of the operational UXO site managers have funded application of the MM and risk analysis process, pending release of the final ESTCP documentation of the MM validation.

## **2.0 TECHNOLOGY**

### **1.6 2.1 Technology description**

The Vortex Lattice UXO Mobility Model (MM) is a 3-dimensional, time-stepped, process-based model for the prediction of exhumation, migration, and subsequent burial of UXO by general bed erosion and local vortex scour. Details of the MM and the most recent Fortran code are provided in Appendix B.

The MM is applicable to a wide variety of coastal, riverine, or estuarine conditions, from the high water line to beyond the closure depth. The MM was validated for the three major coastal classifications (i.e., Collision Coastal/West Coast of CONUS, Trailing Edge/East Coast of CONUS, and Biogenic Reef /Hawaii). The MM was validated using surrogate 5"/38 projectiles, a common UXO size that behaves similar to larger, "cobble-sized" seafloor objects. Limited portions of the validation also included 20 mm surrogates, which behave more like small-grain sediment, such as sand. The burial and sediment transport modules of the original Vortex Lattice Model are already validated for larger 500-lb bomb shapes.

### **1.7 2.2 Technology development**

The MM is adapted from a modification of the Vortex Lattice UXO Scour/Burial Model. For each time step, the model produces a 3-dimensional image of the UXO and the adjacent seabed. The model accepts forcing function inputs from either measurements or forecasts of surface gravity waves, coastal currents, and river discharge or precipitation. The computational methodology for the migration/burial processes is based on the vortex lattice method, which calculates the vortex system shed by the UXO of arbitrary shape. The method of images is used to resolve the ground effects of the vortex system over the seabed based on a formulation derived from Peace and Riley [9]. The induced velocity of the vortex system acting on the seabed causes both bedload and suspended load scour treated by the ideal granular sediment transport equations of Bagnold [10], updated by Bailard and Inman [11]. The reaction forces to the vortex induced velocity field cause migration of the UXO once the moment balance is exceeded. Migration, burial, or exposure by general bed accretion or erosion is accounted for by equilibrium profile changes after Inman et al. [12] and by accretion/erosion waves as formulated by Inman and Bagnold [10] and Inman [13].

Several important modifications to the previous basic VORTEX lattice model were made:

- Algorithms for calculating the near-field effects on UXO were modified to address the complex tapered shapes.

- The overall algorithm for calculating the far-field effects that drive sediment movement was modified. The sediment movement determines when the UXO is and is not buried, which has a major impact on overall UXO migration. The algorithm for calculating the total shape and size of the critical volume of sediment that is active along a given beach was re-created using thermodynamic balance as the basis rather than the past methods based on Dean's models.
- To support the critical volume analysis, an improved method of calculating the closure depth (the depth beyond which there is no net movement of sediment) was developed and incorporated in the MM.

The general flow of the MM, shown in Figure 5, shows the primary modules highlighted in grey.

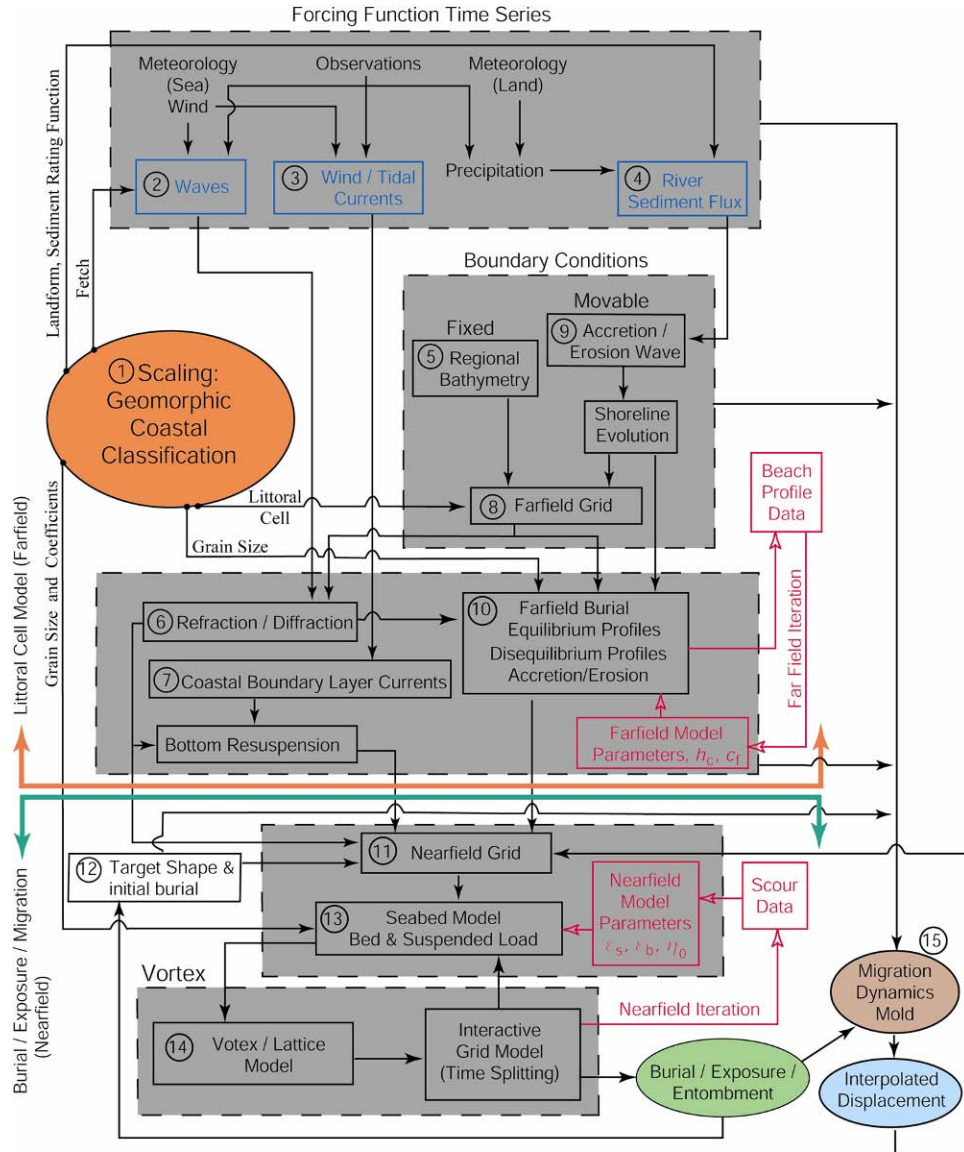


**Figure 5. UXO Mobility Model flow diagram.**

### **2.2.1 Processes Represented and Applicable Coastal Regions**

The MM is a process-based model that incorporates regional (farfield) processes and also local (nearfield) processes acting within several diameters of the UXO. Farfield processes, those that alter the seabed elevation over length scales that are comparatively large with respect to the size of an individual UXO round, usually occur in response to general erosion or accretion. Nearfield processes are due to the flow disturbance caused by the UXO and affect the seabed elevation by local scour as well as induce hydrodynamic forces that cause the UXO to move.

The general relationship between farfield and nearfield processes, depicted in Figure 6, shows how ocean waves can influence the movement of sediment and exposed UXO, thereby resulting in a critical mass of active sediment. Furthermore, the beach profile shown in Figure 7 illustrates beach slope migration either shoreward or seaward, depending upon the season of the year, which, in turn affects the thickness of the critical mass envelope, or depth of permanent entombment. The close-up view in Figure 8 illustrates the forces that must be overcome in order to exceed the threshold of migration and cause UXO movement.

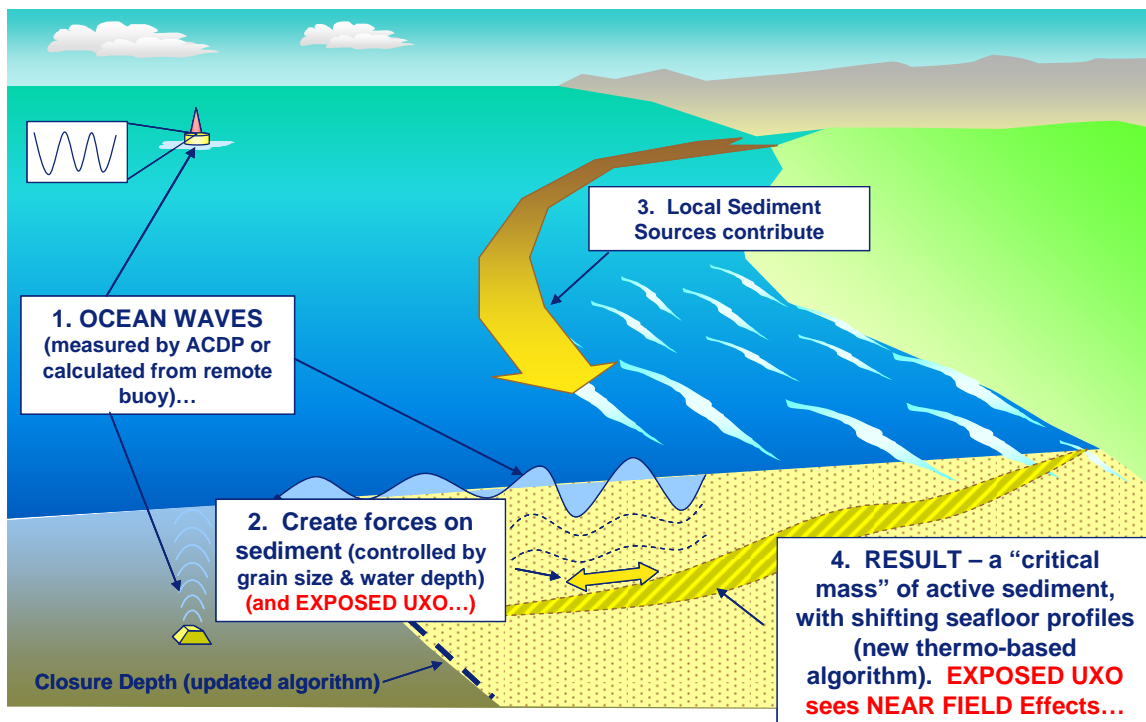




Figure 6. Farfield and nearfield processes for the UXO MM.

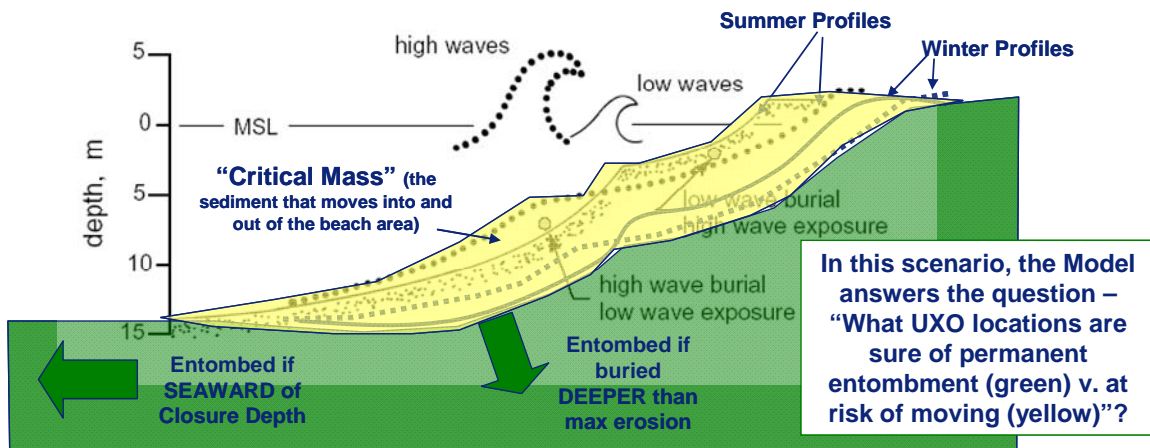
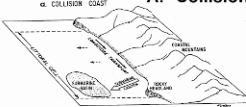
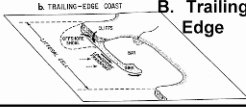
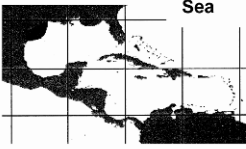
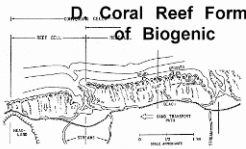


Figure 7. UXO entombment versus nearshore location and critical mass of sediment.



Farfield processes are controlled by the balance between the amount of sediment entering the farfield and the amount leaving. This balance, known as the sediment budget, requires the identification of sediment sources and sinks, which will vary with the type of coastline. Some basic types of coastlines have been identified. The Geomorphic Coastal Classification module in Figure 5 (highlighted in red) is used to select the relative scaling and assigns the sediment sources and sinks to which a particular UXO site belongs. The classification includes three general tectonic types of coasts with their morphologic equivalents and two types associated with latitudinal extremes: 1) collision coasts with narrow shelves and steep coastal topography resulting from collisions between two or more tectonic plates, 2) trailing edge coasts that are on the stable, passive margins of continents with broad shelves and low inland relief, 3) marginal sea coasts that are semi-enclosed by island arcs and thereby fetch limited, and, 4) biogenic coasts that are formed by fringing coral reefs or mangroves. Figure 9 provides schematic examples of the leading order morphology of these coastal types (“geomorphic type”), their characteristics, and representative sites for each.

Geomorphic Type	Boundary Conditions					Model Parameters		
	Morphology (Example)	Sediment Source	Sediment Sink	Closure Depth	Littoral Cell Dimensions	Grid Cell	Grain Size	Bed Roughness, $\eta_0$
 <b>A. Collision</b>	Narrow-Shelf Mountainous Coastal Bluffs (California)	Rivers & Bluff Erosion	Submarine Canyons	15 - 18 m	Longshore: 50 km Cross Shore: 1 - 5 km	Farfield: 70 - 90 m Nearfield: 1 - 4 cm	Beach: 0.2 - 0.3 mm Shelf: 0.06 - 0.10 mm	0.5 - 3 cm
 <b>B. Trailing Edge</b>	Wide-Shelf Plains (Duck, NC)	Headlands & Shelves	Roll-Over Shoals Spit-Extension	10 - 13 m	Longshore: 100 km Cross Shore: 30 - 50 km	Farfield: 40 - 80 m Nearfield: 2 - 7 cm	Beach: 0.2 - 0.4 mm Shelf: 0.06 - 0.15 mm	0.8 - 5 cm
 <b>C. Marginal Sea</b>	a) Narrow-Shelf Mountainous (Korea) b) Wide-Shelf Plains (Corpus Christi) c) Deltaic tideless (Mississippi) d) Deltaic tidal (Bangladesh) Wide-Shelf	Rivers & Deltas	a) Canyons b) Beaches & Barriers c) Delta & Shelf d) Delta Islands, flats, canyons	Narrow shelf: 7 - 10 m Wide shelf: 4 - 7 m Delta: 3 m	Longshore: a) 5-10 km b) 100 km c) 5-200 km d) var Cross Shore: a) 1 - 5 km b) 50 km c) 20-80 km d) var	Farfield: 10 - 20 m Nearfield: 1 - 3 cm	Beach: 0.06 - 0.21 mm Shelf: 0.01 - 0.09 mm Delta: .005 - .05 mm	a-d) 0.1 - 1 cm d) sand waves
 <b>D. Coral Reef Form of Biogenic</b>	Coral Reef Island (Hawaii)	Carbonate Reef Material Volcanic Headlands	Pocket Beaches & Awa Channels to the Shelf	Reef Platform	Longshore: ~2 km Cross Shore: 0.5 km	Farfield: 100 - 150 m Nearfield: 1 - 20 cm	Beach: 0.2 - 0.4 mm Shelf: 0.03 - 0.1 mm	Reef Platform ~1 m Offshore 1 - 15 cm

**Figure 9. Geomorphic coastal classifications used in UXO Mobility Model (Mode 1).**

Although the relative importance of transport processes varies among coastal type, two processes are always important to UXO exhumation and burial. These are seasonal changes in the beach profile and fluxes of sediment into and out of the UXO environment by accretion/erosion waves.

The field demonstrations were conducted in Trailing Edge and Biogenic Reef environments because they represent a substantial fraction of all the sites of interest – and virtually all of the sites with high-energy waves where UXO movement likely occurs. Table 1 shows the percentage of UXO sites that are located in the various coastal classifications.

**Table 1. UXO Site Coastal Classifications.**

<b>Coastal Category</b>	<b>Coastline Sub-Category</b>	<b>Bay/Estuarine Sub-Category</b>	<b>Total</b>
Collision	17%	30%	48%
Trailing Edge	22%	9%	30%
Biogenic Carbonate	9%	4%	13%
Marginal Seas	9%	0%	9%

**Nearfield Processes: Migration, Scour, and Burial.** Nearfield processes occur over length scales on the order of the UXO dimensions and on time scales of a few seconds to hours, primarily governed by local hydrodynamic forces and scour mechanics arising from the disturbance which the UXO creates in the flow.

The UXO and adjacent seabed is subdivided into a set of panels (lattices). The vortex field induced by the UXO is constructed from an assemblage of horseshoe vortices, with a horseshoe vortex prescribed for each panel. This computational technique is known as the vortex lattice method and has been widely used in aerodynamics and naval architecture. The strength of the vortices is derived from the pressure change over each panel associated with the local wave and current velocity. The release of trailing vortex filaments from each panel causes scour of the neighboring seabed.

When viewed in any cross-wake plane, each pair of filaments induces a flow across the seabed that results in scour proportional to the cube of the vortex strength and inversely proportional to the cube of the sediment grain size. This sensitivity of scour to grain size selectively removes the finer grained fraction of the bed material and leaves behind the coarser grained fraction in the scour depression. The coarse material that remains in the scour hole armors the bed against further scour thereby slowing the rate of scour burial.

Scour burial is a shape dependent process that varies with the intensity of hydrodynamic forcing and with bed composition and slope. Because most UXO are bodies of revolution, the burial mechanism proceeds by a series of scour and roll events on a fine sand bottom, whereby the UXO successively scours a depression and then rolls into that depression. In contrast, a flat bottom mine-like objects (e.g., MANTA, ROCKAN, etc.) or UXO resting flat-side down bury by scour and slip sequences involving episodic shear failures (avalanches) of the slopes of the

scoured depression. During these shear failures, the UXO is in a state of sliding friction with the bed and is easily moved by the hydrodynamic forces of waves and currents.

Both of these mechanisms (scour and roll or scour and slip) may be arrested by large scale changes in the bed elevation due to either seasonal profile changes or influx of material by accretion/erosion waves. Both of these mechanisms (scour and roll, and scour and slip) involve movement of the UXO during the burial sequence. Over erosion-resistant beds, waves and currents may cause UXOs to migrate large distances before scour and burial arrests further UXO migration. During lower energy summer condition, sand moves onshore from the shorerise, shifting the bottom profile shoreward, exposing the UXOs and inducing migration. On muddy seabeds during storms, both the UXO and seabed may move as a unit.

### **2.2.2 User Requirements**

To conduct a complete analysis of the risk of human interaction, three basic user skill/experience sets are required:

The technical lead for the overall analysis must be an engineer whose technical background includes a familiarity with ocean processes and the general principles of computer modeling, as well as the general principles of data collection on the types and amounts of human activity in coastal areas. This lead engineer also needs to be experienced in basic project management and be a liaison with the site UXO manager as well. In order to conduct the entire risk analysis, the lead engineer must be able to use ESRI ArcGIS software and the Microsoft Excel spreadsheet program, and be familiar with the overall processes described in the AGD [7].

The lead oceanographer/coastal scientist must be skilled in locating the sources of environmental data (e.g., waves, currents, bottom types, etc.), acquiring those data sets for the time periods of interest, and formatting those data to serve as inputs to the MM. The lead scientist also needs a general understanding of coastal processes, basic hydrodynamics, and related ocean engineering technologies in order to assist in setting up the model inputs and understanding its outputs.

Finally, the MM itself needs to be run by a person skilled in the using basic Fortran programs for computer modeling purposes. The MM is a Fortran program than will run on a variety of professional-grade laptop or desktop computers, so the user must be capable of compiling and running Fortran programs.

Of course the above list of skills and abilities may be provided by various possible combinations of individuals. During various stages of the MM development effort, the analysis work was conducted by as few as two and as many as four to six persons.

The detailed requirements for software, computer hardware, and user skills are described in the User's Manual [14].

### **2.2.3 Previous Mobility Model Efforts**

The NESDI program originally supported efforts to adapt the mine warfare community's VORTEX model and develop the first UXO Mobility Model software. The Navy program also initiated a limited validation test at a single collision coastal site adjacent to Mugu Beach, CA, [5] and conducted a series of Measurement Method Field Tests (MMFT 1 and 2) on the coast of Ocean Shores, Washington, in September 2004 and May 2005 [6].

The Mugu Drifter Test (MDT) used only small-diameter UXO (20mm rounds and surrogates). It served as a proxy for UXO sites belonging to the collision coastline sub-category, one of the eight coastal sub-categories given in the Geomorphic Coastal Classification system [4]. MDT results were used to validate the expected movement of small UXO in a large open coastal movement area (the Santa Barbara cell), which tends to move small UXO offshore like sand.

The MMFT at Ocean Shores used only larger UXO (5"/38 inert and surrogate rounds). MMFT was a short-term test intended primarily to validate the effectiveness of two measurement methods for tracking UXO movement (e.g., physical tethers and acoustic pingers). The durations of the tests were brief, just one to three days each, but the overall test provided a calibration for the part of the MM that addresses the high-energy breaking surf zone, again on a collision coastal beach.

The Navy program supported MM development but completed short term, surf-zone validation for only one coastal type.

### **1.8 2.3 Advantages and Limitations of the Technology**

The major advantage of the MM is that it allows site managers to evaluate the risk of human interaction with UXO at their site and take only those remediation actions that are required. In many cases, the MM can define the limits of UXO mobility and substantially reduce the total area that would otherwise need to be covered in any UXO removal efforts – which saves a lot of money.

The primary limitations of the MM, as with most computer models, are the quantity and quality of the input data. In general, the MM output statistics are driven by the statistics of the following: (a) estimates of original UXO distributions (i.e., type, location, burial depth) and (b) physical oceanography data (i.e., waves, currents). Data for sediment type and local bathymetry are also critical to the MM accuracy, but these tend to be relatively static in time, and therefore more deterministic in nature. The MM does predict and account for changes in local bathymetry from the forcing functions (e.g., seasonal, sand waves, etc.).

To accommodate these variations in data quality, the MM can be run in three distinct Modes (1, 2, or 3). Mode 1 uses default data for the environment given only a general description of the UXO distribution, coastal classification, coarse bathymetry, and a limited set of wave data from distant measurement points; these pre-configured data are based on the coastal classification system described in Sec. 1. Modes 2 and 3 require additional data, up to the point of detailed

modeling of individual UXO items using full spatial sampling of the seafloor properties, *in situ* long-duration wave data sets, and high-resolution bathymetry or imagery (e.g., LIDAR, multi-beam backscatter, side scan sonar, etc.).

The primary factors affecting cost are the size of the area to be modeled, the complexity of the environment (e.g., bottom variability, variations in UXO distribution, etc.), the extent and variability of human activity, and the resultant costs of collecting input data (e.g., bathymetry surveys, UXO distribution surveys, fishing activity surveys, etc.). Costs can range from \$100,000 for a basic desktop Mode 1 analysis of a single site to approximately \$1,000,000 for a complex area.

### **3.0 PERFORMANCE OBJECTIVES**

The performance objectives shown in Table 2 provide the basis for evaluating the performance and costs of using the MM.

**Table 2. UXO Mobility Model Validation Program Objectives**

Performance Objective	Metric	Data Required	Success Criteria	Results
<b>Qualitative Performance Objectives</b>				
MM proves useable by engineers other than software creators.	Review by NAVFAC ESC – selected panel including Navy, Army, and support contractors concludes software is transferable to other users.	Results of attempted MM runs by users other than the software creators.	Users other than the original developers can run the MM software successfully.	Yes. Both NAVFAC ESC and SST staff have been able to run the MM software. There is still value to be gained from the MM developer (Scott A. Jenkins Consulting) as new applications arise.
MM provides credible prediction of movement in support of test planning, ops.	Predictions check against general engineering theory and observations at similar sites.	Graphic presentations of predicted and measured movements of UXO surrogates from both field demonstration sites.	Differences between predicted values and measurements show consistent pattern, and can be reduced to within 20% or less by calibration the MM.	At both the PMRF and FRF Duck sites the MM predictions generally agree with complex movements observed for multiple items. All surrogates remained within planned range of measurements.
<b>Quantitative Performance Objectives</b>				
Field Demonstration collects sufficient quality data to allow validation of MM	Tracking movement of surrogates with accuracy consistent with input data and MM computational resolution	Measured position of the surrogates v. time at the field tests (location and depth of burial)	> 50% of surrogates are tracked successfully at each site. Movements are measured within +/- 10%.	At Hawaii, 73% of the 168 possible data points in the 6 measurements were successful. 100% of the final 3 measurement sets were successful. Measurements were accurate within 1-2 m (<9% of range).
				At FRF Duck, 92% of 120 data points in the 5 main measurements were successful. Measurements were accurate within 1-2 m (<7% of range). Only a sampling of the 20mm was obtained – but no movement observed.
MM validation shows good match between predictions and measurements, with coefficients correctable to positive match.	Model skill factor (ability to correctly predict surrogate movements and burial)	Measured position of the surrogates vs. time at the field tests (location and depth of burial)	$R > 0.8$	MM validation by visual match to measurements is very good. For FRF Duck, $R_{\xi} = 0.87$ for movement and $R_h = 0.93$ for burial. For Hawaii, $R_{\xi} = 0.88$ for movement, $R_h = 0.90$ for burial.



### **1.9 3.1 Qualitative Assessment of Multi-User Capability**

It is important that the MM software be sufficiently user-friendly and robust that it can be used by technical staff other than those who created it. However, this is a specialized software application not intended for general non-technical public use. The code is written in Fortran (an industry standard for such computational software), but running the MM does require professional computer modeling experience. The formatting of the input data and interpretation of the results require the skills of an experienced ocean/coastal processes scientist or engineer.

The MM was beta tested by having the SST IT technician run the MM using only the guidance available in the Applications Guidance Document [7]. The MM also was run successfully on several different laptops, using two different Fortran compilers by NFESC ocean facilities staff and by other SST technical staff.

Given the specialized nature of the MM, it is recommended that the most cost-effective way to apply the MM will be for NAVFAC ESC and support contractors to remain the Center of Expertise in this area. This approach ensures MM continuity beyond the individual scientists and engineers who developed the software and yet does not incur the expense of refining the software to a more generalized, user-friendly format. This Center of Expertise will then be available to organizations seeking to use the software to evaluate an operational site. To date, NFESC has already received several such inquiries from U.S. Army, U.S. Navy, and private entities.

### **1.10 3.2 Qualitative Mobility Model Performance**

As each data set was obtained and reported from the FRF field demonstration, the results were compared against the initial predictions from the MM. The fact that movements were (a) large enough to be measured, (b) within the general range of movements initially predicted and (c) generally consistent with the unexpectedly low-energy wave motions at the site all confirmed that the MM predictions were likely going to be easy to calibrate.

The individual plots of surrogate movements showed that the deeper sites (lower energy) moved less than the shallow sites. The averages of the movements at the FRF tended to be along the shore rather than toward or away from it, which was consistent with the MM initial predictions.

In the PMRF tests, the movement was substantially less than predicted by the initial Mode 1 analysis. There was some concern after the first round of measurements that the MM would not be valid at this site. However, once the detailed LIDAR data were obtained and the complex features of the area were modeled at the Mode 3 level, the reduced flow field (low input) became clear and the resultant very small movements became logical and consistent.

### **1.11 3.3 Field Demonstrations Collect Sufficient Data**

It is very easy to create hundreds or even thousands of data points with the UXO MM simulations by modeling the given UXO type at various locations at a site, with various subsets of historical wave data inputs. In order to provide reasonable statistics from the field

demonstrations measurements it was necessary to have at least a 50 to 100 measured data points for the given UXO type (5"/38 round). It was anticipated that there would be at least 3 to 6 rounds of measurements during the tests, so a minimum of around 16 surrogates were required. Because it was expected that some of the surrogates would either be lost, have their acoustic beacons fail or otherwise not provide a full set of data, 24 surrogates were used at each field test site.

Also, it was necessary that the location measurements be accurate to within approximately 10% of the actual movement distance, or about 1 meter (whichever was larger). This level of accuracy is consistent with the expected error bounds on the basic environmental parameter measurements (e.g., sediment grain size, wave velocities, etc.).

The breadth of the data collection efforts during both of the field tests exceeded the requirements. While there are certainly other locations and conditions under which the MM could be further validated, the fact that not only these two field demonstrations but also both of the prior limited Navy field tests all required very minor calibration of the MM suggests that the basic fluid theory and mathematical modeling methods in the MM are very sound and could be extrapolated to other sites with confidence.

#### **1.12 3.4 Mobility Model Validation Successful**

When the predictions of the calibrated MM were compared to the measured UXO surrogate movements using the basic least-squares skill evaluations criterion, the following results were calculated: for FRF Duck,  $R_{\xi} = 0.87$  for movement and  $R_h = 0.93$  for burial, and for Hawaii,  $R_{\xi} = 0.88$  for movement,  $R_h = 0.90$  for burial. Note that any value greater than  $R=0.8$  is considered to be very good for ocean modeling, so these values are more than within the acceptable limits.

## **4.0 SITE DESCRIPTION**

The U.S. Army Corps of Engineers Engineering Research Division, Field Research Facility (FRF) is located along the Northern Outer Banks in Duck, NC (Figure 10). The area in which the demonstration took place is situated just north of the 1840 ft long pier (Figure 11).

The Pacific Missile Range Facility (PMRF), Kauai, Hawaii, site is located on the southwestern coast of Kauai, HI (Figure 12).



Figure 10. Duck, NC, is approximately 60 miles south of Norfolk, VA.

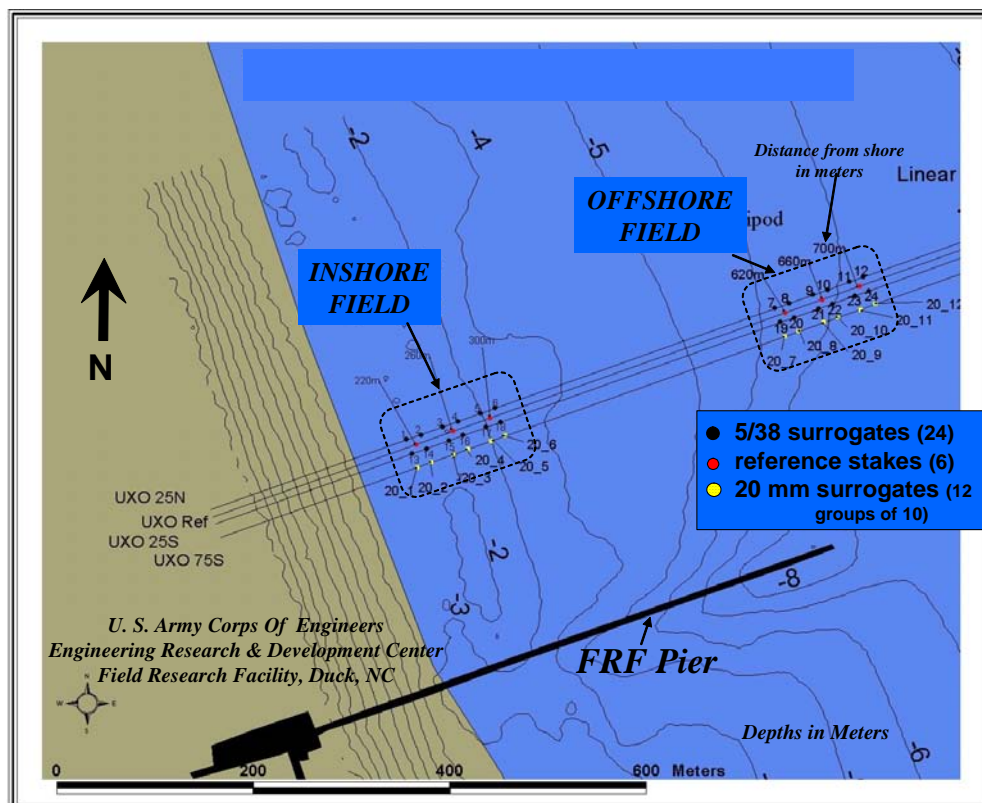
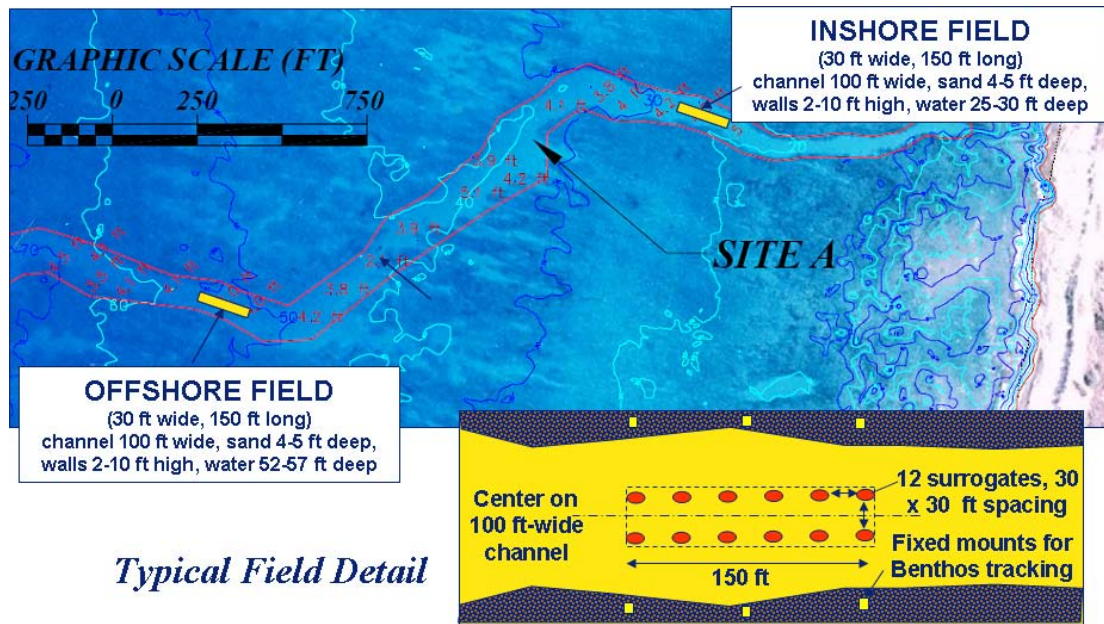


Figure 11. FRF Duck Field Demonstration configuration.



**Figure 12. PMRF Field Demonstration configuration.**

### 1.13 4.1 Site Selection

The following criteria were used to select a demonstration site:

- a. Representative of a major coastal classification. The two most common types of known UXO sites are the Trailing Edge (i.e., shallow coast, as in East Coast of CONUS), and Biogenic Reef.
- b. Controlled access. Areas with limited public access are favored in order to minimize disturbance.
- c. High frequency of high-energy weather events. Areas which experience frequent storms are conducive to measuring surrogate movement.
- d. Environmental permits. The ability to meet environmental permitting requirements is necessary.

The two sites for the UXO ESTCP demonstration/validation program were selected primarily because each represents a broad class of coastal environments in which underwater UXO is found. The initial phase of the Navy UXO Mobility Model program funded an extensive literature and web search, in addition to gathering information contained in reports by the U.S. Environmental Protection Agency (EPA) [15], Tucker [16], Jarrah [17], and the U.S. Army Engineering and Support Center (USAESCH) [18]. This effort identified the sites where underwater UXO are highly likely to exist; those sites are listed in Table 3.

Table 3 is predominantly comprised of Navy sites, though it is not all-inclusive. However, it is typical of the shallow and very shallow water regions necessary for establishing representative coastal scenarios for comprehensive computer modeling of subsurface UXO movement and

burial. This study assumed that ordnance at deeper depths (> 40 ft or the local closure depth, if greater) is permanently entombed or at least will not move. This is probably a reasonable assumption in the absence of oil tanker or other deep draft ship traffic, seabed dredging, marine construction activities – or extreme wave conditions. As weapons technology moves toward precision-guided munitions, the cost and complexity of each unit increases and a shift from bulk palletization to single weapon packaging has occurred. This change from ordinary bombs and large projectiles to sophisticated weapons correlates with a trend from Naval Ammunition Depots (NAD) to Naval Weapons Stations (NWS) and the unit cost translates to more cautious handling with fewer inadvertent losses.

**Table 3. Potential UXO Sites.**

**Coastal Ammunition Loading Sites**

NAD Indian Island, WA  
 NAD Seal Beach, CA  
 NAD Detachment Concord, CA  
 NAD Detachment North Island, CA  
 Ex-Naval Ship Yard Mare Island, CA  
 NWS Yorktown, VA  
 NWS Charleston, SC  
 NWS Mayport, FL  
 Ex-NAD, Jackson Park, WA (former NAD with continuing UXO problems)

**Coastal Live Firing Ranges**

San Clemente, Island, CA (heavy past usage and still active at reduced levels)  
 San Nicholas Island, CA (old gunnery range now used for missile testing)

**Formerly Used Live Firing Ranges**

Kaho’olawe, HI (heavily used naval gunnery, bombing, and ordnance test site)  
 Vieques Island, PR (heavily used naval gunnery, bombing and amphibious exercise site)  
 Culebra Island, PR (40 years of use as gunnery and bombing range)  
 Normans Island, MA (WW II gunnery and bombing)  
 Hingham Island, MA (WW II gunnery and bombing)  
 Panama Canal Zone (multiple formerly used defense sites)  
 Salton Sea Test Range, CA (former navy inland sea small caliber firing range)  
 Ex-Naval Station Adak, AK (extensive UXO of all types)

**Operational Bases with Potential Underwater UXO**

Marine Corps Base Hawaii, (Kaneohe)  
 NWS Dahlgren, VA  
 NS San Diego, CA  
 NAD Earle, NJ

Higher cost and less reliance on large caliber projectiles also translates into less “live firing” and a reduction in new UXO issues on the remaining “Operational Ranges.” Most of the underwater UXO on the firing ranges of concern in this effort is therefore older ordnance that has had ample time to move and bury (i.e., WWII through 1970s vintage on the “Formerly Used Live Firing Ranges” given in Table 3.

Combining the 23 potential UXO problem sites with their associated coastal category/sub-category designations yields the Potential UXO Site Priorities shown in Table 1. These priorities were used as an important criterion in the selection of test sites for the NESDI Research and Development effort. The Navy program tests that preceded the ESTCP program were used to calibrate the modified VORTEX model and collect supporting MM performance data for the Collision Coastal environment (exposed coastal periphery).

The field demonstration at Duck, North Carolina, validated the MM for a Trailing Edge Coastal environment and the field demonstration in Hawaii validated the MM for a Biogenic Reef environment. The Navy UXO site percentages shown in Table 1 and the Navy test results greatly supported the ability to validate MM for 50% of all known UXO sites. More importantly, that 50% of the UXO sites includes nearly all the sites of known high energy and expected high rates of UXO movement. In the “sheltered coastal bays/estuaries” sub-categories the energy is much lower and movement is primarily related to sediment transport; the human interaction risks are generally lower there as well. These sites will eventually need to be calibrated in the future, as well.

Both of the demonstration sites were also selected because they replicate the typical environments in which UXO is found but are not themselves active UXO sites. Since these field demonstrations require installing instrumented surrogates from small boats and diver operations on the seafloor, safety dictated that the operations avoid live UXO if at all possible.

The sites also were attractive because they are either under full military control (FRF Duck) or have very limited civilian access (PMRF, Kauai). The Navy test program environmental reviews for the California and Washington state tests have all shown that there is no significant impact from the short-term testing process, which helped to expedite the permitting processes.

Finally, the environments of both sites were already reasonably well documented because of recent offshore test activities there. FRF is an operational Army test facility that has been used in the past for Navy tests of the migration of seafloor mine shapes. As one of the most instrumented beaches in the world, FRF continually monitors the wave environment and the measures beach profile on a weekly basis. The PMRF site is also well documented because it is a Navy Range.

Choosing the FRF site clearly matched the requirements since it represents the Trailing Edge environment and, being just south of Cape Hatteras, it is normally exposed to hurricanes in the summer and nor’easter storms in the winter. It also is very well instrumented and has a long history of test operations similar to those planned for this program. Permits were easily



obtained, and the FRF Duck staff members were extremely capable and helpful. Their Coastal Research Amphibious (CRAB) vehicle and Lighter Amphibious Resupply Cargo (LARC) vessel provided optimal support for installing, monitoring, and recovering the demonstration items over the many months of the effort.

The Hawaii site selection process took a lot longer since more than one possible site was identified. The PMRF site was eventually approved and it afforded the team with a location representative of many typical biogenic reefs, along with rugged bathymetry, wandering sand channels (awas), and heavy winter storm waves. Fortunately there were LIDAR data available; otherwise, the MM would not have been run in its most intensive mode, Mode 3, to properly account for the awa formations. All Hawaii field operations were conducted by Sea Engineering, Inc. (SEI), whose divers worked from small ocean craft.

#### **1.14 4.2 Demonstration Site/Facility History**

FRF is an active research site since their personnel maintain a comprehensive measurement program even during severe storms when significant coastal change occurs. Their long-term monitoring program of the coastal ocean includes waves, tides, currents, local meteorology, and resultant beach response. Divers and small craft are used in various tests and the beach is profiled by the CRAB on a weekly basis. The site is used by both the USACE and a variety of educational institutions; the primary impact of FRF's busy operations schedule on the demonstration was the occasional schedule conflict with divers and equipment for monitoring.

PMRF also is heavily used as a test facility, though most of the activity takes place on land. The beach area is used by recreational surfers and fishing boats do frequent the area, but none of those activities had any impact on the demonstration. SEI divers were able to work whenever the weather allowed, which was most of the time.

#### **1.15 4.3 Site Geology**

The FRF site is a classic "Trailing Edge" coastal geomorphic environment, as cited in Hammond et al. [4]. The site is characterized by a shallow, relatively flat seafloor extending several miles offshore. The bottom is covered by frequently shifting sand.

The PMRF site is categorized as a typical "Biogenic Reef". The area is composed of hard rock and coral, with awa (sand channels) cutting through it.

#### **1.16 4.4 Munitions Contamination**

For diver safety reasons, these sites were chosen because they are environmentally similar to many UXO sites but have no known underwater ordnance located there.

## 5.0 TEST DESIGN

The basic concept was to install surrogate UXO (5"/38 projectile surrogates) at the representative sites, monitor their burial/movement, and compare the measurements against predictions made by the UXO Mobility Model. Figure 13 illustrates the general concept.

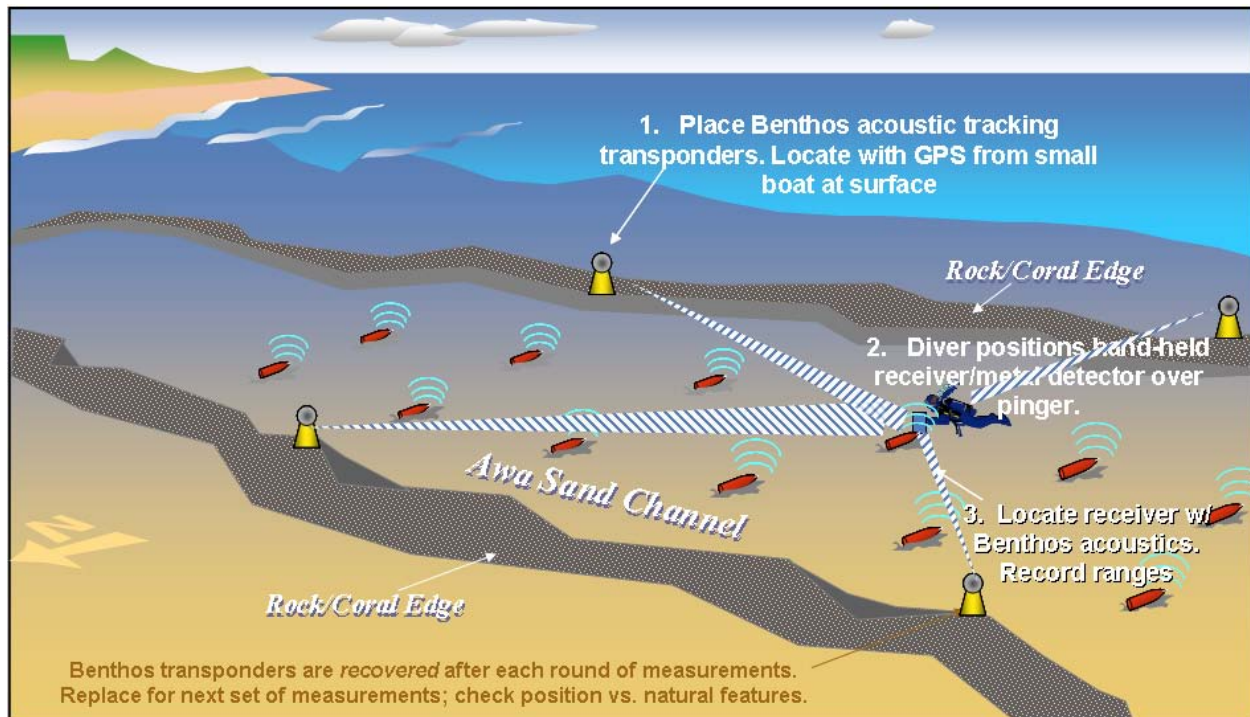


**Figure 13. Field demonstration concept (PMRF Hawaii example).**

### 1.17 5.1 Conceptual Experimental Design

Note that this program was not a demonstration of detection, discrimination, or remediation technologies, but rather it was a series of field demonstrations performed to yield data to validate the MM. Therefore, the discussion in this section focuses on summarizing these efforts and does not address issues relevant to more traditional munitions management projects. The two field demonstrations are described in greater detail in the separate Field Demonstration Reports [1, 2].

#### 5.1.1 Demonstration Setup and Startup

At each field site, 24 x 5"/38 UXO surrogates were placed on the seafloor in various orientations and water depths. Their location, depth of burial, and orientation were then monitored by diver inspections at intervals determined by the occurrence of high-energy environmental events (e.g., storms or large, local wave events). The surrogates were left in place through one local seasonal cycle at PMRF Kauai and for two entire years at FRF Duck.



The 5"/38 surrogates were installed at pre-determined distances from the shoreline from the closure depth to just seaward of the low tide line. By then plotting the actual movements of each individual surrogate, it was possible to investigate data trends as a function of location with respect to the surf zone, weather forcing function conditions, and local sediment properties.

Groups of 20 mm surrogates were initially placed in small groups near the 5"/38 surrogates at FRF. Though the 20 mm surrogates were not individually tracked, they were located and samples collected at the time of the final recovery to determine relative migration distance; it is noted that the 20 mm surrogates were only used at the FRF Duck site and not at PMRF Kauai.

The location of the 5"/38 surrogates was tracked with a variety of methods. The larger surrogates (5"/38) were composed of large metal cores and equipped with acoustic pingers. Divers used hand-held receivers, as well as a Benthos fixed acoustic tracking system, to track the surrogates. Metal detectors were used to further locate the surrogates in conditions of poor visibility or when they were buried. Each location was measured from fixed references by employing acoustical methods, Global Positioning System (GPS) to surface floats, and tape measures, depending on the local conditions at the time.

The primary metrics for a successful demonstration were to collect data on the movement of all or most of the UXO surrogates and to document the environmental conditions that caused those movements (e.g., currents, waves, and seafloor properties). The primary metric for defining a successful MM validation effort was that the observed movement matched the predicted movement well enough to allow final adjustment of the MM parameters to match the observations without changing the basic structure of the MM (i.e., assumptions of basic forces and interactions would remain unchanged). The details of the MM calibration and validation process are described in more detail in following sections.

### **5.1.2 Period of Operation**

The following Gantt chart for the total ESTCP UXO Mobility Model program shows the demonstration periods highlighted in green in Figure 14.

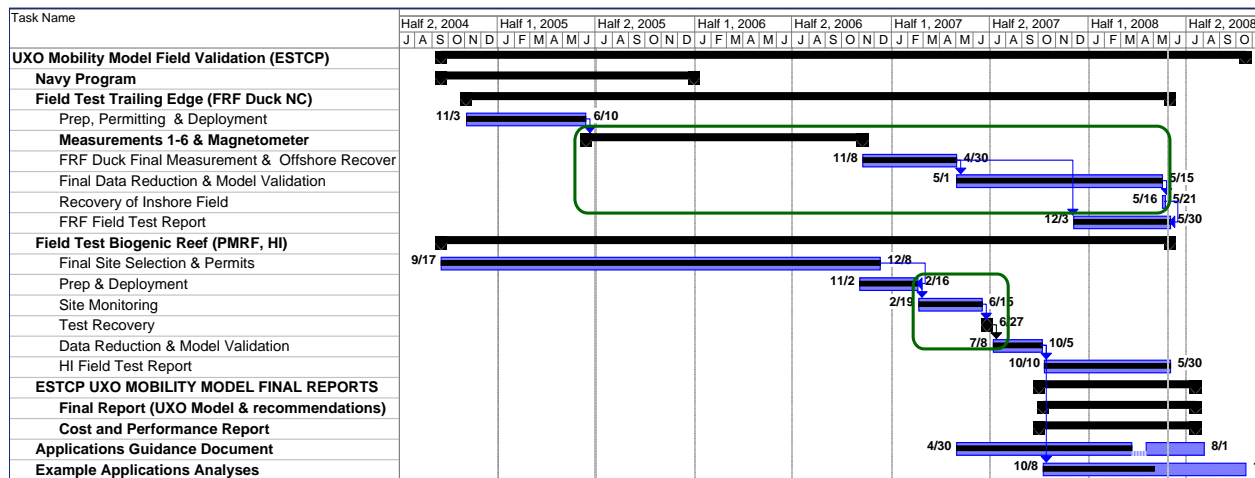


**Figure 14. ESTCP UXO Mobility Model program schedule.**

The FRF demonstration was in place through two full cycles of hurricane season and winter nor'easters, although during the 2005-2007 season, only unusually mild storms occurred at Duck; the hurricanes instead veered south, while the nor'easters remained to the north. The PMRF Kauai demonstration spanned one winter cycle which also uncharacteristically did not experience any extreme events, but rather only moderate winter storms.

## 1.18 5.2 Site Preparations

The primary pre-demonstration effort was the Navy program that developed the MM itself and conducted the initial short-term validation tests at Point Mugu, CA, and Ocean Shores, WA. In addition, there were site visits and preliminary MM analyses performed to aid in the planning of the Field Tests.

### 5.2.1 FRF Duck Pre-Demonstration Analysis

Prior to the demonstration, the FRF site was analyzed by running the MM using historical wave, current, sediment transport, and other seafloor data from the site to determine the expected movement of the UXO as a function of location along and across the coastline profile. That analysis was used to set the final FRF location and initial orientation of each surrogate 5"/38 projectile. MM results were also used to determine the details of the locations of reference stakes and approaches to be used by divers in conducting surveys.

A preliminary dive was conducted at the FRF site to collect small samples of the seafloor sediment across the demonstration area. Dr. Jenkins analyzed the samples at Scripps Institute for sediment type and a standard grain-size analysis was performed. Grain size is an important input to the MM. Besides FRF's permanently deployed instruments that provided waves and currents

data for the site, the team was able to use their extensive historical database of meteorological and oceanographic information from which to make predictions.

The preliminary dive also allowed local procedures and logistics processes to be used as baselines for the initial installation and follow-on monitoring visits.

### **5.2.2 PMRF Kauai Pre-demonstration Analysis**

The SEI support diving team made two preliminary dives at the site to photograph the bottom conditions, confirm the awa configuration, and obtain samples of the sediment (sand) in the awa at the two sites selected for the inshore and offshore fields. There were some delays in locating, obtaining, and then gridding the detailed LIDAR data. To make up for lost time, the hardware and surrogates were installed as soon as the permits allowed, which precluded running the MM for this site prior to deployment. However, analyses of the height of the awa walls were performed to confirm that even in the worst possible storm the surrogates would not move out of the awa and onto the beach; they would remain in the demonstration area so they would not damage local coral, and so they could be closely monitored.

The results already obtained from the FRF site suggested that the acoustic monitoring process would continue to be useful. However, the locations of the Benthos tracking transponders were adjusted to allow for better triangulation calculations.

For safety reasons, none of the efforts were performed at sites known to contain active UXO. However, the validation effort did provide enough data to produce environmental characterizations of each site, while also providing insight into methods for detecting and tracking UXO if desired. The magnetometer tests conducted at FRF Duck showed that 5"/38 UXO can be accurately located by metal detectors if the detector is calibrated and the sensor is properly tracked acoustically.

### **1.19 5.3 System Specifications**

The main hardware for the UXO Field Demonstrations was the surrogate 5"/38 projectiles. They were cast from plastic with a steel core so they represented the correct shape and weight. They were equipped with small Sonotronics acoustic pingers in the nose to facilitate locating them even when buried. Sonotronics underwater acoustic receivers were used to guide divers to the location of the surrogates during each round of measurements. When the surrogates were buried, hand-held metal detectors were used to refine the diver's position within less than 1 meter. The diver's location in the test field was then determined by ranges from two or more Benthos acoustic transponders located at fixed points in or near the field.

The surrogates are shown in Figure 15. For further details on the test hardware, refer to the two separate Field Demonstration Reports [2, 3].



**Figure 15. Surrogate 5''/38 projectiles used in UXO Mobility Model field demonstrations.**

#### **1.20 5.4 Calibration Activities**

The locations computed from the Benthos tracking units were compared against hand-held tape measurements from multiple points. In all cases, the tape measured locations (typically accurate to  $\pm 6$  inches) fell in the center of the acoustic error bounds ( $\pm 1$  meter).

## **6.0 DATA ANALYSIS AND PRODUCTS**

Note that since this program was designed to validate a computer model of UXO movement rather than validating a method of detection or removal of UXO, the following sections do not directly follow the ESTCP March 2008 Final Report outline.

The section begins with a short overview of the required inputs for the MM, the outputs it provides, etc. Then the results of each of the two field demonstrations are analyzed and compared against the MM predictions. The resultant MM calibration and validation are then described.

## 1.21 6.1 Mobility Model Description

The MM model and the associated demonstration efforts, are neither “detection/discrimination” nor “remediation” technologies. Rather, it is instead a “decision support tool”. The operating parameters are considered to be the variables entered into the MM and are described below.

### 6.1.1 Required Input

The MM can be operated in three distinct modes depending on the data that are available for making a burial prediction and the user’s desire to make site specific adaptations to the model’s configuration. When little more than the general coastal setting and the time frame of UXO introduction and initial depth are known, the MM is run in Mode 1. Mode 1 predictions use pre-configured gridding systems, forcing functions, boundary conditions and calibration factors based on the coastal classification system. The seven input parameters required for Mode 1 operation are indicated by the *italicized* entries in **Table 4**.

When information is known about the gross site specific details of a suspected UXO field, then the MM can be run in Mode 2. Mode 2 operation makes burial predictions using pre-configured gridding systems and calibration parameters with user supplied bathymetry, wave and sediment data. The Mode 2 input parameters are the seven *italicized* and 13 underlined entries for parameters listed in **Table 4**.

The MM is run in its most detail intensive configuration as Mode 3. This operational mode is for applications in which contemporary, high-resolution, site-specific information is known about the UXO field. This operational mode was used in field experiments at Ocean Shores in August 2003 and for both of the ESTCP field tests. And Mode 3 is intended for experienced modelers, and allows for customized configurations of all gridding systems, calibration factors, and file structures of forcing functions and boundary conditions. Mode 3 input parameters include all 40 parameters listed below.

**Table 4. UXO Mobility Model Input Parameters.**

<b><u>Farfield Littoral Cell Model Parameters</u></b>	
<i>1</i>	<i>Coastal Type: Collision, Trailing Edge, Marginal Sea/Narrow-Shelf Mountainous, Marginal Sea/Wide-Shelf Plains, Marginal Sea/Deltaic-Tideless, Marginal Sea/Deltaic-Tidal, Arctic Form of Cryogenic, Coral Reef Form of Biogenic</i>
<i>2</i>	<i>Estimated time when UXO entered the environment</i>
<i>3</i>	<i>Time period of prediction</i>
<u>4</u>	<u>Deep water directional wave spectra or discrete height, period &amp; direction estimates of principal band</u>
<u>5</u>	<u>Deep water wave height of antecedent extreme event</u>
<u>6</u>	<u>Wind speed</u>
<u>7</u>	<u>Precipitation or river flow rate data, Q</u>
8	Coefficients (a, b) of sediment rating curve ( $R = aQ^b$ )
9	Grid cell dimension x-axis (Longitude)
10	Grid cell dimension y-axis (Latitude)
11	Number of grid cells along the x-axis (Longitude)
12	Number of grid cells along the y-axis (Latitude)
13	Latitude/longitude of upper left hand corner of farfield grid (Raster formatted grid)
14	Stationary bathymetry file at start of simulation
15	Position of mean shoreline (0.0 m MSL) at start of simulation
16	Distance offshore to closure depth
<u>17</u>	<u>Median grain size of shelf sediments (seaward of closure depth)</u>
18	Grain size distribution of shorerise and bar-berm sediments (as many as 9 size bins)
19	Volume concentration of seabed sediment
<u>20</u>	<u>Tidal harmonic constituents</u>
21	Longshore transport efficiency coefficient
22	Shorerise bottom friction coefficient
23	Breaker dissipation coefficient
24	Angle of internal friction

**Nearfield Scour and Burial Model Parameters**

### **Nearfield Scour and Burial Model Parameters**

- 25 *UXO type*
- 26 User selected grid cell(s) from farfield grid corresponding to UXO sweep area
- 27 *Estimated time of UXO deployment*
- 28 *Time period of prediction*
- 29 *Degree of impact burial*
- 30 Grain size distribution of seabed sediments (as many as 9 size bins)
- 31 Local seabed elevation and slope from user selected grid cell of farfield model
- 32 Local orbital velocity from user selected grid cell of farfield model
- 33 Local tidal velocity from user selected grid cell of farfield model
- 34 Bed roughness
- 35 Seabed drag coefficient
- 36 Bedload transport efficiency
- 37 Suspended local transport efficiency
- 38 Angle of internal friction
- 39 Volume concentration of seabed sediment
- 40 User selected grid cell dimension for unregistered UXO type

Note that these parameters are all measurable by, or derivable from, conventional ocean environmental measurement technology. Existing Defense Mapping Agency (DMA) charts, commercial surveys with multi-beam bathymetry/imagery, and a few selected sub-bottom profiles, a series of core samples, and hindcast coastal wave, tide and current measurements are all sources for the data needed for useful MM operation. The MM is very complete in the parameters it considers, but does not demand new technology or great expense to collect the required data. The inputs allow deterministic simulations of UXO behavior. The MM simulations then allow long-range predictions based on stochastic application of site-specific climatic conditions.

The accuracy of the MM predictions is limited almost entirely by the statistics of the inputs.

#### **6.1.2 Key Outputs**

The primary MM outputs are the predicted rate of burial/unburial and the direction and rate of movement of unburied UXO (i.e., location in x, y, and z vs. time). The primary numerical output is a mathematical relationship between UXO mobility distance and the Shields Parameter, a dynamic parameter that is a measure of the intensity of environmental forcing relative to the inertia of the UXO. The Shields Parameter represents a ratio between the hydrodynamic forces acting to move the UXO and the gravitational forces acting to restrain and bury the UXO. Initial trial runs of the MM on a 5-inch diameter parabola of revolution (surrogate for a 5-inch naval projectile) were found to show a systematic relation between the distance the UXO is transported in a 30-day period ( $\xi$ ) and a form of the Shields parameter,  $\Theta = \sigma^2 H^2 / g' D$ ; where,  $H$  is the wave height,  $\sigma = 2\pi / T$  is the radian frequency of the wave,  $T$  is the wave period,  $D$  is the base diameter of the UXO,  $g$  is the acceleration of gravity,  $g' = g\Delta\rho / \rho$  is a form of reduced gravity, and  $\Delta\rho$  is the density difference between the UXO and seawater density,  $\rho$ . Data

indicate that UXO mobility increases with increasing wave height, with decreasing caliber of the UXO or with decreasing density (specific gravity) of the UXO. More detail is provided in the Navy's Phase One report by Hammond et al. [4].

The MM works anywhere data are available. Baseline analyses can even be performed with very limited knowledge. Mode 1 only requires a general estimate of the coastal classification, and desk-top data on climatology or NOAA wave buoy data sets.

### **6.1.3 Field Demonstration Data Quality**

As is normal for at-sea operations, there were a few erratic or missed data points in the monitoring process. At FRF some of the points were missed because surrogates were buried too deeply at that time, or because weather closed in. At PMRF on one occasion the measurements were offset by one number because a diver mistakenly took a fix on some other buried metal object. However, 70 to 90% of all data were consistent so outlying or missing data points were easily identified and did not obscure the overall accuracy of the validation process. The measurement skill of the divers improved with practice at each site, so the final few measurement sets were (a) more accurate than some of the interim measurements and (b) 100% complete. Both the initial position and the final position of all the surrogates at both the sites were accurately measured.

### **1.22 6.2 Analysis of PMRF (Hawaii) Field Test Data**

The *Vortex Lattice (VORTEX) Scour and Burial Model* was used to predict migration and burial behavior of UXO surrogates of 5"/38 projectiles (Figure 16) when grounded on the seafloor in the near shore of a biogenic reef environment. The reef environment selected for this experiment was the PMRF located off the west coast of the island of Kauai, HI.



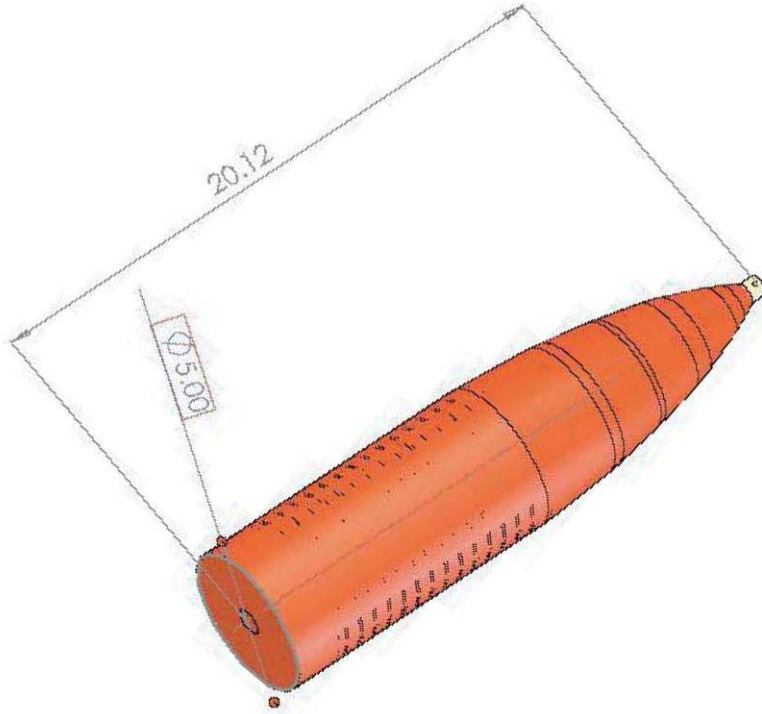


**Figure 16. Dimensions of 5"/38 surrogate used in field demonstrations.**

The forcing function module of the MM (Figure 17) provides time series of waves, currents, and sediment flux. Waves and currents are derived from direct observations by means of Datawell directional wave buoys and Acoustic Doppler Current Profilers (ADCP), to validate model velocity algorithms. Fluxes of river sediment are neglected as explicit boundary conditions, but the presence of those sediments is accounted for in the grain size distributions of the offshore sediments. The wave and current forcing provides excitation applied to the deep water boundary of the farfield computational domain. These boundaries are specified in the boundary conditions module (beige box) in Figure 17, where the farfield computational domain is assembled from a series of boundary-conforming control cells, using a combination of bathymetric data obtained from National Ocean Service (NOS) and United States Geological Survey (USGS) as compiled by the National Geophysical Data Center to assemble the gross morphology of the fringing reef [19, 20, 21, 22, 23]; and LIDAR data to construct bathymetric details of local awa channels (at 1m grid cell resolution) in which the UXO fields were placed.

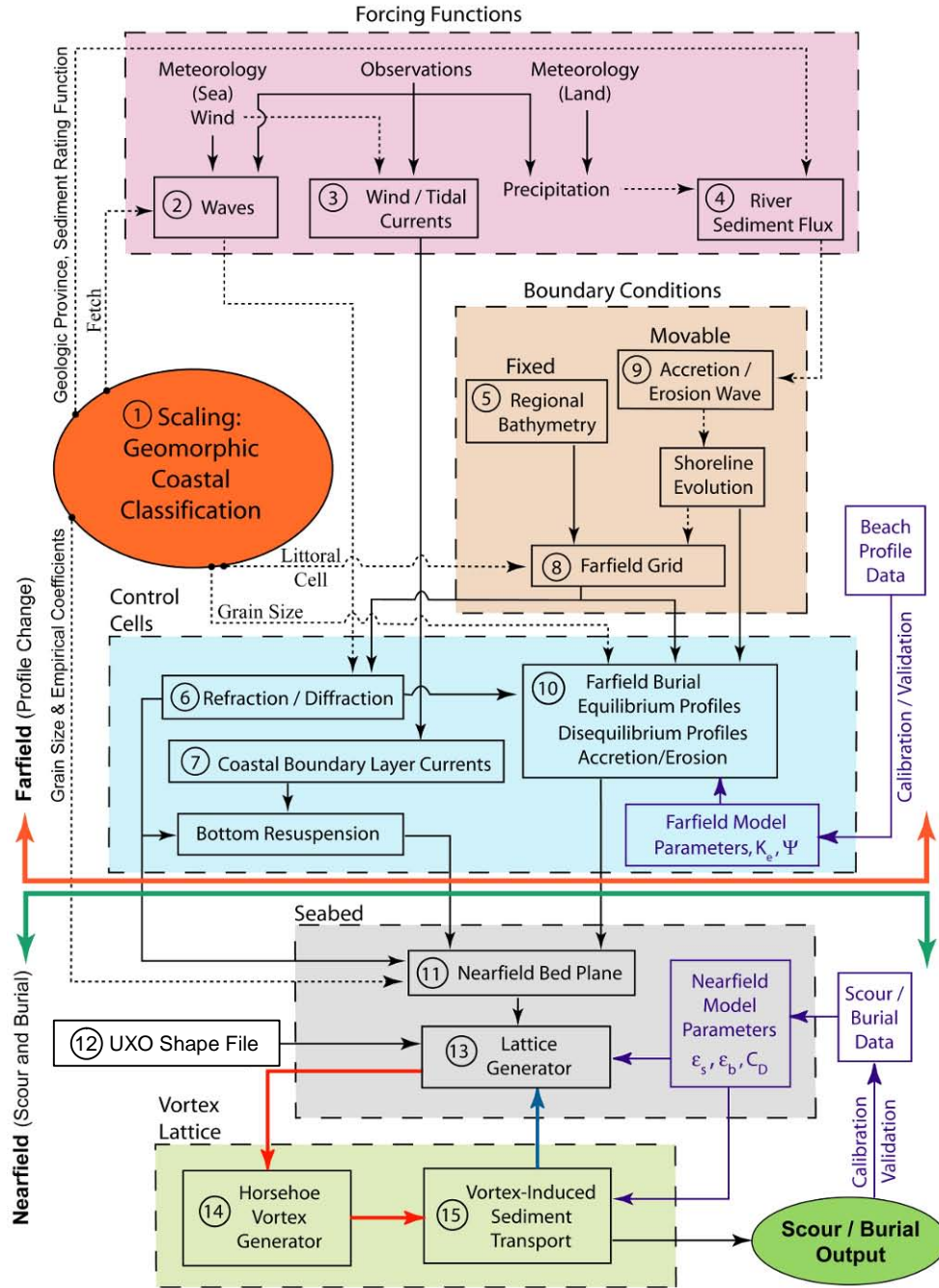


**Figure 17. Vortex Lattice Scour Burial Model.**

With these forcing functions and boundary conditions, the farfield response module (blue box) computes the spatial and temporal evolution of the fluid forcing and bottom elevation along cross-shore profiles of a control cell representing the gross morphology of a fringing reef system (Figure 18). At the PMRF site, these control cells are bounded in the cross shore by the walls of

sand and awa channels cut cross-shore through the lithified reef structures. Predominately carbonate sediments accumulate in these channels along bottom gradients that can be specified by profiles having three matching segments: 1) the stationary profile that extends from the deep water boundary inshore to closure depth  $h_c$ , where profile changes become vanishingly small; 2) the shorerise profile that continues from closure depth to the wave break point; and, 3) the bar-berm profile that begins at the break point and ends at the berm crest. The stationary profile is invariant with time and is given by the regional bathymetry. Bottom elevation changes along the non-stationary profiles of the shorerise and bar-berm are computed by module #10 in the farfield response module (blue box) using equilibrium profile algorithms. The stationary and non-stationary profiles are interpolated to create a Cartesian depth grid within each control cell on which simultaneous refraction and diffraction patterns are computed by module #6 using algorithms to specify fluid forcing by shoaling waves.

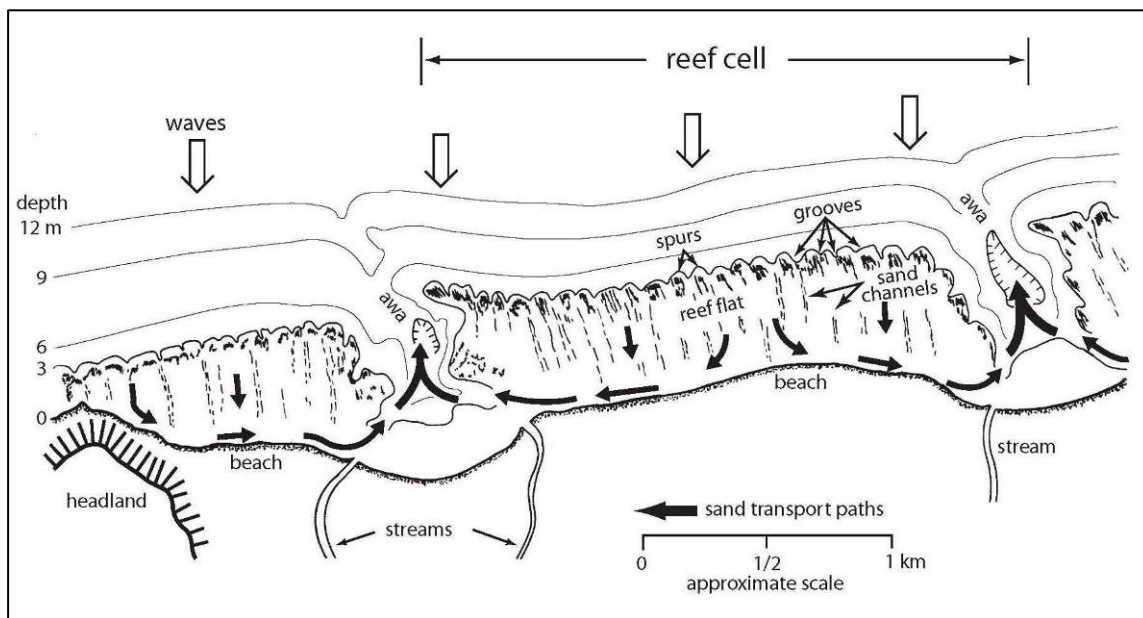


**Figure 18. Schematic diagram of control cells along a fringing reef coast**

Figure 19 illustrates the mechanics of farfield burial at the PMRF site. Part (a) is the envelope of profile change (critical mass). Part (b) is the volume of critical mass from elliptic cycloids. Part (c) is the cross-shore variation in thickness.

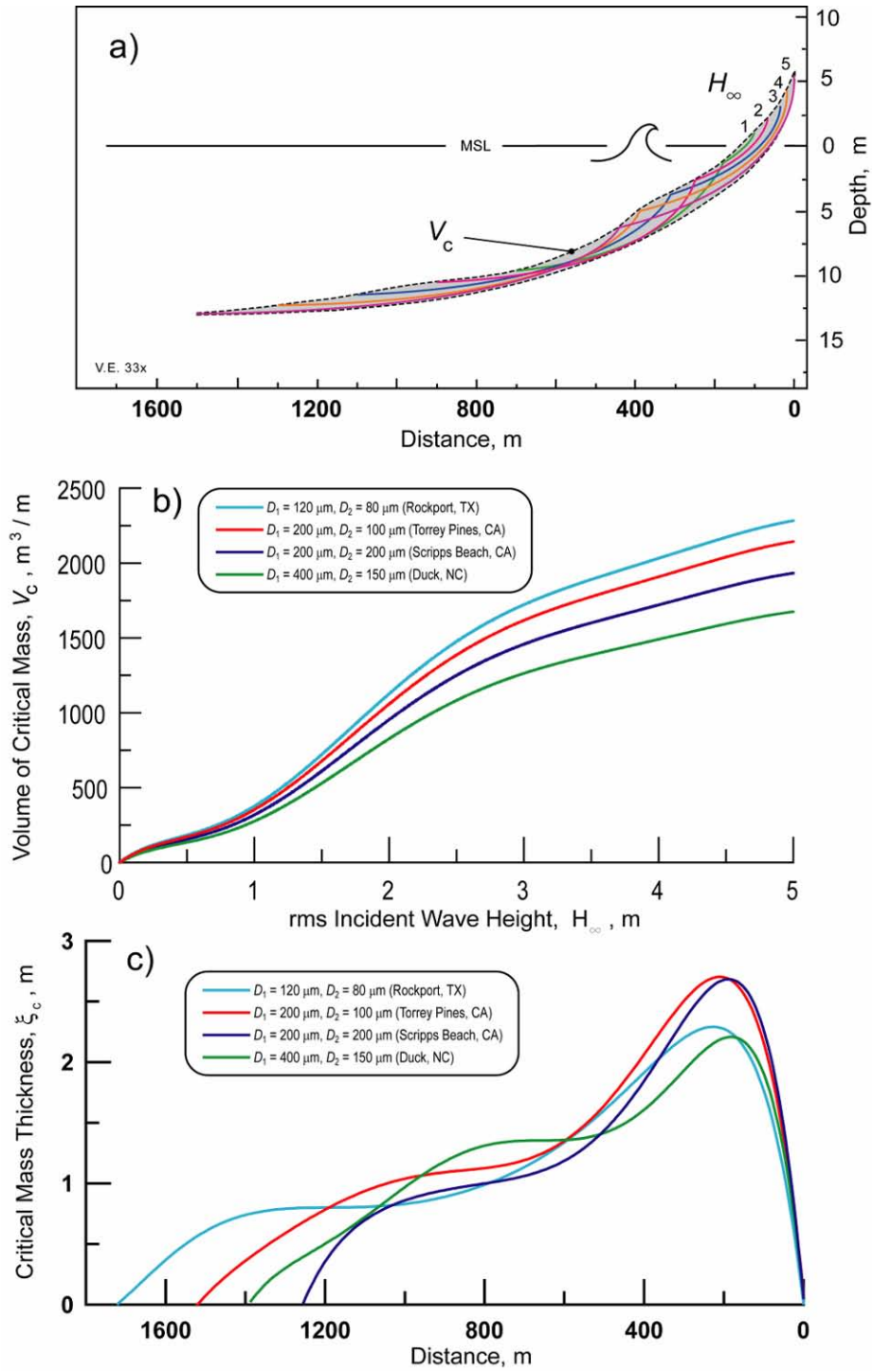


**Figure 19. Farfield burial mechanics.**

Fluid forcing by currents in the farfield are computed in module #7 where wave induced streaming and mass transport are based on algorithms after Longuet-Higgins [24], Lamoure and

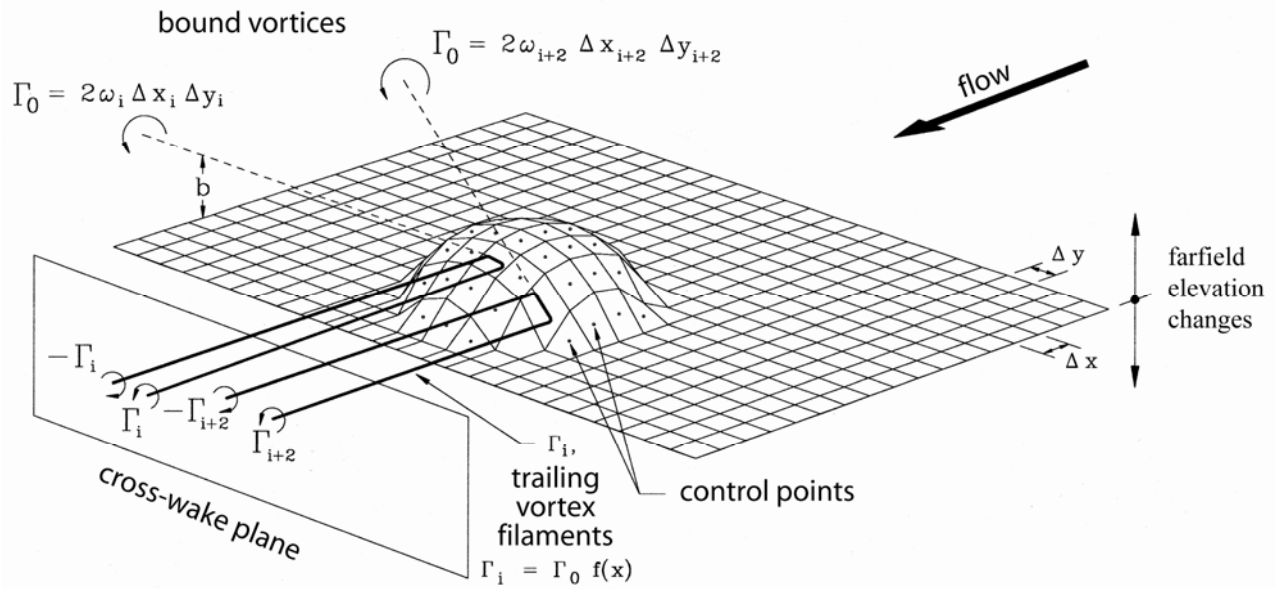
Mei [25], and Longuet-Higgins [26], and shallow water tidal currents follow from algorithms after Connor and Wang [27]. Fluid forcing time series and bottom elevations computed in the farfield response module feed into the nearfield response modules shown below the green line in Figure 17. The farfield throughput is applied to the local seabed boundary conditions module (gray box). These local boundary conditions include two types: 1) the slope and elevation of the seabed plane around the object base derived by module #11 from location in the farfield control cell; and 2) the shape file of the body in question module #12. These two local boundary conditions are used to generate lattice panels by module #13 that defines the object and bedform of the surrounding seabed (Figure 20a). The lattice is the computational domain of the nearfield scour-burial processes in which the method of embedded vortex singularities (vortex lattice method) is applied in module #14 using algorithms after McCormick [28], Van Dyke [29], and Peace and Riley [30]. This method employs horseshoe vortices embedded in the near-bottom potential wave oscillation to drive local sediment transport in module #15 based on ideal granular bed load and suspended load equations after Bagnold [31], Bagnold [32], and Bowen [33]. A horseshoe vortex is specified by module #14 for each lattice panel during every half-cycle of the wave oscillation as shown schematically in Figure 20a. The horseshoe vortices release trailing pairs of vortex filaments into the local potential flow field that induce downwash on the neighboring seabed (Figure 20b), causing scour with associated bed and suspended load transport as computed by module #15. This scour action by trailing vortex filaments can be seen occurring in nature in Figure 20b.

The lattice generation in module #13, horseshoe vortex generation in module #14 and sediment transport computations in module #15 are implemented as a leap-frog iteration in a time-stepped loop shown by the red and blue pathway arrows at the bottom of Figure 17. The leading time step (red arrow) computes the strength of the horseshoe vortex filaments generated by the pressure gradients and shear setup over the lattice panels of the combined body-bedform geometry of the previous (lagging) time step. The bed and suspended load transport induced by these filaments results in an erosion flux from certain neighboring lattice panels on the seabed and a deposition flux on others, based on image lifting line theory as first applied by Jenkins and Wasyl [34] to a mobile sedimentary boundary. The erosion and deposition fluxes of the leading time step are returned in the computational loop to the lattice generator (blue arrow) where those fluxes are superimposed on the lattice geometry of the lagging time step. That superposition produces a new lattice geometry for implementing the next leading time step. By this leap-frog iterative technique, an interactive bedform response is achieved whereby the flow field of the leading time step modifies the bedform of the lagging time step; and that modified bedform in turn alters the flow field of the next leading time step. This lead and lag arrangement is based on the fact that the inertial forces of granular bed near incipient motion are large compared to those of the fluid [31], hence the flow field responds faster to a change in bedform than the bedform can respond to a change in flow field.

Figure 20 illustrates the vortex shedding process and the vortex lattice model. Part (a) shows the lattice and horseshoe vortex system. Part (b) shows horseshoe vortices inducing sediment transport in nature.



a)



b)

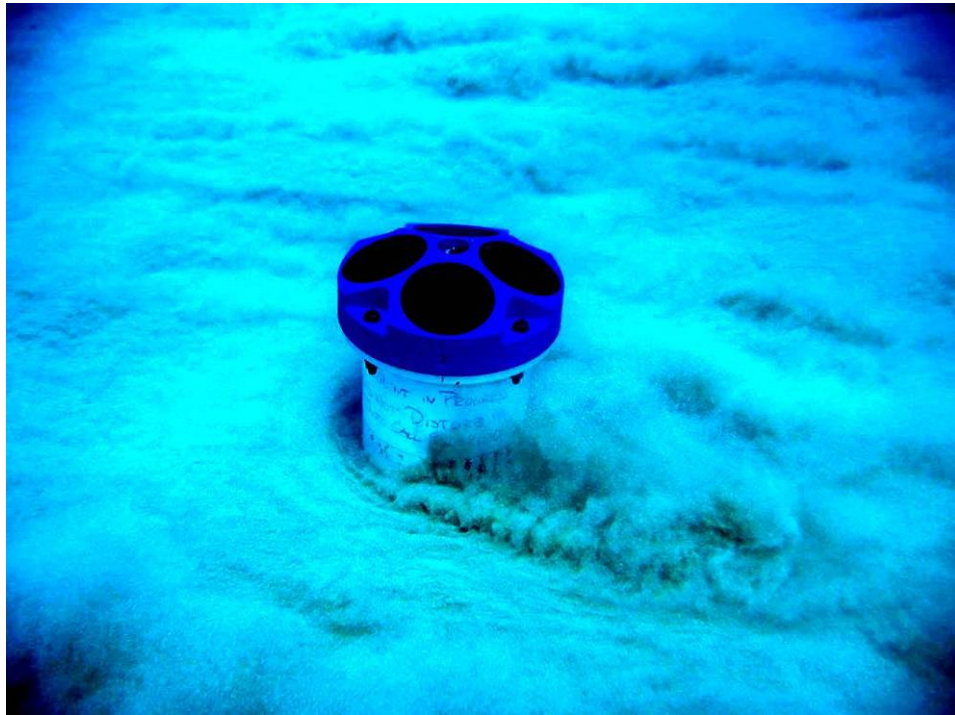


**Figure 20. Vortex lattice method: (a) lattice and horseshoe vortex system, (b) horseshoe vortices inducing sediment transport in nature (photo courtesy Kimball Millikan).**

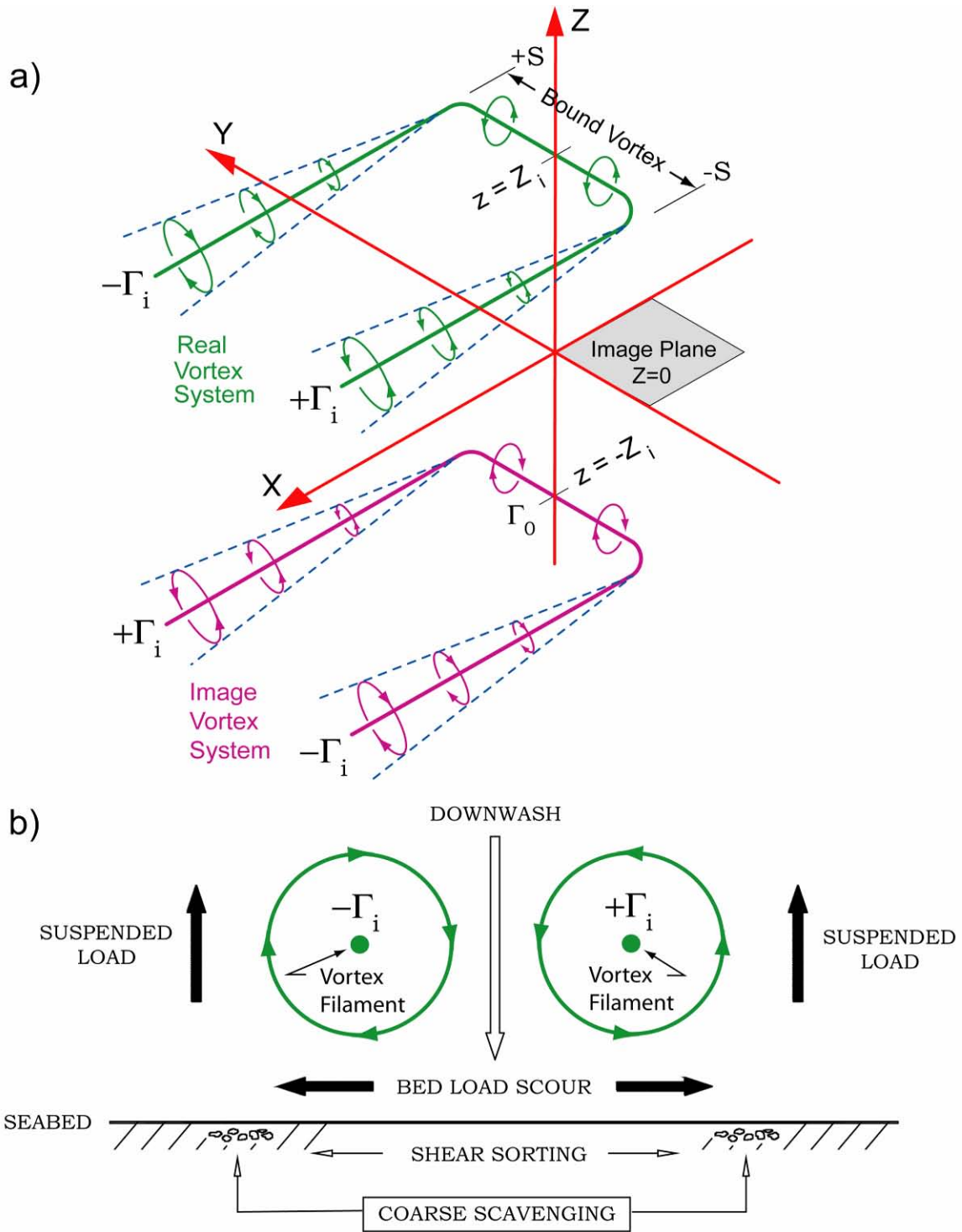


**Figure 21. Illustration of the image vortex method.**

Part (a) of Figure 21 shows the image method for vortex induced velocity at any point near the bed (image plane) due to the horseshoe vortex system of an arbitrary lattice panel. The real

vortex of the lattice panel is diagrammed in magenta. The image vortex is in green. Part (b) is a schematic in the cross-wake plane of a pair of vortex filaments trailing out of the page.

### **6.2.1 PMRF Model Initialization**

#### **Farfield Initialization**

Farfield initialization involves data base constructions and model parameterizations for model inputs above the orange line in Figure 17. A detailed listing of these inputs can be found in Wilson et al. [2]. They are reviewed here in context specific or unique to the PMRF site.

#### Bathymetry

The stationary farfield bathymetry was derived from the National Ocean Service (NOS) digital database as contoured in Figure 22 seaward of the 0m MSL depth contour. This coarse-scale bathymetry defines the basic morphology of the fringing reef system at PMRF along the west coast of Kauai. Gridding is by latitude and longitude with a 3 x 3 arc second grid cell resolution yielding a computational domain of 15.4km x 18.5km. Grid cell dimensions along the x-axis (longitude) are 77.2 meters and 92.6 meters along the y-axis (latitude). This small amount of grid distortion is converted internally to Cartesian coordinates, using a Mercator projection of the latitude-longitude grid centered on PMRF air field. The convention for Cartesian coordinates uses x-grid spacings for longitude and y-grid spacings for latitude. For the non-stationary bathymetry data inshore of closure depth (less than 12m MSL) we use the equilibrium beach algorithms from Jenkins and Inman (2006) [35]. Depth contours generated from these algorithms vary with wave height, period, and grain size and are plotted in Figure 22 landward of the 12m depth contour for the typical seasonal range of wave parameters of the PMRF site during the time frame of February through June 2007.

While Figure 22 defines the gross morphology of the reef platform, the micro-bathymetry of the specific area in which the UXO were placed was resolved with high resolution LIDAR data. Figure 23 gives a co-registration of the LIDAR data (green dots) with the coarse-scale NOS bathymetry and shows the sample density of the LIDAR data over that portion of the PMRF reef where the UXO fields were placed. The relative scale of coarser NOS bathymetry grid cells is shown by the larger patch-work pattern. Sample density of the LIDAR data was typically on the order of 1m, allowing for considerable detail of the area to be resolved around the offshore and inshore UXO sites (Figure 24). Coordinates for the offshore and inshore UXO sites are given in Figure 24a. The inshore site is located in local water depths of 25 ft -30 ft (~8.3m MSL), while the offshore site is at depths of 52 ft - 57 ft (~16.6m MSL). The channel takes several bends and curves in the cross shore direction between the offshore and inshore UXO sites, resulting in vertical convergence and divergence of surge currents flowing over the reef top as apparent in Figure 24b (with current forcing computed by module #7 of Figure 17). This reef-induced divergence tends to make UXO mobility and more sensitive to specific location than is otherwise found on the planar beaches of collision and trailing edge coastlines [4].



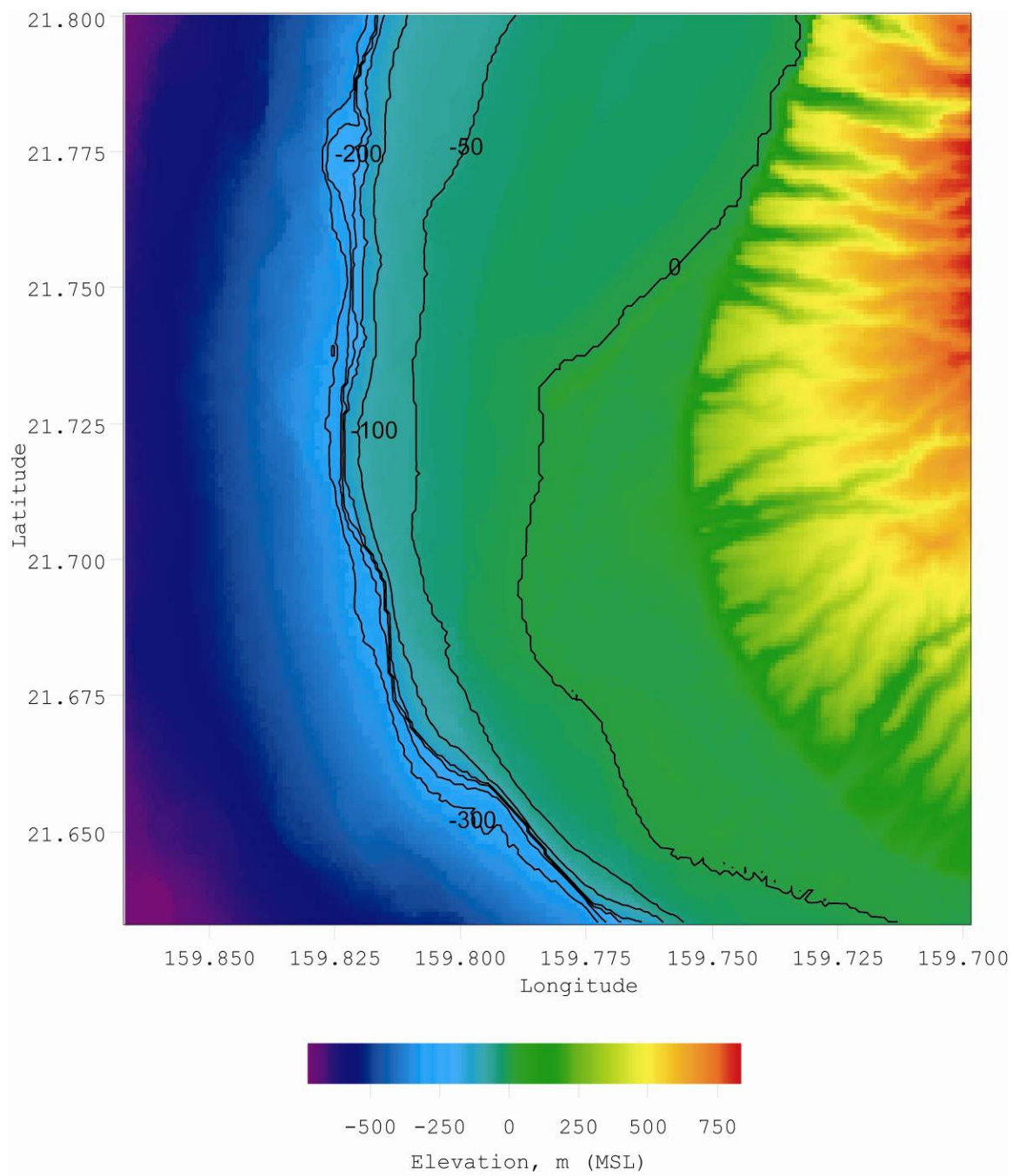


**Figure 22. Composite bathymetry from NOS data base and equilibrium profiles for wave conditions February - May 2007.**

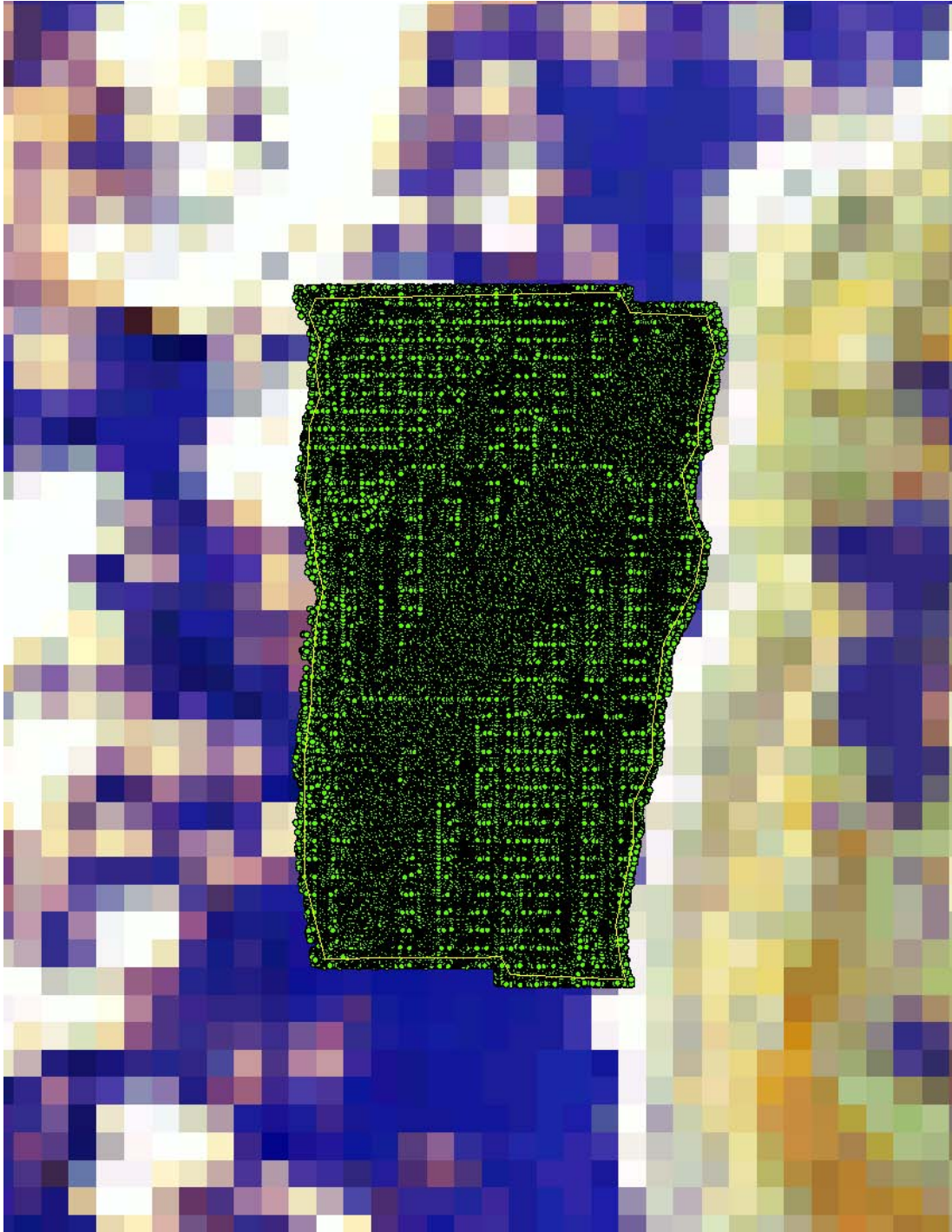
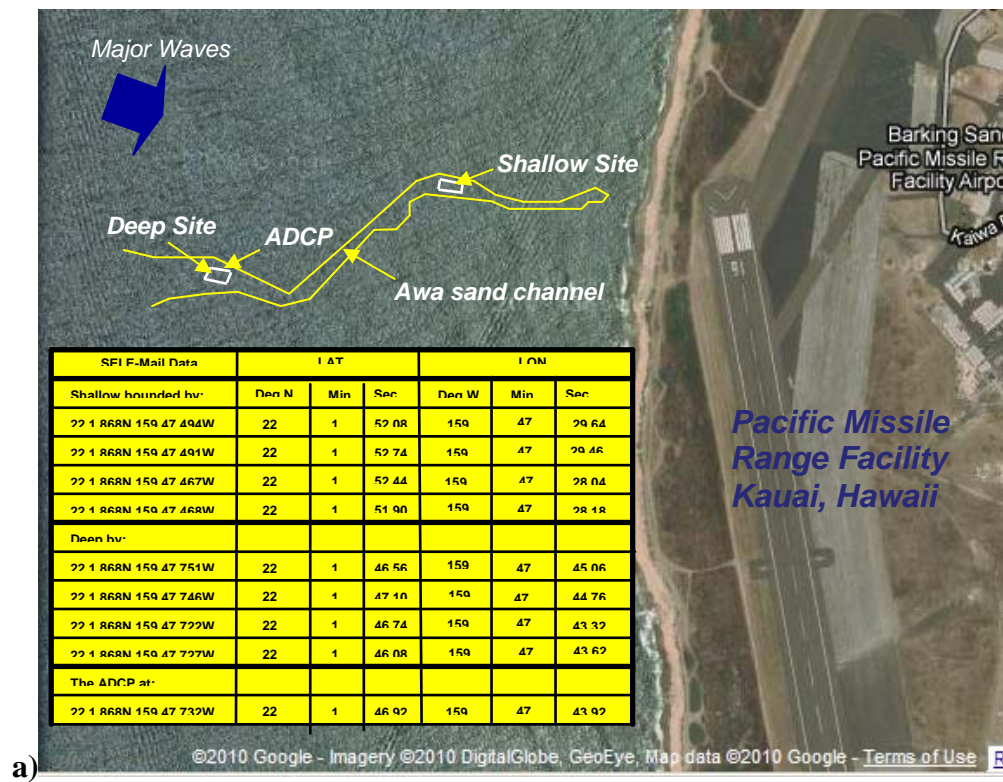


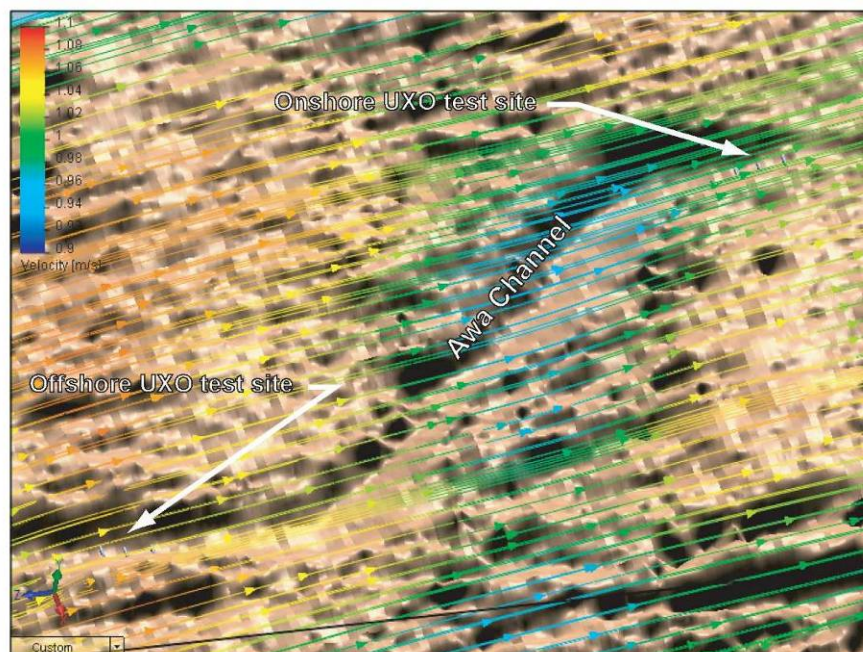
**Figure 23. Sample density of LIDAR high resolution bathymetry data.**





a)

b)



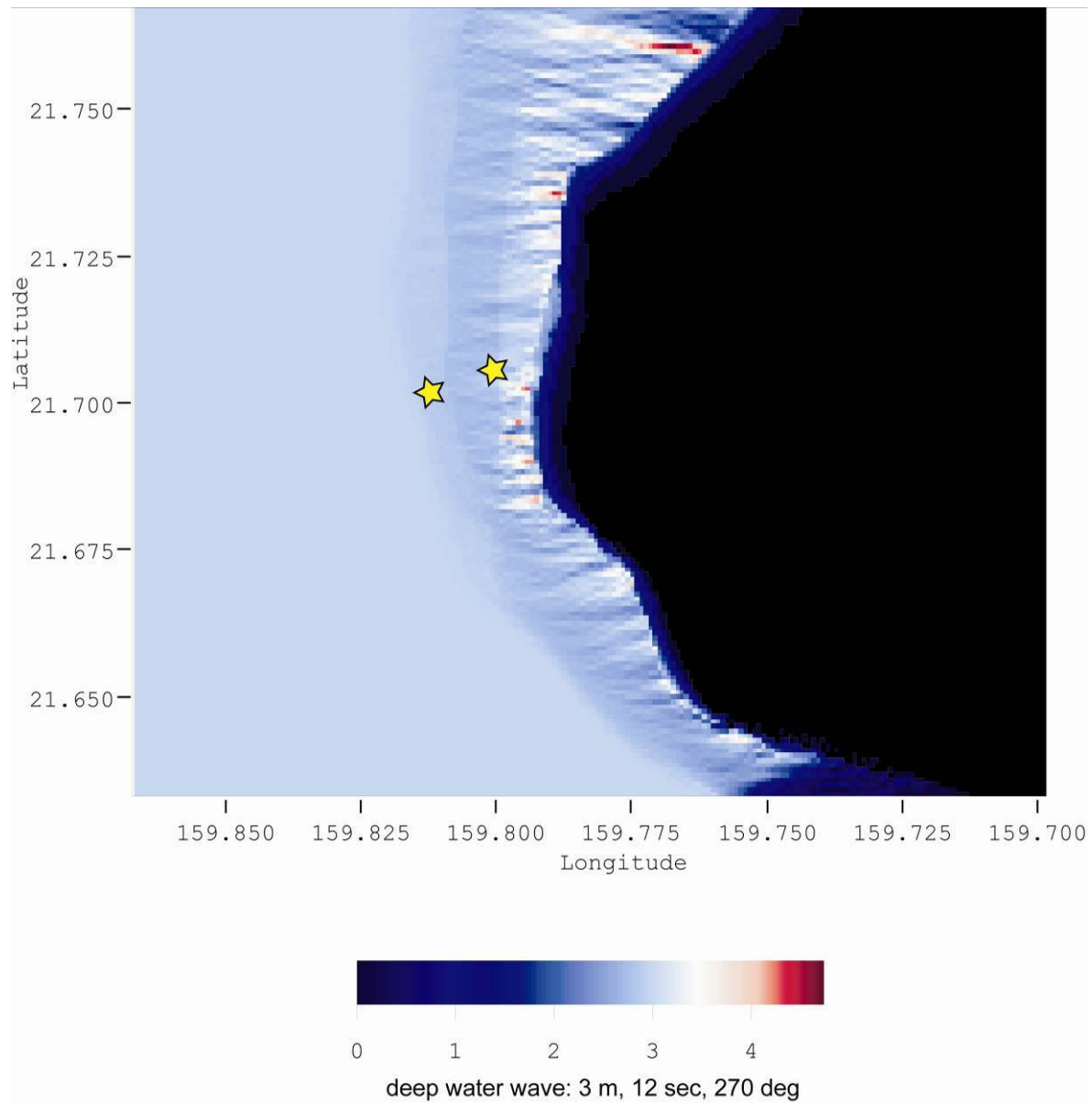
## Figure 24. PMRF offshore and inshore field demonstration sites

Figure 24(a) shows the location of offshore and inshore UXO fields of test surrogates. Figure 24(b) shows high resolution bathymetry derived from LIDAR data of an awa (channel) in fringing reef at PMRF; the instantaneous current magnitude is scaled by the color bar in the upper left corner.

### Wave and Current Forcing

Spatial variation in wave forcing over the reef platform and channel system is derived from refraction/diffraction analysis of directional wave measurements interpolated from an RD Instruments ADCP installation at 22° 1.782'N; 159° 47.732'W near the offshore (deep) UXO site. The ADCP data were back refracted to deep water and forward refracted over the PMRF site shown in Figure 25. The broad-scale refraction/diffraction plot, with inshore and offshore UXO fields denoted by stars, was computed for the largest waves measured by the ADCP during this period with a deep water wave height of 3 m, a 12 sec period, and approaching the coast from 270 degrees, indicative of a swell from the post-frontal side of a distant cold front dropping south from the Gulf of Alaska. Considering that 10m high waves are not uncommon in winter months along the windward coast of Kauai, the measured wave climate in Figure 26 must be considered unusually benign. This observation is enforced by the fact that the summer portion of the wave record shown in this figure produced wave heights comparable to all but the first few weeks of winter waves. The benign wave climate during the experiment combined with the vertical divergence in the flow field over the awa (Figure 26) produced fluid forcing that was generally insufficient to cause large displacements in the 5"/38 UXO surrogates.

While the reef produces bright spots in the refraction pattern along the west coast of Kauai at several locations north of the PMRF test (Figure 25), the refracted waves display small alongshore variation around the UXO sites. The absence of local alongshore gradients in shoaling wave heights produces very small longshore currents from the current prediction algorithms of the model. That assures that the predominant motion over the UXO fields will be up/down channel along the cross-shore axis of the awa. This observation is confirmed by the measured current directions in Figure 27, which on a daily basis are from the west and south west, directed onshore along the axis of the awa.



**Figure 25. Refraction/Diffraction pattern at PMRF test site for highest waves occurring during the experiment (February-May 2007).**

Figure 26 shows the currents for the offshore site, as measured by an RD Instruments 1200 kHz Workhorse Directional Wave Gage and Current Profiling ADCP during the PMRF UXO migration experiment. Measurement location was at 220 1.782°N; 1590 47.732°W near the offshore (deep) UXO site at a depth of 16.6m MSL. Figure 27 shows the currents for that same site.

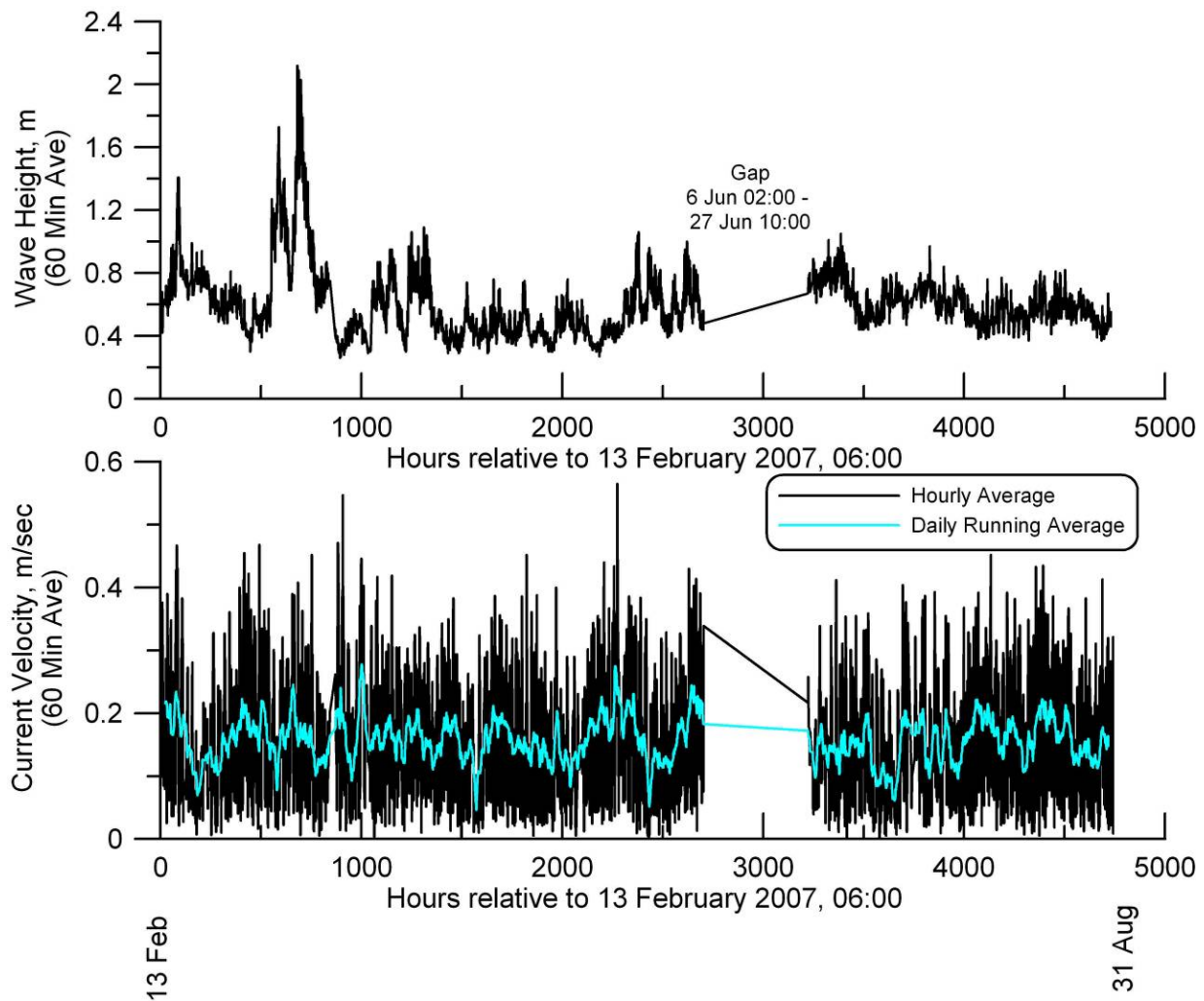


**Figure 26. Wave height (upper) and current magnitude (lower) at the offshore site.**

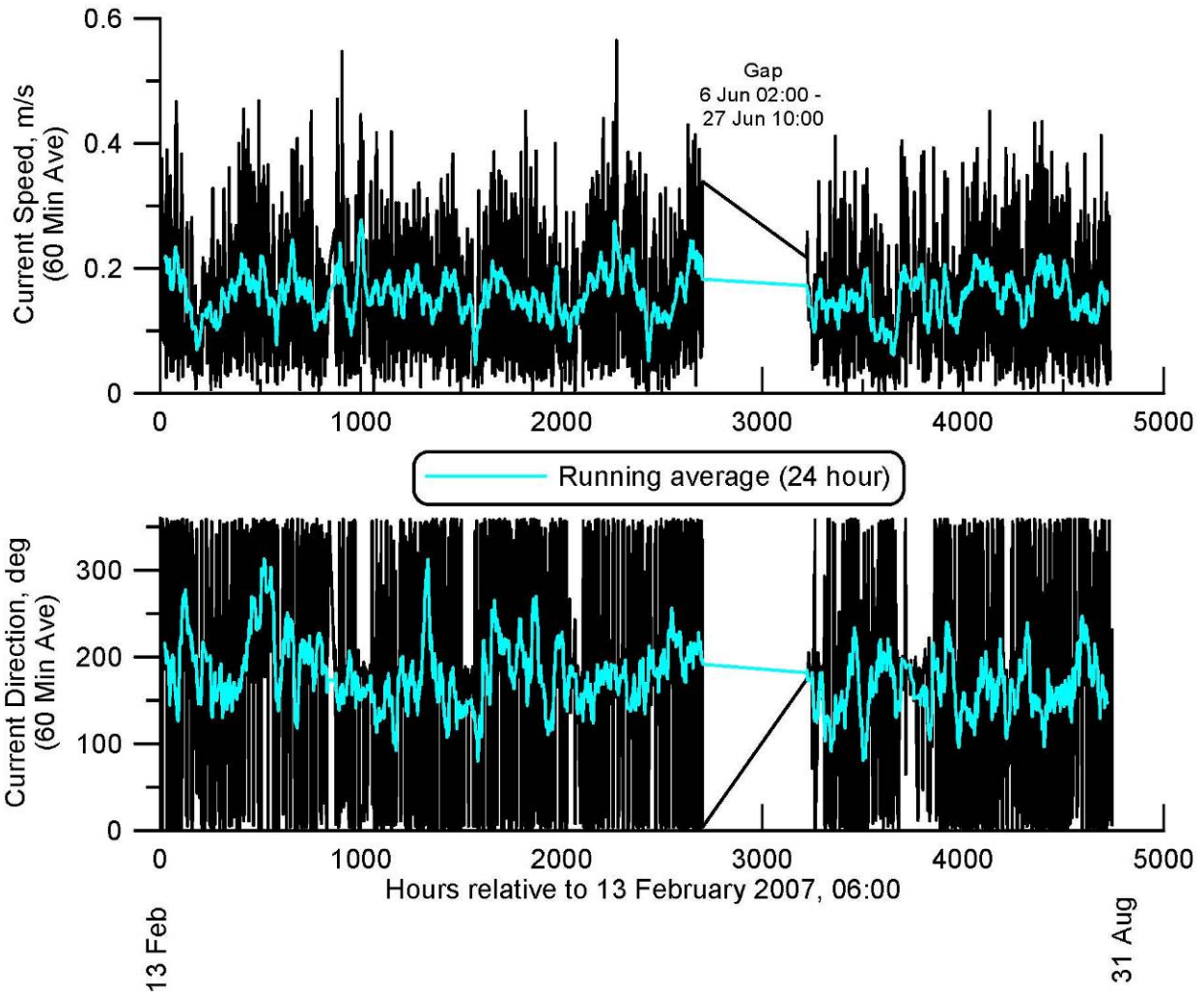


**Figure 27. Current speed (upper) and current direction (lower) during the demonstration.**

### **Nearfield Initialization**

Nearfield initialization involves data base constructions and model parameterizations for model inputs below the green line in Figure 17. A detailed listing of these inputs can be found in Hammond et al. [4]. They are reviewed here in context specific or unique to the PMRF site.

### **Sediment Parameters**

The nearfield of the MM was gridded as described in Section 1.1 for a coarse sand bottom in the awa defined by 14 grain size bins according to the grain size distribution as shown in Figure 28. The pie chart reveals that 70% of these channel sediments are carbonate, derived from biogenic processes and reef fragments. The carbonate sediments comprise the majority of the coarser size bins in Figure 28. The finer fractions are predominately sediments of terrigenous origin and make up about 27% of the awa sediments. Generally, mean grain sizes of sandy sediments from



streams draining the leeward sides of Kauai are smaller than those of streams draining the windward sides [36], and the PMRF site is a leeward location. Most of the terrigenous sands along the PMRF beaches, from the Napali Coast, south through Polihale State Park to Barking Sands, are eroded from the Kokee Highlands, a remnant of a shield volcano that is dissected on its western side by numerous small intermittent streams and outwash areas. Drainage basins under erosion on the leeward side drain older geomorphic surfaces, which when combined with smaller amounts of leeward rainfall, results in a longer duration of predominantly chemical weathering, with greater fining and rounding of eroded sand-sized fractions. The small percentage of organics in the PMRF sand sample is another characteristic of the terrigenous sediment yield of the lee side watersheds. On the other hand, the sediments discharged from drainage basins on the windward side are eroded from younger, more vegetated geomorphic surfaces having steeper gradients exposed to higher rainfall, resulting in larger sand-sized fractions with higher organic content. Therefore, a windward/leeward segregation of grain size parameters is probably necessary when initializing the model for generic biogenic reef environments.

Of course for this particular demonstration season, late winter through spring, the dominant winds and waves are from the west, so the hydrodynamic forcing functions are typical of a windward shore.

In general, the sediment properties of biogenic reef environments as represented by Kauai are distinctly different from those of previously studied UXO experimental sites along collision and trailing edge coastlines [4]. The MMFT and FRF sites on the coasts of Washington and North Carolina, respectively, were comprised almost entirely of well-sorted, fine-grained quartz sediments of terrigenous origin. In contrast, the Kauai site presents a composite of coarse-grained carbonate and fine-grained volcanic sediments that is less well sorted and contains a higher percentage of organics (although not enough to produce granular cohesion). The lithified side walls of the channels in the biogenic reef also introduce longshore barriers to sediment transport, analogous to what is found in densely packed groin fields along well developed coastlines [36]. These obstructions to longshore transport tend to compartmentalize the sediment transport to the along channel axis of the awas.



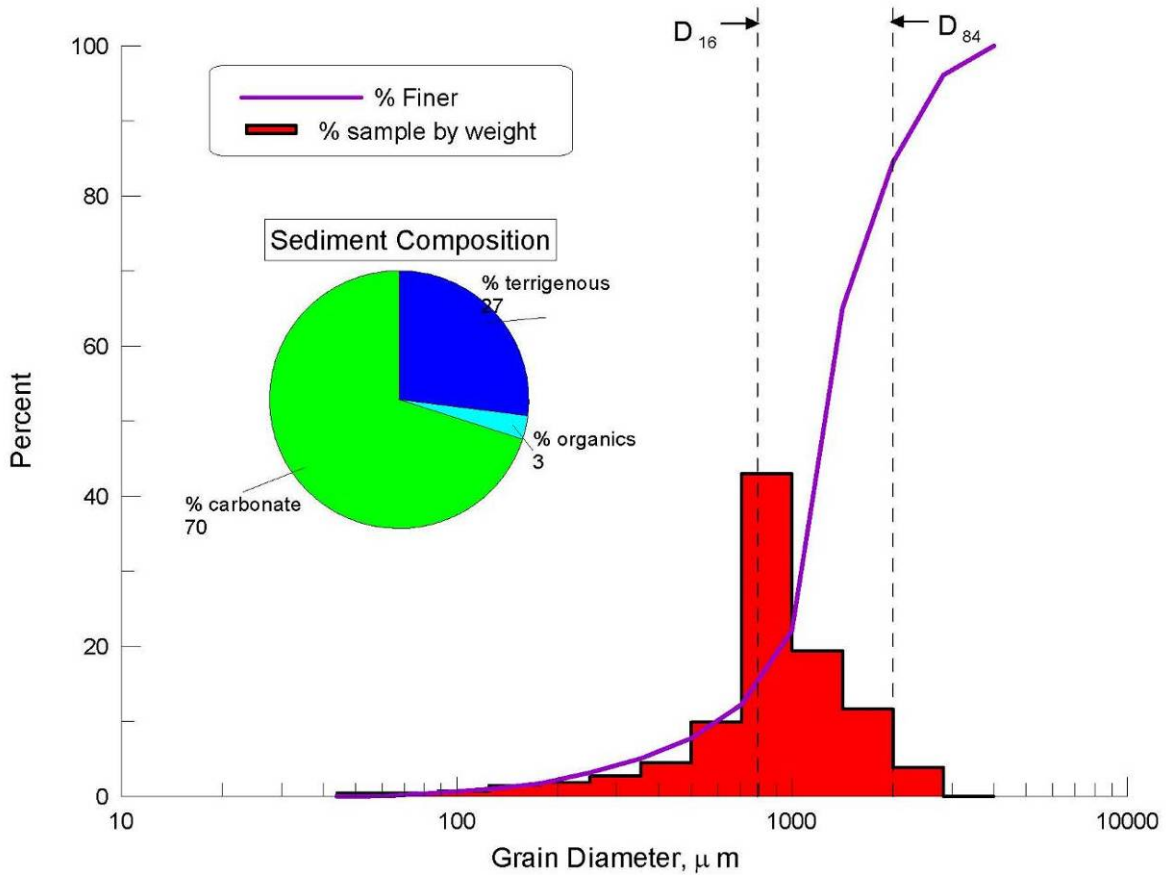


**Figure 28. Grain size distribution of sediment – PMRF Field Test site, Kauai, May 2007; data provided by Sea Engineering, Inc.**

### 6.2.2 UXO Shape Lattice

To provide a systematic and manageable set of inputs for shape specific calibration parameters we concentrated our model simulations on the 5"/38 projectile shown in Figure 16. These rounds were approximated by an elliptic frustrum revolved about the major axis of the round, say the  $y$ -axis, taken for example as the transverse axis to the mean flow as shown in Figure 20. For this orientation the generalized shape of the round can be represented by the analytic expression:

$$R(y) = a - a \left( \frac{y}{S} \right)^\beta \quad (1)$$

Here  $a = D/2$  is the basal radius and  $D$  is the basal diameter of the round;  $R(y)$  is the local radius at any arbitrary location  $y$  along the major axis of the round;  $S$  is the total length of the round as measured along the  $y$ -axis; and  $\beta$  is a constant that adjusts the pointedness of the round. A best fit of equation (1) to the 5"/38 round using the dimensions shown in Figure 16

found that  $\beta = 3.5$ . To accommodate these dimensions and the small radius curves of the shape, the VORTEX shape lattice file was gridded for 3mm grid cells.

### 6.2.3 Burial and Migration on Planar Carbonate Sediment Beds

Prior to considering the nearfield influence of the channel walls on the burial migration response of the UXO at PMRF, we test the performance of the shape lattice files using the coarse-grained carbonate sediment distribution from Figure 28 on a planar bed, (with no extraneous irregularities in either the stream-wise or cross stream directions). Figure 29 presents the modeled instantaneous vortex and scour field produced from an initially planar bed with the UXO resting proud on the bed with the major axis of the round aligned transverse to a train of monochromatic waves with 12 sec period propagating from right to left. The wave oscillatory velocity amplitude at the top of the bottom boundary layer is 96 cm/sec. This velocity amplitude corresponds to the super-critical transport regime [38] for the grain size distribution in Figure 28. In this regime, flow separation with a basal vortex is observed on the down-wave (shoreward) side of the round, inducing formation of a scour hole. As the scour hole deepens, the round slips or rolls into the hole, resulting in migration and burial through what is known either as a scour and slip or scour and roll burial sequence [38, 39, 40, 41, 42]. At the instant the flow field in Figure 29 was calculated, the burial/ migration progression of the UXO had advanced to a state of 55% burial; this flow diagram is typical of the 24 surrogates that were installed at PMRF. The UXO surrogate is shown 55 % buried in a coarse sand bottom under a wave crest propagating from left to right at super-critical velocity amplitude.

At an advanced stage in the burial/migration progression referred to as *lock-down*, burial becomes sufficiently extensive that migration is no longer possible [38, 41, 42]. For excitation by monochromatic waves of various periods and heights, the distance a UXO migrates before lock-down sets up has a monotonic dependence on a parameter of dynamic similitude referred to as the Shield's parameter. This parameter is a measure of the intensity of environmental forcing relative to the inertia of the UXO. Explicitly, the Shields parameter,  $\Theta$ , represents a ratio between the hydrodynamic forces (drag and lift) acting to move the UXO and the gravitational forces acting to restrain and bury the UXO, where

$$\Theta = \frac{u^2}{g'D} \quad (2)$$

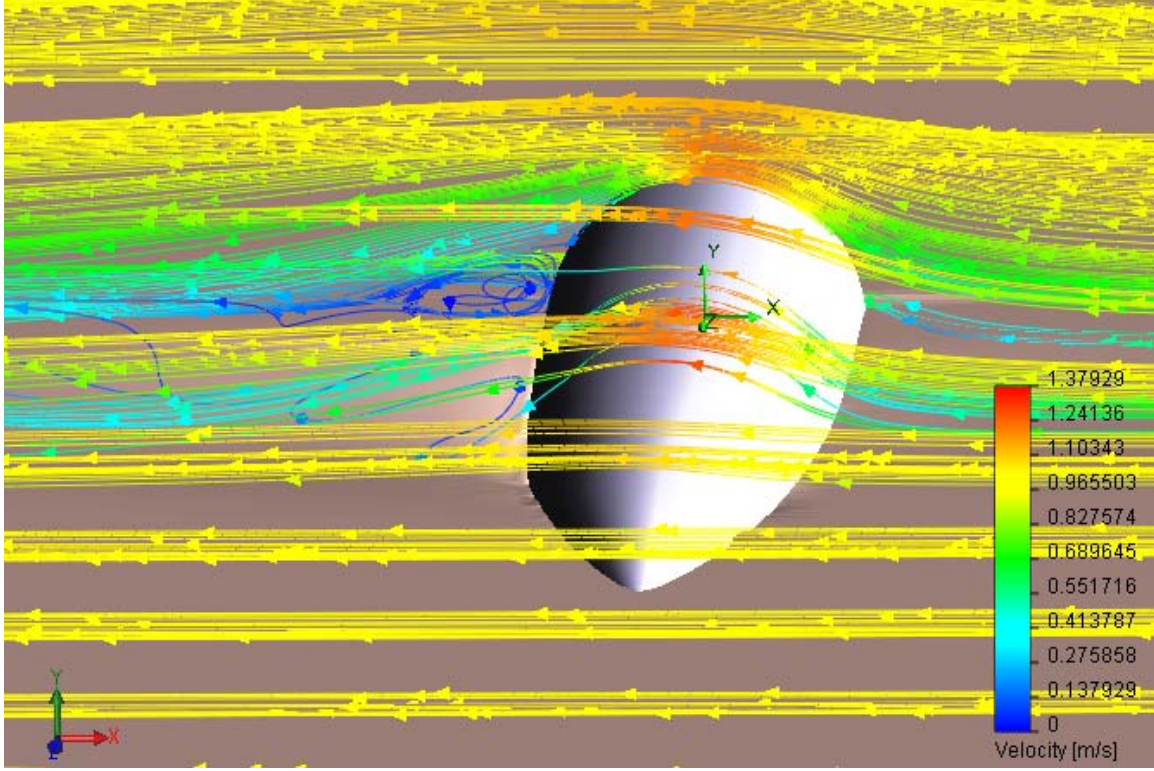


**Figure 29. Simulation of vortex and scour field in the nearfield grid of the 5''/38 UXO surrogate.**

In equation (2),  $u$  is the oscillatory wave velocity amplitude at the top of the bottom boundary layer;  $D$  is the basal diameter of the UXO;  $g' = g \Delta\rho / \rho$  is a form of reduced gravity,  $g$  is the acceleration of gravity; and  $\Delta\rho$  is the density difference between the UXO and seawater density,  $\rho$ . Planar bed simulations of the type shown in Figure 29 indicate that UXO mobility increases with increasing wave velocity (proportional to wave height and inversely proportional to wave period); with decreasing caliber of the UXO; or with decreasing density (specific gravity) of the UXO. Planar bed simulations using the wave velocities measured at PMRF (Figure 27) reveal that with the exception of a few storms early in the deployment the Shields parameter for the most part was sub-critical, meaning that  $\Theta \leq 7$ ; Jenkins et al. [38], Donohue and Garrison [41], Inman and Jenkins [42], and Fu et al. [36] for additional details regarding sub- and super-critical transport regimes). When the Shields parameter is sub-critical, very little movement of the UXO occurs because hydrodynamic moments associated with drag, lift are insufficient to overcome the restraining moments due to gravity [36, 38]. The reasons for this condition during the PMRF demonstration are due to a combination of benign wave climate and vertical divergence of the wave induced surges and streaming over the reef channels.

#### 6.2.4 Eddies and Secondary Flows from Awa Channel Sidewalls

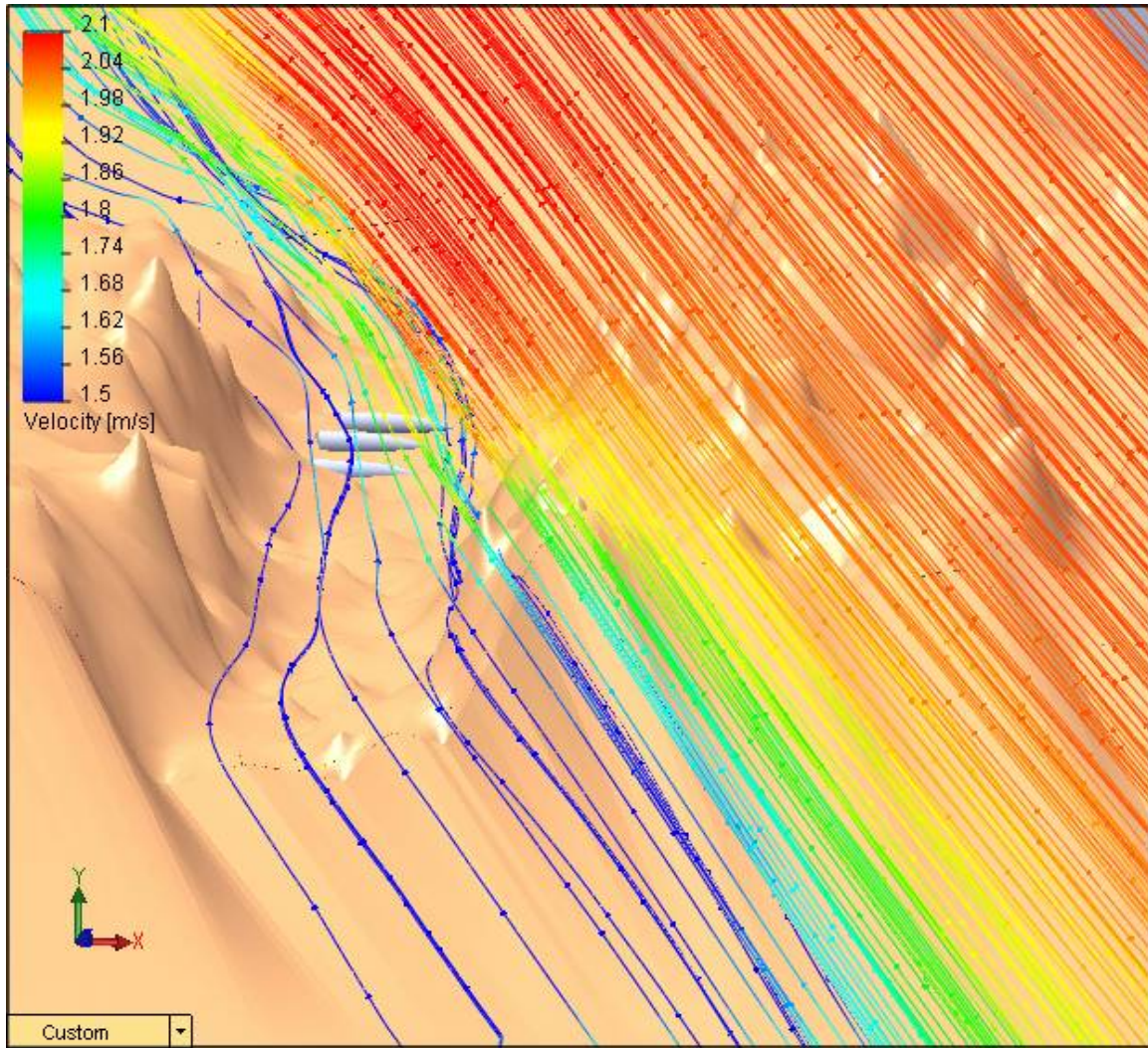
Awa side wall influence on the nearfield flow dynamics are one of the most unique features of the biogenic reef environments. Figure 30 shows a typical edge of the awa site for the 13 February to 27 June 2007 UXO experiment. Note the wall surface roughness and curvature of the lithified reef structures. They were not previously encountered at the other UXO experimental sites (collision and trailing edge coasts, see Fu et al. [36]). Both the gridded LIDAR data and underwater photos of the test site reveal that the channels introduce both curvature effects and roughness effects on the flow of wave surges and wave induced streaming. These flow disturbances undoubtedly produce eddies that could induce additional vortex scour to the nearfield of the UXO over and above that excited directly by the UXO shape. This increases the modeling challenge by forcing us to expand the nearfield grid to include the prominent features of awa side walls in the immediate neighborhood of the UXO site. It is neither practical nor numerically efficient to extend the 3mm resolution of the shape lattice of the UXO across tens of meters of adjacent awa channel sidewalls. Therefore we nested a coarser scale lattice of the awa wall geometry around the UXO shape lattice and embedded it inside the farfield grid of the reef platform. This merely required replicating existing code to create a secondary nested grid inside module #13 of the model architecture (see Figure 17). Grid resolution was set at 0.5m for the secondary nested grid of the sidewall geometry around the UXO field.

Figure 31 gives a MM simulation of the curvature effects of the awa in the neighborhood of the offshore UXO field. The channel features were resolved by the nested nearfield grid at 0.5m grid cell accuracy using LIDAR data in Figure 23. Vertical divergence of the flow field between the top of the reef and the bottom of the channel is accentuated over the UXO field because it is sited on the inside of the channel bend for onshore directed surges and wave-induced streaming. There is also a tendency for the near channel bottom flow to develop secondary meanders that can introduce cross-flow components over the UXO surrogates. The primary consequence of these secondary flows and vertical divergence phenomena is to promote sub-critical flow conditions over the UXO that retard migration while promoting burial.



**Figure 30. Awa channel sidewall at intersection with carbonate sedimentary floor at PMRF; photo courtesy of Sea Engineering, Inc.**





**Figure 31. Simulation of vertical divergence and secondary flows induced by curvature of awa axis in the vicinity of the offshore site at PMRF, Kauai.**

The second major influence of the awa sidewalls stems from the encroachment of shoulders of the sidewalls into the sand channel. These shoulders project a rather large scale disturbance into the primary up/down channel, along axis flows. These disturbances in turn can generate rather large scale eddies, much larger than those shed by the relatively small body radius of the UXO. In Figure 32, the nested secondary grid of the MM was used to simulate these large scale channel vortices near two of the twelve UXO in the offshore field. This simulation is representative of the sub-critical channel surges recorded by the ADCP in Figure 26 for which  $u \sim 0.4$  m/sec. In spite of the low velocities in the bottom of the channel, the encroaching sidewall is able to excite a large channel eddy with high vertical velocity component  $w \sim 0.2$  m/sec.

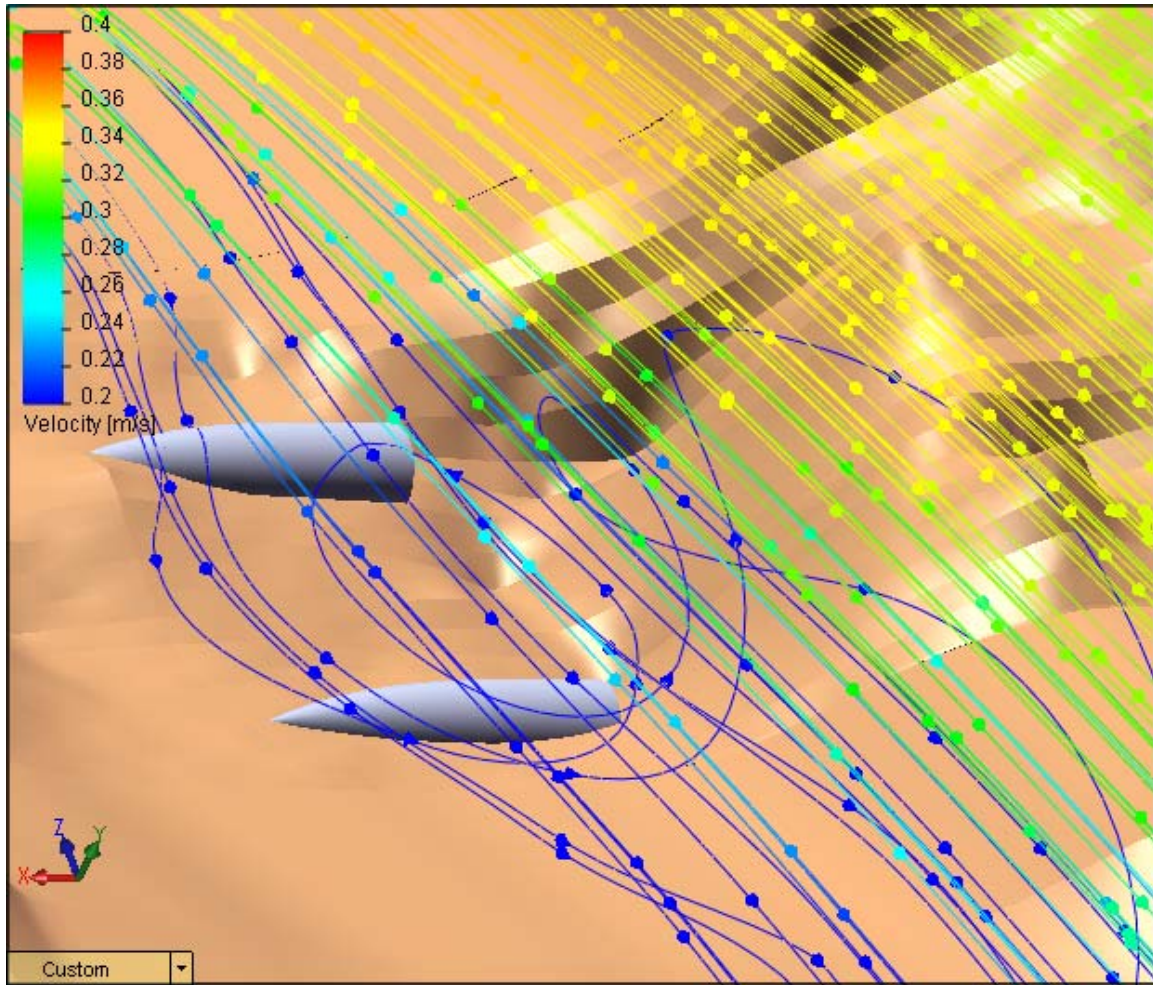


**Figure 32. Simulation of large scale eddies over UXO induced by encroaching shoulders of awa sidewalls in the vicinity of the offshore site at PMRF, Kauai.**

Vertical velocities of this magnitude in the nearfield of the UXO are capable of excavating large scour depressions into which the UXO can readily roll [38, 39, 40, 41, 42]. Thus, large external channel eddies can facilitate UXO migration even when the Shields parameter remains sub-critical.

### **6.2.5 UXO Migration/Burial Model Performance at PMRF Experiment**

The model performance is tested against data from two separate UXO sites deployed in an awa in the nearshore of PMRF, Kauai, HI, between 13 February and 27 June 2007. The details of the lay-down pattern of 12 each UXO surrogates of a 5"/38 naval rounds that were deployed at each of the two test sites (24 surrogates in total) is shown in Figure 33. At both the offshore and inshore sites, surrogates were laid in two along-channel rows 30 ft apart at 30 ft spacing with six surrogates in each row. The surrogates were deployed on 13 February 2007 and thereafter the



position and burial depths of some or all of the surrogates was measured on 22 February, 2 March, 21 March, 13 April, 9 May, 31 May, and 27 June 2007.

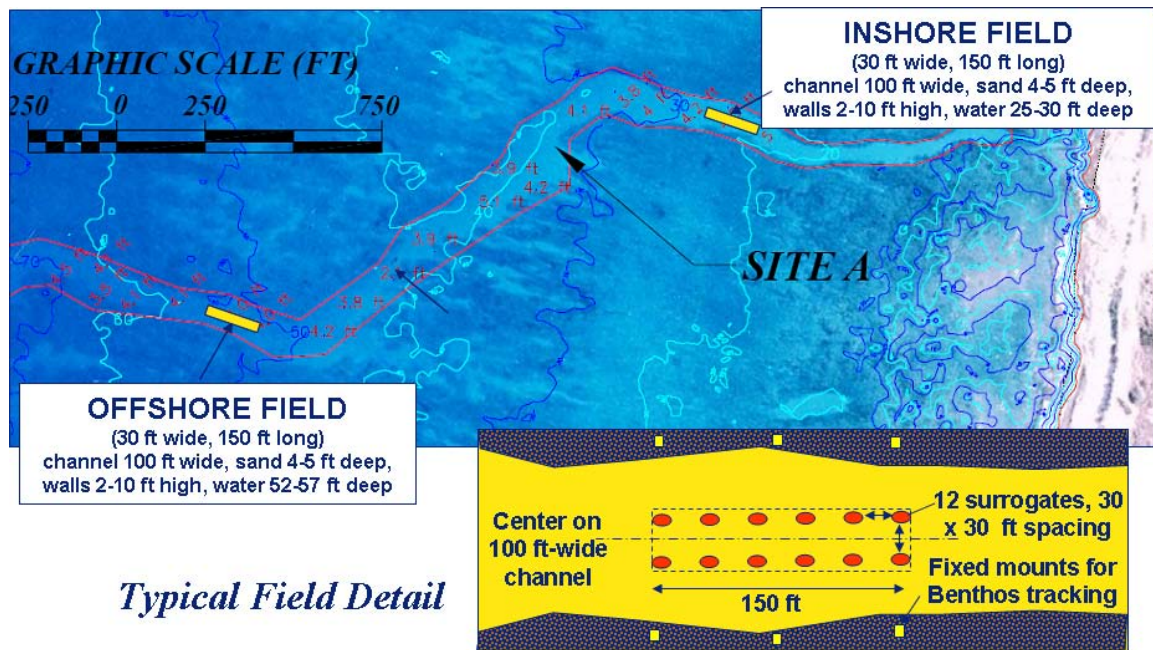


**Figure 33. Details of lay-down pattern of UXO surrogate fields at PMRF.**

Because the surrogates all became buried during the experiment, the primary method for locating the surrogates was an acoustic ranging technique utilizing embedded pingers and four transponders mounted about the perimeter of each test site. Figure 34 gives a schematic of the technique that was perfected at earlier UXO experiments at Ocean Shores, Washington, and Duck, North Carolina [2]. Because of reverberation concerns from the awa sidewalls at PMRF, the accuracy of this acoustic ranging technique was verified during the 13 April 2007 survey, when the acoustic range data was compared against tape measurements between each of the four transponders and the UXO specimens. The acoustic measurements showed a consistent underestimation of the range to the surrogates. This error averaged 0.6m and had a standard deviation of 0.4 m. The acoustic range data was subsequently corrected for this systematic error.

Burial depths were measured by penetration probes that were inserted into the sand bed at the surrogate locations indicated by the acoustic range data. Probes were hand driven by divers and refusal depths recorded manually. All refusal depths were substantially less than the known thickness of the sediment cover in the awa, which averaged 4-5 ft (~140 cm). Consequently refusal depth was taken as equivalent to burial depth.



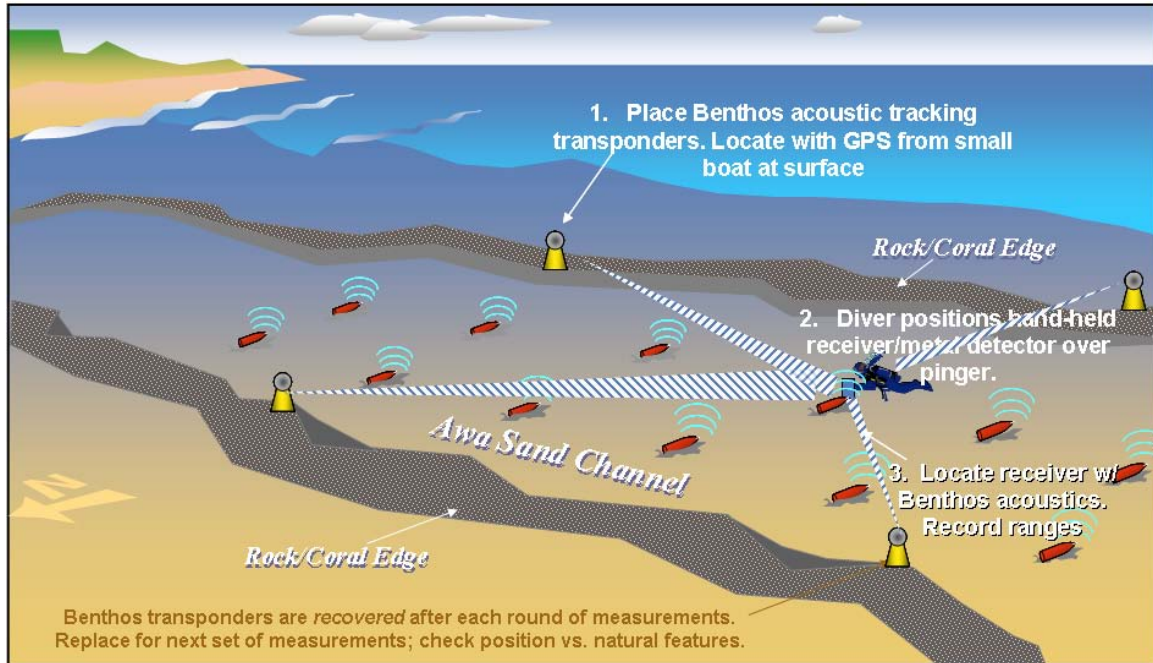


**Figure 34. Schematic of acoustic transponder ranging technique for locating position of UXO surrogates during the PMRF experiment.**

#### 6.2.5.1 Model Predictions of UXO Migration and Burial Rates

Migration and burial of each of the 24 UXO in the inshore and offshore sites at PMRF (Figure 33) were simulated by the MM for the wave and current forcing measured by the ADCP and the grain size distribution. Wave forcing measured at the offshore site by the ADCP was corrected to the inshore site using refraction/diffraction analysis. The vertical divergence and large scale eddies induced by the awa side wall geometry was computed separately for the offshore and inshore sites. These simulations were based on the high resolution bathymetry applied to nested secondary gridding of the channel as demonstrated in Figure 31 and Figure 32.

Figure 35 gives the MM simulated migration and burial rates during the entirety of the PMRF experiment averaged over the 12 surrogates in the inshore test site. Blue crosses indicate the individual simulations of migration for each wave measurement in Figure 26 that caused some increment of migration to occur.

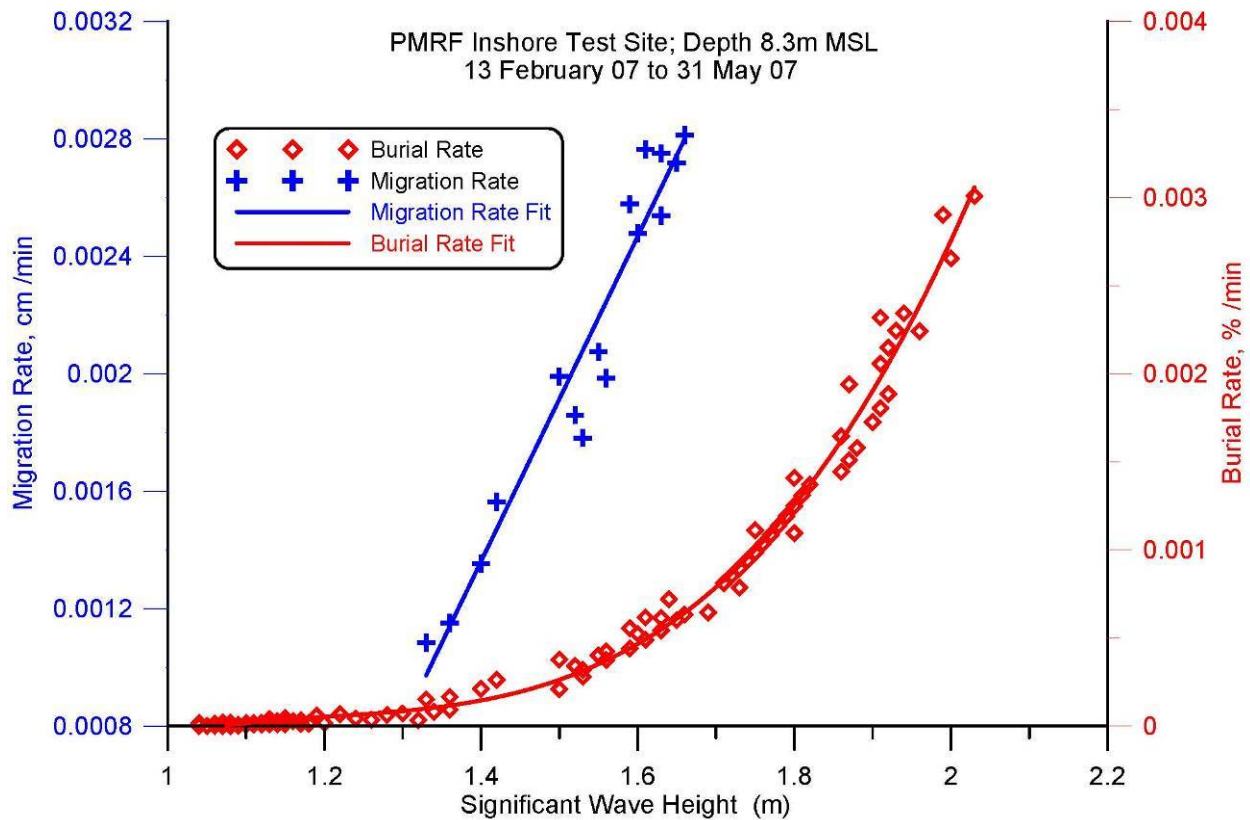


**Figure 35. VORTEX model simulation of migration and burial rates of 5"/38 UXO surrogates at the inshore site at 8.3m depth as a function of measured wave heights.**

Similarly, the red diamonds in Figure 35 give simulations of burial for each wave measurement in Figure 26 that caused some increment of burial to occur. Here burial is expressed in terms of burial depth as a % of the diameter (caliber) of the round. The obvious difference in the numbers of blue crosses versus red diamonds indicates that relatively few wave events caused the rounds to actually move. This reflects the fact that the surrogates became completely buried under many centimeters (20-50 cm) of overburden, whereas migration is halted by lock-down that sets up while the surrogates are still only partially buried. The solid blue and red lines in Figure 35 are best-fit polynomials to the simulated points generated by the individual wave events. No model realizations are shown for waves heights less than 1m because smaller waves produce bottom velocities at 8.3m depth that are less than the threshold of motion of the median grain size of sediment.

The scatter about each of the fit lines in Figure 35 is due to the wave period dependence of migration and burial rate, which for these shallow water conditions is second order relative to wave height dependence. From this outcome, the average threshold of migration for the 5"/38 UXO surrogates appears to be at a significant wave height of approximately 1.3 m at water

depths of 8.3 meters. From this threshold, migration rates increase rapidly with increasing wave height, roughly tripling with an increase of only 0.3 m in wave height. While this process occurs, burial rates increase at first slowly, from negligibly small rates at threshold of migration wave heights, to rapidly increasing rates as burial lock-down is approached, which takes place in the neighborhood of significant wave heights of 1.6 m. Maximum migration rates are approximately 0.0028 cm/min. Beyond burial lock-down, the burial rate continues to accelerate until total burial is achieved, when the scour burial mechanism vanishes and only farfield burial from bottom profile change can effect any subsequent burial. Scour burial maximums for the 5"/38 surrogates occur at significant wave heights of approximately 2m at a rate of 0.003 % per minute, though this result is somewhat controlled by the particular sidewall effects of the awa at the inshore site.

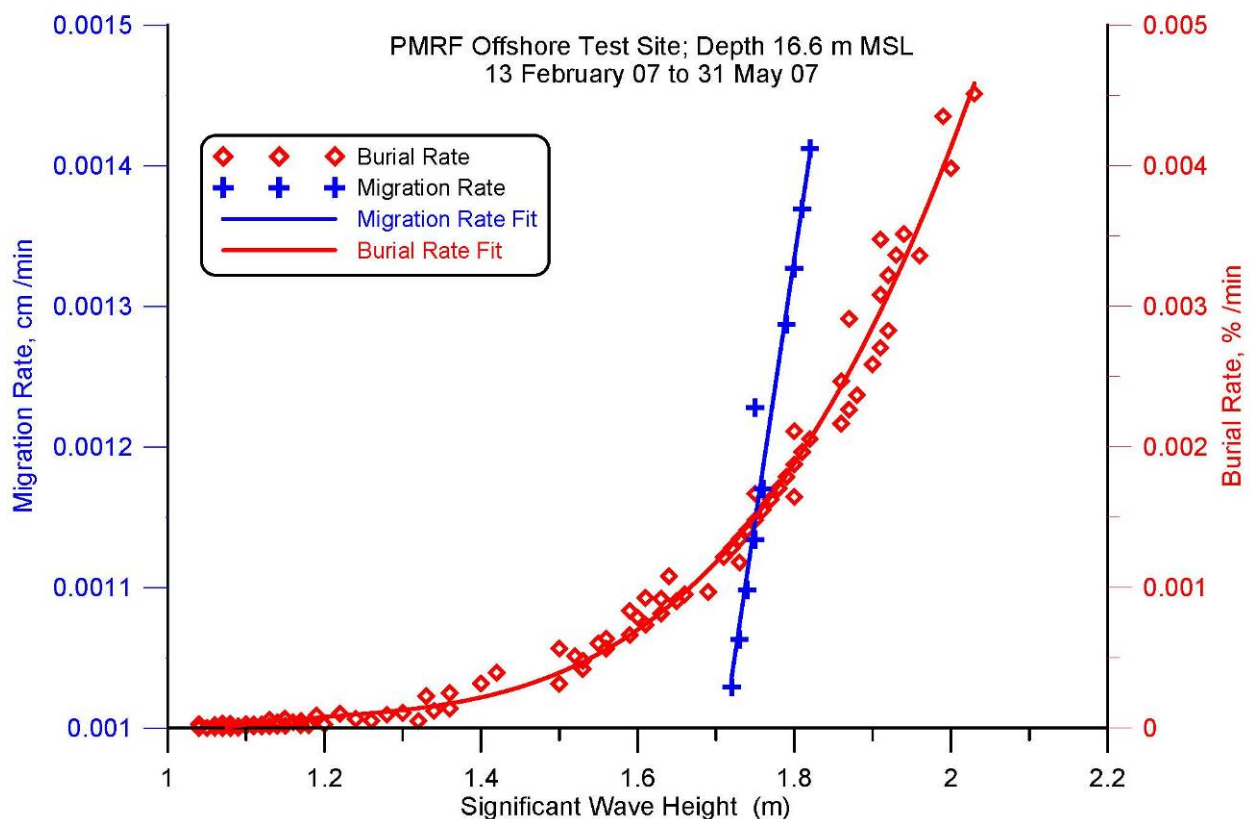


**Figure 36. VORTEX Model simulation of migration and burial rates of 5"/38 UXO surrogates at the offshore site at 16.6m depth as a function of measured wave heights**

Figure 36 provides the average simulated migration and burial rates for the 12 surrogates in the offshore test site at PMRF at 16.6m mean depth. Again, blue crosses indicate the simulations of migration for each wave measurement that caused some increment of migration to occur; and, red diamonds give simulations of burial for each wave measurement that caused some increment

of burial to occur; where burial is expressed in terms of burial depth as a % of the diameter of the round. For clarity, the axes in Figure 36 were re-scaled for the differences in dynamic range. Upon comparing Figure 36 with Figure 35, it is apparent that the threshold wave height for migration of the UXO surrogates in the offshore array is substantially higher (increasing to a significant wave height of 1.7m), primarily due to depth attenuation of the wave orbital velocity in the deeper waters of the offshore site. For the same reason, there are fewer numbers of wave events that induce migration at the deeper offshore site; compare numbers of blue crosses in Figure 36 with those in Figure 35. However, once the UXO surrogates in the offshore array begin to move, their migration rate increases rapidly, increasing 140% with a 0.1m increase in wave height above threshold of migration and reaching a maximum migration rate 0.0015 cm per minute at significant wave heights greater than 1.8m. This maximum migration rate is approximately one half that of the surrogates in the inshore array and occurs at a substantially higher significant wave height (1.8 m vs. 1.6 m), again because of depth attenuation in orbital wave velocities. At their maximum migration rate, surrogates in the offshore array are burying at 0.0019 % per minute while surrogates in the inshore array are burying at approximately 1/3 that rate, or 0.0005 % per minute. Thus, surrogates in the offshore array reach burial lock-down sooner and thereby have less time to migrate off-station.

Maximum burial rates of surrogates in the offshore array are 0.0045 % per minute at a significant wave height of 2m, or about 50% faster than for surrogates in the inshore array. While this may be partly understood in terms of slower migration rates going hand-in-hand with higher burial rates, it is not intuitive when considering that burial rates tend to increase with orbital velocity while orbital velocity decreases with increasing depth. Our interpretation of this specific and somewhat paradoxical result is that the large scale eddies induced by the awa sidewalls are more active and well developed at the offshore site, and this action increases scour burial rates induced by relatively smaller orbital velocities.

#### **6.2.5.2 Predictive Skill of Model Predictions**

Here we apply two approaches to assessing the predictive skill of the quantitative model predictions of the magnitude of migration and burial of UXO surrogates at PMRF. By the first approach, we construct probability density functions of migration and burial magnitudes predicted by the model and compare them with the probability density functions assembled from the observed outcomes of the experiment. Because the experimental outcomes involve small ensemble statistics, we merge the results of all 24 surrogates from the inshore and offshore test sites (Figure 33) into a single set of probability density functions. By the second approach, we compute predictive skill factor  $R$  from the mean squared error between the predicted and measured outcomes.

To generate predictions of migration and burial magnitudes from the rates in Figure 35 and Figure 36, we integrate those rates (as computed for each surrogate) over the duration of each migration or burial rate-inducing wave event. Figure 37a presents the probability density function (histogram) of the predicted UXO migration distances for all 24 surrogates at PMRF. A total of 312 realizations of migration distance were constructed from the rates (blue crosses) in Figure 35 and Figure 36. These are contrasted with the 24 measured realizations of migration

distance that make up the measured probability density function in Figure 37b. The peak, spread and shape of the predicted and measured probability density functions of migration in Figure 37 are quite similar, although the granularity of the measured distribution is much coarser owing to the relatively small numbers of observations. Both distributions give a mean migration distance of about 1m and a maximum migration of slightly more than 3m. In both the predicted and observed outcomes, migration was almost exclusively along the axis of the awa channel.

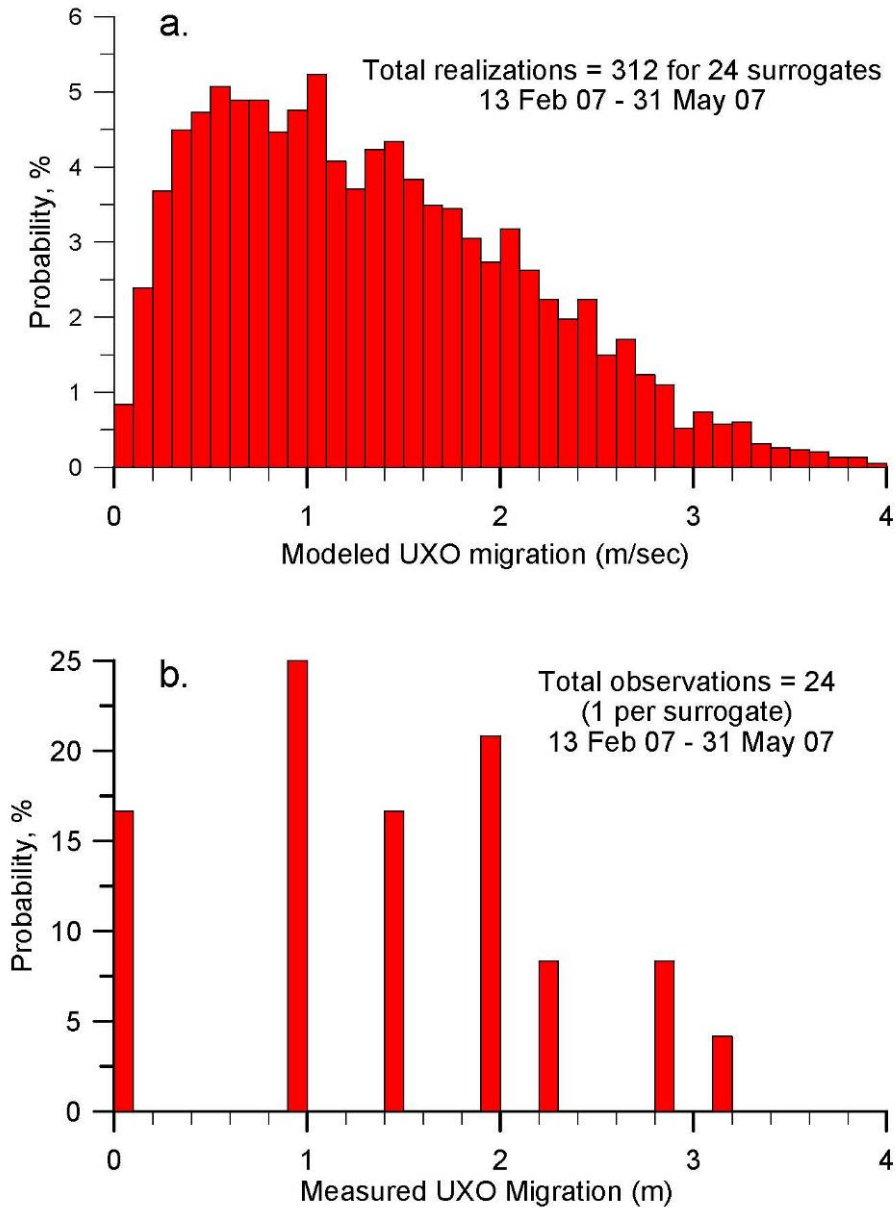


**Figure 37. Comparison of modeled probability density function for UXO migration (a) versus the measured probability density function (b) for all surrogates at the PMRF test sites, 13 February – 27 June 2007.**

Migration at PMRF was approximately double the values measured for the same type of surrogates deployed on a collision coast at Ocean Shores Washington. Although the Pacific Northwest deployment took place over the span of only 1 to 2 days – very brief by comparison to PMRF – the surrogates were placed directly in the surf zone instead of fully submerged offshore. Similarly, migration magnitudes at PMRF were on average about 1/3 what was observed for

similar surrogates deployed on a trailing edge coast at Duck, NC. The length of the FRF Duck deployment was approximately seven times the duration of the PMRF experiment. None of the three UXO experiments observed effects from any extreme event storms. With these gross comparisons, it is evident that a certain degree of monotonic migration behavior exists over the time UXO spend in the environment in the absence of extreme events.

Figure 38 compares the predicted versus measured probability density functions for UXO burial at PMRF during the period 13 February to 27 June 2007. The larger numbers of burial-inducing wave events in Figure 35 and Figure 36 produced nearly 10 times more realizations (3,806) of predicted burial in Figure 38a. The comparison with measured probability density function for burial in Figure 38b is quite satisfying, despite the small ensemble of measured statistics. Again, the peak of the measured distribution, its breadth, and shape are all faithfully mimicked by the modeled distribution in Figure 38a. Mean burial depths are approximately 20 cm while maximum burial depths are slightly over 40 cm. These burial depths are greater than what was observed during the brief deployment at Ocean Shores, Washington, and on a par with the inshore surrogates at Duck, NC.

Using the analytical statistical approach to error assessment, we compute the predictive skill factor  $R$  of the UXO migration distance,  $\xi$ , and burial depth,  $h$ , as quantified by an estimator adapted from the mean squared error. The foundation reference for the skill factor, its definition, and acceptable limits was originally treated in Gallagher et al. [43].

It was later used in the equilibrium beach profile paper that now is considered the keystone reference for this type of modeling: Jenkins and Inman's "Thermodynamic solutions for equilibrium beach profiles" [35].

For burial depth the skill factor would have the following form adapted from Gallagher et al. [43]:

$$R_h = 1 - \frac{1}{N\hat{\sigma}_i} \left\{ \sum_{i=1}^{i=N} [\hat{h}(i) - h(i)]^2 \right\}^{1/2} \quad (3)$$

where  $\hat{h}(i)$  is the measured burial depth for  $i = 1, 2, \dots, N$  observations,  $h(i)$  is the predicted burial depth for the  $i^{th}$  observation, and  $\hat{\sigma}_i$  is the standard deviation of all observations over the period of record.

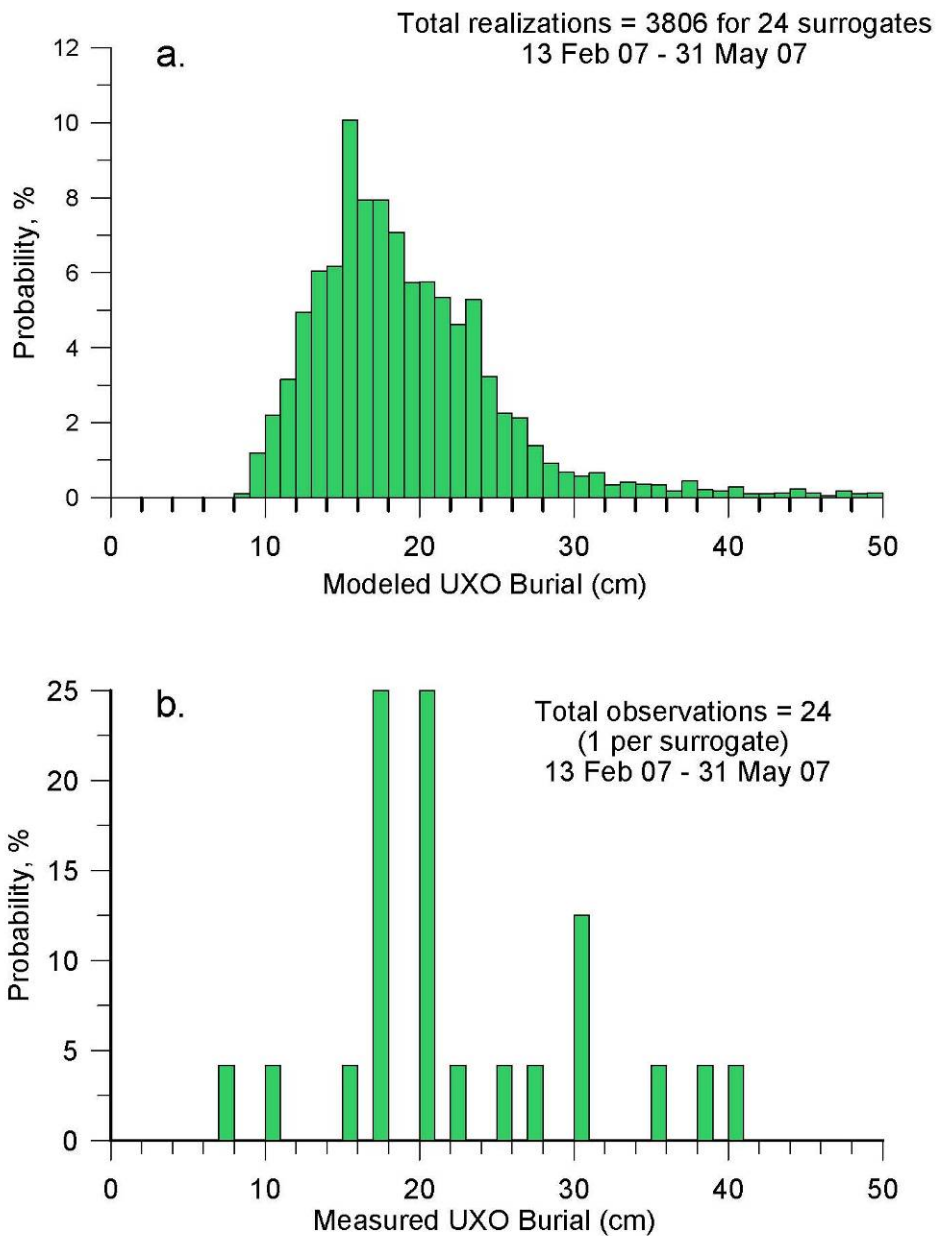


**Figure 38. Comparing probability density functions for UXO burial of all surrogates during the PMRF demonstration: modeled (a) versus measured (b).**



For migration distance the skill factor would have the form:

$$R_{\xi} = 1 - \frac{1}{N\hat{\sigma}_i} \left\{ \sum_{i=1}^N [\hat{\xi}(i) - \xi(i)]^2 \right\}^{1/2} \quad (4)$$

where  $\hat{\xi}(i)$  is the measured migration distance for  $i = 1, 2 \dots N$  observations,  $\xi(i)$  is the predicted migration distance for the  $i^{th}$  observation. Based on these formulations and the predicted versus measured outcomes in Figures 21 & 22, the skill factor for migration at PMRF was calculated at  $R_{\xi} = 0.88$  and  $R_h = 0.90$  for burial. For coastal processes modeling and mine burial prediction in particular, any skill factor in excess of 0.8 is considered to be a good result [43].

### 6.2.5.3 Conclusions From PMRF (Hawaii) Field Test

A process-based MM was developed and exercised during the winter-spring season at two separate offshore sites on the leeward side of a biogenic reef environment off the west coast of the island of Kauai, HI, at PMRF. The MM generated simulations of hydrodynamic forcing, and UXO migration and burial that were in general agreement with the ensemble results from 24 inert surrogates of a 5"/38 projectile that were monitored between 13 February and 27 June 2007. The field demonstration met all objectives, except that no "extreme" weather event occurred during this effort. All the required data were collected and all field demonstration surrogates and associated instruments were successfully recovered.

The following conclusions are derived from the demonstration results and the following MM calibration and validation analysis:

- The biogenic reef environment is the most challenging UXO modeling problem encountered to date because of the complex micro-bathymetry associated with the awa that cut through the fringing reef. Awa side walls influence the nearfield flow dynamics, presenting a tedious challenge to the requirement for a regular gridding of the model domain. Meeting this challenge did not necessitate generating new MM code, but did require the availability of high resolution LIDAR bathymetry data and considerable computer memory for operating on the resulting dense grids. Reef channels introduce both curvature effects and roughness effects to the flow of wave surges and wave induced streaming. These flow disturbances produce vertical divergence in the flow over UXO and introduce large scale eddies to the nearfield of the UXO that induce additional scour to that excited directly by the UXO shape.
- Awa channels confine a sediment cover of complex composition that alters parameters of the granular transport equations in the model. The composition of this sediment cover varies considerably between the windward and leeward sides of these biogenic reef environments, requiring a separate set of granular parameters for the opposing sides of the reef environment. Typically 70 % of awa sediments are carbonate, derived from

biogenic processes and reef fragments. The carbonate sediments comprise the majority of the coarser size bins. The finer fractions are predominately sediments of terrigenous origin and generally make up about 27 % of reef channel sediments, while 3 % are organics, a major portion of which is also of terrigenous origin. These terrigenous sediments and organics are delivered to the reef environment by small local intermittent streams and headward erosion of sea cliffs. Generally, mean grain sizes of sediments from streams draining the leeward sides are smaller than those of streams draining the windward sides.

- Model predictions and measurements were presented for 24 surrogates of a 5"/38 projectile divided equally between a shallow water inshore site in 8.3 m local depth and a deeper offshore site in 16.6 m local depth. Both sites occupied the same area that made several turns and bends between the two sites. The average threshold of migration for the 5"/38 UXO surrogates at the shallow site appears to be at a significant wave height of approximately 1.3 m. From this threshold, migration rates increase rapidly with increasing wave height, roughly tripling with an increase of only 0.3 m in wave height. While this occurs, burial rates increase at first slowly from negligibly small rates at threshold of migration wave heights to rapidly increasing rates as burial lock-down is approached, at significant wave heights of approximately 1.6 m. Maximum migration rates are approximately 0.0028 cm/min. Beyond burial lock-down, the burial rate continues to accelerate until total burial is achieved, whence the scour burial mechanism vanishes and only farfield burial from bottom profile change can effect any subsequent burial. Scour burial maximums for the inshore site occur at significant wave heights of about 2m at a rate of 0.003 % per minute (although this result is somewhat controlled by the particular sidewall effects of the channel at the inshore site). The threshold wave height for migration of the UXO surrogates at the offshore array is substantially higher and increases to a significant wave height of approximately 1.7m, primarily due to depth attenuation of the wave orbital velocity in the deeper waters of the offshore site. For the same reason, there are fewer numbers of wave events that induce migration at the deeper offshore site. However, once the UXO surrogates at the offshore site begin to move, their migration rate increases rapidly with wave height, reaching a maximum migration rate 0.0015 cm per minute at significant wave heights greater than 1.8m. This maximum migration rate is about one half that of the surrogates at the inshore site and occurs at a substantially higher significant wave height (1.8 m vs. 1.6 m), again because of depth attenuation in orbital wave velocities. At their maximum migration rate, surrogates in the offshore array are burying at 0.0019 % per minute while surrogates in the inshore array are burying at about 1/3 that rate, or 0.0005 % per minute. Thus, surrogates in the offshore array reach burial lock-down sooner, and thereby have less time to migrate off-station. Maximum burial rates of surrogates in the offshore array are 0.0045 % per minute at a significant wave height of 2m, or about 50% faster than for surrogates in the inshore array. This is not an intuitive result when considering that burial rates tend to increase with orbital velocity while orbital velocity decreases with increasing depth. Our interpretation of this specific and somewhat paradoxical result is that the large scale eddies induced by the area sidewalls are more active and well developed at the offshore

site, and this action increases scour burial rates induced by relatively smaller orbital velocities.

- Two approaches were applied to assessing the predictive skill of the quantitative model predictions of the magnitude of migration and burial of UXO surrogates at PMRF. The first approach was to construct probability density functions of migration and burial magnitudes predicted by the model and compare them with the probability density functions assembled from the observed outcomes of the experiment. The second approach computed predictive skill factor,  $R$ , from the mean squared error between the predicted and measured outcomes. The peak, spread, and shape of the predicted and measured probability density functions of migration are quite similar. Both distributions give a mean migration distance of approximately 1m and a maximum migration of slightly greater than 3m. In both the predicted and observed outcomes, migration was almost exclusively along the axis of the wave. The peak of the measured burial probability distribution, its breadth, and shape are all faithfully mimicked by the modeled distribution. Mean burial depths are about 20 cm while maximum burial depths are slightly greater than 40 cm. These burial depths are greater than what was observed during the brief deployment at Ocean Shores, Washington, and are on a par with the inshore surrogates at Duck, NC. The skill factor for migration at PMRF was calculated at  $R_{\xi} = 0.88$  and  $R_h = 0.90$  for burial. For coastal processes modeling and mine burial prediction in particular, it is noted that any skill factor greater than 0.8 is considered to be a good result.

### **1.23 6.3 Analysis of FRF Duck Field Test Data**

The Vortex Lattice (VORTEX) Scour and Burial Model module within the MM was used to predict migration and burial behavior of UXO surrogates of 5"/38 naval projectiles (Figure 15) when grounded on the seafloor in the near shore of a trailing edge coastal environment. The environment selected for this experiment was the USACE Field Research Facility (FRF) located on the Atlantic Ocean near the town of Duck, North Carolina.

Waves and currents are derived from direct observations by means of the directional wave arrays and Acoustic Doppler Current Profilers (ADCP) maintained by the Field Research Facility at Duck Pier. Fluxes of river sediment are neglected as explicit boundary conditions, but the sediments are accounted for in the grain size distributions of the offshore sediments. The wave and current forcing provides excitation applied to the deep water boundary of the farfield computational domain. These boundaries are specified in the boundary conditions module where the farfield computational domain is assembled from a series of boundary-conforming control cells using a combination of bathymetric data obtained from NOS and United States Geological Survey (USGS) [19, 20, 21, 22, 23] as compiled by the National Geophysical Data Center. From these data bases, the gross morphology of the barrier sand spits and continental shelf along the Outer Banks (Figure 39) were assembled.

With these forcing functions and boundary conditions, the farfield response module (blue box in Figure 17) computes the spatial and temporal evolution of the fluid forcing and bottom elevation along the two littoral cells that comprise the Outer Banks (Figure 39). At the FRF site, these littoral cells are bounded in the cross shore by Cape Henry to the north, Cape Hatteras in the mid-reach where the angle of the coastline makes a dog-leg departure toward the southwest, and Cape Lookout to the south. FRF Duck is located just east of Albemarle Sound, in the center of Figure 39.

Predominately quartz sediments of glacial origin produce cross shore bottom gradients having three matching profile segments: 1) the stationary profile that extends from deep water in the mid-continental shelf region, inshore to closure depth  $h_c$ , where profile changes become vanishingly small, 2) the shorerise profile that continues from closure depth to the wave break point; and, 3) the bar-berm profile that begins at the break point and ends at the berm crest.

The stationary profile is invariant with time and is given by the regional bathymetry. Bottom elevation changes along the non-stationary profiles of the shorerise and bar-berm (Figure 40a) are computed in the farfield response module using equilibrium profile algorithms after Nordstrom and Inman [44], Inman [45], Inman and Chamberlain [46], Stauble [47], and Stauble and Cialone [48]. The stationary and non-stationary profiles are interpolated to create a Cartesian depth grid within each littoral cell on which simultaneous refraction and diffraction patterns are computed to specify fluid forcing by shoaling waves.

Fluid forcing by currents in the farfield are computed where wave induced streaming and mass transport are based on algorithms after the works of Stauble [49], Jenkins and Inman [50], and Kirby [51] and shallow water tidal currents follow from algorithms after Dalrymple et al. [52]. Fluid forcing time series and bottom elevations computed in the farfield response module are through-put to the nearfield response modules shown below the green line in Figure 17. The farfield throughput is applied to the local seabed boundary conditions module (gray box). These local boundary conditions include two types: 1) the slope and elevation of the seabed plane around the object base derived from location in the farfield control cell; and 2) the shape file of the body in question. These two local boundary conditions are used to generate lattice panels that define the object and bedform of the surrounding seabed (Figure 20a). This lattice is the computational domain of the nearfield scour-burial processes in which the method of embedded vortex singularities (vortex lattice method) is applied using algorithms after Longuet-Higgins [53], Lamoure and Mei [54], and Longuet-Higgins [55]. This method employs horseshoe vortices embedded in the near-bottom potential wave oscillation to drive local sediment transport based on ideal granular bed load and suspended load equations after Connor and Wang [56], McCormick [57], and Van Dyke [58]. A horseshoe vortex is specified for each lattice panel during every half-cycle of the wave oscillation as shown in Figure 20. The horseshoe vortices release trailing pairs of vortex filaments into the local potential flow field that induce downwash on the neighboring seabed (Figure 20b), causing scour with associated bed and suspended load transport as computed. This scour action by trailing vortex filaments can be seen occurring in nature in Figure 21.

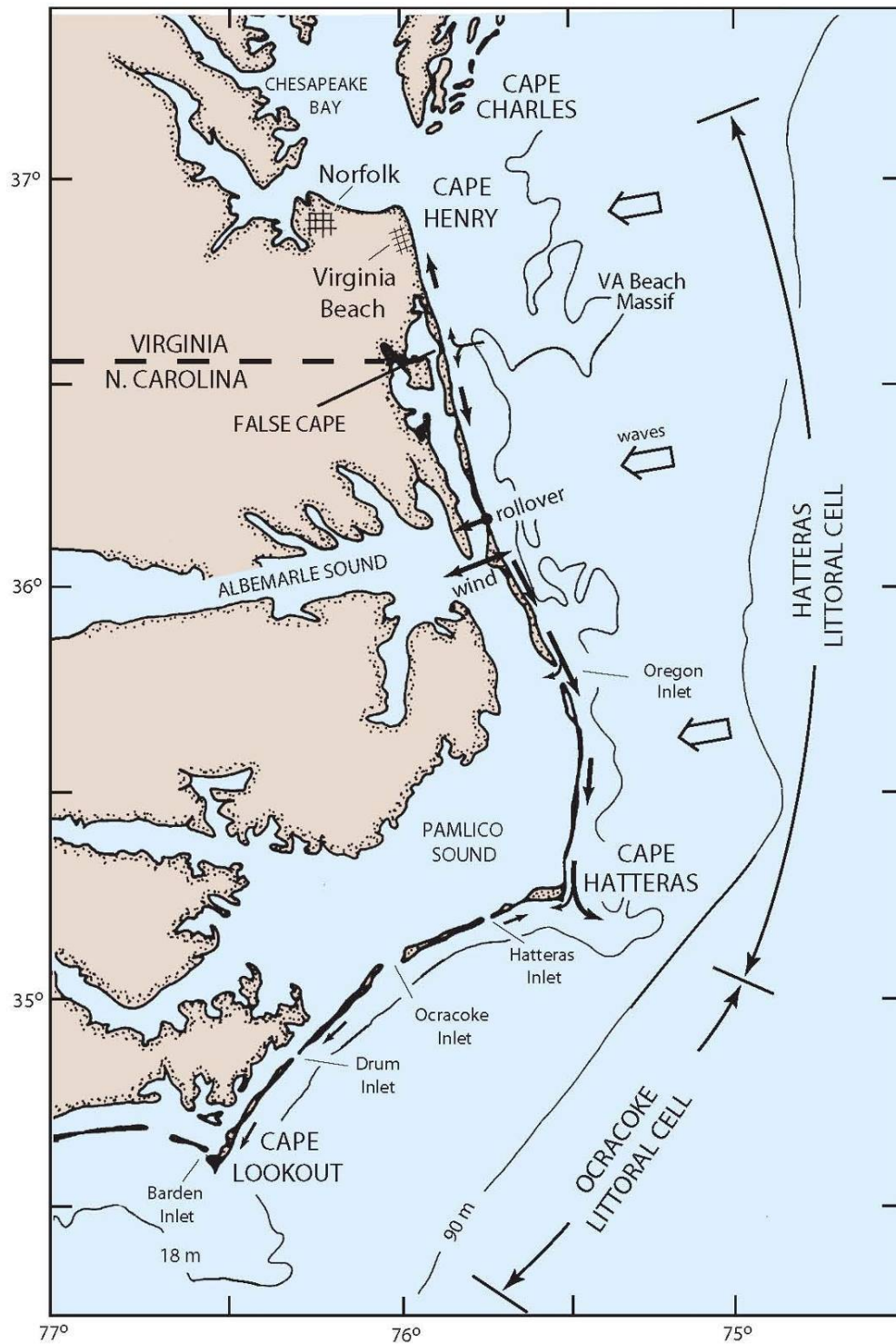


**Figure 39. Hatteras and Ocracoke littoral cells along the outer banks of North Carolina.**

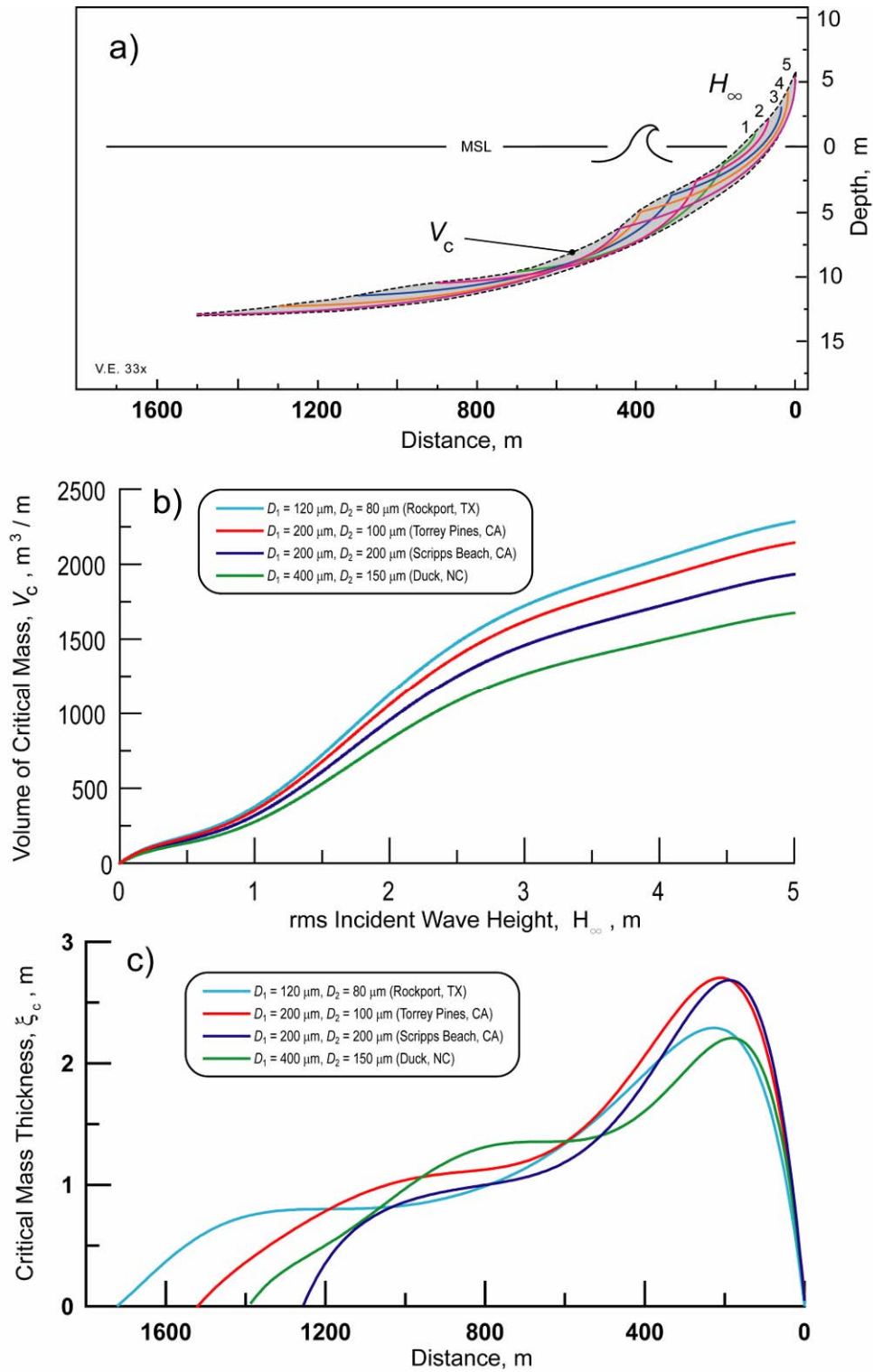


**Figure 40. Critical mass cross-section (a), volume (b) and thickness vs. distance (c).**

The lattice generation, horseshoe vortex generation, and sediment transport computations are implemented as leap-frog iterations in a time-stepped loop. The leading time step computes the strength of the horseshoe vortex filaments generated by the pressure gradients and shear setup over the lattice panels of the combined body-bedform geometry of the previous (lagging) time step. The bed and suspended load transport induced by these filaments results in an erosion flux from certain neighboring lattice panels on the seabed and a deposition flux on others, based on image lifting line theory as first applied by Jenkins et al. [37] to a mobile sedimentary boundary. The erosion and deposition fluxes of the leading time step are returned in the computational loop to the lattice generator (blue arrow) where those fluxes are superimposed on the lattice geometry of the lagging time step. That superposition produces a new lattice geometry for implementing the next leading time step. With this leap-frog iterative technique, an interactive bedform response is achieved whereby the flow field of the leading time step modifies the bedform of the lagging time step; and that modified bedform in turn alters the flow field of the next leading time step. This lead and lag arrangement is based on the fact that the inertial forces of granular bed near incipient motion are large compared to those of the fluid [58], hence the flow field responds faster to a change in bedform than the bedform can respond to a change in flow field. The codes have been linked end-to-end in the latest generation of the MM found in Appendix B.

### **6.3.1 Model Initialization**

#### **Farfield Initialization**

Farfield initialization involves data base constructions and model parameterizations for MM inputs. A detailed listing of these inputs can be found in Wilson et al. [2] and are reviewed here in context with the uniqueness of the FRF site.

#### Bathymetry and Construction of Farfield Grid

The stationary farfield bathymetry was derived from the NOS digital database compiled by the National Geophysical Data Center [19, 20], and was subsequently assembled in a farfield grid as contoured by the white lines in Figure 41. Depth contours are labeled in yellow based on meters below the 0 m MSL contour. This coarse-scale bathymetry defines the basic shelf and nearshore morphology of the Outer Banks littoral system, including the Hatteras Littoral Cell and the Ocracoke Littoral Cell, where FRF is located in the Hatteras Littoral Cell north of Oregon Inlet at the place designated by the green star in Figure 41. The system of barrier islands and sand spits that control the beach and shoreline dynamics of this highly variable littoral system are defined by the 0 m MSL contour, evident in the satellite photo in the inset at the lower right hand corner of Figure 41. The farfield grid is assembled from a 2,401 x 2,401 point array (5,764,801 grid points) formatted by latitude and longitude using 3 x 3 arc second grid cell resolution and yielding a computational domain of 168.1 km along the x-axis (longitude) and 222.3 km along the y-axis (latitude). This is the largest grid on which the MM has computed UXO transport and



burial to date, and was necessitated by the broad-scale longshore fluxes of sediment and mass exchange occurring between the Hatteras and Ocracoke Littoral Cells.

The small amount of grid distortion between x- and y- length scales in the farfield grid is compensated internally during a transformation to Cartesian coordinates using a Mercator projection centered on FRF. For the non-stationary bathymetry data inshore of closure depth (less than -12 m MSL), the equilibrium beach algorithms from Jenkins and Inman (2006) [35] were used. Depth contours generated from these algorithms vary with wave height, period and grain size and are contoured in Figure 41 for the range of wave parameters measured at the FRF site (at the locations shown in Figure 42) for the two largest storms occurring during the UXO experiment, (Figure 43 and Figure 44).

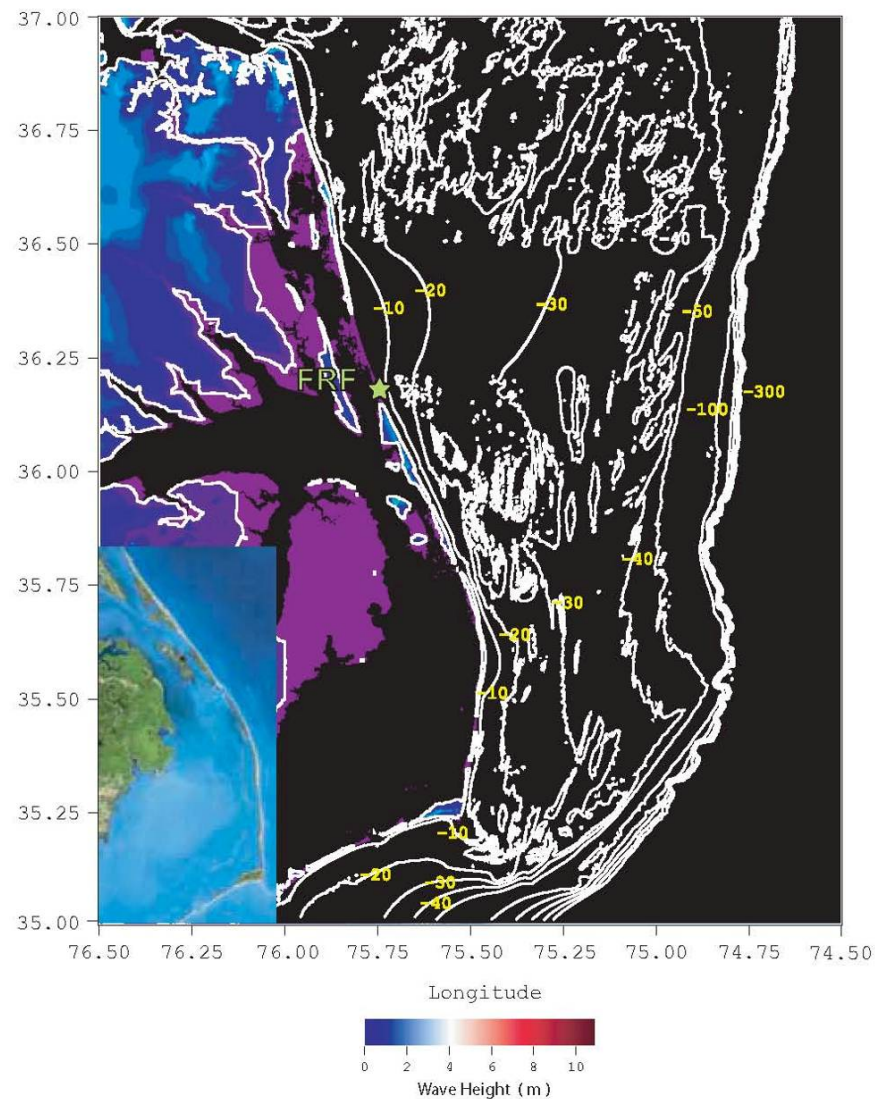


**Figure 41. Regional bathymetry for littoral cell and refraction/diffraction analysis.**



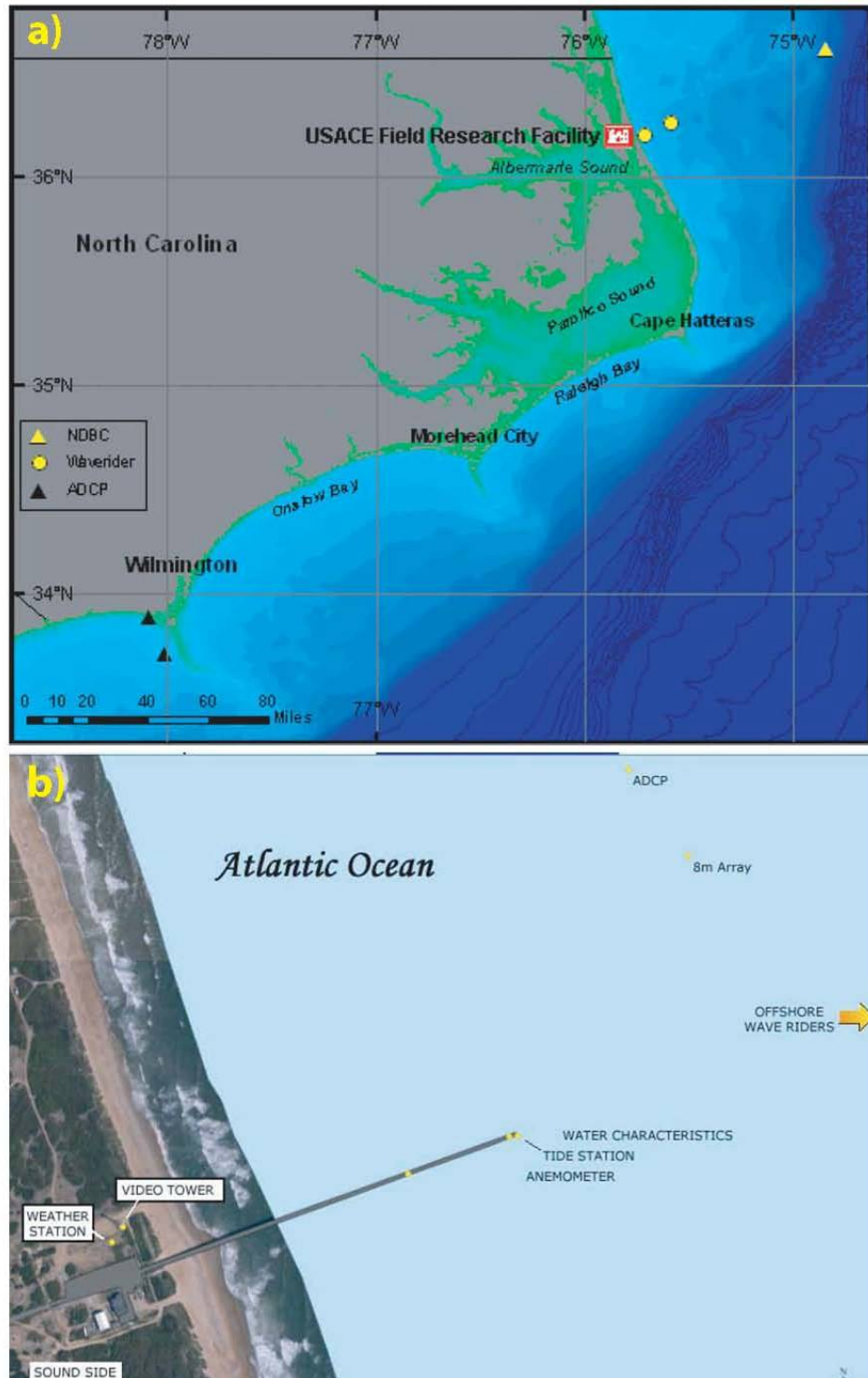


**Figure 42. Charts of FRF coastal area with locations of wave measurement and other instrumentation.**

While Figure 41 defines the broad-scale morphology of the shelf and barrier island system of the Outer Banks, the micro-bathymetry of the near-shore bar system in which the UXO were placed was resolved with high resolution survey data taken monthly by the routine beach monitoring program maintained by FRF using their CRAB. These surveys were used to calibrate the elliptic cycloid algorithms of the model to predict profile evolution over the duration of the simulation, 22 June 2005 to 16 February 2006.

The UXO surrogates were placed in two groups (inshore group and offshore group) along two cross-shore parallel lines next to FRF profile range lines # 76 and # 85. During the first two months of the deployment, July and August 2005, there were only small profile changes along these two range lines as the wave climate was dominated by benign short period summer wind waves. During the September through November 05 time frame, several moderate early winter storms brought waves up to 3m height (Figure 43 and Figure 44 ), resulting in the development of complex longshore bar and trough bed forms. The type-b cycloid algorithms in the MM were found to give the best fit to the profiles having these bar-trough bed forms. The type-b cycloid has been built into the G-95/ FRF version of the VORTEX code (Appendix B) using the general solution algorithm:

$$h = \frac{\pi \varepsilon x}{2I_e^{(1)}} \left( \frac{1 - \cos \theta}{\theta - \sin \theta} \right) = r(1 - \cos \theta) \quad (1)$$

Here  $h$  is the local depth;  $x$  is the on-off shore position;  $r$  is the radius vector measured from the center of the cycloid ellipse whose semi-major and semi-minor axes are  $a, b$ ;  $\varepsilon$  is the eccentricity of the cycloid ellipse given by  $e = \sqrt{1 - b^2/a^2}$ ;  $I_e^{(1)}$  is the elliptic integral of the first kind; and  $\theta$  is the angle of rotation of the cycloid (see Jenkins and Inman [35] for additional details). The cycloids are given by the trajectory of a point on the circumference of an ellipse that rolls seaward in the cross-shore direction under the plane of  $h = 0$ . This trajectory defines the elliptic cycloid and the segment traced by the first half of a rotation cycle ( $0 < \theta < \pi$ ) of the rolling ellipse is the equilibrium beach profile.

The depth of water at the seaward end of the profile ( $\theta = \pi$ ) is  $h = 2b$  for the type-b cycloid. The length of the profile  $X$  is equal to the semi-circumference of the ellipse:

$$X = \frac{2bI_e^{(1)}}{\varepsilon} \cong \frac{\pi b}{\varepsilon} \sqrt{\frac{2 - e^2}{2(1 - e^2)}} \quad \text{at } \theta = \pi \quad (\text{type-b cycloid}) \quad (2)$$

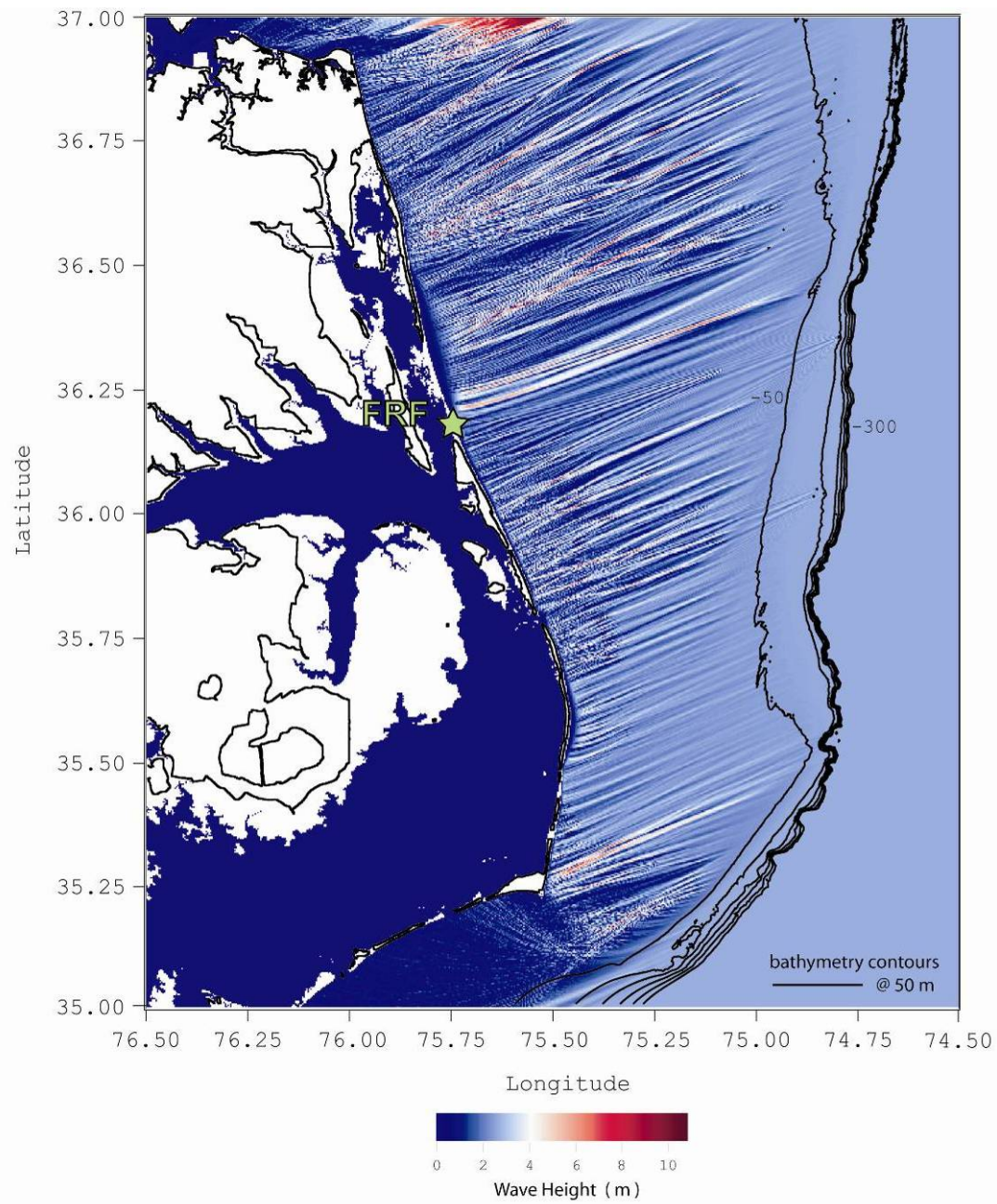


**Figure 43. Refraction/diffraction pattern for storm of 25 October 2005.**

Figure 43 shows the wave patterns for 25 October 2005.  $H = 3.12\text{m}$ ,  $T = 10.5\text{ sec}$ ,  $\alpha = 52\text{deg}$ .

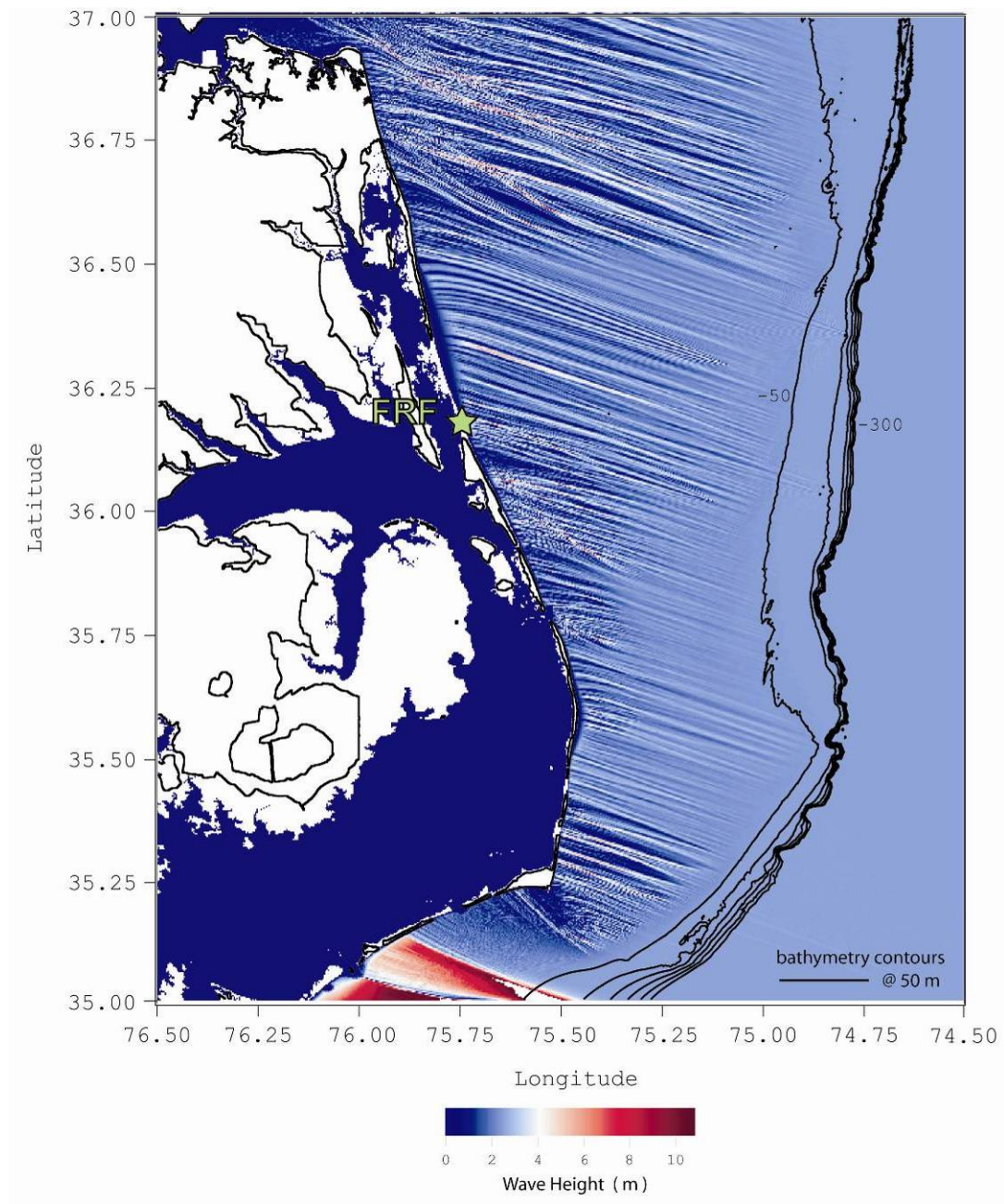


**Figure 44. Refraction/diffraction pattern for storm of 16 September 2005.**

Figure 44 shows the wave patterns of 16 September 2005.  $H = 2.96\text{m}$ ,  $T = 9.1\text{ sec}$ ,  $\alpha = 11.6\text{ deg}$ .



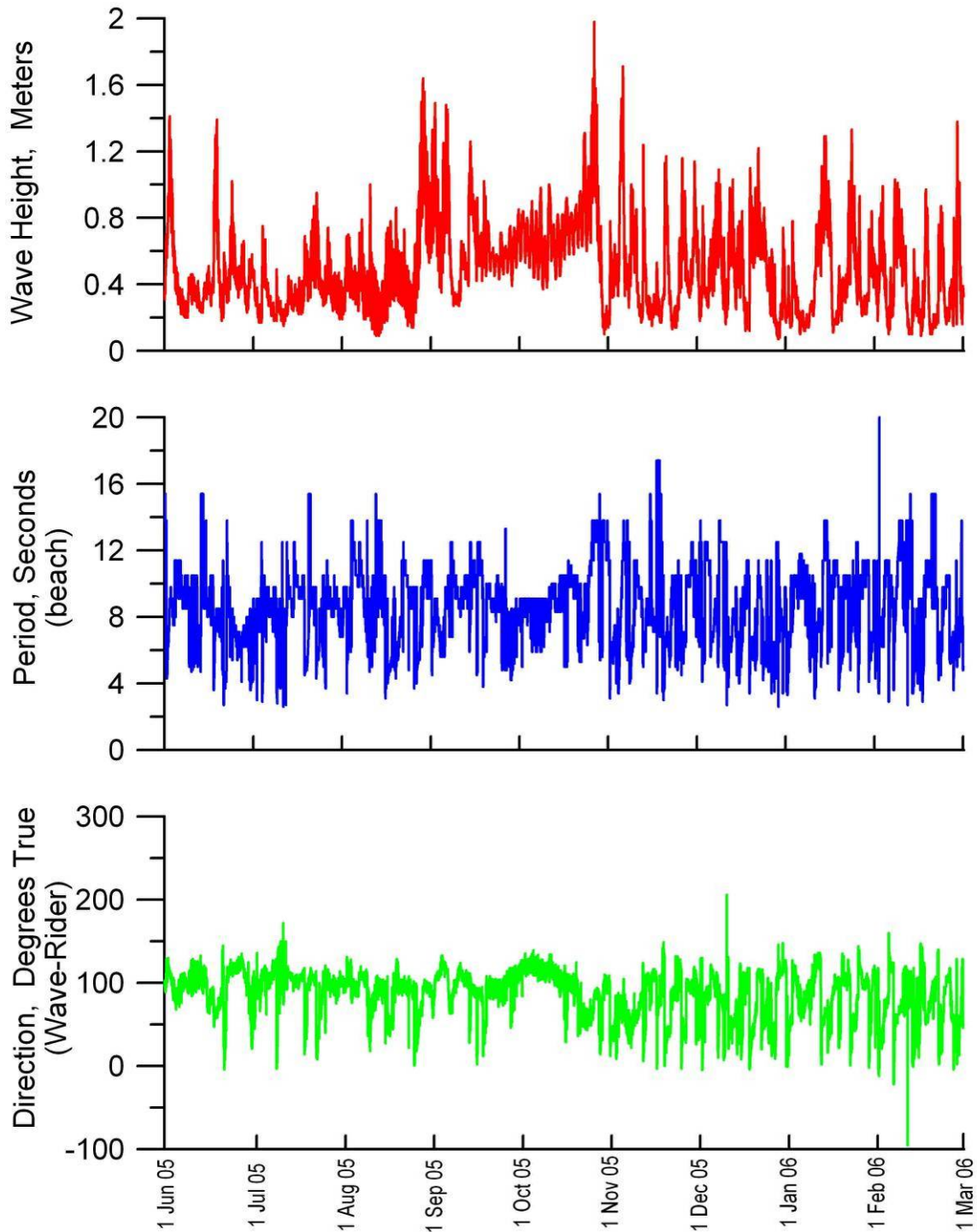


**Figure 45. Wave data during Rounds 1-4 UXO mobility demonstration at FRF Duck, NC.**

Figure 45 shows the wave height, surfzone (red), (b) wave period (blue), and (c) wave direction (green) 1 June 2005- 1 March 2006.

The measured FRF surveys along FRF ranges lines #76 and #85 were used to calibrate the parameters ( $e, b$ ) in equations (1) and (2) using a best fitting process that minimizes the mean squared error between the type-b cycloid and the measured profile.

An interesting feature of these calibrated cycloid profiles using the supporting survey data is that the closure depth was only  $h_c \cong 6$  m to 7m when normally it is about twice that value. The explanation for this beach profile anomaly was the unusually benign wave forcing that persisted throughout the experiment.

### Wave and Current Forcing

Spatial variation in wave forcing over the barrier island system of the Outer Banks is derived from refraction/diffraction analysis over the farfield grid as shown in Figure 43 and Figure 44, based on directional wave measurements from instrumentation maintained by FRF. This instrumentation includes a directional wave buoy in 17m water depth (Sensor #630), pier-mounted pressure sensors at 2m depth, (Sensor # 651) and an ADCP and pressure sensor array installed at 8m depth. The directional wave buoy data provided deep water boundary conditions in the calculation of the regional variation in the shoaling wave field based on refraction/diffraction analysis. Figure 43 provides spatial detail of the shoaling waves from an early northeaster storm occurring 25 October 2005, showing how the shelf bathymetry breaks up the incoming northerly waves into a series of directional beams along the Outer Banks. Figure 44 shows the corresponding shoaling response to southerly waves generated along the leading edge of a trailing cold front that passed over the region on 16 September 2005. In either case, directional beams induced by the shelf bathymetry produced pronounced patterns in the nearshore of shadows (regions of locally smaller waves) and bright spots (regions of locally higher waves). Wave-driven nearshore currents flow away from bright spots and converge on shadows. The northerly waves in Figure 43 are found to produce considerable banding between shadows and bright spots immediately to the north of Duck Pier where the UXO fields were placed between range lines # 76 and #85. The along shore variation in wave height between these shadows and bright spots produces considerably divergence of drift with associated rip cells and complex bar formations (Figure 46).

Repeated wave shoaling computations with the buoy data (sensor #630) of the kind shown in Figure 43 and Figure 44, combined with the wave pressure measurements from Duck Pier (Sensor #651) allowed us to assemble an unbroken time series of wave height, period, and direction (Figure 45) that spanned the full nine month deployment of the UXO experiment (Rounds 1-4). The most notable feature of this record was the occurrence of unusually small wave heights during the fall and winter months. Normally wave heights of 5-8 m are quite common along the outer Banks during this time of year. The benign wave climate encountered during the Rounds 1-4 of the UXO experiment was the essential environmental feature determining the nature of the outcome, an outcome that for the most part showed only modest movement of the UXO with deep burial.

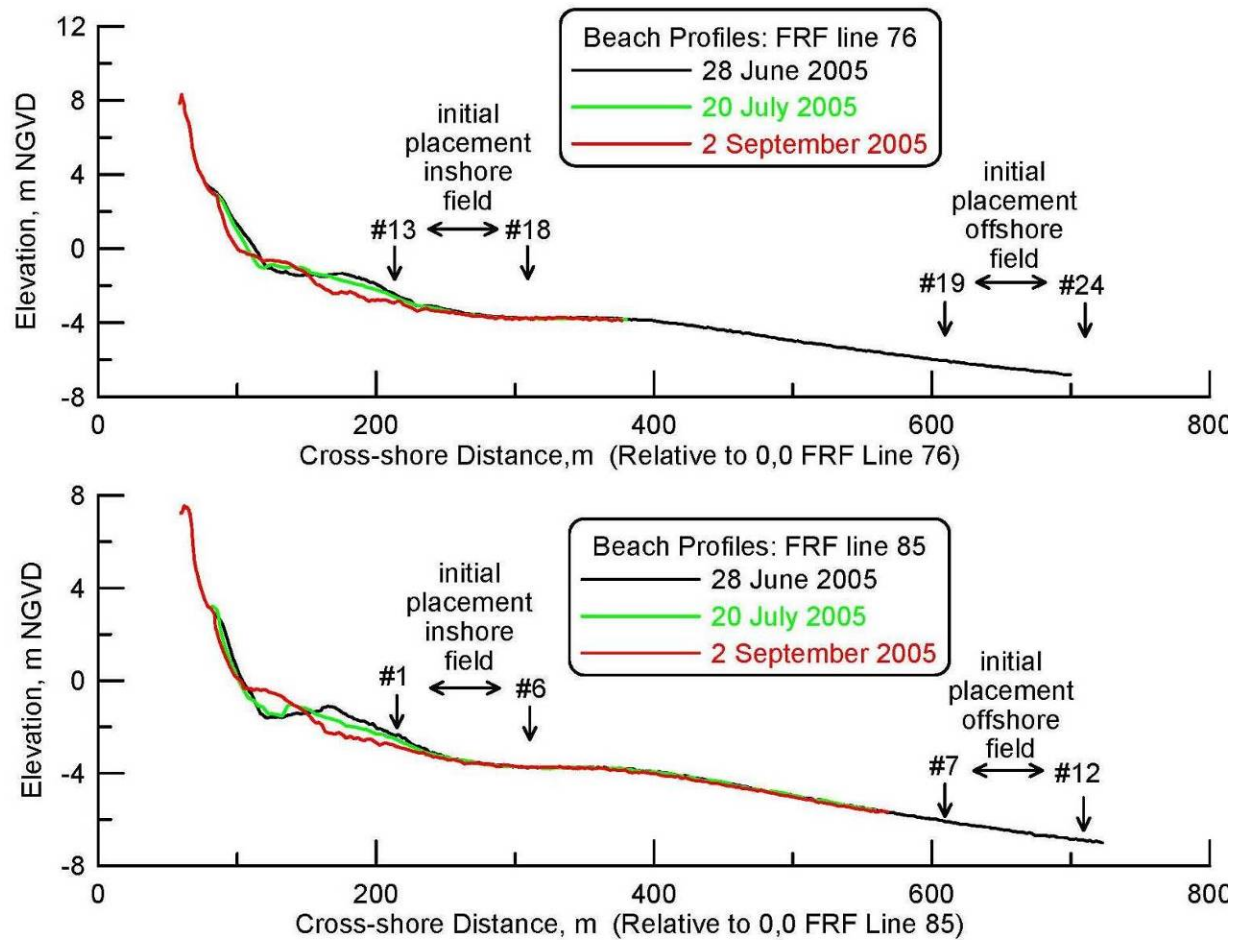


**Figure 46. Beach profile variation during UXO demonstration, FRF Duck, NC, 28 June – 2 September 2005.**

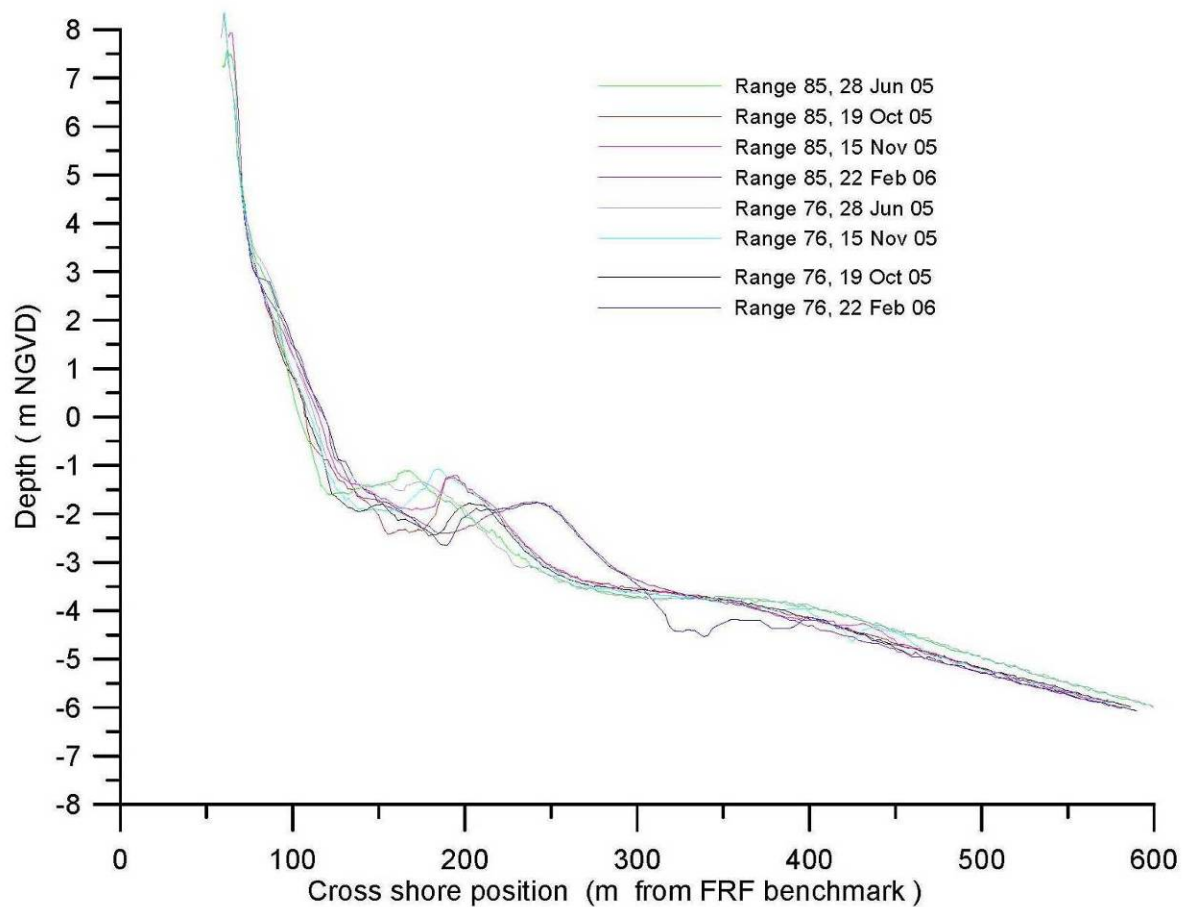


**Figure 47. Beach profile variation during UXO demonstration FRF, Duck, NC, 28 June 2005 – 22 February 2006.**

### **Nearfield Initialization**

Nearfield initialization involves data base constructions and model parameterizations for MM inputs. A detailed listing of these inputs can be found in Wilson et al. [2]. They are reviewed here in context specific or unique to the FRF site.

### Sediment Parameters

The nearfield of the model was gridded for a fine to medium coarse sand bottom that was parameterized by 20 grain size bins according to the grain size distribution shown in Figure 48. The cumulative distribution in this figure (purple line) reveals that the Duck sand is well sorted by the wave action, and mineral analysis indicates it is predominately quartz of glacial origin [60]. The median grain size is 565 microns, with 70% of the sediment comprised of medium-coarse sand between 450 microns and 750 microns. These sediment characteristics are well suited to the ideal granular relations used in the MM. Based on these sediment grain sizes, wave



heights, and UXO placements on the active beach profile, the thickness of the critical mass, the depth of permanent entombment, is  $\xi_c = 220$  cm for the inshore UXO group;  $\xi_c = 140$  cm for the offshore group; and the critical mass of sand (volume of sand that must be removed to expose buried UXO) is  $V_c = 600 \text{ m}^3$  to  $1200 \text{ m}^3$  per meter of shoreline (Figure 47).

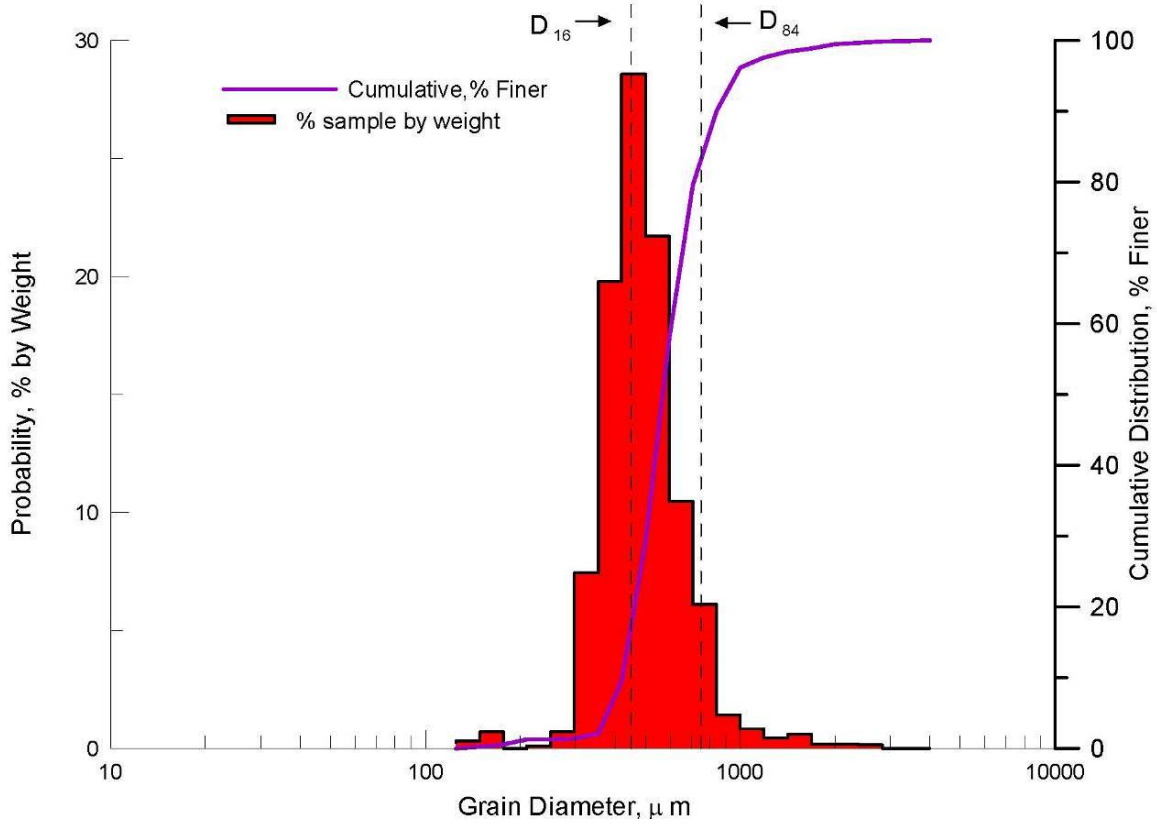


**Figure 48. Grain size distribution of sediment for FRF Duck, #B6-S1, 1 September 2005.**

#### UXO Shape Lattice

To provide a systematic and manageable set of inputs for shape specific calibration parameters we concentrated our model simulations on the 5"/38 Naval projectile. These rounds were approximated by an elliptic frustrum revolved about the major axis of the round, say the y-axis, taken for example as the transverse axis to the mean flow.. For this orientation the generalized shape of the round can be represented by the analytic expression:

$$R(y) = a - a \left( \frac{y}{S} \right)^\beta \quad (3)$$

Here  $a = D/2$  is the basal radius and  $D$  is the basal diameter of the round;  $R(y)$  is the local radius at any arbitrary location  $y$  along the major axis of the round;  $S$  is the total length of the round as measured along the y-axis; and  $\beta$  is a constant that adjusts the pointedness of the

round. A best fit of equation (1) to the 5"/38 round dimensions found that  $\beta = 3.5$ . To accommodate these dimensions and the small radius curves of the shape, the VORTEX shape lattice file was gridded for 3mm grid cells. The dry bulk mass of the 5"/38 surrogate rounds was nominally  $\rho_s V_0 g = 22.8$  kg.

### 6.3.2 Burial and Migration from Mode 1 Analysis

Prior to considering the influence of the local bathymetry and forcing history on the burial migration response of the UXO, we test the MM in Mode 1 using the UXO shape lattice files on the Duck grain size distribution for a flat planar bed with constant wave forcing. Figure 49 presents the modeled instantaneous vortex and scour field produced from a 5"/38 UXO resting proud on the bed with the major axis aligned transverse to a train of monochromatic waves with 12 sec period propagating from right to left. The wave oscillatory velocity amplitude at the top of the bottom boundary layer is 100 cm/sec. This velocity amplitude corresponds to the super-critical transport regime [37] for the grain size distribution in Figure 48. In this regime, flow separation with a basal vortex is observed on the down-wave (shoreward) side of the UXO, inducing formation of a scour hole. As the scour hole deepens, the round slips or rolls into the hole, resulting in migration and burial through what is known either as a *scour and slip* or *scour and roll* burial sequence [38, 39, 40, 41, 42].

At an advanced stage in the burial/migration progression referred to as *lock-down*, burial becomes sufficiently extensive that migration is no longer possible [38, 39, 42]. For excitation by monochromatic waves of various periods and heights, the distance a UXO migrates before lock-down occurs has a monotonic dependence on a parameter of dynamic similitude referred to as the Shields' parameter. This parameter is a measure of the flow inertia relative to the inertia of the UXO. Explicitly, the Shields parameter,  $\Theta$ , represents a ratio between the hydrodynamic forces (drag and lift) acting to move the UXO and the gravitational forces acting to restrain and bury the UXO, where

$$\Theta = \frac{u^2}{g'D} \quad (4)$$

Figure 49 illustrates the lockdown stage typical of the surrogates that were installed at FRF. The UXO surrogate is shown 64% buried in a medium-coarse sand bottom under a wave crest propagating from right to left at super-critical velocity amplitude.

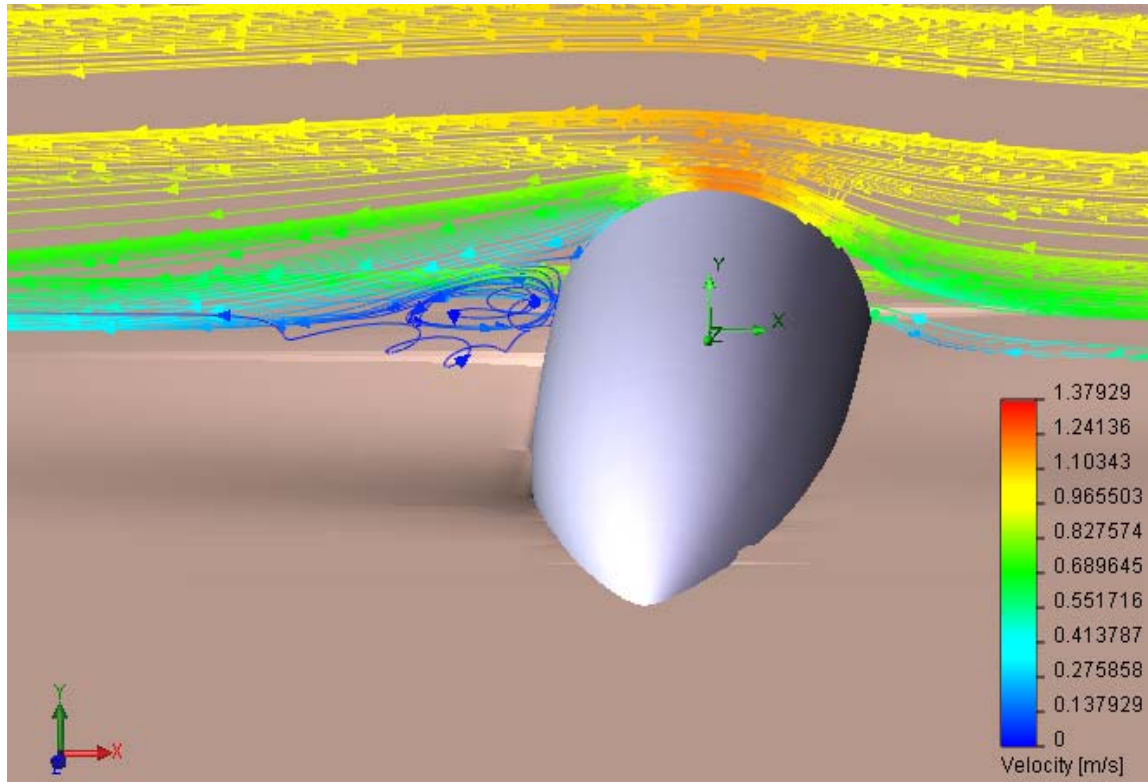


**Figure 49. Simulation of vortex and scour field from a Mode 1 simulation of the 5"/38 UXO surrogate.**

In equation (2),  $u$  is the oscillatory wave velocity amplitude at the top of the bottom boundary layer;  $D$  is the basal diameter of the UXO;  $g$  is the acceleration of gravity;  $g' = g(\Delta\rho/\rho)$  is the reduced gravity; and  $\Delta\rho = \rho_s - \rho$  is the density difference between the UXO and seawater density,  $\rho$ . Flat bed simulations of the type shown above indicate that UXO mobility increases with increasing wave velocity (proportional to wave height and inversely proportional to wave period); with decreasing caliber of the UXO; or with decreasing density (specific gravity) of the UXO.

For shallow water waves in the typical Outer Banks period band of 9 to 12 sec, Mode 1 analysis shows there is little burial or migration of the 5"/38 UXO for wave heights less than 0.4 m (sub-critical regime), see Jenkins et al. [38], Donohue and Garrison [41], and Inman and Jenkins [42] for more details regarding sub- and super-critical transport regimes. Once wave height exceed 1.2 m, migration and burial proceed rapidly (super-critical regime) until burial lock-down arrests further migration. At that point, further migration is only possible if broad scale bed erosion of the bed reduces the degree of burial. Recurrence analysis of the wave height time series indicates that wave heights were sub-critical 48.8% of the duration of the deployment during Rounds 1-4 of the UXO experiment at FRF, Duck NC, and that super-critical conditions persisted only 5.4% of that deployment due to the benign nature of the wave climate. Thus, the

observed migration was the result of relatively rare super-critical wave events, and only some of those events would actually move the UXO because super-critical waves had to occur concurrently with beach profile shifts in order to re-expose the UXO and release them from burial lock-down. These kinds of temporal interplay can not be resolved by the simple Mode 1 analysis. Instead, they depend on the history of the wave forcing and burial/migration response. These temporal relationships and their statistics of recurrence will be addressed in the following section.

### **6.3.3 UXO Migration/Burial Model Performance at FRF Experiment**

The MM performance in Mode 3 is tested against data from two separate UXO sites deployed at FRF, Duck, NC, between 22 June 2005 and 15 February 2006. Figure 50 gives the details of the lay-down pattern in relation to the FRF Research Pier and the local bathymetric features. Twelve UXO surrogates of a 5"/38 naval round were deployed at each of the two test sites for a total of 24 surrogates. The in-shore field (surrogate #s 1-6 and 13-18) was located on the north side of the FRF Pier in a nominal depth of 2m to 3m MSL, while the off-shore field (surrogate #s 7-12 and 19-24) was laid at depths between 6-7 m MSL. At both the offshore and inshore sites, surrogates were laid in two along-channel rows parallel to FRF survey range lines #76 to the north and #85 to the south Figure 51. The surrogates were set at nominally 20m spacing in the cross-shore direction, with six surrogates in each row. The surrogates were laid on 22 June 2007 and thereafter the position and burial depth of each surrogate was measured at six intervals referred to as "Rounds". Round 1 measurements were made on 27 June 2005, Round 2 on 12 August 2005, Round 3 on 20 October 2005, Round 4 on 15 February 2006, Round 5 on 26 July 2006, and Round 6 on 3 August 2006. Both burial and migration were measured during Rounds 1-4. Thereafter, only burial was measured for a few selected surrogates. Since burial and migration are coupled phenomena, the analysis and modeling validation focused on Rounds 1-4.

In Figure 50 black dots denote 5"/38 surrogates, red dots denote reference stakes, and the yellow dots are groups of 20 mm surrogates, the latter of which only a small sample was recovered.

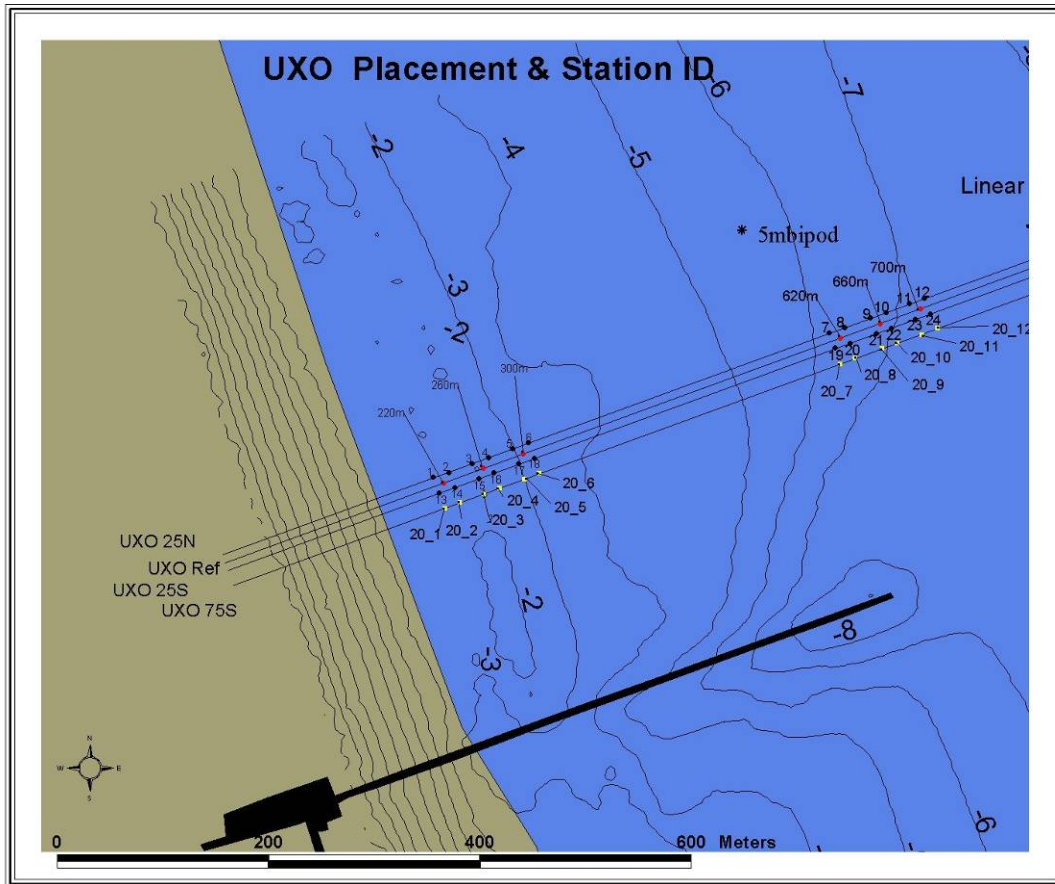


**Figure 50. Details of lay-down pattern of UXO fields at the FRF site.**

Because the surrogates all became buried during the experiment, the primary method for locating the surrogates was an acoustic ranging technique utilizing embedded pingers in the surrogates, each with a unique code for identification. Once the surrogate was located by its pinger, position was triangulated from distances measured to three reference stakes implanted in the seabed along the cross-shore axis of each group, as shown schematically in Figure 52. Two distance measurement techniques were used: tape measurements and acoustic ranging using a Benthos Model DRI-267A directional range finder. The accuracy of the acoustic ranging measurements were found to be within 5% of tape measurements of distances of 20m to 40m, or an uncertainty of typically less than 1m. Acoustic ranging was the predominant technique used to ascertain UXO position throughout Rounds 1-4 because it was faster to implement, while tape measurements were particularly difficult to make in the shallow inshore group where the tape would tend to stream out over curved paths in the wave surge.

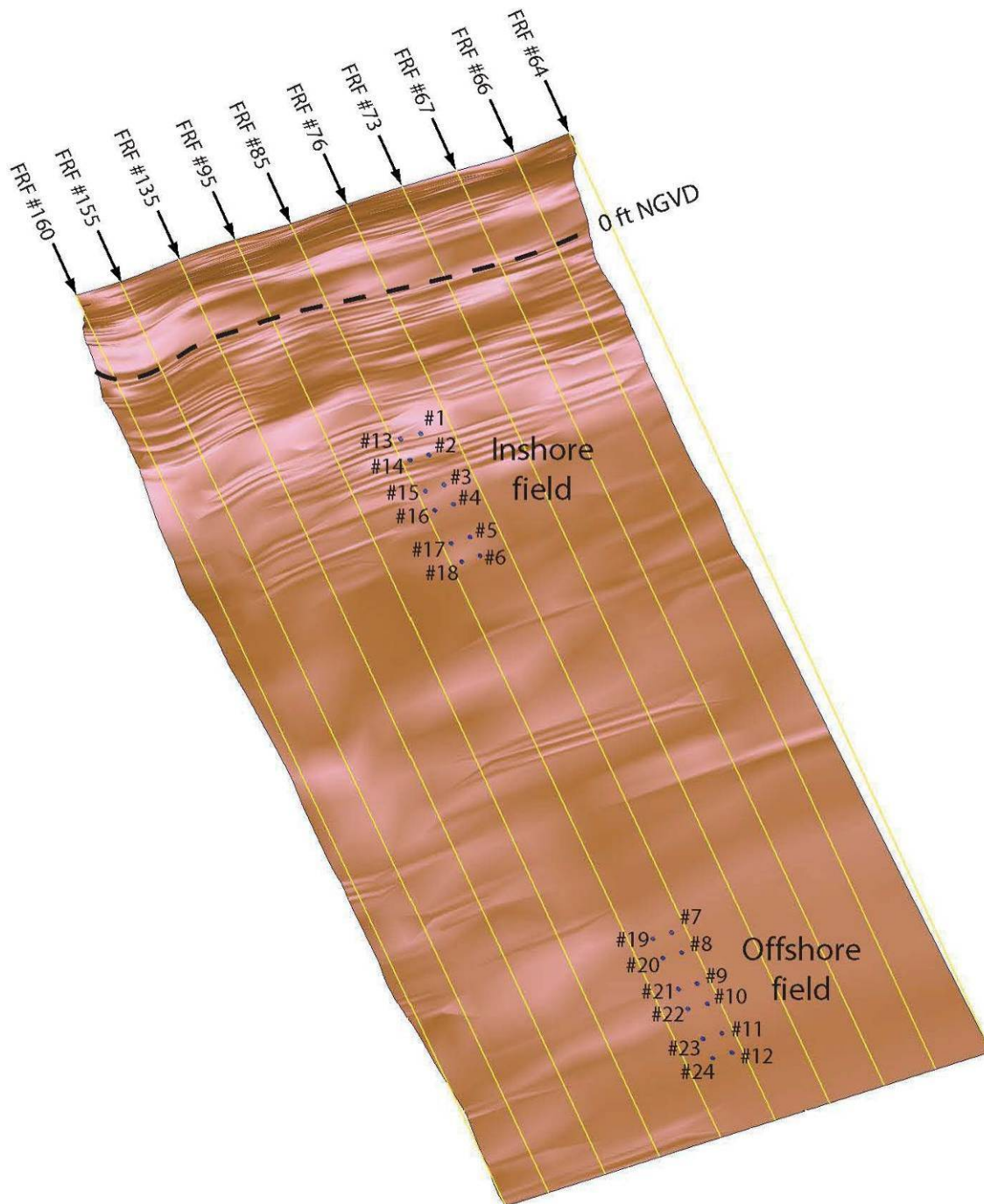


**Figure 51. Three dimensional rendering of UXO deployment at FRF Duck, NC, June 2005.**

Burial depths were measured manually by divers by probing into the bottom with a small diameter bar until refusal depth was reached. When this technique failed to obtain refusal depth once the UXO became buried 1m or more, burial was calculated from elevation changes in the



surveyed profiles at the location of the UXO along FRF ranges #76 and #85 (cf. Figure 46). The largest profile changes that caused the deepest degree of burial were associated with the continuously evolving parallel bar systems that are ubiquitous in the near shore of the Outer Banks. Figure 51 shows the extent of the parallel bar system in the neighborhood of the UXO fields based on a three dimensional reconstruction of the shore rise and bar berm from FRF beach profile surveys taken along FRF Ranges #64 - #160 at the time of the Round 1 measurements, 5 days after the initial installation. Note the longshore expanse of bar systems derived from on-range profile variations shown in Figure 46 and Figure 47. These bar systems migrated continuously throughout the remaining measurement cycles taken during Rounds 2-4 of the experiment, as evidenced by the profile variations in Figure 46, particularly in the neighborhood of the inshore group. The migration of these sand bars lead to episodic re-exposure of buried UXO, leading to additional short periods of migration between the various measurements between Rounds 1 and 4.

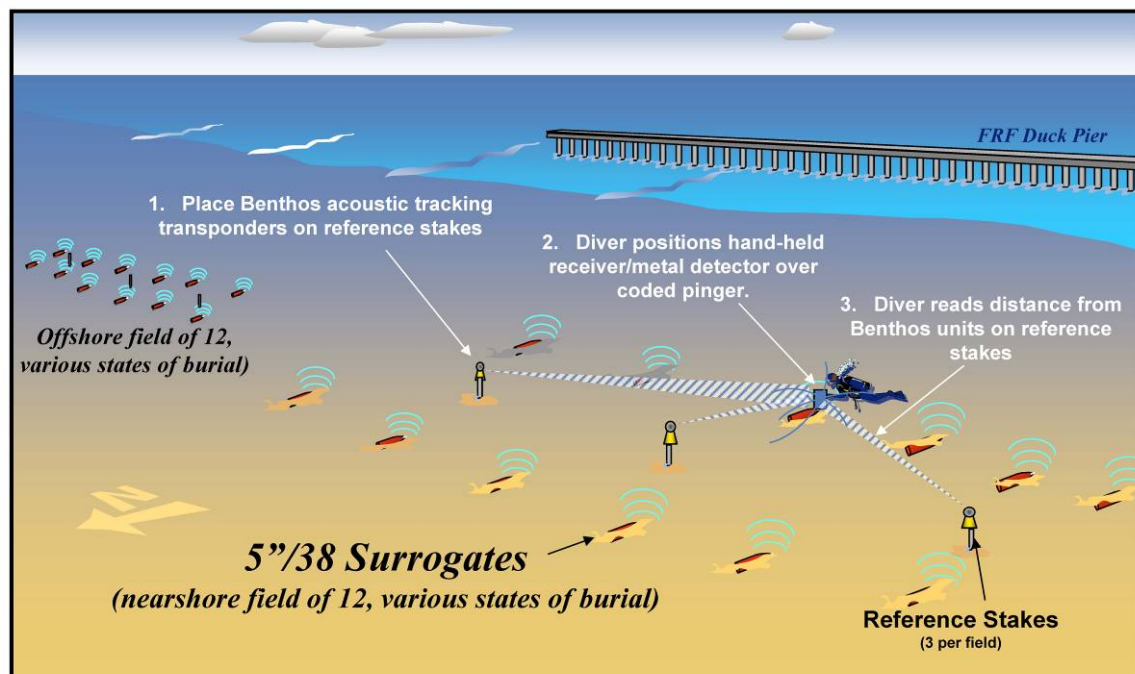


**Figure 52. Schematic of acoustic directional ranging technique for locating position of UXO surrogates during the FRF experiment.**

### 6.3.3.1 Model Predictions of UXO Migration and Burial Rates

Migration and burial of each of the 24 UXO in the inshore and offshore test sites at FRF were simulated by the MM in Mode 3 configuration using the measured wave forcing, fine-scale bathymetry and the grain size distribution. The MM computed burial and migration at time step intervals of  $\Delta t = 20$  minutes.

Figure 53 and Figure 54 provide the MM simulations of time evolutions of burial and migration for two of the most active 5"/38 UXO surrogates, #3 in the Inshore Group and #11 in the

Offshore Group. Those simulations show the time evolutions for these two surrogates during Round 1, 22-27 June 2005. Figure 55 and Figure 56 show the time evolutions during Round 2, 27 June-12 August 2005. Figure 57 and Figure 58 show the time evolutions during Round 3, 12 August - 20 October 2005. Figure 59 and Figure 60 show the time evolutions during Round 4, 20 October 2005 - 15 February 2006. In each of these plots, migration distance (blue) and burial depth (red) are predictions of changes (in scalar lengths) relative to horizontal position and burial depth at the start of each round. For the start of Round 1, the initial position and burial depth are taken as zero; thereafter, the starting horizontal position and burial depth are the end points of the preceding round. In each panel of Figure 53, the migration distance is read from the outer left-hand vertical axis; burial depth is read from the outer right-hand vertical axis; and wave height is plotted in gray according to the inner left-hand vertical axis. For the Inshore Group (Figure 53, Figure 55, Figure 57, and Figure 59), migration was primarily along shore towards the north and south with the convention that transport to the south (in the direction of predominant littoral drift) is taken as positive, while movement toward the north is negative.

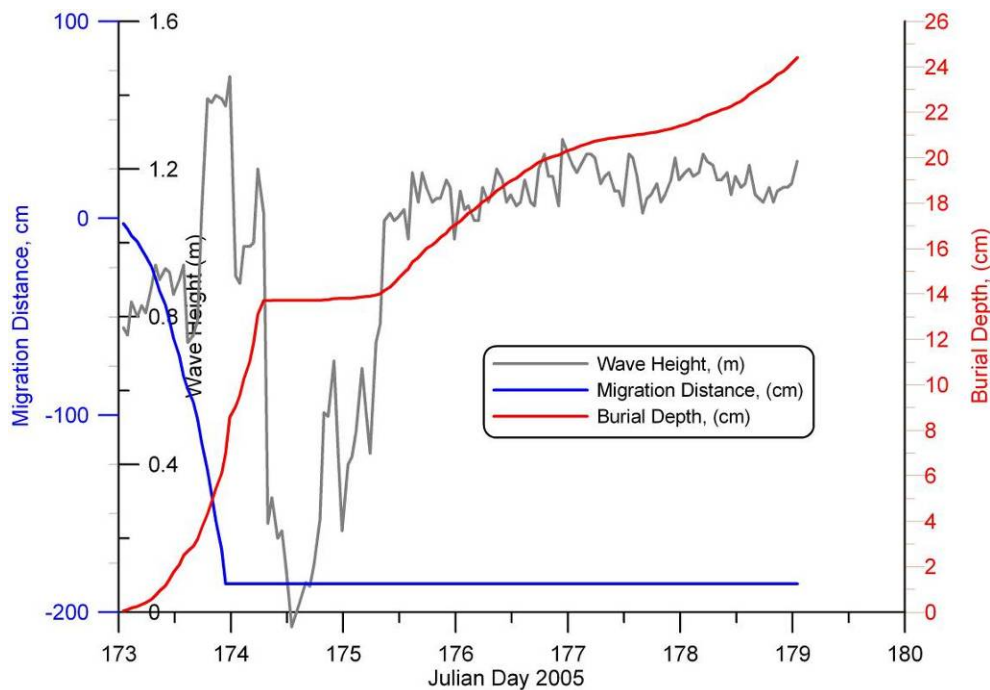


**Figure 53. MM simulation of migration and burial sequence of 5''/38 surrogate #3, Inshore Group, Round 1, FRF Duck, 22-27 June 2005.**



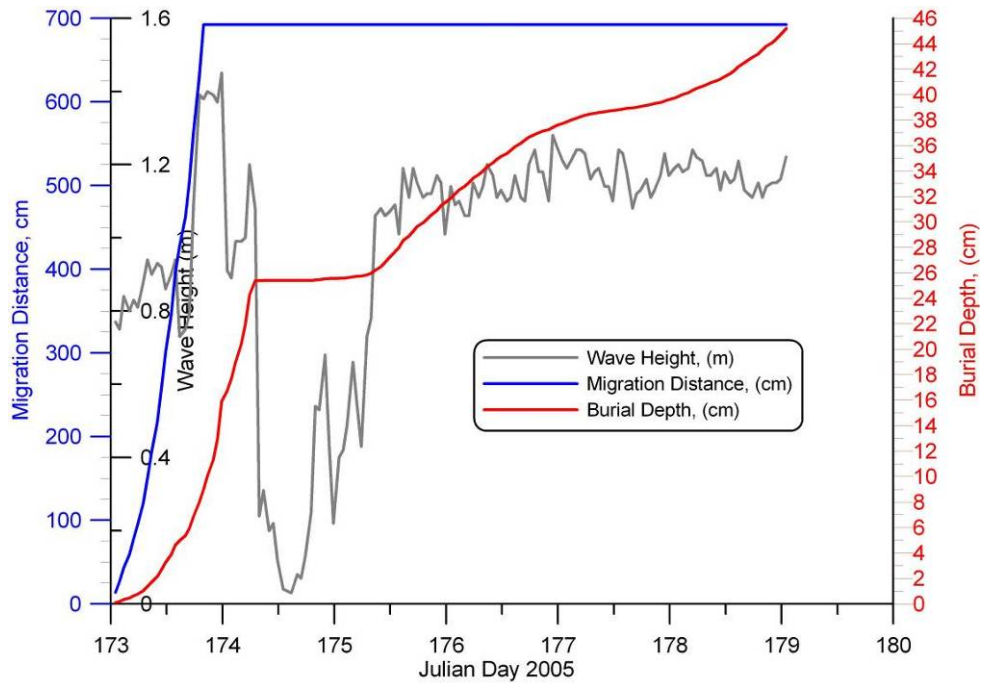


**Figure 54. MM simulation of migration and burial sequence of 5''/38 surrogate #11, Offshore Group, Round 1, FRF Duck, 22-27 June 2005.**

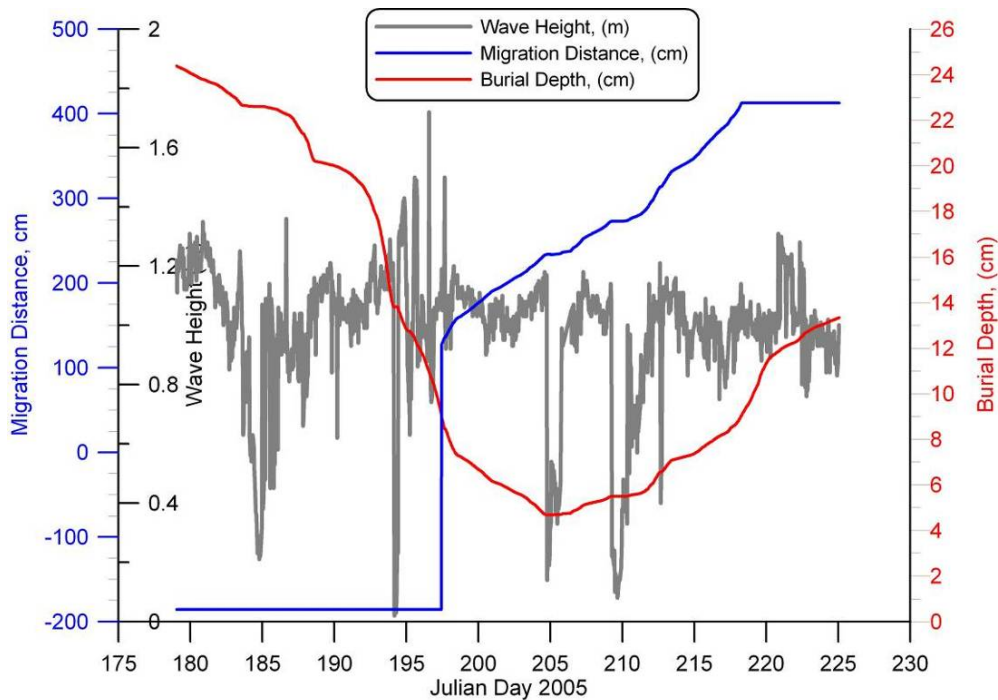


**Figure 55. MM simulation of migration and burial sequence of 5''/38 surrogate #3, Inshore Group, Round 2, FRF Duck, 27 June – 12 August 2005.**

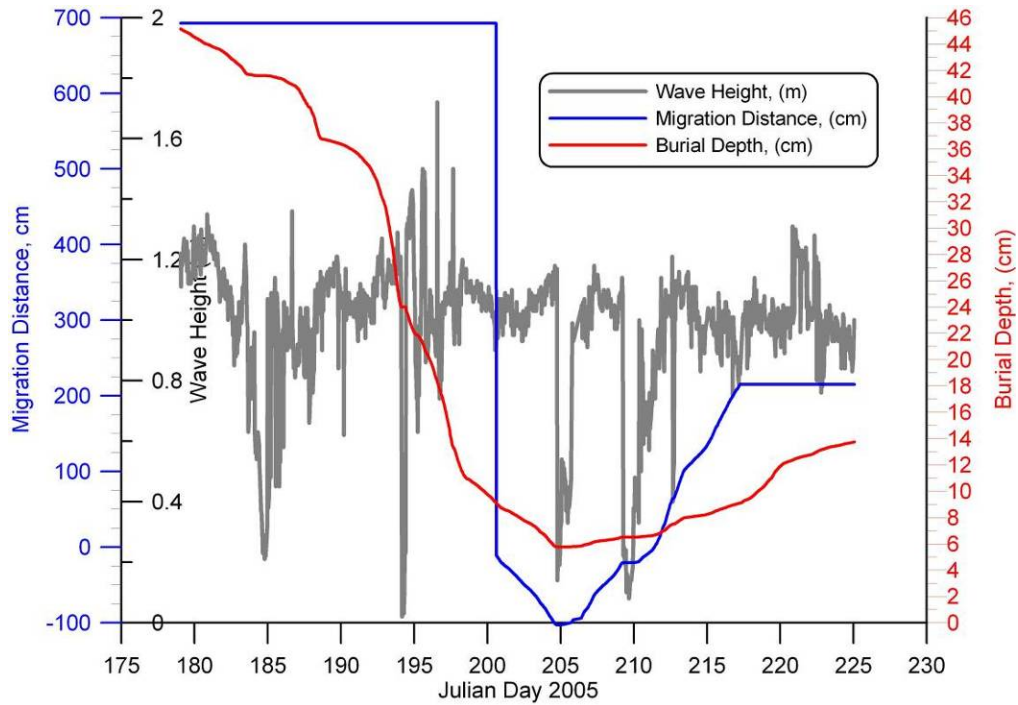


**Figure 56. MM simulation of migration and burial sequence of 5''/38 surrogate #11, Offshore Group, Round 2, FRF Duck, 27 June – 12 August 2005.**

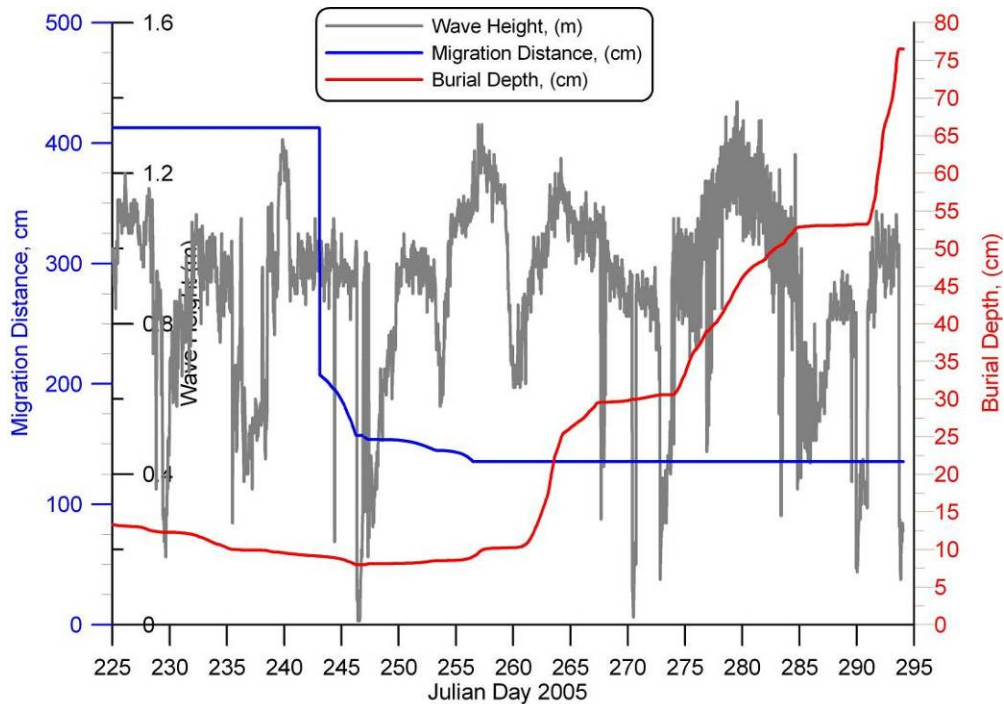


**Figure 57. MM simulation of migration and burial sequence of 5''/38 surrogate #3, Inshore Group, Round 3, FRF Duck, 12 August – 20 October 2005.**

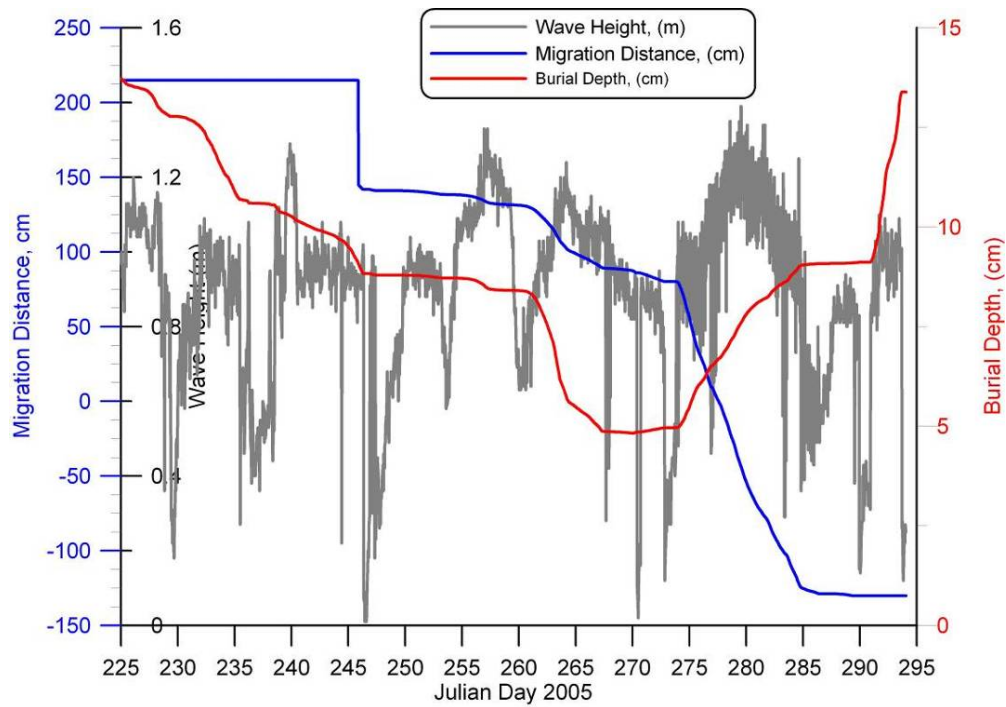


**Figure 58. MM simulation of migration and burial sequence of 5''/38 surrogate #11, Offshore Group, Round 3, FRF Duck, 12 August – 20 October 2005.**

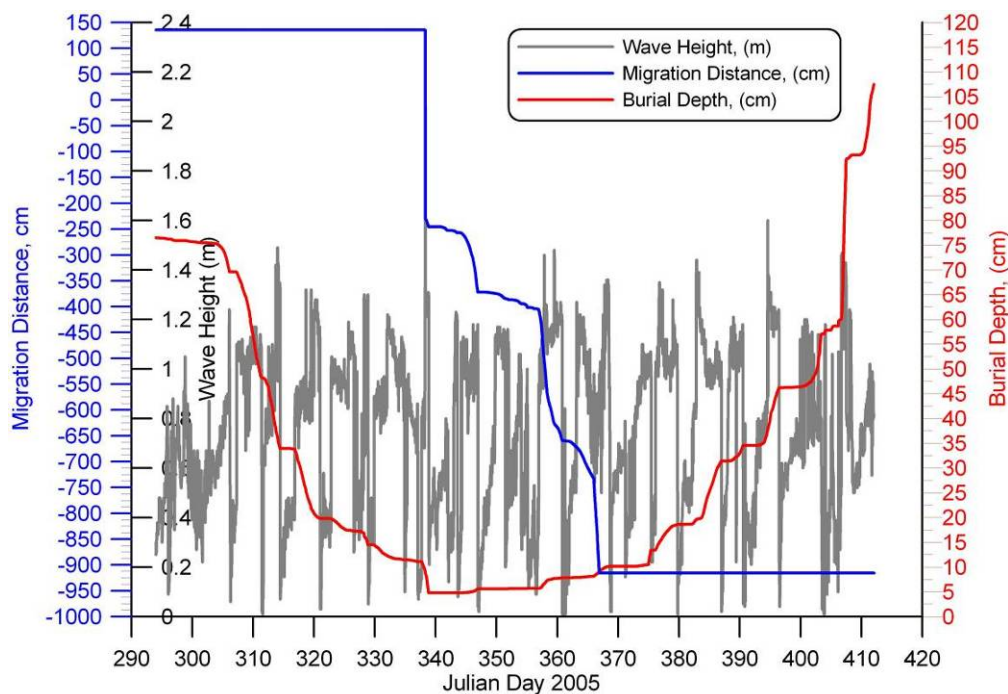


**Figure 59. MM simulation of migration and burial sequence of 5''/38 surrogate #3, Inshore Group, Round 4, FRF Duck, 20 October 2005 – 16 February 2006.**

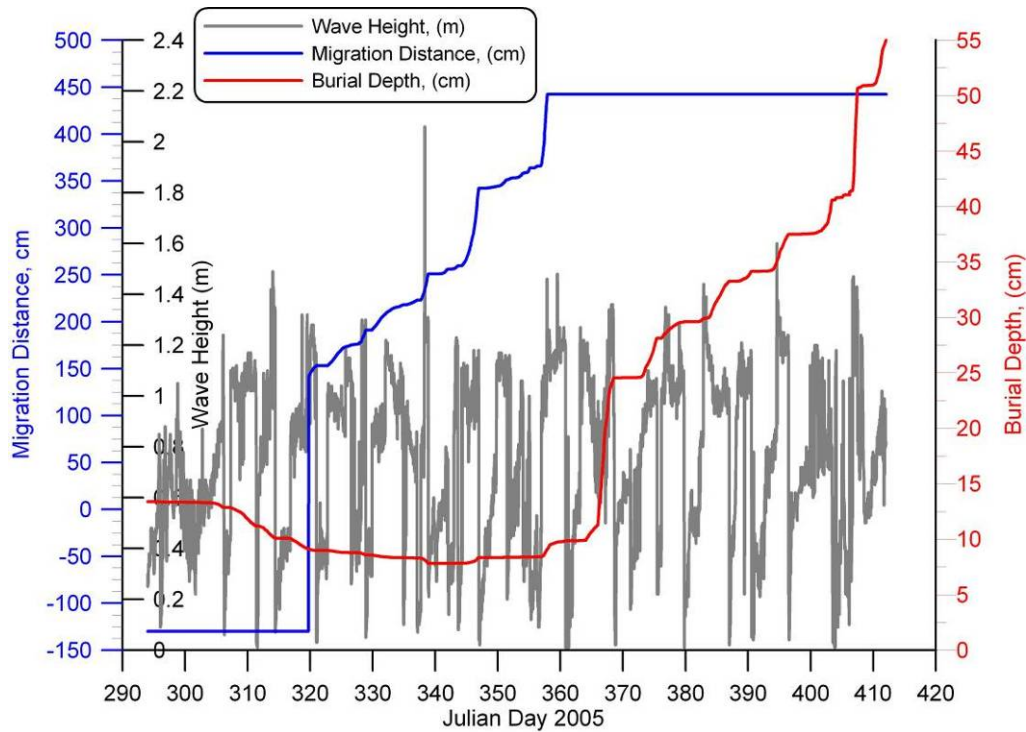


**Figure 60. MM simulation of migration and burial sequence of 5''/38 surrogate #11, Offshore Group, Round 4, FRF Duck, 20 October 2005 – 16 February 2006.**

With the Offshore Group (Figure 54, Figure 56, Figure 58, and Figure 60), migration was primarily on/off shore with the convention that transport off shore is taken as positive, while movement onshore is negative. So that migration and burial in both the Inshore and Offshore Groups can be compared to a common wave height reference, the wave heights plotted in Figure 53 through Figure 60 are from the wave rider buoy in 17m water depth (Sensor #630), prior to being shoaled into the specific location of a particular surrogate. Burial depth was measured from the bottom of the surrogate at its basal end, with the time axis shown in these figures given in terms of Julian Day relative to the start of year 2005.

Some of the largest movements of the UXO surrogates (both in the Inshore and Offshore Groups) occurred in the first two days of Round 1 when burial was initially small immediately after installation. In this minimal burial state the UXO are particularly susceptible to mobility if sufficiently large waves occur to give rise to a supercritical transport state ( $H_0 \geq 1.2$  m). Figure 53 indicates that this was indeed the case for surrogate #3 that was placed in the middle of the northern most row of the Inshore Group. The MM simulation computed that surrogate #3 moved a distance  $\xi(i) = 186$  cm from its initial lay-down position. (Diver surveys measured a net excursion of 2.0 m for surrogate #3 during Round 1). The direction of movement calculated by the MM was principally long shore towards the north, counter to the prevailing long-term net littoral drift (cf. Figure 55), but in general agreement with diver surveys. It is also noted that the high rate of initial migration for surrogate #3 was abruptly halted by burial lock-down; no further movement of the surrogate occurred during the remainder of Round 1, as burial progressively

increased to a burial depth of  $h(i) = 23.4$  cm, which was more than sufficient to entirely bury the 5"/38 surrogate.

A larger migration excursion was played out during Round 1 in the Offshore Group. Figure 54 calculates that surrogate #11 at the seaward end of the Offshore Group initially moved  $\xi(i) = 692$  cm before burial arrested further movement. Divers measured net movement of surrogate #11 to be 7.8m during Round 1. This movement was predominantly down-slope and offshore also in general agreement with diver acoustic ranging observations. The larger amount of movement of surrogate #11 versus surrogate #3 is apparently the result of steeper local bed slopes associated with the seaward sloping face of a sand bar and trough bedform. Because the bedform migrated under the influence of the 1.4 m high shoaling waves, total burial of surrogate #11 was significantly larger and was computed to be  $h(i) = 45.2$  cm by the end of Round 1 (approximately double that realized for surrogate #3). High burial rates abruptly arrest high migration rates associated with the scour and roll progression involved with the migration mechanics of round bottom shapes like the 5"/38 naval projectiles [38, 40, and 42].

Once the UXO is fully buried, as occurred by the end of Round 1, subsequent movement is only possible if bottom profile variation of the type shown in Figure 47 results in re-exposure to a sufficient degree that releases the UXO from burial lock-down and permits it to undergo additional scour and roll progressions [38, 42]. In the MM, re-exposure of the UXO is the result of a complex interplay between the wave refraction/diffraction time history and the cycloid equilibrium profile algorithms. Computations of this interplay are only possible in the Mode 3 operation of the model because it requires time variability in the wave forcing, and spatial variability in the bathymetry. In the FRF model runs of Rounds 1-6, the time variation of wave height and direction (when shoaled over the broad-shelf bathymetry, cf. Figure 43) produces time variability in the parameters of the type-b cycloid bottom profiles; and it is that profile variability that can re-expose a UXO and render it susceptible to further migration sequences. During all the diver surveys conducted in Rounds 1-6, the UXO surrogates were always entirely buried, and yet these surrogates were found in different locations during each survey round. The only explanation for how these buried surrogates moved between survey rounds is provided by the simulations of the MM that calculated interim re-exposure events that were not observed by divers.

Figure 55 shows one such re-exposure event occurring with surrogate #3 during Round 2 at Julian Day 198 (17 July 2005). As the bar-berm profile re-adjusted to wave heights  $H_0 \geq 1.6$  m, the burial depth was reduced to  $h(i) \leq 7$  cm, thereby exposing the 5"/38 surrogate and allowing it to scour and roll. As the burial depth continued to decline to less than 4.5 cm, surrogate #3 executed a large amplitude scour and roll progression of several meters, retracing its migration route from Round 1 and trending along a general longshore pathway directed towards the south. It continued to migrate in this direction for several weeks but at a declining rate as the degree of burial gradually increased; resulting in burial lockdown at Julian Day 218 (6 August 2005), whence no further migration occurred. By the end of Round 2, surrogate #3 had migrated a distance of  $\xi(i) = 413$  cm to the south of its initial deployment location at the start of Round 1.

Altogether, MM calculates an incremental migration distance of  $\Delta\xi(i) = 599$  cm during Round 2, ending up totally buried at the end of Round 2 at a relatively shallow burial depth of only  $h(i) = 13.4$  cm. The simulated migration distances in Figure 55 compare with a net movement of 4.2 m measured by divers for surrogate #3 over Rounds 1 and 2, and a measured incremental movement of 5.1 m for Round 2.

Migration and burial dynamics were also active on the sand bars of the Offshore Group during Round 2. Figure 56 shows that the MM predicted initially no further movement of surrogate #11 until the bar shifted and the UXO became exposed on Julian Day 201 (20 July 2005). Once exposed with only 5.7 cm of the surrogate buried, it abruptly moved almost 8m in less than a day. This initial movement was shoreward, which was down slope on the shoreward face of the bar-trough bed form. This large initial excursion was the result of both gravity and radiation stress of the shoaling waves coupling together in the same direction. Once the surrogate had scoured and rolled to the trough of the bed form, migration was halted for a time, circa Julian Day 205 (24 July 2005). Thereafter, the surrogate gradually scoured and rolled about 3 m back seaward, eventually re-burying and becoming locked down under about 1 cm of overburden at a net distance of  $\xi(i) = 215$  cm from its initial starting position the beginning of Round 1. This compares to a net transport of 1.9 m measured by divers from the beginning of Round 1 until the end of Round 2. The incremental movement calculated by the MM for surrogate #11 during Round 2 was  $\Delta\xi(i) = 478$  cm, as compared with 5.9 m measured by divers.

Unfortunately, the acoustic ranging data for the positions of the most shoreward surrogates in the Inshore Group was too poor during Round 3 to provide ground truth, but we do know from the measured profiles along ranges FRF # 76 and #85 that these surrogates were buried under about 0.75 m of sand overburden. Figure 57 provides insight from the MM calculations on what surrogate #3 in the Inshore Group likely did during Round 3. In the early portions of Round 3, surrogate #3 was buried under only a couple of centimeters of over burden, which was gradually eroded away as the bar-berm profile shifted, re-exposing and unlocking the surrogate circa Julian Day 243 ( 31 August 2005). Once this occurred, it abruptly moved about 2m back toward the north, followed by more gradual northward scour and roll progress until the degree of burial increased sufficiently by Julian Day 257 (14 September 2005) to re-establish burial lock down and arrest any further movement. Thereafter, the bar-berm profile continued to transition from a summer-type equilibrium to a more winter type equilibrium configuration, increasing the depth of burial of surrogate #3 to  $h(i) = 76.5$  cm by the end of Round 3. During Round 3, the MM predicted an incremental movement of surrogate #3 of  $\Delta\xi(i) = 277$  cm toward the north, but still leaving the surrogate a net distance of  $\xi(i) = 136$  cm south of the initial placement at the start of Round 1.

Round 3 acoustic ranging measurements showed that surrogate #11 in the Offshore Group migrated shoreward an incremental distance of 3.76 m from its prior location at the end of Round 2. The MM simulation in Figure 58 calculated an incremental shoreward movement of  $\Delta\xi(i) = 345$  cm for surrogate #11 during Round 3, resulting in a net movement of  $\xi(i) = 130$  cm



shoreward of the initial placement at the start of Round 1. The time evolution of this movement was shown in Figure 58 to follow re-exposure and unlocking from shallow burial circa Julian Day 246 (3 September 2005), with continued gradual shoreward migration of the surrogate over the next 40 days. At Julian Day 285 (12 October 2005), surrogate #11 experienced burial lock down at its end point position for Round 3 and subsequently buried under less than a centimeter of sand overburden. Thus, the computed direction and magnitude of migration of surrogate #11 were in general agreement with diver observations, while the calculated burial depth was consistent with measured beach profiles along ranges FRF # 76 and #85.

A number of moderately high waves occurred during Round 4 (20 October 2005 – 16 February 2006) and produced substantial surrogate movement in both the Inshore Group (Figure 55) as well as the Offshore Group (Figure 60). In these plots, the time axis is in Julian Days relative to 2005, so that the days exceeding Julian Day 365 correspond to occurrences in the year 2006. The Round 4 MM simulation for surrogate # 3 in Figure 59 shows that it remained immobile in a state of deep burial until sufficient erosion had occurred to the bottom profile of the Inshore Group to cause re-exposure circa Julian Day 338 (4 December 2005). Once this occurred, surrogate #3 abruptly moved toward the north about 4 m, and continued a progressive northward migration for about a month when burial lock-down halted further movement circa Julian Day 369 (4 January 2006). Thereafter, burial continued to advance as the bar-berm profile shifted further into a winter equilibrium state, leaving surrogate #3 buried as much as  $h(i) = 107$  cm by the end of Round 4. The incremental movement of surrogate #3 during Round 4 was calculated by the MM to be  $\Delta\xi(i) = 1,051$  cm, which compares well with a measured incremental movement of 10.4 m based on acoustic ranging measurements. The MM calculation of net movement of surrogate #3 from the beginning of Round 1 until the end of Round 4 was  $\xi(i) = 915$  cm north of its initial placement. This agrees closely with a measured net movement of 9.1 m, suggesting that the MM calculations for surrogate #3 during Round 3, when no measurements were available, must have been accurate.

Similar accuracy during Round 4 was also obtained with the MM for surrogate #11 in the Offshore Group. Figure 60 shows that surrogate #11 was re-exposed by bottom profile shifts on Julian Day 320 (16 November 2006) and begin migrating abruptly offshore at first, and continuing its offshore migration for another 40 days. Burial began increasing abruptly near the end of 2005, and surrogate #11 ceased further migration on Julian Day 358 (24 December 2005). Continued self-similar offshore shifts of the shore rise profile increased burial depth of surrogate #11 to  $h(i) = 54$  cm by the end of Round 4. The incremental movement of surrogate #11 during Round 4 was predicted by MM to be  $\Delta\xi(i) = 572$  cm as compared to a measured value of 5.6 m. The net movement of surrogate #11 from the beginning of Round -1 until the end of Round 4 was  $\xi(i) = 443$  cm offshore of its initial placement, as compared to a measured value of 4.0 m.



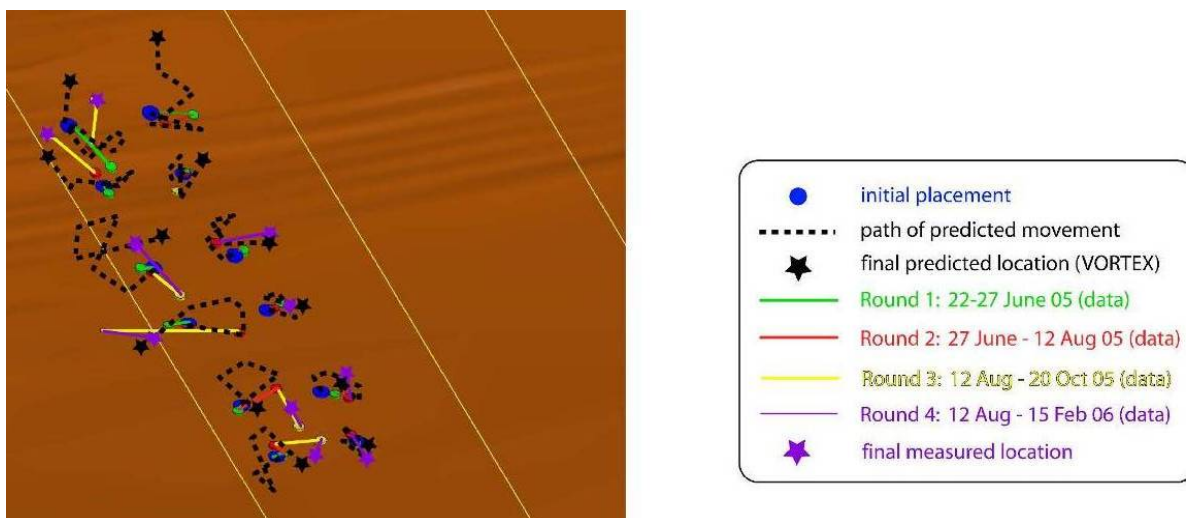


**Figure 61. Predicted vs. measured UXO migration in Inshore Field, FRF Duck, NC, Rounds 1-4, 22 June 2005 – 16 February 2006**

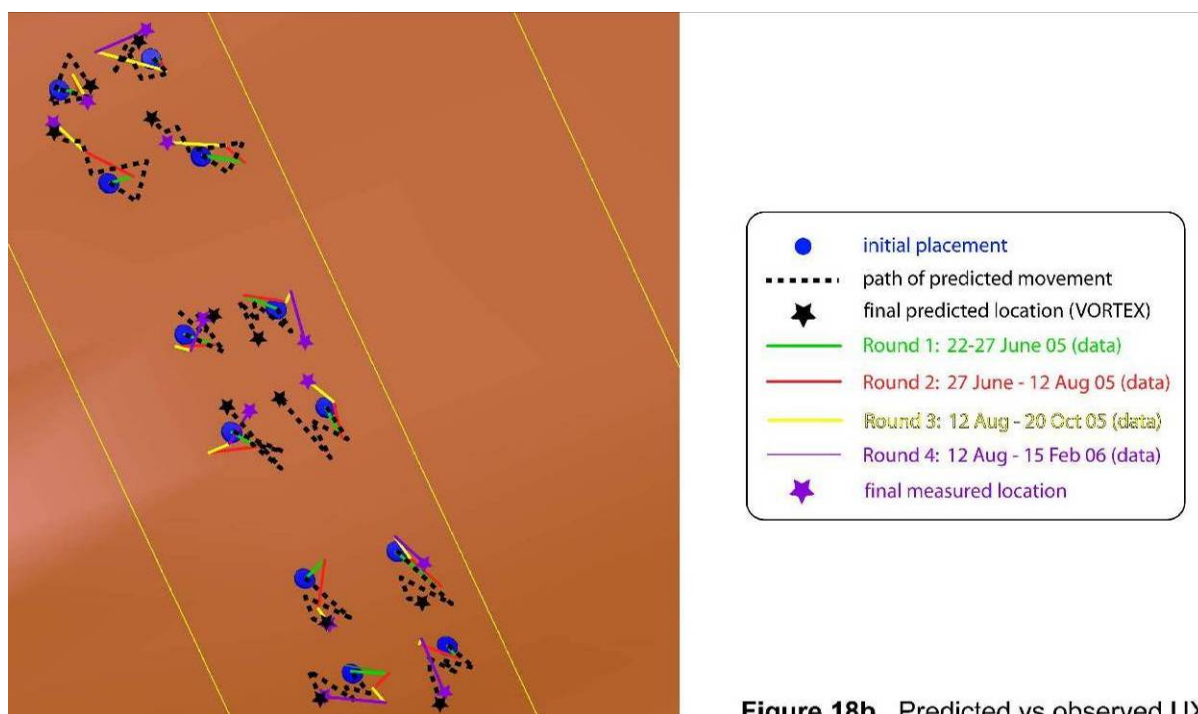


**Figure 18b. Predicted vs observed UX**

**Figure 62. Predicted vs. measured UXO migration in Offshore Field, FRF Duck, NC, Rounds 1-4, 22 June 2005 – 16 February 2006.**

A comparison of the predicted versus observed migration trajectories for Rounds 1-4 is shown in Figure 61 for all the surrogates in the Inshore Group, and in Figure 62 for all the surrogates in the Offshore Group. In these trajectory maps the initial position at the start of Round 1 is designated by a blue circle and the measured end point by a purple star. The measured legs of the

trajectories for each round are indicated by the colored line segments; Round 1 displacements are indicated in green, Round 2 displacements are in red, Round 3 displacements are in yellow, and Round 4 displacements are shown in purple. The modeled migration trajectories are shown as a dashed black line, with the predicted end-point at the end of Round 4 indicated by a black star. The identification number of each surrogate in Figure 61 and Figure 62 can be deduced from Figure 51. In general the predicted trajectories show the correct trends with respect to the direction of net movement and are within 1m of the observed magnitude of movement, which in turn is within demonstrated measurement error using the acoustic ranging technique.

To quantify the statistical accuracy of the migration predictions of the MM, we construct probability density functions from the ensembles of measured and predicted movement. Figure 63a presents the probability density function (histogram) of the measured UXO migration distances for all 24 surrogates at FRF. A total of 80 realizations of migration distance were constructed from the diver measurements from Rounds 1-4. These are contrasted with the 96 simulated realizations of migration distance that make up the modeled probability density function in Figure 63b. The peak, spread and shape of the predicted and measured probability density functions of migration in Figure 63 are quite similar. The MM predicts a mean transport distance of 3.5 m as compared to an observed mean of 4.6m, an agreement within measurement error. The MM slightly over-predicts the spread in transport outcomes, predicting a maximum transport distance of 14.3 m and a minimum of 0.5m as compared to an observed maximum of 12.6m and an observed minimum of 0.7m. However, the standard deviation of the modeled transport is slightly less than observed, with the MM giving  $\sigma_i = 1.9$  m versus the observed  $\sigma_i = 2.6$  m. This is to be expected when comparing a process-based model to stochastics from a field experiment.

Two of the 24 surrogates were not recovered after Round 4, and these were allowed to remain in place until 3 August 2006 in what was referred to as Rounds 5-6. These included one surrogate from the Inshore Group (# 18) and the other from the Offshore Group (#23). While the positions of these were not monitored, their burial depth was determined at the time of extraction on 3 August 2006. To test the MM's ability to make a long term prediction, simulations of the migration and burial of these two surrogates were performed for the period from 16 February 2006 until 3 August 2006. Figure 64 gives the migration/burial prediction of surrogate #18 of the Inshore Group during Rounds 5-6. MM results predicted no additional migration following Round 4 due to the very deep burial state. At the end of Round 4 and the beginning of Rounds 5-6, the model predicted a burial depth of  $h(i) = 251$  cm. Over the course of Rounds 5-6, the bottom profile transitioned from a winter equilibrium to a summer equilibrium and burial depth for surrogate #18 was predicted to decline to  $h(i) = 43$  cm by 3 August 2006; this compared to a measured burial depth of 0.51 m at the time surrogate #18 was extracted.

In the Offshore Group, MM predicted somewhat more active movement for surrogate #23 (Figure 65). Here the surrogate was re-exposed circa Julian Day 143 (23 May 2006) and migrated an incremental distance of  $\Delta\xi(i) = 277$  cm over a period of about 50 days before become re-buried to a depth of  $h(i) = 18$  cm by the end of Rounds 5-6. This compares to a

measured burial depth of 0.15 m for surrogate #23 at the time of extraction. Thus the MM demonstrated a high degree of accuracy in predicting the burial of these two surrogates over a full calendar year.

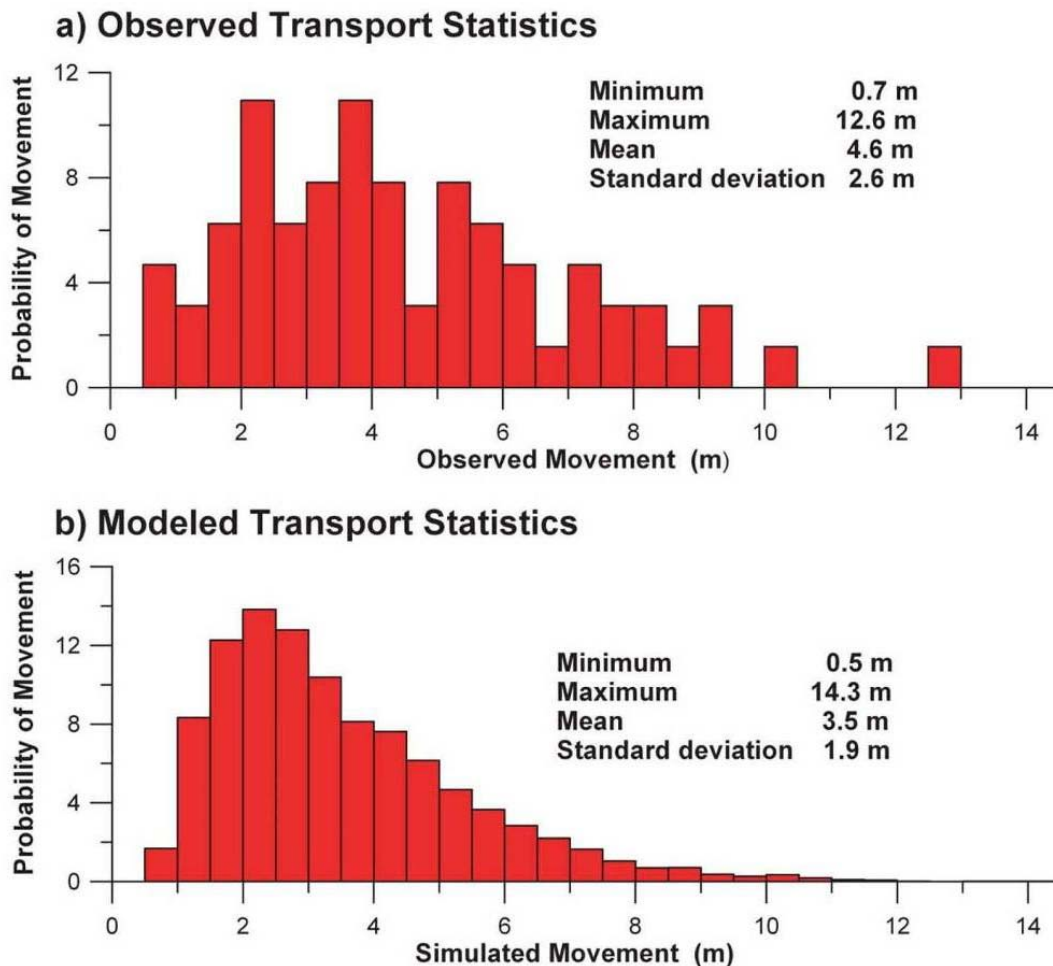


**Figure 63. Predictive skill for all surrogate movement, Rounds 1-4, FRF Duck, NC.**

The measured and predicted burial ensembles were assembled into probability density functions based on 98 separate observations and predictions. Figure 66 compares the predicted versus measured probability density functions for UXO burial at FRF during Rounds 1-6. The comparison with measured probability density function for burial in Figure 66a is quite satisfying, despite the small ensemble statistics. Again, the peak of the measured distribution, its breadth, and shape are all faithfully mimicked by the modeled distribution in Figure 66b. The model predicts a mean burial depth of 89.6 cm as compared to an observed mean of 84.9 cm. The model slightly under-predicts the spread in burial outcomes, predicting a maximum burial depth of 257.6 cm and a minimum of 11.3 cm. This compares to an observed maximum of 264.6 cm and an observed minimum of 1.85 cm. The standard deviations are virtually the same for

both the observed and modeled distributions,  $\sigma_i = 58 - 59$  cm. These burial depths are significantly greater than what was observed during the brief deployment at Ocean Shores, Washington.

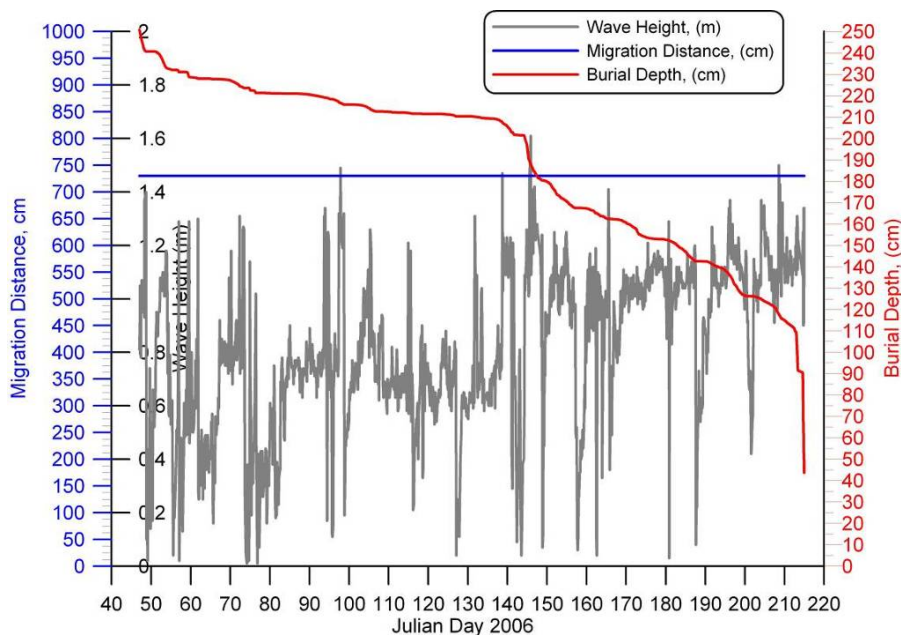


**Figure 64. MM simulation of migration and burial sequence of 5''/38 UXO surrogate #18 in Inshore Group, during Rounds 5-6 at FRF Duck, NC, 16 February – 3 August 2006.**

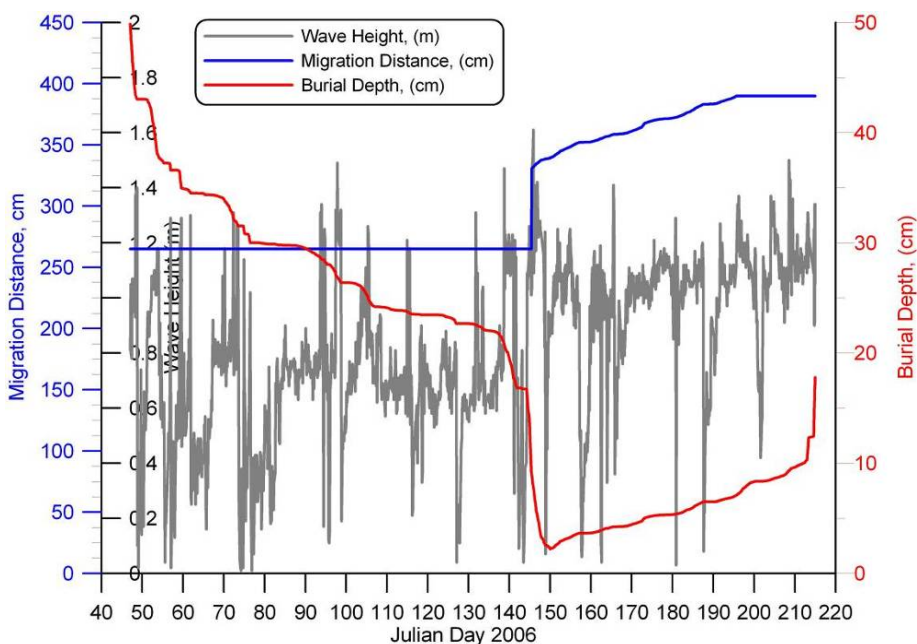


**Figure 65. MM simulation of migration and burial sequence of 5''/38 UXO surrogate #23 in Offshore Group, during Rounds 5-6 at FRF Duck, NC, 16 February – 3 August 2006.**

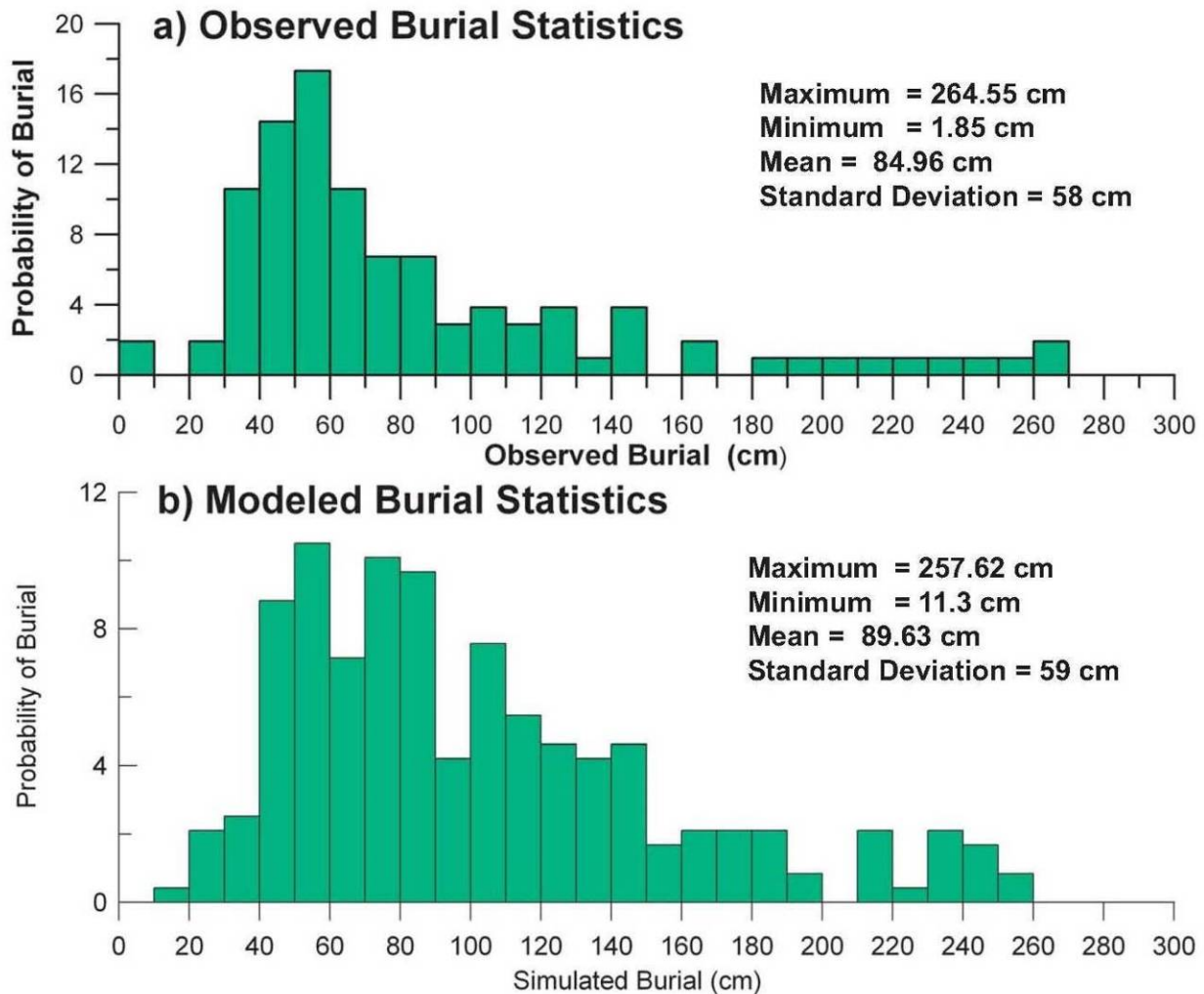


**Figure 66. Predictive skill for surrogate burial, Rounds 1-4, FRF Duck, NC; (a) Measured probability density function versus (b) predicted probability density function.**

### 6.3.3.2 Predictive Skill of Model Predictions

A predictive skill factor,  $R$ , was computed from the mean squared error between the predicted and measured outcomes. The foundation reference for the skill factor, its definition, and acceptable limits was originally treated in Gallagher et al. [43].

It was later used in the equilibrium beach profile paper that now is considered the keystone reference for this type of modeling: Jenkins and Inman's Thermodynamic solutions for equilibrium beach profiles" [35].

Two approaches are applied to assess the predictive skill of the quantitative MM predictions of the magnitude of migration and burial of UXO surrogates at FRF. With the first approach, probability density functions are produced for migration and burial magnitudes predicted by the MM and compared with the probability density functions assembled from the observed outcomes of the experiment. Because the experimental outcomes involve small ensemble statistics, we merge the results of all 24 surrogates from the inshore and offshore test sites into a single set of probability density functions. By the second approach, we compute predictive skill factor,  $R$ , is computed from the mean squared error between the predicted and measured outcomes.

Using the analytical statistical approach to error assessment, we compute the predictive skill factor  $R$  of the UXO migration distance,  $\xi$ , and burial depth  $h$  as quantified by an estimator adapted from the mean squared error. For burial depth the skill factor would have the following form adapted from Tucker [16]:

$$R_h = 1 - \frac{1}{N\hat{\sigma}_i} \left\{ \sum_{i=1}^{i=N} [\hat{h}(i) - h(i)]^2 \right\}^{1/2} \quad (5)$$

where  $\hat{h}(i)$  is the measured burial depth for  $i = 1, 2...N$  observations,  $h(i)$  is the predicted burial depth for the  $i^{th}$  observation, and  $\hat{\sigma}_i$  is the standard deviation of all observations over the period of record. For migration distance the skill factor would have the form:

$$R_\xi = 1 - \frac{1}{N\hat{\sigma}_i} \left\{ \sum_{i=1}^{i=N} [\hat{\xi}(i) - \xi(i)]^2 \right\}^{1/2} \quad (6)$$

where  $\hat{\xi}(i)$  is the measured migration distance for  $i = 1, 2...N$  observations,  $\xi(i)$  is the predicted migration distance for the  $i^{th}$  observation. Based on these formulations and the predicted versus measured outcomes in Figure 63 and Figure 66, the skill factor for migration at FRF was calculated at  $R_\xi = 0.87$  and  $R_h = 0.93$  for burial. For coastal processes modeling and mine burial prediction in particular, any skill factor in excess of 0.8 is considered to be within acceptable limits [43].

### 6.3.3.3 Conclusions from FRF Duck Field Demonstration Analysis

The field demonstration was entirely successful, with the following summary conclusions made based upon the analyses conducted to date:

- All 24 5"/38 surrogates were installed as planned and were tracked for 22 to 28 months, despite the fact that they were all found buried for each of the 7 sets of measurements.
- Measurable movement occurred, generally within the range of initial predictions.
- The predicted depth of burial matched the measured depth consistently.

- The general nature of the horizontal movements matched the model predictions. After a period of nearly two years, the average movement was within 24% of the predicted location, which is almost at the limit of accuracy of the tracking system.
- The presence of biofouling on the 5"/38 surrogates, and its absence on the 20mm surrogates, are both consistent with the Model predictions.

In addition, the following detailed conclusions were derived from the MM validation for the FRF Duck field test site:

- The trailing edge coast environment of the Outer Banks is a challenging UXO modeling problem that requires very large farfield model grids to adequately resolve the highly variable nearshore bathymetry that ultimately controls the burial/migration evolution. The farfield grid is assembled from a 2,401 x 2,401 point array (5,764,801 grid points) formatted by latitude and longitude using 3 x 3 arc second grid cell resolution and yielding a computational domain of 168.1 km along the x-axis (longitude) and 222.3 km along the y-axis (latitude). This is the largest grid on which the MM has computed UXO transport and burial to date and was necessitated by the broad-scale longshore fluxes of sediment and mass exchange occurring between the Hatteras and Ocracoke Littoral Cells. Spatial variation in wave forcing over the barrier island system of the Outer Banks is derived from refraction/diffraction analysis over the farfield grid based on directional wave measurements from instrumentation maintained by FRF. This instrumentation includes a directional wave buoy in 17m water depth (Sensor #630), pier-mounted pressure sensors at 2m depth, (Sensor # 651) and an ADCP with a pressure sensor array installed at 8m depth. The nearfield of the model was gridded for a fine to medium coarse sand bottom that was parameterized by 20 grain size bins according to the *in situ* grain size distribution. The FRF Duck sand is well sorted by the wave action and mineral analysis indicates it is predominately quartz of glacial origin. The median grain size is 565 microns, and 70 % of the sediment is comprised of medium-coarse sand between 450 microns and 750 microns. The UXO surrogates were placed in two groups (inshore group and offshore group) along two cross-shore parallel lines next to FRF profile range lines # 76 and # 85. The in-shore field (surrogate #s 1-6 and #s 13-18) was located on the north side of the FRF Pier in a nominal depth of 2m to 3 m MSL, while the off-shore field (surrogate #s 7-12 and #s 19-#4) was laid at depths between 6-7m MSL.
- Some of the largest movements of the UXO surrogates, in both the Inshore and Offshore Groups, occurred in the first two days of Round 1 when burial was initially small immediately after installation. In this minimal burial state, the UXO are particularly susceptible to mobility if sufficiently large waves occur to give rise to a supercritical transport state ( $H_0 \geq 1.2$  m). The high rate of initial migration was subsequently found to be abruptly halted by burial lock-down, whence no further movement of the surrogates occurred. Once the UXO is fully buried, as observed during each diver inspection, subsequent movement is only possible if bottom profile variation results in re-exposure to a sufficient degree that releases the UXO from burial lock-down and permits it to



undergo additional scour and roll progressions. Three such re-exposure events were calculated by the MM during Rounds 1-4 of the experiment, and a fourth was calculated for surrogate #23 during Rounds 5-6.

- In the MM, re-exposure of the UXO is the result of a complex interplay between the wave refraction/diffraction time history and the cycloid equilibrium profile algorithms. Computations of this interplay are only possible in the Mode 3 operation of the model because it requires time variability in the wave forcing, and spatial variability in the bathymetry. In the FRF model runs of Rounds 1-6, the time variation of wave height and direction (when shoaled over the broad-shelf bathymetry) produces time variability in the parameters of the bottom profile algorithms; and it is that profile variability that can re-expose a UXO and render it susceptible to further migration sequences. The type-b cycloid algorithms in the MM were found to give the best fit to the FRF bottom profiles that are well known for having complex and highly variable bar-trough bed forms. The type-b cycloid has been built into the G-95/ FRF version of the VORTEX code (Appendix B) that was used exclusively for the model analysis of this study. An interesting feature of the calibrated cycloid profiles using the supporting survey data is that the closure depth was only  $h_c \cong 6$  m to 7 m, when normally it is about twice that value. The explanation for this beach profile anomaly was the unusually benign wave forcing that persisted throughout the experiment. The thickness of the critical mass (depth of permanent entombment) is  $\xi_c = 220$  cm for the inshore UXO group;  $\xi_c = 140$  cm for the offshore group; and the critical mass of sand (volume of sand that must be removed to expose buried UXO) is  $V_c = 600$  m<sup>3</sup> to 1200 m<sup>3</sup> per meter of shoreline.
- The most accurate model predictions of migration were obtained with surrogate #3 in the Inshore Group and surrogate # 11 in the Offshore Group. The MM calculation of net movement of surrogate #3 from the beginning of Round 1 until the end of Round 4 was  $\xi(i) = 915$  cm north of its initial placement. This agrees closely with a measured net northerly movement of 9.1 m using acoustic ranging techniques. The net movement of surrogate #11 from the beginning of Round 1 until the end of Round 4 was  $\xi(i) = 443$  cm offshore of its initial placement, as compared to a measured value of 4.0 m of offshore movement.
- The most accurate model predictions of burial were obtained during Rounds 5-6 with surrogate #18 in the Inshore Group and surrogate # 23 in the Offshore Group. Over the course of Rounds 5-6, the bottom profile transitioned from a winter equilibrium to a summer equilibrium and burial depth for surrogate #18 was predicted to decline to  $h(i) = 43$  cm by 3 August 2006. This compared to a measured burial depth of 0.51 m at the time surrogate #18 was extracted. In the Offshore Group, VORTEX predicted active movement for surrogate #23. Here the surrogate was re-exposed circa Julian Day 143 (23 May 2006) and migrated an incremental distance of  $\Delta\xi(i) = 277$  cm over a period of about 50 days before become re-buried to a depth of  $h(i) = 18$  cm by the end of Rounds

5-6. This compares to a measured burial depth of 0.15 m for surrogate #23 at the time of extraction.

- Two approaches were applied to assessing the predictive skill of the quantitative model predictions of the magnitude of migration and burial of UXO surrogates at FRF. By the first approach, we construct probability density functions of migration and burial magnitudes predicted by the model and compare them with the probability density functions assembled from the observed outcomes of the experiment. By the second approach, we compute predictive skill factor,  $R$ , from the mean squared error between the predicted and measured outcomes.
- A total of 80 realizations of migration distance were constructed from the diver measurements from Rounds 1-4. These are contrasted with the 96 simulated realizations of migration distance that make up the modeled probability density function. The peak, spread and shape of the predicted and measured probability density functions of migration are quite similar. The model predicts a mean migration distance of 3.5 m as compared to an observed mean of 4.6 m, an agreement within measurement error. The model slightly over-predicts the spread in migration outcomes, predicting a maximum migration distance of 14.3 m and a minimum of 0.5 m; compared to an observed maximum of 12.6 m and an observed minimum of 0.7 m. However, the standard deviation of the modeled migration is slightly less than observed, with the model giving  $\sigma_i = 1.9$  m versus the observed  $\sigma_i = 2.6$  m. This is to be expected when comparing a process-based model to stochastics from a field experiment.
- The measured and predicted burial ensembles were assembled into probability density functions based on 98 separate observations and predictions during Rounds 1-6. The peak of the measured distribution, its breadth, and shape are all faithfully replicated by the modeled distribution. The model predicts a mean burial depth of 89.6 cm as compared to an observed mean of 84.9 cm. The model slightly under-predicts the spread in burial outcomes, predicting a maximum burial depth of 257.6 cm and a minimum of 11.3 cm. This compares to an observed maximum of 264.6 cm and an observed minimum of 1.85 cm. The standard deviations are virtually the same for both the observed and modeled distributions,  $\sigma_i = 58$  -59 cm.
- The skill factor for migration at FRF was calculated at  $R_\xi = 0.87$  and  $R_h = 0.93$  for burial. For coastal processes modeling, and mine burial prediction in particular, any skill factor in excess of 0.8 is considered to be a good result [43].

## 7.0 PERFORMANCE ASSESSMENT

### 1.24 7.1 Performance Criteria

The primary metric for gauging the success of each Field Demonstration was collecting data on the movement of all or most of the UXO surrogates and documenting the environmental conditions that caused those movements (i.e., currents, waves, seafloor properties, etc.). The primary metric for success of the MM validation effort was that the observed movement matched the predicted movement well enough to allow final adjustment of the model parameters to match the observations without changing the basic structure of the MM (assumptions of basic forces and interactions). The performance criteria for the validation program and for the MM are shown in Table 5.

**Table 5. UXO Mobility Model Validation Performance Criteria.**

<b>Performance Criteria</b>	<b>Criteria Description</b>	<b>Primary or Secondary</b>
MM proves useable by engineers other than software creators.	MM software studied and exercised by NAVFAC ESC and SST staff.	Primary
Field Demonstrations allow sufficient quality data to be collected and allow Model to be validated.	Movements measured and data recovered from at least 50% of large surrogates and 10 % of the 20 mm surrogates.	Primary
MM validation shows good match between predictions and measurements, with coefficients correctable to positive match.	Either R or $r^2 > 0.8$ at each site.	Primary
MM provides credible predictions of movements in support of demonstration planning.	MM used for each site to predict movement in planning demonstrations. Resultant movement stays within bounds of demonstration.	Secondary

### 1.25 7.2 Performance Confirmation Methods

Table 6 summarizes the performance confirmation methods.

**Table 6. Performance confirmation methods.**

<b>Performance Criteria</b>	<b>Expected Performance Metric (pre demo)</b>	<b>Performance Confirmation Method</b>	<b>Actual (post demo)</b>
MM proves useable by engineers other than software creators.	MM software studied and exercised by NAVFAC ESC and SST staff.	NAVFAC ESC and SST staff ran MM on various computers and compiler software	Both NAVFAC ESC and SST staff have been able to use the software (run the MM). However, there is still value from the MM developer (Scott A. Jenkins Consulting) as new applications arise.
Field Demonstrations allow sufficient quality data to be collected and allow Model to be validated.	Movements measured and data recovered from at least 50% of large surrogates and 10 % of the 20 mm surrogates.	All field observations and measurements by divers recorded by hand and then tabulated.	At FRF Duck, 92% of 120 data points in the 5 main measurements were successful. Measurements were accurate within 1-2 m (<7% of range). Only a sampling of the 20mm was obtained – but no movement observed. At Hawaii 73% of the 168 possible data points in the 6 measurements were successful. 100% of the final 3 measurement sets were successful. Measurements were accurate within 1-2 m (<9% of range).
MM validation shows good match between predictions and measurements, with coefficients correctable to positive match.	Either R or $r^2 > 0.8$ at each site.	Probability density function (PDF) of field measurements compared against PDF of MM predictions.	MM validation by visual match to measurements is very good. For FRF Duck, $R_\xi = 0.87$ for movement and $R_h = 0.93$ for burial For Hawaii, $R_\xi = 0.88$ for movement, $R_h = 0.90$ for burial.
MM provides credible predictions of	MM used for each site to predict movement in	Preliminary Mode 1 MM analyses conducted for	At both the PMRF and FRF Duck sites the MM predictions generally agree with complex

movements in support of demonstration planning.	planning demonstrations. Resultant movement stays within bounds of demonstration.	each site, along with independent estimates of maximum movement (away limits, etc.)	movements observed for multiple items. All surrogates remained within planned range of measurements.
---	---	---	--

Specifically, the MM itself was validated by the standard criteria used for software simulation validation. There are two commonly used metrics for validating model performance in a quantitative manner. These are the skill factor, R, and the coefficient of determination,  $r^2$ . The predictive skill factor, R, of the model solutions for migration distance, h, is measured by the following estimator adapted from the mean squared error

$$R_{\xi} = 1 - \frac{1}{N\hat{\sigma}_i} \left\{ \sum_{i=1}^{i=N} [\hat{\xi}(i) - \xi(i)]^2 \right\}^{1/2} \quad (3)$$

where  $\hat{h}(i)$  is the measured migration distance for  $i = 1, 2 \dots 9$  temporal observations,  $\xi(i)$  is the predicted migration distance for time, i, and  $\hat{\sigma}_i$  is the standard deviation of all observations over the period of record.

The coefficient of determination,  $r^2$ , is used as a measure of predictive skill for the migration parameters (distance and direction) and is calculated from the usual form

$$r^2 = \frac{SSe}{SSe - SSR} \quad (2)$$

where SSe is the residual sum of squares given by the sum of the squares of the difference between the predicted and observed values, and SSR is the regression sum of squares given by the sum of the differences between the average of all observed values and the predicted value at each time, i.

Both are based on the mean-squared variation between measured migration distance and predicted migration distance. For the MM to be of merit, it must at least be capable of achieving a value greater than 0.5 for either R or  $r^2$ . If the model can do better than  $R > 0.8$  or  $r^2 > 0.8$ , then it is considered to be a highly predictive model. A perfect model achieves  $R = r^2 = 1.0$ .

The level of validation achieved in the ESTCP tests is sufficient for bringing the MM into widespread use, and therefore not only directly benefits the individual program users but will also establish a DoD-wide base of experience. This process provides field experience for the widest possible range of site environmental conditions and UXO types. Such experience established relationships between site characteristics and controlling MM parameters that can

subsequently be used to expedite calibration for all remaining sites. In turn, users are now able to interpolate MM results for future un-calibrated sites instead of initiating a new extrapolation process.

### **1.26 7.3 Performance In Extreme Conditions**

The UXO Mobility Model (MM) was validated at various levels and for four different coasts. These validations took place in weather conditions that would best be described as “normal” or “average” at the sites:

- At Point Mugu, CA, the test took place throughout a typical Southern California winter, with only normal storms (no El Niño or other major events).
- At Ocean Shores, WA, the test took place during just a single, moderate winter storm.
- At FRF Duck, NC, the demonstration was in place for two full years, but during both years, all the hurricanes bypassed the Carolina coast and moved south into the Gulf of Mexico (i.e., Katrina, Rita, etc.). Only the low-energy end of several nor’easter winter storms reached the site.
- At PMRF Kauai, HI, the waves were generated from only a normal winter, and the UXO surrogates were in a protective awa, or sand channel. They also were in relatively deep water because of local concerns for possible damage to the coral if the UXO were moved out of the awa.

Nevertheless, these validations address conditions that would occur well over 99 % of the time at typical UXO sites. A 10-year storm lasting an entire two weeks would thus comprise only 0.4% of the total time period, which is relatively minimal.

However, extreme events have the potential to provide more movement than all the other 99% of the exposure time combined. For example, simulations of a 10-year event at the Washington state site showed that with 20 foot waves over a period of just a few days, the UXO would have moved 664 feet and wound up on shore above the high tide line (Figure 67). By comparison, the MM predicts that sustained normal wave action in the area would move UXO just a few feet and leave it buried most of the time. That prediction was validated by the MMFT Test at Ocean Shores, WA [2].

Therefore, it remains reasonable to determine the validity of the UXO Mobility Model for “extreme” events.

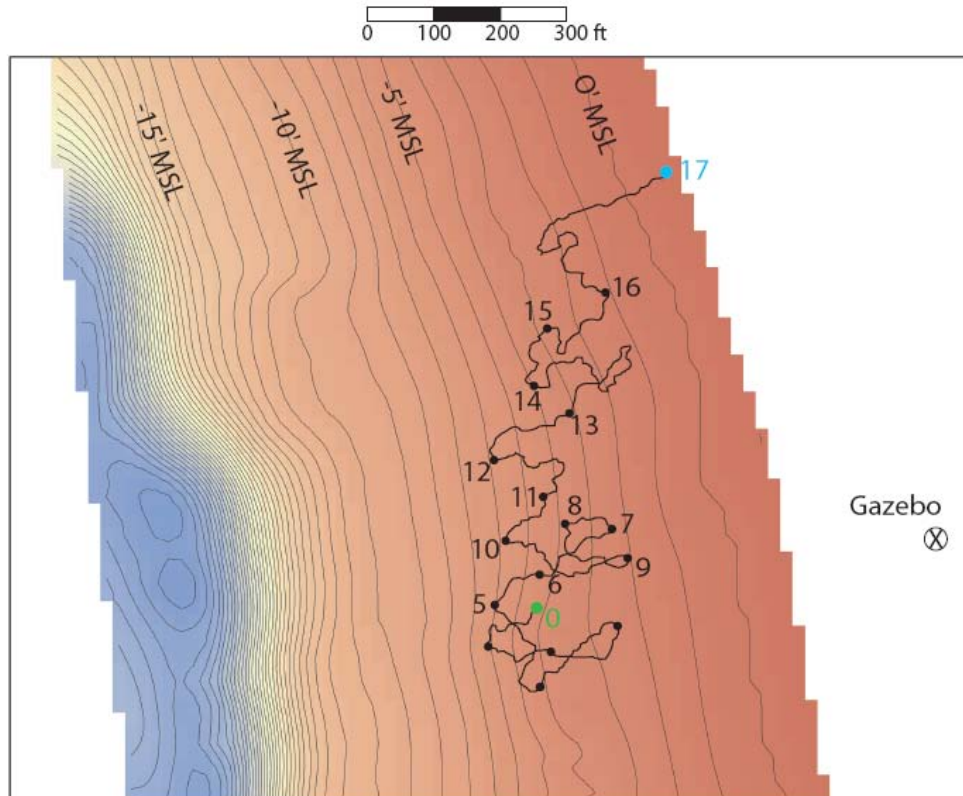


**Figure 67. Extreme case simulation of migration trajectory for 5" naval projectile during storm series, 17 Nov - 4 Dec 2003, Pacific Beach, WA: Hmax = 20.3 ft, net migration 664 ft.**

### 7.3.1 Background

In order to evaluate the level of validation, it is necessary to first review the foundation of the MM. The two primary elements of the MM are the modules which take into account the farfield and nearfield processes. The farfield modules model the external environmental forcing functions, which primarily consist of incoming waves and currents. The nearfield modules model the resulting small-scale hydrodynamics, vortex shedding, sediment scour, and resultant UXO burial, unburial, and movement and reburial cycles.

In all of the field tests, the results of the MM measured movements matched the model predictions with only minor calibrations required. Those tests included seafloor wave conditions ranging from very benign (e.g., sheltered away, calm weather on the FRF Duck coast, etc.) to the conditions directly under 2m breaking waves on the shallow hard beach of the Ocean Shores coast in Washington state. The tests included a variety of seafloor sediment properties, slopes, and sediment depths, etc. Of note is the fact that when large waves, and even breaking waves, were input to the MM, the software still functioned properly with no mathematic or logic errors.



As a result, the nearfield modules of the MM are well calibrated and validated for a very wide range of seafloor conditions; if the input data from the farfield modules are valid, there is high confidence that the output from the nearfield modules will be valid as well. Therefore, the issue becomes one of validating the farfield inputs, which take into account the wave models.

### **7.3.2 Modeling Incoming Waves**

The REF/DIF (refraction/diffraction) model used in the MM is very widely used and accepted, and acts as an industry standard. Also, for each of the ESTCP program field demonstrations, the predictions from the REF/DIF model were compared against ADCP measurements from the same site, which compared favorably and were also within the measurement accuracy of the ADCP itself.

Even so, the seafloor water movement predictions of the REF/DIF model have not been directly validated under the extreme wave conditions of hurricanes or similar storms in the nearshore area where breaking waves occur. The problem is that direct-measurement buoy systems will not survive the forces of those waves to provide data throughout the storm. Even bottom-mounted instruments are frequently lost or fail in such conditions. Oil companies own particularly extensive wave data sets since they heavily instrument their large oil platforms. However, those data are very-closely held and proprietary, and therefore not suitable for the public distribution required of ESTCP reports; the information also does not include wave data for the immediate near-shore environment.

Therefore, the existing wave models of water velocity at the seafloor are not entirely calibrated and validated for the most extreme, shallow water wave conditions. However, it is important to consider that the models do replicate the surface shape of waves as they are affected by their approach to shore. Since the alteration of wave shape with decreasing water depth is driven by the interaction with the seafloor, it is reasonable to assume that the model approximation of that interaction is reasonably accurate. Otherwise the calculations of the resultant wave shape, height, period, etc., would not be as accurate as they are.

Therefore, it is reasonable to conclude that the existing wave models, which are taken into account under the farfield inputs, do provide an estimate of water velocity at the seafloor in extreme conditions that is sufficiently accurate to support a statistically-based risk analysis of UXO movement. Whatever errors are produced by the wave model itself are likely smaller than those associated with the other inputs to the MM, such as the initial estimates of UXO population and distribution, variations in sediment grain size over the area of analysis, variations in UXO shape with marine growth, sediment outflow rates from nearby estuaries, etc.

### **7.3.3 Effect of Extreme Events on Overall Risk Analysis**

It also is useful to consider the overall impact of an extreme event on the total risk of human interaction at a UXO site. Extreme events such as hurricanes always produce other kinds of damage to structures on or near the shore, as well as changes in the beach structure itself. They only occur every few years and they draw much attention when they do take place. If there are

known UXO in the nearshore area, emergency management forces can be alerted to the possibility of UXO moving ashore (or into other offshore areas) and specific steps can be taken to safely clear the UXO as part of emergency response cleanup efforts. Essentially, these occurrences are unusual events, and the response to them can be conducted under controlled conditions, with special awareness of possible UXO risks. As a result, the actual risk to public safety from UXO after extreme events is generally less than if the UXO were to migrate ashore, or move into previously clear areas, without any special alerts made to the public. Even a less-than-fully-validated model of the probability of UXO movement into public areas in extreme events will still provide a useful decision tool. The site manager will be able to decide whether it is more cost-effective to try to clear all the UXO from the potential movement source in advance, or take action upon whatever moves after an extreme event occurs.

### **7.3.4 Summary of Present Validation for Extreme Events**

The nearfield modules have been directly validated for a wide range of inputs, and the farfield wave model were indirectly validated by inference from its fidelity in modeling wave shape. It is therefore reasonable to conclude that extrapolation of the UXO Mobility Model to analysis of extreme wave events will not introduce any significant errors beyond those associated with the other basic MM inputs.

Also, UXO movement into public areas after extreme events can be generally predicted and appropriate emergency response forces alerted. The UXO can be handled under relatively controlled conditions as part of the response to the extreme weather event, so public safety is at considerably less risk than if the UXO appear without any weather indicators.

The UXO Mobility Model is directly validated as a tool to provide warning of UXO movement under those “normal” conditions and is validated by inference as a tool to generate alerts for movement under extreme weather event conditions.

## **8.0 COST ASSESSMENT**

### **1.27 8.1 Cost MODEL**

Per the Federal Remediation Technologies Roundtable (FRTR) *Guide to Documenting and Managing Cost and Performance Information for Remediation Projects* (EPA 542B 98-007, Oct 98), “The total cost for an application should not include other project phases/activities, such as preliminary assessment/site investigation, remedial investigation/feasibility study, remedial design, or post-closure surveillance and long-term monitoring.” Since the UXO Mobility Model is a basic tool to support all of the “other project phases/activities”, the cost structure of this section will not include most of the items in the standard format that pertain to the actual remediation process.

The operational costs of using the MM and associated IM are substantially less than the costs that were required to develop and validate the two models. The primary cost elements for using the MM, in generally descending order, are:

- Data acquisition (climatology, bathymetry, seafloor conditions, human use activities, UXO history and distribution). The costs can be minimal if the site is already well documented, but can be as much as several hundred thousand dollars for each small site if in situ surveys are required.
- Data formatting and processing for use (gridding bathymetry, deriving UXO population – can be as much as a few months of labor)
- MM computer operations (typically less than a few weeks of labor)
- Report development
- Customer liaison

Since the MM is applied in steps (Mode 1, 2, 3 as required), the total cost of using the MM is controlled by the level of detail required, and by the site-specific results obtained as the analysis proceeds.

The actual costs of the MM development and validation are provided here for reference, along with example estimates of costs for various levels of site analysis.

#### 8.1.1 Development and Validation Costs

The Navy program that developed the UXO Mobility Model and provided the initial limited validation started in December 2002 and concluded in December 2005. The entire ESTCP UXO Mobility Model validation program started in June 2004 and concluded in June 2008. The program spanned 5 years and the total expenditure was approximately \$1,795,750. The ESTCP investment was approximately \$1,278,000.

Table 7 summarizes the program costs. The investment was divided between the MM development work (28%) and the field validation effort (72%).

**Table 7. UXO Mobility Model program cost summary.**

	Navy	ESTCP	TOTAL
<b>MOBILITY MODEL DEVELOPMENT</b>			<b>\$498,375</b>
FY02-FY04	\$143,375		
FY05-FY08		\$355,000	
<b>MOBILITY MODEL VALIDATION</b>			<b>\$1,297,375</b>
Pt. Mugu Test	\$119,188		
Measurement Method Field Test	\$255,188		
FRF Duck, NC, Demonstration		\$404,320	
PMRF Kauai, HI, Demonstration		\$433,320	
Example Application Analysis		\$85,360	
	<b>\$517,750</b>	<b>\$1,278,000</b>	<b>\$1,795,750</b>

## 1.28 8.2 COST DRIVERS

As discussed above, the main cost drivers on the use of the MM and IM are the acquisition and processing of the environmental data required as inputs to the models. The best way to illustrate the range of those costs is by example.

The costs to apply the MM at full-scale sites are separated into three phases of analysis. The detailed process of applying the MM to a full-scale site is described in Wilson et al. [7], the Applications Guidance Document.

### Mode 1 Screening Analysis

The first phase uses only Mode 1 of the MM. All of the inputs for this phase are composed of existing data available from a “desk-top” study. Default values are used for many of the MM inputs, based on the general coastal type. The primary purpose of the Mode 1 analysis is to determine areas that are *not* at risk of human exposure to UXO. Therefore, these are areas in which either (a) there are no UXO of concern or (b) the UXO is permanently entombed – buried at depths below any known or forecast human activities (i.e., fishing, dredging, etc.). The term “permanently” is limited by the worst-case storm activity ever recorded or forecast for the site. Table 8 shows an example cost estimate for a basic Mode 1 screening analysis of a typical UXO “site”.

The assumptions made in this cost estimate are as follows:

- UXO site manager liaison is provided via NAVFAC
- Analysis performed by support contractors (e.g., engineers/computer analysts)
- UXO site managers have Mode 1 level data available, including:
  - general estimate of history of UXO type and distribution
  - basic bathymetry (NOAA charts or past local surveys)
  - defined areas of responsibility (boundaries)
  - summary of type and location of human use (e.g., fishing, recreation, dredge, etc.)
- Initial analysis performed without travel (no site visits)
- Baseline “site” is a single section of coastline (e.g., small bay, offshore from firing range, etc.)
- Duration of Mode 1 phase is approximately 3-6 months.

Note that the word, “site”, in this context refers to a relatively small, contiguous area of UXO with dimensions on the order of a few kilometers, such as a small bay, firing range, etc. Estimates for larger “sites” such as an entire island, a major coastline, etc., are developed as multiples of single sites.

**Table 8. Nominal cost of Mode 1 screening analysis of a single UXO site.**

<b>MODE 1 SCREENING ANALYSIS</b>	
Initial contact, problem definition, liaison	\$20,000
Preliminary screening (set up ARCGIS, plot areas of use, define closure depth)	\$20,000
Mode 1 analysis of UXO movement at selected points in risk areas (no Model modifications)	\$30,000
Preliminary analysis of risk of human interaction	\$8,000
Initial report & recommendations	\$8,000
Program management	\$10,000
<b>Mode 1 Total</b>	<b>\$96,000</b>

Unless either (a) the desktop data for the Mode 1 are unusually complete and detailed or (b) the Mode 1 analysis clearly shows that even conservative estimates place virtually all the UXO at the site at very low risk of human interaction, it will be necessary to conduct a more detailed analysis, using additional site-specific data inputs (Mode 2).

### **Mode 2 Detailed Analysis**

The Mode 2 analysis is only conducted on those parts of the site that are not clearly shown to be low risk by the Mode 1 analysis. Mode 2 requires input data for the local environmental conditions that are not normally available for UXO sites. However, the Mode 2 analysis does not involve any direct surveys of the UXO distribution itself. The assumptions for the Mode 2 Detailed Analysis phase are as follows:

- Mode 1 was previously completed
- UXO site manager liaison is provided via NAVFAC
- Analysis performed by support contractors (e.g., engineers/computer analysts)
- Environmental site surveys required (though a UXO survey is not)
  - bathymetry (LIDAR or multibeam backscatter (MBBS) for details of depth at 2-5m spacing, <1 m resolution)
  - bottom samples to determine sediment properties
  - on-site wave measurements are necessary to refine the REF/DIF model
  - on-site human use surveys are conducted to obtain fishing data, etc.
- Climate and human use studies cover one annual cycle
- Mode 2 phase lasts about 18 months after Mode 1.

Mode 2 will likely meet the analysis needs for most sites.

The costs to apply the MM at full-scale sites varies considerably with the size and location of the site (e.g., area to be modeled, cost of data to be collected), complexity of the bathymetry, level of

human use, etc. The size of UXO sites ranges from as little as a square kilometer for one bay at Vieques, PR, 100 km<sup>2</sup> for the offshore area of Camp Perry on Lake Erie, 150 km<sup>2</sup> for the entire coastline of Kaho'olawe, HI, and 240 km<sup>2</sup> for the firing range off Ft. Monroe, VA. Each of those could be surveyed in a single day by aircraft at approximately \$50,000 per day, plus mobilization costs. The subsequent post-processing of the data costs approximately \$1000/km<sup>2</sup>. Therefore, the total price for LIDAR survey of typical UXO sites range from about \$90,000 for the Vieques area to as much as  $\approx$  \$310,000 for the Ft. Monroe area. For an example mid-sized site, the estimated cost is as shown in Table 9; note that the dominant costs are associated with the site surveys.

**Table 9. Estimated cost of Mode 2 Detailed Analysis.**

<b>MODE 2 DETAILED ANALYSIS</b>	
Detailed Mode 2 phase program plan	\$10,000
Bathymetry survey (LIDAR or MBBS)	\$200,000
On-site sediment sampling & ADCP (four seasons)	\$95,000
Human use surveys (fishing, boating, diving, etc.)	\$30,000
Update Mode 1 ARCGIS and data sets	\$15,000
Mode 2 Analysis of UXO movement at selected points in risk areas.	\$50,000
Updated analysis of risk of human interaction	\$12,000
Mode 2 Report	\$12,000
Program management	\$35,000
<b>Total</b>	<b>\$459,000</b>

### Mode 3 Enhanced Analysis

Mode 3 adds the final input detail of enhanced estimates of the UXO initial distribution. Since obtaining this type of information is the most expensive, and potentially dangerous data to collect, it is only added to the process when the desk-top data on UXO distributions are not credible due to such issues as age, inconsistencies, etc., and either (a) there is clear evidence of substantial risk of human interaction or (b) large-scale UXO movements are predicted that require more accurate estimates. The development of enhanced UXO distribution estimates involves several possible technologies and considerable on-site effort and cost. It begins with additional analysis of historical data to convert recorded UXO entry (e.g., air drops, gunnery, etc.) into expected impact with the seafloor and initial burial. This data is matched against more refined on-site surveys of the seafloor itself to locate and identify UXO that are not entirely buried. The final step is to locate buried UXO using sub-bottom profilers, magnetometers, diver, checks, etc.

The assumptions for a Mode 3 Enhanced Analysis cost estimate are as follows:

- Mode 1 and 2 were previously completed
- Mode 3 is only used for cases of high risk, or if UXO data are questionable
- UXO site manager liaison is provided via NAVFAC

- Analysis performed by support contractors (e.g., engineers/computer analysts)
- Mixture of means used to develop UXO distribution baseline:
  - impact analysis (historical firing records and physics of impact)
  - analysis of previous bottom imagery to detect surface UXO
  - new visual searches of seafloor (e.g., ROV, towed fish, divers)
  - new acoustic surveys (e.g., imagery, sub-bottom)
  - magnetometer surveys
- Costs vary considerably with size and location of site and type of UXO
- Mode 3 phase spans approximately 12 months beyond Mode 2 phase (6 months survey, 6 months analysis)

Table 10 shows an example estimate of the costs of this additional Mode 3 Enhanced Analysis phase.

**Table 10. Mode 3 Enhanced Analysis cost estimate.**

<b>MODE 3 ENHANCED ANALYSIS</b>	
Detailed Mode 3 phase program plan	\$5,000
Impact analysis (historical firing records plus physics of impact)	\$8,000
Analysis of previous bottom imagery (for surface UXO)	\$10,000
New visual searches of seafloor (ROV, towed fish, divers)	\$200,000
New acoustic surveys (imagery, sub-bottom)	\$200,000
Magnetometer surveys	\$50,000
Run Mode 3 simulations (updates Mode 2 results at key points).	
Estimate half-life of UXO survey data v. remediation schedule	\$30,000
Updated analysis of risk of human interaction	\$12,000
Mode 3 Report	\$12,000
Program management	\$50,000
<b>Total</b>	<b>\$577,000</b>

## 1.29 8.3 Cost BENEFITS

### 8.3.1 Cost Comparison

There are no other available computer models to which the MM can be compared to determine competitiveness. The most instructive comparison is the cost of applying the MM versus the potential savings in remediation efforts.

In any event, the cost of using the MM to define areas of high risk will be small compared to alternative approaches such as sweeping the total area of possible UXO contamination, which can easily cost many tens of \$M per site. As of this writing, the MM is also the only tool that allows credible analysis of sites to be conducted to verify that risk either is already at an acceptably low level, and therefore does not require comprehensive clean up costs, or to set the depth and area of cleanup so that it covers the entire risk area and avoids the need to sweep the area again later if adjacent UXO migrate into the swept area after cleanup. Also, analysis at the



Mode 1 level reduces the need for Mode 2 data collection, and, in turn, Mode 2 reduces need for Mode 3 to be conducted.

One way to quantify the value and compare the cost of using the MM is to estimate the Return On Investment (ROI). That is, compare the cost savings produced by the MM, less the investment costs, as a fraction of the investment costs. The equation for ROI is:

$$\text{ROI} = (\text{Savings} - \text{Investment}) / \text{Investment}$$

An ROI of 0 is the break-even point where the savings equals the investment.

Of course there are other non-economic benefits associated with using the MM, such as reducing risk, demonstrating good faith efforts, etc. However, this analysis solely focuses on cost benefits.

The primary cost benefit from the UXO Mobility Model is to reduce the size of the area requiring cleanup and remediation. The MM shows where UXO are permanently entombed deeper than any human interaction will occur. It also provides the limits of UXO movement, so it bounds the need for “preventative” clearance measures.

The actual ROI depends heavily on the derived percent reduction in required cleanup, which will not be known until the MM is applied to specific sites. However, it is possible to bound the ROI.

For example, in 2004, the approximation of “best-possible” ROI was determined as follows:

- The estimated cost to clean up three major underwater UXO sites (Mare Island, Vieques, Kaho’olawe) was  $\approx$  \$2,764M.
- The estimated cost of the UXO Mobility Model development and validation program was \$1.32M (note that no estimates for operational use were available at that time).
- IF the MM program then showed that NO cleanup was required at those three sites, which is unlikely, but a “best case” scenario, the ROI would then be equivalent to

$$\frac{(\$2,764 - \$1.32)}{\$1.32} = 2092$$

This value translates into savings that are 2092 times the cost of using the MM – a significant ROI.

Now that the development program is concluded, it is possible to develop a more realistic estimate of the ROI.

- First, there is now a better estimate of the cost to use the MM. A Mode 1 screening analysis can be performed for a single site for approximately \$200k. However, if detailed *in situ* surveys of the UXO baseline population are required, it could cost as much as

\$1M per site. These two estimates range from \$0.6M (minimum) to \$3.0M (maximum) for the three sites. Also, the cost correction for inflation makes the 3-Site total cleanup cost equal to  $\approx \$3,233\text{M}$ .

- Second, the analysis can consider the example sites and how much cleanup area might actually be reduced by using the MM analysis to better estimate of savings.
- As a final step, the minimum amount of cleanup reduction required to equal the future investment costs, the break-even point, can be determined.

Note that the \$1.5M development costs are sunk and not part ROI for future investments.

For the updated “Best Case” scenario (parallels the 2004 approach),

$$\text{ROI} = (\$3233\text{M} - \$3\text{M})/\$3\text{M} = 1077$$

which translates into savings = 1077x MM use costs.

**To refine the ROI further, consider the following three figures showing the same three example sites used in the original analysis: Mare Island Naval Shipyard (Figure 68), Vieques (Figure 69), and Kaho’olawe (Figure 70).** In each figure, the maximum area requiring remediation is outlined, along with an example of the possible reduction in area allowed by the results of the MM.

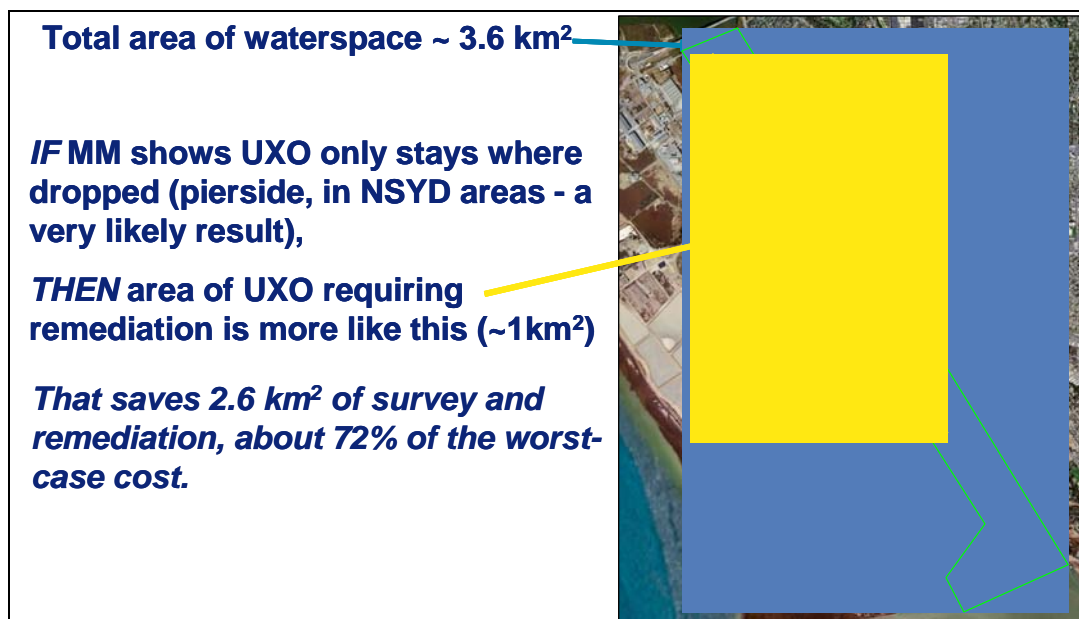


**Figure 68. Mare Island Naval Shipyard UXO remediation area comparison.**

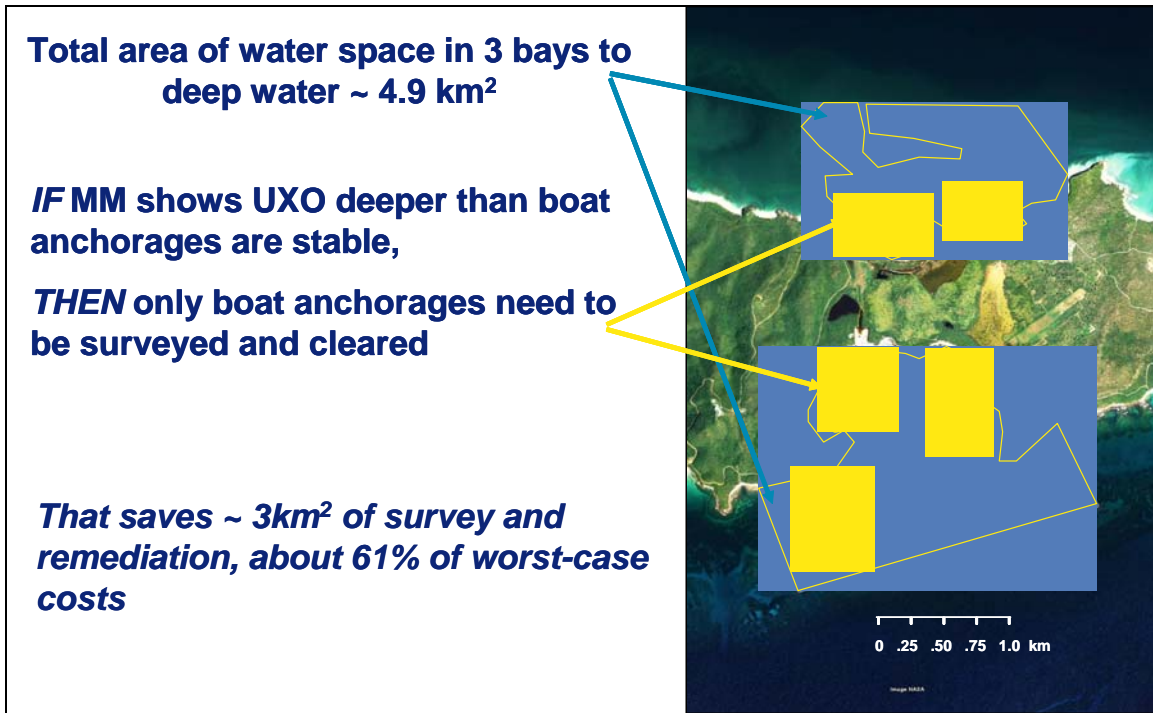


**Figure 69. Vieques range UXO remediation area comparison.**

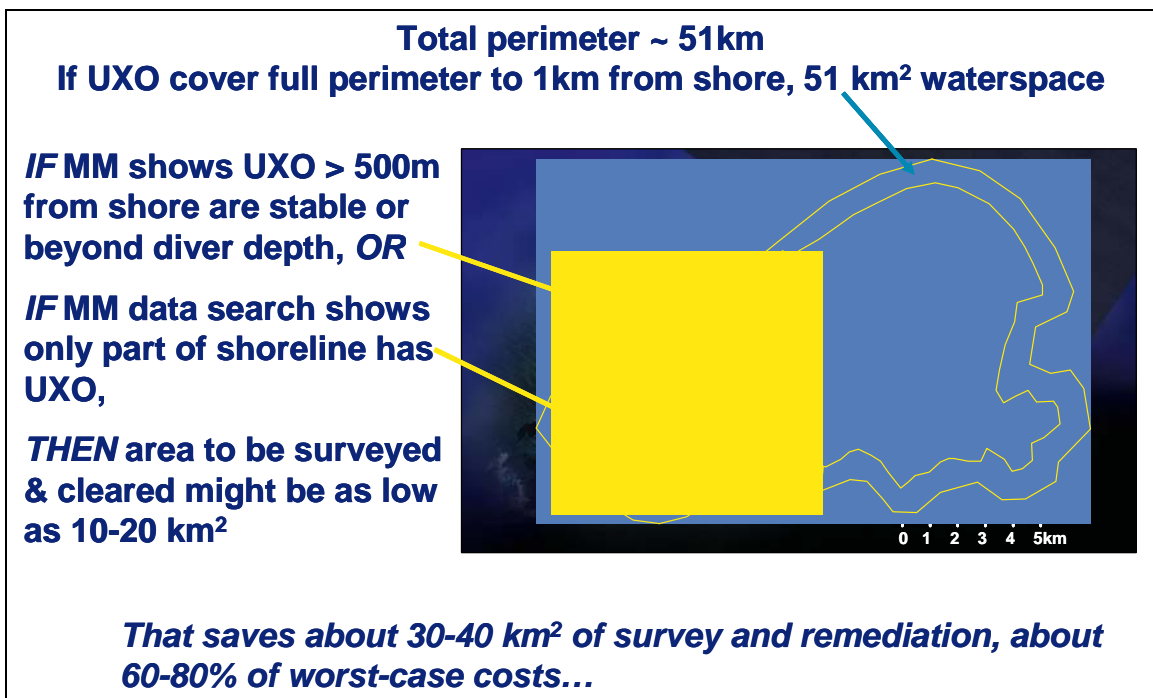


**Figure 70. Kaho'olawe Island UXO remediation area comparison.**

For these more realistic scenarios, the savings average  $\approx 75\%$  of the worst-case. Therefore,

$$\text{ROI} = [(0.75 \times \$3233) - \$3] / \$3 = 807$$

which still signifies that the savings is equivalent to 807 x MM use costs, a good investment by almost any standard.

The break-even point, or  $\text{ROI} = 0$ , occurs when MM usage saves just \$3M, which is 000928 x worst case costs (less than 0.1%); this is only 0.06 km<sup>2</sup>, or an area of seafloor approximately 245 x 245 m<sup>2</sup> (one football field per site).

Clearly, the cost to use the MM will virtually always be much less than the savings it produces in reduced area requiring survey and remediation.

### 8.3.2 Basis of Costs

Note there are essentially no required annual costs for this MM. The software does not require updates since it is written in Fortran code. Both the commercial ABSOFT and the freeware GNU compilers have been used.

A normal professional-grade laptop or desktop computer unit is required. The computer to be used to execute the MM software should meet the configuration shown in Figure 71. The Intel processor is not important; however, the installed processor must be operating with Window XP SP2 or later. The 2GB of installed memory is critical to execution of the larger code modules. While an internet connection is not necessary to run the UXO model it is useful to obtain software updates to both the Windows operating system and compiler and to obtain data. See the User's Manual [14] for further details.

As with any software model that predicts a hardware system response to environmental forcing functions, two primary costs are inherent in using the model:

- a. Collecting data on the initial hardware configuration
- b. Collecting historical data from which to predict the environmental forcing functions.

The cost of actually running the MM itself is very low at typically a few days or weeks of engineering labor. The MM runs on a typical high-end engineering desktop computer, so there is no computer time cost. A simulation of UXO migration and burial for a 60 day long period using the coarsest time step of 6 hours produces 136 MB of output for a migration burial solution. For the full compliment of solutions at 1 hour time steps with shifted gridding for small caliber munitions, the storage memory requirement is estimated to be roughly 540 MB using the present equation solver based on vortex lattice panels. On a 500 MHz desktop PC, run time is presently 5 min. / time step. On a more advanced platform such as a SGI Octane with approximately 2 GB and 8 CPUs, the run time is approximately 1 hour for a 60-day long simulation or 15 sec/time step.

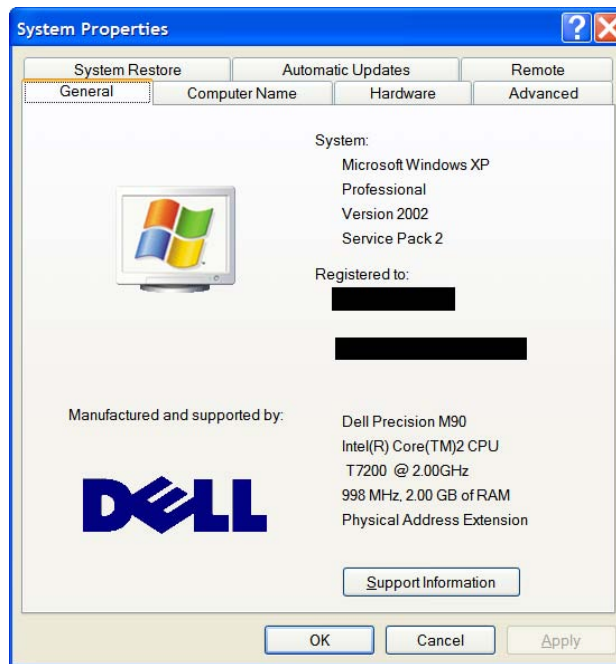


**Figure 71. Computer configuration.**

### 8.3.3 Cost Drivers

In the case of the UXO Mobility Model, collecting data to establish the initial configuration of the hardware, such as the distribution of UXO, can easily become the most expensive task. This is the case because at most sites there are only limited records of the UXO distribution, particularly in water. Also, much of the UXO has been in place for many seasonal cycles and is likely not where it originally landed, or in the original state of burial. Therefore at least some limited in-water surveys would be beneficial to provide a credible baseline to start the model. Given the limited state of the art of UXO location technology, the size of the areas to be surveyed and the generally high day rate costs of at-sea operations, it is likely that several tens of thousands of dollars would be required for even a minimal sampling survey. While a more credible survey could cost several hundred thousand dollars, a full survey could cost millions of dollars.

Fortunately, the MM itself can be used as a “what-if” advisor to help focus the survey. The MM can be applied to the various sub-environments of a given area of interest to determine in which areas UXO would be subject to unburial and movement if it does exist there. Only those areas would then need to be surveyed.

The second cost item is the collection of data to define the environmental parameters. Fortunately, most sites already have a historical data base for the primary environmental forcing function, weather. The key to this task is in the experience and skill of the oceanographer or coastal scientist assigned to locate, process, and format the data as input to the MM. However,

even with an experienced scientist/technician processing the data, it can require a few weeks of effort to process a large site data base.

There also may be added costs incurred for collecting seafloor sediment samples and local sediment sources data (e.g., rivers, etc.). Typically a few tens of thousands of dollars per site would provide the key data required to support the MM.

The primary cost drivers in using the MM are all related to data collection. The costs for a site could be as minimal as approximately \$96k for a basic Mode 1 screening and to approximately \$1M or more for a full Mode 2-3 analysis of a complex site with high risk conditions.

#### **8.3.4 Life Cycle Costs**

The UXO Mobility Model has little if any cost associated with its maintenance over its life. Each site-specific application will have its own defined set of costs. The total costs of using the MM will depend on how many times it is used and the complexity of the sites to which it is applied.

## **9.0 IMPLEMENTATION ISSUES**

### **1.30 9.1 Environmental Checklist**

The application of the UXO Mobility Model itself requires no environmental permits, as there is no field activity in the modeling process. The acquisition of survey data would require standard permits for operating aircraft or vessels with multi-beam sonars, but those are standard commercial operations with very low environmental impact. Bottom sample collection by divers, use of ADCP instruments, etc., for site monitoring would fall in the same general category.

All of the activities associated with the use of the MM are extremely low-impact environmentally. In fact, the overall result of use of the MM is to actually improve the environment by minimizing risk of human exposure to UXO.

### **1.31 9.2 Other Regulatory Issues**

The primary dissemination of information concerning the UXO Mobility Model to regulatory agencies will be via the ESTCP publications program. In addition, the MM developers expect to submit various papers for publication in technical journals.

### **1.32 9.3 End-User Issues**

The primary end users for this technology include the operators and managers of the 23 identified Navy UXO sites, as well as the dozens of other Army UXO sites.

The MM also will be used by higher-level administrative organizations such as Navy Regional Commands and Systems Commands in the development of environmental programs, decisions regarding investment in new UXO cleanup technology etc.

The Army has similar requirements. No Air Force or Coast Guard requirements have been identified at this time, although Coast Guard responsibilities for port security may at some point lead them to a requirement to understand UXO behavior on the seafloor of the approaches to ports and other estuaries.

The primary questions regarding MM expressed by ESTCP and potential users have been (a) validity of the MM and (b) cost to use the MM. The ESTCP program has effectively answered question (a) because the MM is validated in a wide range of operating environmental conditions. Although the weather did not provide any truly extreme cases during the Field Demonstrations, the MM was easily calibrated over the full range of “normal” storm conditions, including breaking waves. Extrapolation for major storm events is likely to be sufficiently accurate to engineering analysis of site risks. The costs are documented above, and are very small compared to the savings that result from reduction of the areas requiring remediation.

There also were concerns regarding issues related to conducting surveys of UXO distribution and then analyzing the stability of the UXO. This program did not directly address the politics of that issue. However, in the Example Applications Analysis presently in progress (Camp Perry, Ohio, Lake Erie Impact Range) has shown that only a very small fraction of the total UXO in the Impact Range is mobile. The MM analysis has shown that only the UXO very near shore (within the area of ice rafting or extreme shoreline reconfiguration in rare storms) moves to shore. The EAA also confirmed the results of the USACOE field testing and dredging operations in the Toussaint River. Those very positive results will be of considerable value and help focus future UXO risk mitigation efforts considerably. .

There are no procurement issues with this software. It is government-owned and can be copied for government use. It is likely that contractors bidding on UXO surveys and cleanup contracts will be given the output from the MM by NAVFAC ESC personnel. There is no known commercial application for the software beyond support for military UXO planning and risk mitigation.

The UXO Mobility Model was validated by this ESTCP program and as of this writing, no competing technology with this particular focus exists to support munitions response operations.



## 10.0 REFERENCES

- [1] DeVisser, A. et al., 2004, “*Environmental Security Technology Certification Program (ESTCP) Demonstration Plan 200417 Predicting the Mobility and Burial of Underwater Unexploded Ordnance (UXO) Using the Modified VORTEX Model*,” October 2004 through April 2006, 16 November 2004.
- [2] Wilson, J.V. et al., 2008, “(ESTCP) 200417 Predicting the Mobility and Burial of Underwater Unexploded Ordnance (UXO) Using the UXO Mobility Model, FIELD TEST REPORT (FRF Duck, NC),” NAVFAC ESC Technical Report (in publication).
- [3] Wilson, J.V. et al., 2008, “(ESTCP) 200417 Predicting the Mobility and Burial of Underwater Unexploded Ordnance (UXO) Using the UXO Mobility Model, FIELD TEST REPORT (PMRF Barking Sands, Kauai, Hawaii),” NAVFAC ESC Technical Report (in publication).
- [4] Hammond, R., Jenkins, S.A., and J. Wasyl, 2003, “Underwater Munitions of Concern Migration and Burial Model: Phase 1 Report: Parameter Definition,” 34 pp, June 2003.
- [5] Wilson, J., 2004, “UXO Migration Field Test Point Mugu Lagrangian Drifters FINAL REPORT “, Sound and Sea Technology Report 04-13, 23 September 2004.
- [6] Wilson, J., et al., 2005, “UXO Measurement Method Field Tests (MMFT1&2) and Mobility Model Modification FINAL REPORT”, Sound & Sea Technology Report 05-07 31 December 2005.
- [7] Wilson, J.V. et al., 2008, “UXO Mobility Model Application Guidance Document”, NAVFAC ESC Technical Report, (in publication).
- [8] Wilson, J.V. et al., 2008, “UXO Mobility Model Example Application Analysis – Lake Erie”, NAVFAC ESC Technical Report, (in publication).
- [9] Peace, A.J. and N. Riley, 1983, “A viscous vortex pair in ground effect,” *Journal of Fluid Mechanics*, v. 129, 409-26.
- [10] Bagnold, R.A., 1963, “Mechanics of Marine Sedimentation” in *The Sea*, v. 3, *The Earth Beneath the Sea*, edited by M.N. Hill, p. 507-528, Wiley Interscience, New York, London, 963 pp.
- [11] Bailard, J.A. and D.L. Inman, 1979, “A Re-examination of Bagnold’s Granular-Fluid Model and Bed Load Transport Equation” *Journal of Geophysical Research*, v. 84, n. C12, p. 7827-33.

- [12] Inman, D.L., M.H.S. Elwany, and S.A. Jenkins, 1993, “Shorerise and Bar-Berm Profiles on Ocean Beaches” *Journal of Geophysical Research*, v. 98, no. C10, p. 18,181-199, October 1993.
- [13] Inman, D.L., 1987, “Accretion and Erosion Waves on Beaches”, *Shore & Beach*, v. 55, n. 3/4, p. 61-66.
- [14] Garrood, D. et al., 2008, “UXO Mobility Model Users’ Manual”, NAVFAC ESC Technical Report (TBD), in publication.
- [15] Environmental Protection Agency, Office of Solid Waste and Emergency Response, “Used or Fired Munitions and Unexploded Ordnance at Closed, Transferred, and Transferring Military Ranges - Interim Report and Analysis of EPA Survey Results”, EPA 505-R-00-01,” April 2000.
- [16] Tucker, L., Personnel Communication, 2003, “UXO clearance, Jackson Park, exNAD”, April 2003.
- [17] Jarrah, D.H., 2001, “Predicting Underwater Corrosion Rates of Unexploded Ordnance (UXO) – Definition and Governing Parameters”, NAVFAC ESC, Nov. 2001.
- [18] USAESCH, United States Army Engineering and Support Center, “Ordnance and Explosives Program Fact Sheets”, <http://www.hnd.usace.army.mil/oew/factshts>.
- [19] National Oceanic and Atmospheric Association (NOAA), National Data Buoy Center, 2003. Available: <http://ndbc.noaa.gov>.
- [20] CDIP, 2008, “Coastal data information program,” <http://cdip.ucsd.edu/>, 2008.
- [21] Oceanographic and Atmospheric Master Library (OAML), 2004, Available: <http://navy.ncdc.noaa.gov/products/oaml.html>.
- [22] USGS, 2008, “National Water Information System: Web Interface,” <http://waterdata.usgs.gov/nwis/>.
- [23] National Geophysical Data Center, 2008, [http://www.ngdc.noaa.gov/mgg/gdas/gd\\_designagrid.html](http://www.ngdc.noaa.gov/mgg/gdas/gd_designagrid.html).
- [24] M.S. Longuet-Higgins, 1953, “Mass transport in water waves,” *Phil. Trans., Ser. A*, vol. 245, p. 535-581.
- [25] Lamoure, J. and C. C. Mei, 1977, “Effects of horizontally 2-dimensional bodies on mass-transport near sea bottom,” *J. Fluid Mech.*, vol. 83, no. 3, pp. 415–433.
- [26] Longuet-Higgins, M.S., 1970, “Steady currents induced by oscillations around islands,” *J. Fluid Mech.*, vol. 42, no. 4, p. 701-720.

- [27] Connor, J.J. and J.D. Wang, 1973, "Finite element modeling of two-dimensional hydrodynamic circulation," MIT Technical Report #MITSG 74-4, p. 1-57.
- [28] McCormick, B.W., 1979, *Aerodynamics, Aeronautics, and Flight Mechanics*. New York: John Wiley & Sons.
- [29] Van Dyke, M., 1975, *Perturbation Methods in Fluid Mechanics*. Stanford, CA: Parabolic, 271 pp.
- [30] Peace, A.J. and N. Riley, (1983), "A Viscous Vortex Pair in Ground Effect," *J. Fluid Mech.*, vol. 129, pp. 409–426, April 1983.
- [31] Bagnold, R.A., 1956, "The flow of cohesionless grains in fluids, *Philos. Trans. R. Soc. London Ser. A*, 249(964), 235–297.
- [32] Bagnold, R.A., 1963, "Mechanics of marine sedimentation," In *The Sea, Ideas and Observations on Progress in the Study of the Seas*, vol. 3, *The Earth Beneath the Sea, History*, edited by M. N. Hill, pp. 507–528, Wiley, New York.
- [33] Bowen, A.J., 1980, "Simple models of nearshore sedimentation: beach profiles and longshore bars," in *The Coastline of Canada: Littoral Processes and Shore Morphology*, Paper 80-10, edited by S. B. McCann, pp. 1–11, *Geol. Surv. of Can.*, Ottawa, Ont..
- [34] Jenkins, S.A. and J. Wasyl, 1990, "Resuspension of estuarial fine sediments by tethered wings," *J. Coastal Res.*, vol. 6, no. 4, p. 961-980.
- [35] Jenkins, S.A. and D. L. Inman, 2006, "Thermodynamic solutions for equilibrium beach profiles," *J. of Geophysical Res.*, vol. 111, C02003, doi:10.1029/2005JC002899, 21 pp.
- [36] Fu, S.S., Tau, C., Prasad, M., Wilkens, R.H., and L.N. Frazer, 2004, "Acoustic properties of coral sands, Waikiki, Hawaii," *J. Acoust., Soc. Am.* 115 (5), Pt 1, pp. 2013-2020.
- [37] Inman, D.L. and R. Dolan, 1989, "The Outer Banks of North Carolina: Budget of Sediment and Inlet Dynamics Along a Migrating Barrier System," *J. Coastal Research*, vol. 5, no. 2, pp. 193–237.
- [38] Jenkins, S.A., D. L. Inman, M. D. Richardson, T. F. Wever, and J. Wasyl, 2007, "Scour and Burial Mechanics of Objects in the Nearshore," *IEEE Jour Ocn Eng*, vol. 32, no. 1, pp. 78-90, Jan. 2007.
- [39] D. L. Inman and S. A. Jenkins, 1996, "A Chronology of Ground Mine Studies and Scour Modeling in the Vicinity of La Jolla," *Scripps Institution of Oceanography: University of California, San Diego, SIO Reference Series* 96-13.

- [40] R. F. Dill, 1958, "The Burial and Scouring of Ground Mines on a Sandy Bottom," San Diego, CA: U. S. Navy Electronics Laboratory, Research Report NEL 861.
- [41] Donohue, J.J. and L. E. Garrison, 1954, "An Evaluation of Mine Behavior Observations in Four Test Areas," Narragansett Marine Laboratory: Univ. Rhode Island, Reference 54-13.
- [42] Inman, D.L. and S. A. Jenkins, 2002, "Scour and Burial of Bottom Mines, A Primer for Fleet Use," Scripps Institution of Oceanography: Univ. of California, San Diego, SIO Reference Series 02-8, 2002. Available: <http://repositories.cdlib.org/sio/reference/02-8/>.
- [43] Gallagher, E. L., S. Elgar, and R. T. Guza, 1998, "Observations of sand bar evolution on a natural beach", J. Geophys. Res., 103(C2), 3203–3215.
- [44] Nordstrom, C.E. and D. L. Inman, 1975, "Sand level changes on Torrey Pines Beach, California," U. S. Army Corps of Engineers, Coastal Engineering Research Center Miscellaneous Paper 11-75.
- [45] Inman, D.L., 1953, "Areal and seasonal variations in beach and nearshore sediments at La Jolla, California," U. S. Army Corps of Engineers: Beach Erosion Board Technical Memorandum 39.
- [46] Inman, D.L. and T. K. Chamberlain, 1955, "Particle size distribution in nearshore sediments," Finding Ancient Shorelines: Society of Economic Paleontologists and Mineralogists, Special Publication 3, pp. 106-129.
- [47] Stauble, D.K., 1992, "Long-term profile morphodynamics: field research facility case history," U. S. Army Corps of Engineers: Coastal Engineering Research Center Technical Report CERC-92-7.
- [48] Stauble, D.K. and M.A. Cialone, 1996, "Sediment dynamics and profile interactions: DUCK94", Coastal Engineering - Proceedings of the twenty-fifth international conference, Vol. 4, ASCE.
- [49] Stauble, D.K., 2005, "A review of the role of grain size in beach nourishment projects," U.S. Army Engineer Research and Development Center, Coastal and Hydraulics Laboratory, <http://www.fsbpa.com/05Proceedings/02-Don%20Stauble.pdf>.
- [51] Kirby, J.T., 1986 "Higher-order approximations in the parabolic equation method for water-waves," J. Geophysical Res., vol. 91, no. C1, p. 933–952, 1986.
- [52] Dalrymple, R.A., J. T. Kirby, and P.A. Hwang, 1984, "Wave diffraction due to areas of energy dissipation," J. Waterway Port, Coast, and Ocean Engineering., vol. 110, p. 67-79.
- [53] Longuet-Higgins, M.S., 1953, "Mass transport in water waves," Phil. Trans., Ser. A, vol. 245, p. 535-581.

- [54] Lamoure, J. and C.C. Mei, 1977, "Effects of horizontally 2-dimensional bodies on mass transport near sea bottom," J. Fluid Mech., vol. 83, no. 3, pp. 415–433.
- [55] Longuet-Higgins, M.S., 1970, "Steady currents induced by oscillations around islands," J. Fluid Mech., vol. 42, no. 4, p. 701-720.
- [56] Connor, J.J. and J.D. Wang, 1973, "Finite element modeling of two-dimensional hydrodynamic circulation," MIT Technical Report #MITSG 74-4, p. 1-57.
- [57] McCormick, B.W., 1979, "Aerodynamics, Aeronautics, and Flight Mechanics"s. New York: John Wiley & Sons.
- [58] Van Dyke, M., 1975, "Perturbation Methods in Fluid Mechanics." Stanford, CA: Parabolic, 271 pp.

### Appendix A. Points Of Contact.

<b>POINT OF CONTACT Name</b>	<b>ORGANIZATION Name Address</b>	<b>Phone/Fax/e-mail</b>	<b>Role In Project</b>
Barbara Sugiyama	NAVFAC ESC	<a href="mailto:barbara.sugiyama@navy.mil">barbara.sugiyama@navy.mil</a>	Principal Investigator
Alexandra De Visser	NAVFAC ESC	<a href="mailto:alexandra.devisser@navy.mil">alexandra.devisser@navy.mil</a>	Co PI
Jeff Wilson	Sound & Sea Technology	<a href="mailto:jwilson@soundandsea.com">jwilson@soundandsea.com</a>	SST Project Manager, Demonstration Design
Bill Daly	Sound & Sea Technology	<a href="mailto:wdaly@soundandsea.com">wdaly@soundandsea.com</a>	SST Senior Field Test Engineer
Ian McKissick	Sound & Sea Technology	<a href="mailto:imckissick@soundandsea.com">imckissick@soundandsea.com</a>	SST Field Test Engineer, Surrogates, Instruments
Scott Jenkins	Dr. Scott A. Jenkins Consulting	<a href="mailto:sjenkins@ucsd.edu">sjenkins@ucsd.edu</a>	UXO Mobility Model Development, Site Analysis
Dr. William Birkemeier	USACE ERDC FRF	<a href="mailto:william.birkemeier@usace.army.mil">william.birkemeier@usace.army.mil</a>	FRF Duck Field Test Planning, Logistic Support, Diving Ops
Robert Rocheleau	Sea Engineering, Inc.,	<a href="mailto:bohr@seaengineering.com">bohr@seaengineering.com</a>	Hawaii Field Test Planning, Logistic Support, Diving Ops

## Appendix B. UXO Mobility Model Fortran Code

```
c.....UXO_transport_frf_duck_w_cycloid_29mar07.for
c***THIS PROGRAM IS CONFIGURED TO RUN ON A 29 Character wave file name (ie.
waves_frf_22jun05-15feb06.dat)
c  which has wave height in centimeters in non-uniform timesteps with a
c  mean interval of 6.44 hours*****
c
      DIMENSION time(5000),ang(5000),per(5000),wht(5000)
      dimension r(90601),s(90601),b(90601)
      dimension x(301),y(301),gama(301),gamb(301),gam(301)
      dimension z_mark(301,301)
      dimension gam2(301),gama_2(301),gamb_2(301)
      dimension scour(301,301,250),bot(301,301,250)
      dimension bury(5000),bur(5000)
      dimension u0(5000),u2(5000),whx(5000)
      character*12 bofile2
      character*5 fname(1500)
c
c9mar07
      dimension alam(5000),ucross(5000),vlong(5000),xcross(5000)
      dimension ylong(5000),shield(5000),theta(5000)
c
      character*20 ofile
      character*29 wavefile
c
c27mar07 cycloid stuff
      dimension dept(3001),wvnum(3001)
      dimension whtme(366)
      double precision depce(366),depcp(366),ac(366),bc(366)
      character*6 fname2(366)
      character*1 cc
CCCC_____cycloid ellipse arrays_____
      DIMENSION angc(2000),xd(2000)
      Dimension slope(2000),circle(2000)
      dimension cycloid(2000)
      character*20 ofile2
      character*12 breakshr
      dimension brkcol(2401),brkhgt(2401),brkang(2401),brkdep(2401)
      Dimension depmsl(2401)
      integer krow(2401),mslcol(2401)
c
1000 format(a12)
```



```

1001 format(a29)
1111 format(a20)
c
    open(19,file='UXO_transport_frf_duck_w_cycloid_29mar07.inp'
    &,status='old')
c***input parameters particular to wave induced burial
    read(19,1001)wavefile
    read(19,*)mstart
    read(19,*)mend
c***input parameters particular to UXO shape generation
    read(19,1000)ofile
    read(19,*)ix
    read(19,*)xinv
    read(19,*)jy
    read(19,*)yinv
    read(19,*)depth
    read(19,*)b_dia
    read(19,*)h
    read(19,*)point
c***input parameters particular to UXO scour
    read(19,*)z_plane
    read(19,*)delx
    read(19,*)dely
    read(19,*)cl
    read(19,*)cf
    read(19,*)g
    read(19,*)rhom
    read(19,*)alpha
    read(19,*)tauc
    read(19,*)str
    read(19,*)r_test
    read(19,*)s_test
    read(19,*)ak_bot
    read(19,*)tcon
    read(19,*)winu
    read(19,*)winl
    READ(19,*)cdir
    READ(19,*)effic
    read(19,*)akx
    read(19,*)htmin
    READ(19,1100)bofile2
    READ(19,*)ass
    READ(19,*)aks
    READ(19,*)tdown

```

```
READ(19,*)tshift
READ(19,*)eff2
READ(19,*)eff3
READ(19,*)akwave0
READ(19,*)akwave2
READ(19,*)icoast
```

c..9mar07

```
READ(19,*)ax
READ(19,*)ay
READ(19,*)dbar
READ(19,*)scrit
READ(19,*)xuxo
READ(19,*)yuxo
READ(19,*)bplane
READ(19,*)burmove
READ(19,*)dir_thr
```

c

CYCLOID Inputs 27mar07

```
read(19,*)gm
read(19,*)ak
read(19,*)beta
read(19,*)akm
read(19,*)akd
read(19,*)vdepce
read(19,*)bs
read(19,*)nrange
READ(19,*)ecc
READ(19,*)akxc
READ(19,*)crit
READ(19,*)refdia
READ(19,*)aka
READ(19,*)dia2
READ(19,*)akbr
READ(19,*)ibrbm
READ(19,*)zone
READ(19,*)xshift
READ(19,*)i_cycloid
READ(19,'(a)')cc
read(19,1111)ofile2
read(19,1000)breakshr
READ(19,*)krefrow
READ(19,*)nuxorow
READ(19,*)sx
READ(19,*)sy
```

```

        READ(19,*)ktotal
CYCLOID END
        akd=akd*(refdia/dia2)**aka
c
c xoffset is the distance in meters (sx = irowixshiftgrid cperpendicular to coastli
c
        pi=ACOS(-1.0)
        write(*,*)g,gm,mend
c....OPEN/READ Breaker/shoreline file ie, "duckbath.bra" determine column
c of 0 MSL
        OPEN(UNIT=30,FILE=breakshr,STATUS='OLD')
        yoffset=(krefrow-nuxorow)*sy
        do 157 k=1,ktotal
        READ(30,*)krow(k),brkcol(k),brkhgt(k),brkang(k),brkdep(k),
        &mslcol(k),depmsl(k)
        if(krow(k).EQ.krefrow)krefcol=mslcol(k)
        if(krow(k).EQ.nuxorow)xoffset=(mslcol(k)-krefcol)*sx
157  continue
c
C.....open wave period-height-direction files
        OPEN(UNIT=2,FILE=wavefile,STATUS='OLD')
c...wave height read in cm
        mcount=0
        DO 105 m=1,5000
        READ(2,*,end=1105)time(m),per(m),wht(m),ang(m)
        mcount=mcount+1
        whx(m)=(wht(m)/((2.0*2.0*pi/per(m))**0.5))*((g/depth)**0.25)
        u0(m)=(whx(m)/2.0)*((g/depth)**0.5)
        u2(m)=akwave2*u0(m)
        alam(m)=(2.0**0.4)*(wht(m)**0.2)*(((2.0*pi/per(m))**2.0)/
        &(g*0.8))**0.2
105  CONTINUE
1105  write(*,*)mcount
        write(*,*)time(1),per(1),wht(1),ang(1)
        write(*,*)time(mcount),per(mcount),wht(mcount),ang(mcount)
c
        nblines=mcount
c
c
1100  format(a12)
C*****begin UXO_br3 logic*****
c
c..open time output file
        OPEN(UNIT=4,FILE=bofile2,STATUS='unknown')

```

```

c
c
91000  format(4f12.5)
c      write(*,*)nblines
c
      do 9155 n=1,nblines
      time(n)=time(n)-tcon
      bury(n)=0.0
      bur(n)=0.0
c..change absolute time to relative time by subtracting tcon
9155  continue
c
      ymine=htmin
      ss=0.0
      gr=0.0
      gr1=0.0
      gr2=0.0
c
c..9mar07
      xcross(1)=xuxo
      ylong(1)=yuxo
      write(*,*)xcross(1),ylong(1)
c***START OF BURY and BUR LOOP*****
      DO 9406 n=2,nblines
      nm1=n-1
      if(icoast.EQ.3)then
      if(ang(n).GE.winu)ang(n)=winu
      if(ang(n).LE.winl)ang(n)=winl
      endif
      if(icoast.EQ.1)then
      if(ang(n).LE.winu)ang(n)=winu
      if(ang(n).GE.winl)ang(n)=winl
      endif
c..keep incident waves inside of window icoast=1 east facing, icoast=3 west coast
      np1=n+1
      delt=(time(np1)-time(n))*31536000.0
      theta(n)=ang(n)-cdir
      energy=1.0/8.0*g*whx(n)**2
      cn=0.5*g*per(n)/(2.0*pi)*SIN(theta(n)*2.0*pi/360.0)*
&COS(theta(n)*2.0*pi/360.0)
c ..
      abcn=ABS(cn)
      asc=abcn*ass
      ptr=energy*cn*effic/(1.64*0.6*1000000.0*g*1000000.0)

```

```

c
c..correct instantaneous transport back to meters ptrm
    pt=ptr*delt
    if(time(n).LT.tdown)then
        gr1=gr1+ABS(pt)
    ELSE
        gr1=gr1-ABS(pt)*eff2
    ENDIF
    gr2=gr2+ABS(pt)*eff3
    gr=gr1+gr2
c
    ymine=htmin-(gr*htmin)
CCCCCCCCCCC...inner loop
c
c
CC.5DEC06***HERE IS THE DEFINITION:
C BURY(n) is the UXO silhouette above seabed as a fraction of cross section
C BUR(n) is the dimensional burial depth (cm) below seabed.
    bury(n)=ymine/htmin
    bur(n)=(1.0-bury(n))*h
    ucross(n)=u0(n)*COS(theta(n)*2.0*pi/360.0)
    vlong(n)=u0(n)*SIN(theta(n)*2.0*pi/360.0)
c..migration calculated in meters relative to initial position xuxo,yuxo using
C SST sign conventions (Solidworks).
    shield(n)=u0(n)**2.0/(1.65*g*b_dia)
    if(shield(n).GT.scrit.AND.bury(n).GT.burmove)then
        ylong(n)=vlong(n)*delt*ay/100.0+ylong(nm1)
        if(theta(n).LT.dir_thr)then
            xcross(n)=-1.0*ucross(n)*delt*ax/100.0+xcross(nm1)
        else
            xcross(n)=ucross(n)*delt*ax/100.0+xcross(nm1)
        endif
    else
        xcross(n)=xcross(nm1)
        ylong(n)=ylong(nm1)
    endif
c
    if(n.GE.mstart.AND.n.LE.mend)write(*,*)n,bury(n),bur(n)
    &,xcross(n),ylong(n),shield(n),theta(n)
9406    continue
c
c
    kbur=0
    DO 9408 n =1,nblines

```

```

time(n)=time(n)+tshift
write(4,92000)time(n),bury(n),bur(n),xcross(n),ylong(n),shield(n)
&,theta(n)
    kbur=kbur+1
9408 continue
92000 format(7f15.5)
    rewind(4)
c
    write(*,*)kbur
c
C*****end UXO_br3 logic*****
c
c
C$$$$$$$$$$$$$$$$$$$$ BEGIN TIMESTEP LOOP $$$$$$$$$$$$$$$$$$$$$$
    i1=0
    i2=0
    i3=0
    i4=0
    i5=0
    OPEN(UNIT=14,FILE=ofile2,STATUS='unknown')
c***can't run past the end of the wave record
    if(mend.GT.nblines)mend=nblines
    do 888 m=mstart,mend
        write(*,*)m,mend
C***DISPERSION RELATIONSHIP
c..convert wave height to meters for cycloid program
    whtme(m)=wht(m)/100.0
    mcountc=mcountc+1
c
c
c..for EVERY wave in time series do ALL OF THE FORTRAN
    freq=1.0/per(m)
    sigma=2.0*pi*freq
    shaldep=ak*gm*(per(m)**2.0)/(2.0*pi)
c
c
c..Wave number array generated for every depth 0-300m for each wave
    do 1010 i=1,3001
        dept(i)=(3001-i)*0.1
c..... depth array generated from 300 m to 0 m, by 0.1 m
        wvnum(i)=0.0
        if(dept(i).LE.0)go to 1090
        if(dept(i).LT.shaldep)then
            wvnum(i)=sigma/((gm*dept(i))**0.5)

```

```

        go to 1090
    endif
    yj=(sigma**2*dept(i))/gm
    xj=yj
c
    do 1030 k5=1,100
    ht=tanh(xj)
    f=yj-xj*ht
    if (abs(f) .lt. 0.000001) go to 1040
    fd=-1.0*ht-(xj/cosh(xj)**2)
    xj=xj-(f/fd)
1030    continue
c
c    write(*,1050)
1050    format(' subroutine disp does not converge!!! ')
1040    wvnum(i)=xj/dept(i)
1090    continue
1010    continue
C***END OF DISPERSION RELATIONSHIP
c*****output file names 1-99999
c*****i1=ones digit, i2=tens digit, i3=100s digit, i4=1000s, i5=10000s
    i1=i1+1
    if(i1.EQ.10)then
        i2=i2+1
        i1=0
    if(i2.EQ.10)then
        i3=i3+1
        i2=0
    if(i3.EQ.10)then
        i4=i4+1
        i3=0
    if(i4.EQ.10)then
        i5=i5+1
        i4=0
    endif
    endif
    endif
    endif
c
    in1=48+i1
    in2=48+i2
    in3=48+i3
    in4=48+i4
    in5=48+i5

```



```

fname(m)=CHAR(in5)//CHAR(in4)//CHAR(in3)//CHAR(in2)//CHAR(in1)
fname2(m)=CHAR(in5)//CHAR(in4)//CHAR(in3)//CHAR(in2)//CHAR(in1)
&//cc
write(*,*)fname2(m)
c...open cycloid profile output files 27mar07
  OPEN(UNIT=11,FILE=fname2(m),STATUS='unknown')
c
c
c
  ep=akm/(akm-1.0)
  depcp(m)=bs*whtme(m)*((beta/(bs*whtme(m)*akm))**ep)
  dst=vdepce
c
c
  do 400 n=1,100
c find wave number associated with depce(m)
  kn=0
  do 600 ind=1,3001
    if(dept(ind).LT.depce(m).AND.kn.EQ.0)then
      kn=1
      wn=wnum(ind)
    endif
600    continue
    if(n.EQ.1)then
      fun_hy=wn*depce(m)
      if(ibrbm.EQ.1)then
        depce(m)=akbr*whtme(m)
      else
        depce(m)=akd*whtme(m)/SINH(fun_hy)
      endif
    else
      kj=0
      do 601 ip=1,3001
        if(dept(ip).LT.depce(m).AND.kj.EQ.0)then
          kj=1
          wn=wnum(ip)
        endif
601    continue
        fun_hy=wn*depce(m)
        if(ibrbm.EQ.1)then
          depce(m)=akbr*whtme(m)
        else
          depce(m)=akd*whtme(m)/SINH(fun_hy)
        endif

```

```

endif
400 continue
c
ac(m)=depce(m)/2.0
bc(m)=depce(m)/2.0
write(*,*)whtme(m),depce(m),wn
c
c
CCCC_____cycloid ellipse
section_____
c
c set eccentricity equal to parameter snum
c
iuxo=0
DO 777 n=2,nrange
angc(n)=0.1*n
c convert angc(n) to radians
angc(n)=angc(n)*pi/180.0
c apply stretching factor to cross shore coordinate xd...
if(i_cycloid.EQ.1)then
c.TYPE-A
fe=((2.0-(ecc**2.0))/2.0)**0.5
rad=((SIN(angc(n))**2.0)+((1.0-(ecc**2.0))
&*((COS(angc(n))**2.0))
dr=-1.0*(ecc**2.0)*(SIN(angc(n))*COS(angc(n)))/rad
dh=SIN(angc(n))+((1.0-COS(angc(n)))*dr)
dx=1.0-COS(angc(n))+((angc(n)-(SIN(angc(n))))*dr)
rc=(1.0-(ecc**2.0))**0.5*(ac(m)/(rad**0.5))
xd(n)=(rc*fe*(angc(n)-(SIN(angc(n))))/akxc)+xshift
cycloid(n)=rc*(1.0-(COS(angc(n))))+(-1.0*zone)
else
c.TYPE-B
fe=((2.0-(ecc**2.0))/(2.0*(1.0-(ecc**2.0))))
rad=((1.0-(ecc**2.0))*((SIN(angc(n))**2.0))+
&*((COS(angc(n))**2.0))
dr=(ecc**2.0)*(SIN(angc(n))*COS(angc(n)))/rad
dh=SIN(angc(n))+((1.0-COS(angc(n)))*dr)
dx=1.0-COS(angc(n))+((angc(n)-(SIN(angc(n))))*dr)
rc=bc(m)/(rad**0.5)
xd(n)=(rc*fe*(angc(n)-(SIN(angc(n))))/akxc)+xshift
cycloid(n)=rc*(1.0-(COS(angc(n))))+(-1.0*zone)
endif
c
c apply stretching factor to slope

```

```

    slope(n)=(dh/dx)*(akxc/fe)
c  check slope(n) using slope of circular cycloid
    dhc=SIN(angc(n))
    dxc=1.0-COS(angc(n))
c    circle(n)=(dhc/dxc)
    circle(n)=(dhc/dxc)*akxc
c  convert angc(n) back to degrees
    angc(n)=angc(n)*180.0/pi
c
c write cycloid at each xuxo in wave timeseries
    if(xd(n).GE.xuxo.AND.iuxo.EQ.0)then
        write(*,*)m,xd(n),cycloid(n)
        write(14,*)m,xd(n),cycloid(n)
    iuxo=1
    endif
c
c..add in xoffset, write cycloid profile
    xd(n)=xd(n)+xoffset
    write(11,*)xd(n),cycloid(n)
777  CONTINUE
    if(xd(nrange).LT.xuxo)then
        write(*,*)m,xd(nrange),cycloid(nrange)
        write(14,*)m,xd(nrange),cycloid(nrange)
    endif
c...End 27mar07
c
C*****BEGIN SHAPE FILE LOGIC*****
CBurial Algorithm for bur in cm
c*****burial based on wave file
c
c..xinv and yinv already in cm
    xmid=(xinv*(ix-1))/2.0
    ymid=(yinv*(jy-1))/2.0
    if(bur(m).GT.h)then
        b_rad=0.0
    else
        b_rad=(b_dia/2.0)*(((h-bur(m))/h)**(1.0/point))
    endif
C
    open(3,file=ofile,status='unknown')
    DO 10 i=1,ix
        r(i)=((i-1)*xinv)-xmid
10  continue
c

```

```

        DO 15 j=1,jy
        s(j)=((j-1)*yinv)-ymid
15      continue
c
        k=0
        DO 20 i=1,ix
        do 30 j=1,jy
        k=k+1
        Ruxo=(r(i)*r(i)+s(j)*s(j))**0.5
c
        if(Ruxo.GT.b_rad)then
        b(k)=bplane
        else
        b(k)=h-bur(m)-(h*((Ruxo/b_rad)**point))
        endif
c
c
c
        write(3,920)r(i),s(j),b(k)
30      continue
20      continue
        rewind(3)
920    format(3f10.3)
C
c*****Beginning on cn_scour_osc*****
        b1=-1.0*3
        b2=-1.0*4
        b3=-1.0*5
        b4=-1.0*8
        b5=-1.0*10
        a0=1.0
        a1=5.410*(10**b1)
        a2=6.670*(10**b2)
        a3=1.173*(10**b3)
        a4=9.241*(10**b4)
        a5=2.729*(10**b5)
c
        gam0=0.5*c1*u0(m)*delx
c**oscilatory
        gam0_2=0.5*c1*u2(m)*delx
c**
        pi=3.14159
c
        open(9,file='z_mark.txt',status='unknown')

```

```

c
  ipt=ix*jy
c.....read 3 dimensional shape file
  icount=0
  do 100 k=1,ipt
    read(3,*)r(k),s(k),b(k)
    icount=icount+1
100  continue
c  write(*,*)icount
  rewind(3)
c
  kount=0
c.....read 3 dimensional shape file a second time to establish marker location
  do 110 i=1,ix
    do 120 j=1,jy
      read(3,*,end=111)dumr,dums,z_mark(i,j)
      kount=kount+1
120  continue
110  continue
111  continue
  write(*,*)kount
  rewind(3)
c
c
  if(m.NE.1)go to 166
  do 160 i=1,ix
    write(9,2000)(z_mark(i,j),j=1,jy)
160  continue
166  continue
c
c
  icount=0
  do 200 k=1,ipt
    icount=icount+1
c****part of sing point test
  if(r(k).EQ.r_test.AND.s(k).EQ.s_test)then
c.....re-initialize scour x-y grid
  do 131 i=1,ix
    do 141 j=1,jy
      scour(i,j,m)=0.0
141  continue
131  continue
  endif
c*****

```

```

    if(b(k).EQ.0.0)go to 200
    zmb=z_plane-b(k)
    zmb2=zmb**2
    zpb=z_plane+b(k)
    zpb2=zpb**2
c
    do 210 i=1,ix
    im1=(i-1)
c **calculate position relative to grid center offset by 1/2 grid cell to
c***prevent singularity at 0
    xgrid=im1*xinv-(xinv*ix/2)
    x(i)=xgrid-r(k)
    x1=x(i)
    x2=x(i)**2
    xs1=str*x(i)
    xs2=(str*x(i))**2
    gama(i)=a0+(a1*xs1)-(a2*xs1**2)+(a3*xs1**3)
    gamb(i)=(-1.0*a4*xs1**4)+(a5*xs1**5)
    gam(i)=(gama(i)+gamb(i))*gam0
    if(gam(i).LT.0.0)gam(i)=0.0
c**oscillatory vortex filament
    gama_2(i)=a0-(a1*xs1)-(a2*xs1**2)-(a3*xs1**3)
    gamb_2(i)=(-1.0*a4*xs1**4)-(a5*xs1**5)
    gam2(i)=(gama_2(i)+gamb_2(i))*gam0_2
    if(gam2(i).GT.0.0)gam2(i)=0.0
c***
c
    do 220 j=1,jy
    jm1=(j-1)
c **calculate position relative to grid center offset by 1/2 grid cell to
c***prevent singularity at 0
    ygrid=jm1*yinv-(yinv*jy/2)
    y(j)=ygrid-s(k)
    yps=y(j)+dely
    yps2=yps**2
    yms=y(j)-dely
    yms2=yms**2
    p1=gam(i)/(4.0*pi)
    aj24=p1*zmb/(x2+zmb2)*((yps/(x2+yps2+zmb2))-(yms/(x2+yms2+zmb2)))
    aj25=p1*zpb/(x2+zpb2)*((yps/(x2+yps2+zpb2))-(yms/(x2+yms2+zpb2)))
    u1=aj24+aj25
    aj26=p1*(zmb/(zmb2+yms2))*(1+(x1/(x2+zmb2+yms2)))
    aj27=p1*(zpb/(zpb2+yms2))*(1+(x1/(x2+zpb2+yms2)))
    aj28=p1*(zmb/(zmb2+yps2))*(1+(x1/(x2+zmb2+yps2)))

```





```
c
c
  write(*,*)xoffset,yoffset
stop
end
```